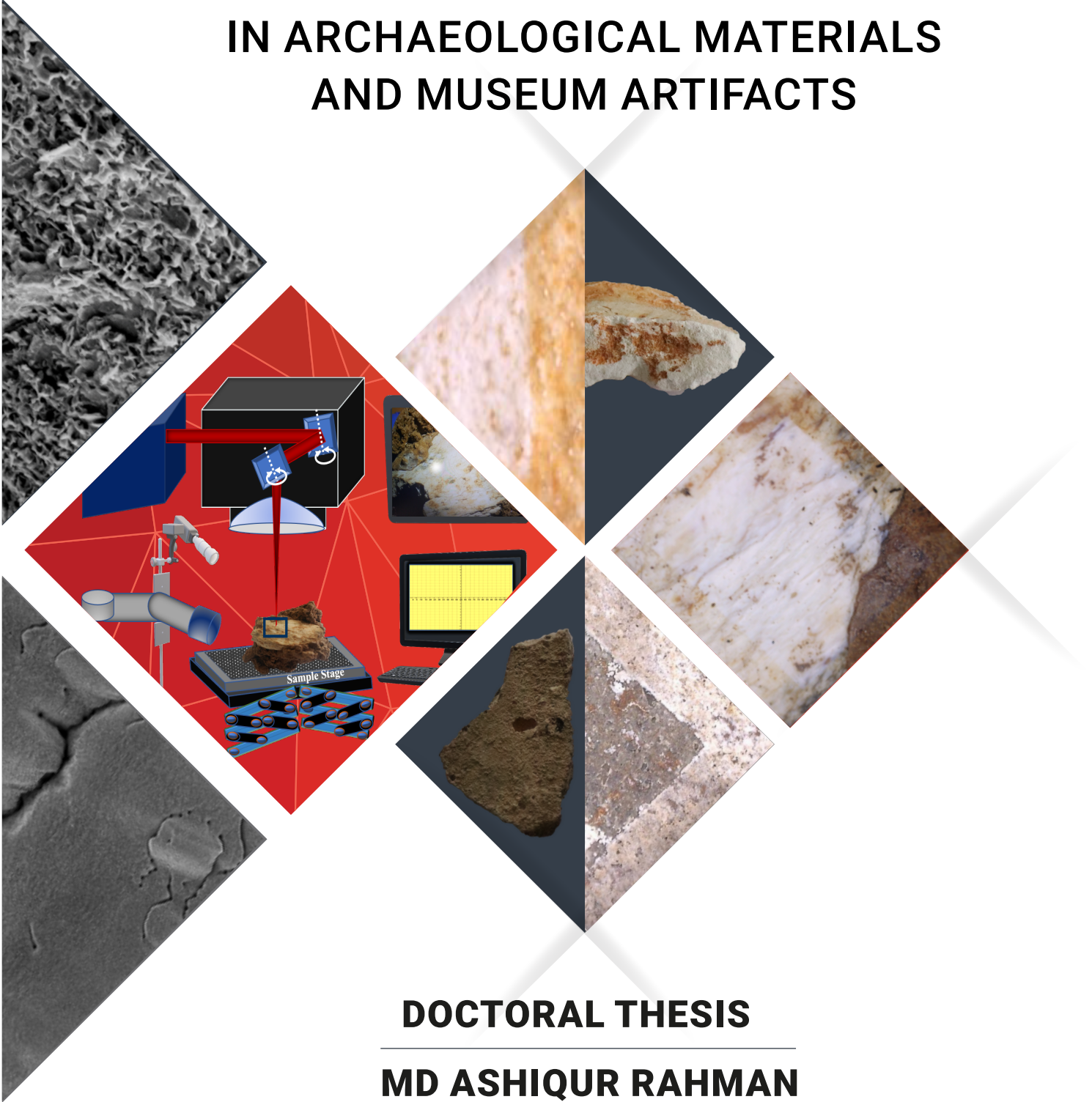




ED-ARCHMAT



LASER BASED INTERVENTION IN ARCHAEOLOGICAL MATERIALS AND MUSEUM ARTIFACTS



DOCTORAL THESIS
MD ASHIQUR RAHMAN



UNIVERSIDAD
DE BURGOS



UNIVERSIDADE
DE ÉVORA



CONSEJO SUPERIOR DE INVESTIGACIONES CIENTÍFICAS



INMA
INSTITUTO DE NANOCIENCIA
Y MATERIALES DE ARAGÓN



Universidad
Zaragoza



DOCTORAL THESIS

LASER BASED INTERVENTION IN ARCHAEOLOGICAL MATERIALS AND MUSEUM ARTIFACTS

MD ASHIQUR RAHMAN

SUPERVISORS

**GERMÁN F. DE LA FUENTE
M^a PILAR ALONSO ABAD
NICK SCHIAVON**

SPAIN, JUNE 2022



**To my beloved parents
my lovely wife and my son**

ACKNOWLEDGEMENT

All praises be upon Allah, the almighty, for enabling me to complete this doctoral thesis work with accuracy and precision, for giving me sound health, strength, courage, patience and perseverance throughout those three years of PhD candidature.

First and foremost, I would like to offer my heartfelt sense of gratitude, reverence and sincerity to the honorable co-supervisor of this thesis, Dr. Germán F. de la Fuente, Professor of Research at the Spanish National Research Council (CSIC: INMA), for selecting such an important topic, and taking the responsibility to nurture me as a researcher. It was an excellent chance to benefit from his extensive knowledge and expertise in the field of Laser. I am grateful for his scholarly guidance, research insight, expert suggestion, active engagement and tiresome efforts for the whole period of the thesis, and apparently continuous motivation during my PhD project, which made my attempts successful. I have learned a lot and been impressed by his extraordinary attention to detail, ethics and integrity, superb professional behavior, and determination, which will undoubtedly shape my future academic research career.

I would like to express my sincere thanks and profound gratitude to the two honorable co-supervisors of this thesis, Dr. Maria Pilar Alonso Abad, Professor at the University of Burgos, and Dr. Nick Schiavon, Professor at the University of Evora, and Dr. Luis Alberto Angurel Lambán, Professor at the University of Zaragoza, for their scholarly engagement in the experiments and data analyses throughout my PhD. I was benefitted enormously from their exceptional knowledge and insight in the fields of laser fundamentals and applications, characterization techniques, and archaeological and cultural heritage materials science. I would like to express my sincere appreciation for their extremely useful comments, constructive criticisms, suggestions and timely support in the detailed discussion on my project topics and data analyses through my project. It was a wonderful opportunity to expand my understanding of laser-based intervention of different significant archaeological materials and statistical analyses from their broad experience in these fields.

I would like to express my gratefulness and sincere thanks to Dr. José Miguel Carretero Díaz, Professor at the University of Burgos, and Dr. Rodrigo Alonso Alcalde, Director at the Museo de la Evolución Humana, for their great support in providing enormous archaeologically important samples, opportunities with the laboratory and archaeological sites visits, and facilities to learn the background of the significant archaeological materials subjected to this thesis work. Their comments and opinions on the different traditional cleaning methods of the archaeological samples helped me to understand the real-world impact of my research findings.

I must acknowledge the valuable time and effort, and would like to express my gratefulness to Dr. Rémy Chapoulié, Professor at the University of Bordeaux Montaigne, for helping me to develop the knowledge in the acquisition and analysis of the revealed data from my thesis, and for continuous support with valuable comments throughout my candidature.

I also express my gratefulness to Mr. Evan Maina Maingi, ESR-11 at the ED-ARCHMAT Project, University of Burgos, for his continuous support in order to learn more about archaeology and the perspectives of the archaeological conservations and restorations.

I would also like to mention Ms. Emma Rebecca Lythgoe, Mr. Ruben Gallo Gonzalez, Ms. Helena Espadaneira, Mr. Sergio Gonzalo Peco, Ms. Cristina Sierra Lite, Ms. Lola Márquez Ortiz, Ms. Concepción Marco Pérez, Mr. Ander Guerrero Ruiz, Ms. Macarena Esteban, Ms. Marisol Martín, and all the other

administrative and supportive staff at the INMA, University of Zaragoza, University of Burgos and University of Evora for their kind cooperation and outstanding administrative supports.

I am very thankful to Ms. Ana Cristina Gallego Benedicto, Ms. Gala Simón Ramírez, Ms. M.^a Concepción Sánchez Sierra, Mr. Guillermo Antorrena, and all the other technical staff at the INMA (CSIC: University of Zaragoza) and the University of Evora who helped in the acquisition and analysis of the characterization of different samples and laser cleaning data.

I would like to express my thanks to researchers within the wider ED-ARCHMAT community from whom I received assistance or support throughout my doctoral research.

I am grateful and would like to cordially thank all the professors, group members, colleagues, department staff, friends, well-wishers, and all those who directly or indirectly helped me in this thesis work.

A special thank goes out to my parents (Md. Nurul Islam and Mrs. Anjumara Begum), my family members and friends who have prayed for me and supported me during this stressful PhD candidature time. My wife (Mosa. Asma Akter) has been a constant source of love, care, encouragement, support, and sacrifice throughout my time in the PhD program. The name of Mr. Ahnaf Abdullah Rahman, my son, the precious gift from the Almighty born in the second year of my PhD candidature, deserves worthy mention. His heavenly smile helped me be less stressed psychologically throughout the last years.

At last, I feel pleasure to acknowledge the ED-ARCHMAT project, supported by H2020-MSCA-ITN-EJD/ED-ARCHMAT action funding under the Marie Skłodowska-Curie grant agreement, No 766311. Partial support obtained from Departamento de Ciencia, Universidad y Sociedad del Conocimiento of Gobierno de Aragón (research group T54_20R). The Atapuerca research project is financed by Ministerio de Ciencia, Innovación y Universidades project PGC 2018-093925-B-C33. Fieldwork at the Atapuerca sites is funded by the Junta de Castilla y León and the Fundación Atapuerca. The archaeological materials presented in this work was made available by the Laboratory of Human Evolution of the University of Burgos, in close collaboration with the "Colección Museística de Castilla y León" of the Junta de Castilla y León, and Museo de la Evolución Humana (Burgos); we acknowledge Professor Juan Luis Arsuaga for the permit to analyze the sample. The use of Servicio General de Apoyo a la Investigación and the National Facility ELECMI ICTS, node "Laboratorio de Microscopías Avanzadas" at the University of Zaragoza is acknowledged. This work is part of the ongoing collaboration between INMA (CSIC-University of Zaragoza) and University of Burgos, under the auspices of Unidad Asociada de I+D+I al CSIC "Vidrio y Materiales del Patrimonio Cultural (VIMPAQ)".

The Author
University of Burgos
June 2022

TABLE OF CONTENTS

<i>Table of Contents</i>	<i>i</i>
<i>Abstract</i>	<i>vii</i>
<i>Abstract (in Spanish)</i>	<i>ix</i>
<i>Aims and methodology</i>	<i>xi</i>
<i>Overview of the thesis</i>	<i>xiv</i>

CHAPTER ONE

GENERAL INTRODUCTION

1.1. Motivation behind the research.....	1
1.2. Laser cleaning in conservation.....	5
1.2.1. Laser cleaning fundamentals	7
1.2.2. Laser cleaning parameters	8
1.2.3. How does laser provide value to cleaning?	10
1.3. Conventional cleaning methods in conservation.....	12
1.3.1. Mechanical cleaning in conservation	12
1.3.2. Chemical cleaning in conservation.....	14
1.4. Archeological sites	15
1.4.1. Sierra de Atapuerca	15
1.4.2. Sima de los Huesos.....	18
1.4.3. Fuente Mudarra	19
1.4.4. La Paredaja	20
1.4.5. El Portalón de Cueva Mayor	21

CHAPTER TWO

LASER CLEANING IN CULTURAL HERITAGE

Summary	25
2.1. Introduction.....	25
2.2. Laser systems used in conservation/restoration	28
2.3. Laser based interventions on Archaeological Bones.....	29
2.4. Laser based interventions on Stones	33
2.5. Laser based interventions on archaeological Ceramic Materials	40
2.6. Laser based interventions on archaeological Iron Objects.....	43
2.7. Discussion	48
2.8. Conclusions.....	50

CHAPTER THREE
EXPERIMENTAL TECHNIQUES

Summary	55
3.1. Laser systems and parameters	55
3.1.1. Ultrafast femtosecond (fs) lasers	55
3.1.2. Sub-nanosecond (sub-ns) lasers.....	58
3.2. Laser pulse scanning modes.....	59
3.2.1. Burst pulse mode	59
3.2.2. Continuous beam scanning mode	60
3.3. Irradiation parameters that utilized to define the laser cleaning protocol	62
3.3.1. Irradiance for a single laser pulse	63
3.3.2. Energy distribution of the Gaussian laser beam profile.....	64
3.3.3. Irradiance for burst pulse mode	65
3.3.4. Irradiance for beam scan mode.....	65
3.3.5. Irradiance value as the standard for the calculation.....	69
3.4. Surface characterization techniques	69
3.4.1. Technical Photography	70
3.4.2. Optical Microscopy (OM)	70
3.4.3. Scanning Electron Microscopy with Energy Dispersive X-ray Spectrometry ...	71
3.4.4. X -ray Photoelectron Spectroscopy (XPS)	73
3.4.5. X-ray Diffraction (XRD).....	74
3.4.6. Fourier Transform Infrared Spectroscopy (FTIR).....	75
3.4.7. Infrared (IR) Thermal Camera.....	76

CHAPTER FOUR
SUB-NS-PULSED LASER CLEANING

Summery	81
Abstract.....	82
4.1. Introduction.....	82
4.2. Materials and methods	86
4.2.1. Materials	86
4.2.2. Experimental.....	87
4.2.2.1. Laser irradiation of Pleistocene bone.....	87
4.2.2.2. Characterization	89
4.3. Results and discussion	90
4.4. Conclusions	98

CHAPTER FIVE

IMPACT OF WAVELENGTH & PULSE DURATION

Summary	103
5.1. Background of the study	103
5.1.1. Laser parameters in artifacts cleaning	103
5.1.1.1. Influence of wavelengths	104
5.1.1.2. Influence of pulse durations	105
5.1.1.3. Other parameters	106
5.1.2. Archaeological bone diagenesis	106
5.1.3. Objectives of the chapter	108
5.2. Materials and methods	109
5.2.1. Pleistocene bone	109
5.2.2. Laser cleaning systems and parameters	109
5.3. Results and discussion	111
5.4. Conclusions	125

CHAPTER SIX

FEMTOSECOND UV LASER IN BONE CLEANING

Summary	129
6.1. Introduction	129
6.1.1. Bone diagenesis	129
6.1.2. Laser cleaning potentials	131
6.1.3. Ultrafast fs pulsed laser	131
6.1.4. Objectives of this chapter	132
6.2. Material and method	133
6.2.1. Significant archaeological bone	133
6.2.2. Laser cleaning system and parameters	134
6.3. Results and discussion	134
6.4. Conclusions	146

CHAPTER SEVEN

LASER FOR FLINTS CLEANING

Summary	149
7.1. Flints	150
7.1.1. Flint patination	150

7.1.2. Color of the flint patina	151
7.1.3. Laser intervention of flints	151
7.1.4. Objective of this chapter.....	152
7.2. Materials and methods	153
7.2.1. Neogene and Cretaceous Flints	153
7.2.2. Laser irradiation parameters applied to flint artifacts.....	154
7.3. Results and discussion	154
7.4. Conclusions.....	167

CHAPTER EIGHT

fs LASER INTERVENTION ON CERAMIC ARTIFACTS

Summary	171
8.1. Motivation of the research	171
8.2. Materials and methods	174
8.2.1. Ceramic artifacts.....	174
8.2.2. Laser cleaning systems and parameters.....	176
8.3. Results and discussion	178
8.3.1. FESEM-EDS analysis of the pottery sherd-2 before laser	178
8.3.2. Femtosecond laser cleaning on pottery sherds	182
8.3.2.1. Femtosecond n-IR laser cleaning on pottery sherds	185
8.3.2.2. Femtosecond Green laser cleaning on pottery sherds	187
8.3.2.3 Femtosecond UV laser cleaning on pottery sherds	189
8.3.3. SEM-EDS and XRD analysis of the laser cleaning outcomes.....	190
8.4. Conclusions.....	193

CHAPTER NINE

fs VISIBLE LASER FOR IRON OBJECT CLEANING

Summary	197
9.1. Background of the study	197
9.1.1. Iron objects conservation.....	198
9.1.2. Objective of this study.....	199
9.2. Material and method	200
9.2.1. Iron object.....	200
9.2.2. Laser irradiation parameters applied to iron object	201
9.3. Results and discussion	201

9.3.1. Corrosion crusts characterization by SEM-EDX.....	201
9.3.2. Laser cleaning for iron object.....	203
9.3.2. Laser cleaned surface characterization by SEM-EDX	205
9.4. Conclusions.....	206

CHAPTER TEN

GENERAL CONCLUSIONS

10.1. Conclusions.....	211
10.1.1. Archaeological bones cleaned by laser.....	213
10.1.2. Archaeological stones cleaned by laser	214
10.1.3. Archaeological ceramic materials cleaned by laser.....	215
10.1.4. Archaeological iron object cleaned by laser.....	216
10.2. Recommendations for further work	216
General Conclusions (in Spanish).....	218-224

REFERENCES & APPENDIX

References.....	227-254
Appendix.....	255-258

ABSTRACT

Laser technology has evolved rapidly over the last decades, providing newly developed laser systems which are capable of emitting in a diversity of wavelengths, powers and pulse durations. In addition, modern lasers are becoming compact in size and, in many cases, portable or transportable and without liquid refrigerants, which paves the way for their full exploitation in many applications, including those which affect restoration of Cultural Heritage (CH) and preservation of Archaeological museum artifacts. Even at the time lasers were more intensive, much less compact and with emission characteristics far from what they offer today, many examples appeared in the literature, and in restoration of monuments, demonstrating their potential in the CH field. Although nowadays lasers are the subject of many published works on different archaeological and CH artifacts, their use in these fields still needs more attention and further improvements, particularly in view of their latest technological advances. In essence, the latter advantages may pave the way to safer laser cleaning protocols that may be easy to implement for the effective conservation of fragile and sensitive surfaces. This thesis work reviews a wide range of laser cleaning applications and the accompanying laser-material interaction regimes that may affect the conservation of archaeological bones, stones, ceramics and iron objects, in an attempt to focus on the methodological techniques used to address typical cleaning challenges. Since published findings have been often found to be inconsistent with each other, difficulties were identified in matching the suitability of a laser cleaning procedure with a specific type of artifact, suggesting that laser cleaning outcomes are case-dependent.

Controlled laser irradiation parameters using recently developed femtosecond (fs) and sub-nanosecond pulsed laser technology with an emission wavelength in the near Infrared (1030 nm, 1064 nm), visible (515 nm) and Ultraviolet (343 nm, 355 nm) regimes have been assessed on selected archaeological artifacts unearthed from several archaeological sites of *Sierra de Atapuerca* (Burgos, Spain). The ablation, damage and cleaning threshold values in burst pulse and beam scanning mode have been identified in removing contaminants and degradation products while assessing the underlying substrate surface damage. The impact of wavelength and pulse duration has also been explored to optimize the laser's emission parameters, thus localizing its interaction within the outermost surface of the substrate. Wavelength, irradiance and pulse repetition rate were among the parameters considered to evaluate the potential that these types of lasers offer towards an increased cleaning efficiency.

Optical Microscopy (OM), Infrared (IR) Thermal Cameras, Scanning Electron Microscopy with Energy Dispersive X-ray Spectrometry (SEM-EDS), X-ray Photoelectron Spectroscopy (XPS), Fourier Transform Infrared Spectroscopy (FTIR), and X-ray Diffractometry (XRD) were used to characterize the contaminated artifacts before and after the laser treatment, while evaluating the degree of damage produced to the original artifact's surface.

The study reveals the capability of different lasers in the successful conservation of artifacts, indicating their ability to remove unwanted material with nanoscale precision, while providing control over ablation depth, avoiding heat accumulation, physicochemical transformations, and mechanical damage to the underlayers. The ultrafast femtosecond pulsed laser in different wavelengths, adapted to a variety of contaminant removal problems, appears to offer attractive solutions based on proper selection of laser intensity and its temporal and spatial distribution to manage laser-artifact interactions. In essence, a specific laser cleaning protocol was proposed concerning each laser cleaned artifact surface, owing to the controllability of laser irradiation parameters and the results from physico-chemical and microstructure studies whereby changes upon laser irradiation were properly characterized. The findings from this thesis work highlight the importance of systematically assessing the cleaning outcomes to develop more effective, operative and safer laser cleaning procedures. It is hoped that these will provide conservators/restorers with very useful information on the improved use of lasers for the preservation of historically relevant artifacts. In addition, this work serves as a valuable beginning point for conservation specialists who intend to do more research on the laser cleaning of ancient artifacts. The current thesis finishes with a number of case studies that might be pursued in the near future to achieve improved cleaning for the preservation of archaeological and cultural heritage objects.

ABSTRACT

(IN SPANISH)

La tecnología láser ha evolucionado rápidamente en las últimas décadas, proporcionando sistemas láser recientemente desarrollados, que son capaces de emitir en una diversidad de longitudes de onda, potencias y duraciones de pulso. Además, los láseres modernos se están volviendo compactos en tamaño y, en muchos casos, portátiles o transportables y si refrigerante líquidos, lo que allana el camino para su pleno aprovechamiento en muchas aplicaciones, incluidas las que afectan a la restauración del Patrimonio cultural (PC) y la conservación de piezas de museos arqueológicos. Incluso hace tiempo los láseres eran más intensivos, muchos menos compactos y con unas características de emisión alejadas de las que ofrecen hoy en día; aparecieron muchos ejemplos en la historiografía y en la restauración de monumentos, demostrando su potencial en el campo del PC. Aunque hoy en día los láseres son objeto de muchos trabajos publicados sobre diferentes piezas arqueológicas y del PC, su uso en estos campos aún necesita más atención y mejoras, particularmente en vista de sus últimos avances tecnológicos. En esencia, las últimas ventajas pueden allanar el camino hacia protocolos de limpieza con láser más seguros que pueden ser fáciles de implementar para la conservación efectiva de superficies frágiles y sensibles. Este trabajo de tesis revisa una amplia gama de aplicaciones de limpieza láser y los regímenes de interacción láser-material que las acompañan y que pueden afectar la conservación de huesos, piedras, cerámicas y objetos de hierro arqueológicos, en un intento de centrarse en las técnicas metodológicas utilizadas para abordar los desafíos típicos de la limpieza. Dado que a menudo se ha encontrado que los hallazgos publicados son inconsistentes entre sí, se han identificado dificultades para hacer coincidir la idoneidad de un procedimiento de limpieza con láser, con un tipo específico de pieza, lo que sugiere que los resultados de la limpieza con láser dependen del caso.

Los parámetros de irradiación láser controlados que utilizan tecnología láser pulsada de femtosegundos (fs) y subnanosegundos desarrollada recientemente con una longitud de onda de emisión en los regímenes infrarrojo cercano (1030 nm, 1064 nm), visible (515 nm) y ultravioleta (343 nm, 355 nm) han sido evaluados en piezas arqueológicas desenterradas en varios yacimientos arqueológicos de la Sierra de Arapuerca (Burgos, España). Los valores de umbral de ablación, daño y limpieza en modo de pulso de ráfaga y escaneo de haz se han identificado en la eliminación de contaminantes y productos de degradación mientras se evalúa el daño de la superficie del sustrato subyacente. También se ha explorado el impacto de la longitud de onda y la duración del pulso para optimizar los parámetros de emisión del láser, localizando así su interacción dentro de la superficie más externa del sustrato. La longitud de

onda (no se ha estudiado este tipo de fenómenos, solo se ha observado el efecto de diferentes longitudes de onda), la irradiancia y la tasa de repetición de pulsos fueron algunos de los parámetros considerados para evaluar el potencial que ofrecen estos tipos de láser para una mayor eficiencia de limpieza.

La microscopía óptica (OM), las cámaras térmicas infrarrojas (IR), la microscopía electrónica de barrido con espectrometría de rayos X de dispersión de energía (SEM-EDS), la espectroscopía de fotoelectrones de rayos X (XPS), la espectroscopía infrarroja transformada de Fourier (FTIR) y la difracción de rayos X (XRD) se han utilizado para caracterizar las piezas contaminadas antes y después del tratamiento con láser, mientras se evaluaba el grado de daño producido en la superficie de la pieza original.

El estudio revela la capacidad de diferentes láseres en la conservación con éxito de las piezas, lo que indica su capacidad para eliminar material no deseado con precisión a nanoescala, al mismo tiempo que proporciona un control sobre la profundidad de la ablación, evitando la acumulación de calor, las transformaciones físico-químicas y el daño mecánico a las capas subyacentes. El láser pulso ultrarrápido de femtosegundos en diferentes longitudes de onda, adaptado a una variedad de problemas de eliminación de contaminantes, parece ofrecer soluciones atractivas basadas en la selección adecuada de la intensidad del láser y su distribución temporal y espacial para gestionar las interacciones láser-pieza. En esencia, se ha propuesto un protocolo de limpieza láser específico para cada tipo de superficie de pieza limpiada con láser, debido a la capacidad de control de los parámetros de irradiación láser y los resultados de los estudios físico-químicos y de microestructura mediante los cuales se caracterizaron adecuadamente los cambios en la irradiación láser. Los descubrimientos de este trabajo de tesis resaltan la importancia de evaluar sistemáticamente los resultados de limpieza para desarrollar procedimientos de limpieza láser más efectivos, operativos y seguros. Se espera que estos brinden a los conservadores/restauradores información muy útil sobre el uso mejorado de los láseres para la preservación de piezas históricamente relevantes. Además, este trabajo sirve como un valioso punto de partida para los especialistas en conservación que tienen la intención de investigar más sobre la limpieza de piezas históricas con láser. La presente tesis finaliza con una serie de casos de estudio que podrían desarrollarse en un futuro próximo para lograr una limpieza mejorada para la conservación de piezas arqueológicas y del patrimonio cultural.

AIMS AND METHODOLOGY

The focal aim of the research is “Laser based intervention in Archaeological Materials and Museum Artifacts”.

Hereafter, the core objective of this research work is to open a leading edge approach in the realm of laser cleaning in the field of conservation, as well as to assess promising cleaning solutions to safeguard archaeological materials and museum stored artifacts by developing scalable, state-of-the-art laser cleaning methodologies.

This study focuses on the following specific goals:

- i. Definition and comparison of the state-of-the-art conservation methods and their influence on selected archaeological materials and museum stored artifacts, particularly in the field of Archaeology and Paleontology, specifically on bones, flints, ceramics and iron objects.
- ii. Evaluation of laser sample interaction taking into account laser emission parameters and the material physicochemical properties.
- iii. Establishment of laser tool selection criteria for decontamination/conservation of museum artifacts.
- iv. Development of a dynamic, automated, or semi-automated laser conservation method; hence, advancing the understanding of laser-sample interactions with archaeological objects of value.
- v. Comparison of laser cleaning-based methods vs. alternative tools (mechanical and chemical cleaning).
- vi. Analyze the possibilities that the new ultra-short pulse lasers open in CH materials conservation, thereby developing laser processing protocols to apply short pulse lasers in actual samples.
- vii. Select problems associated with archaeological artifacts and CH material of historical value (origin and use).
- viii. Develop skills necessary to select, operate safely and apply lasers in CH and Archaeology.

In order to achieve successful laser cleaning, the proposed methodology has been accomplished mainly in three significant steps:

- i) physicochemical characterization of the artifacts before laser intervention to improve our understanding of their condition,

-
- ii) laser interventions on the artifacts considering a diversity of treatments to determine the ablation, cleaning and damage threshold values, and
 - iii) physicochemical characterization after laser intervention for advancing the knowledge of laser interactions with archaeological artifacts; hence develop practical criteria and protocols to apply lasers to valuable museum artifact conservation.

For developing this improved laser cleaning methodology, the following steps were planned:

1. Utilize different physicochemical characterization techniques for every single artifact irrespective of type ‘before and after laser cleaning’ to compare the mineralogical, elemental and compositional information as a single specific area-by-area of objects;
2. Choose different laser cleaning technologies and possibilities from literature reviews that apparently lead to the most efficient and outstanding cleaning solution;
3. Select and apply the best cleaning parameters following the laser performance on avoiding the subsurface damage when cleaning;
4. Return to using the physicochemical characterization techniques in order to confirm reliably that laser cleaning didn’t produce any alteration or damage to the substrate surface of the artifact;
5. Develop the data set for threshold cleaning and damage values for different specific artifacts, and examine extensively for similar samples with the same cleaning problem several times;
6. Analyzing the performance, problems, difficulty, and feasibility of the laser techniques for large scale applications;
7. Develop the protocols and find substitutes to increase the cleaning performance and further application to different types of artifacts;
8. Conclude and reveal other interesting observations on the laser cleaning process, etc.

The flow chart for the laser cleaning experiments approach has been utilized throughout this thesis work presented in the Fig. I. In order to fulfil the thesis project aims, numerous distinct objective-oriented methodology has been experimented on diverse sort of artifacts with varied cleaning issues, till revealing the final outcomes of different laser cleaning applications.

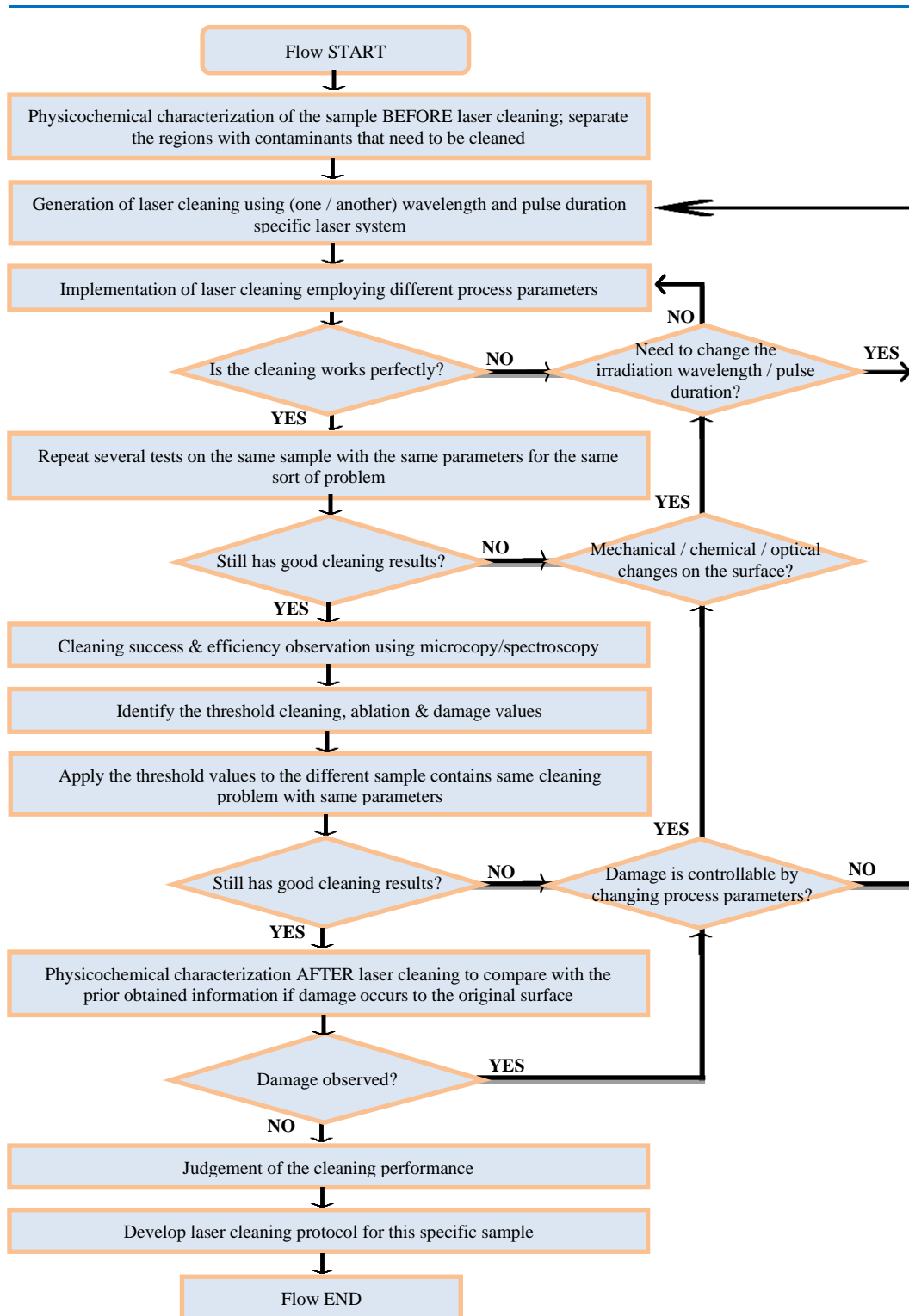


Fig. I: Flow chart of the laser cleaning methodology applied in this research work.

OVERVIEW OF THE THESIS

This thesis contains ten main chapters and two appendices. These chapters introduce the thesis structure and provide some background information to show the technological aspects of this research. They follow the same order as the developed works with the following content:

Chapter 1 discusses the motivation behind this thesis work and the general introduction of laser cleaning techniques in the conservation of cultural heritage materials. An introduction to the conventional cleaning conservation methods and the primary information regarding all the archaeological sites from where the artifacts were excavated and used in this research work is presented.

Chapter 2 reviews state-of-the-art laser cleaning and the associated laser-material interaction regimes, emphasizing the methodological strategies employed to handle typical cleaning problems, specifically for the conservation of four distinct archaeological materials. The findings highlight the significance of carefully examining cleaning outcomes to design more effective, operational, and safer laser cleaning profiles and instruct conservators about whether laser cleaning is an option for preserving such artifacts in their care.

Chapter 3 summarizes the experimental data of all five laser techniques used in this thesis investigation. The irradiation parameters used to establish the laser cleaning technique have also been presented, as have the burst pulse and laser beam scan modes. Additionally, a summary of the various techniques used in this thesis to characterize the materials is provided.

Chapter 4 presents the effects of controlled sub-nanosecond (sub-ns) pulsed laser irradiation on a Pleistocene bone at emission in the near-Infrared (n-IR) range. As a result, identifying the most efficient burst-mode laser cleaning settings revealed a better understanding of the laser interaction with contaminants and degradation products in the outermost bone layers, while minimizing any damage to the underlying original bone surface. Laser cleaning of bone archaeological artifacts may now be done more safely and effectively, as threshold cleaning and substrate damage values have been established using this laser technology. In addition, the cleaning conservation was consistent with the fact that Manganese (Mn) mineralization in bone may develop as a result of a longer burial period.

Chapter 5 discusses the effect of wavelength and pulse duration on removing a hard blackish contaminants crust on Pleistocene bone via laser ablation. Cleaning was performed using a sub-ns pulsed laser emitting at 355 and 1064 nm, and a femtosecond (fs) pulsed laser emitting at 343 nm. The cleaning effectiveness of the contaminated bone surface was determined using the laser beam scanning mode, where wavelength-dependent absorption, pulse repetition rate, and material thermal characteristics were all evaluated. This chapter aims to identify realistic cleaning parameters and improve laser procedures for cleaning archaeological bone from a conservation and restoration standpoint.

Chapter 6 addresses the fs ultrafast pulsed laser technology, which has recently emerged as a viable alternative for cleaning CH artifacts, because of its ability to manage ablation depth while avoiding undesirable photothermal and photochemical damage. A significant Pleistocene bone was cleaned of surface contaminants, degradation products, and cemented soil crusts using a fs laser with an emission wavelength in the Ultraviolet (UV) regime. Ablation and damage threshold values were determined in laser beam scanning mode, along with the most efficient cleaning parameters. This study demonstrates the capabilities of this newly developed fs UV laser for effective archaeological bone conservation.

Chapter 7 provides a comparative investigation of the removal of dark, compact, yellowish and reddish-colored encrustation on Neogene and Cretaceous flints using n-IR and UV sub-ns, and UV fs laser pulses respectively with different pulse durations. Laser techniques were used to irradiate optically absorbent colored encrustation, which was then subjected to ablation, optical characteristics, and photomechanical effects. Apart from describing in detail the technical conservation and physical issues related to stone cleaning, considerable effort was made to investigate the application potential for the discoloration effect associated with different pulse regimes and wavelengths.

Chapter 8 discusses how laser technology can be used to clean ceramic artifacts, which the restoration community hasn't given much attention till today. This study explores laser application to remove concretions or hardened solid crusts while minimizing mechanical and chemical interruption of historic surfaces. Three different wavelength-based ultrafast fs lasers have been investigated in order to overcome the drawback of longer pulse duration, which permits heat and shock waves to penetrate the substrate and potentially cause damage to historic surfaces. It has been explored how fs pulses efficiently ablate very thin surface layers in nanometer ranges that are too short to enable heat or shock waves to penetrate deeply into the substrate.

Chapter 9 explores the possibilities of employing laser cleaning to remove a range of surface corrosion from a single iron object using ultrafast UV fs laser. Multiple analytical analyses were performed on the irradiated surfaces of the sample to define the difference of original surface and corroded surface, and to identify any laser-induced changes taking into account the darkening phenomena of the iron surface. The assessment of the laser cleaning procedure highlighted how important it is to optimize the laser's characteristics, particularly the pulse duration and wavelength.

Chapter 10 provides the reader with more elaborate conclusions of laser for *in situ* cleaning of materials with archaeological interest, and reveals the outcomes of aims and objectives of this research work. The outcomes from this study are presented, evaluated and compared within the laser techniques employed to this thesis, and comments on the laser cleaning methodologies and protocols are made. Finally, this chapter delivers the recommendations for future work.

The references section provides references to the objectives of the thesis. The Appendix-A section provides the acronyms and abbreviations has been used throughout this thesis, and finally the different units used in this thesis investigation is listed in Appendix-B.

CHAPTER: 1

GENERAL INTRODUCTION

CHAPTER ONE

GENERAL INTRODUCTION

1.1.Motivation behind the research

Cultural Heritage (CH) conservation is predominantly an ethical responsibility of our civilization towards the forthcoming generations, but it is also a big challenge for multi-disciplinary scientific advancement and modern technology. More and more sophisticated scientific instrumentation is increasingly needed to fully understand and solve many conservation problems involving archaeological materials and museum-stored artifacts as well as monuments and historical sites. The role of heritage conservators and restorers community must also be significantly improved [1][2]. Every sector working on the study of cultural heritage, techniques and applications are counted as vital for the research and analysis of artifacts conservation. Although traditional artwork conservation techniques, specifically chemical and mechanical cleaning have been in use for a much longer period of time, the laser cleaning technique represents one of the most significant contributions of physics to artwork conservation in the last five decades. It has been a fascinating field of research, but has received little attention from the heritage conservation and restoration community [3][4].

The word “LASER” stands for ‘Light Amplification by Stimulated Emission of Radiation’. As one of the most significant technological discoveries of the 20th century, the laser is widely regarded as one of the most important advancements in modern technology. In 1917, Einstein discovered a quantum mechanism known as stimulated emission, which led to the development of this technology. Stimulated emission generates light rays that are particularly single color (monochromatic), coherent (light waves are in phase), travel in a single direction, and travel with the highest intensity. Although it seems like a very recent invention, it has actually been with us for over half a century; the theory was first figured out in 1957 [5], and the first functional laser was built in 1960 [6]. Notably, lasers produce just one wavelength of light; this wavelength is defined by the difference in energy between the electron’s excited and fundamental (or lower excited) states, when such transition is radiative. In addition, a main property of laser light is that it is collimated, can be sharply focused and can travel great distances, even to the moon and back!

The fundamental characteristics of a laser beam, such as monochromaticity, coherence, collimation, and low divergence, as well as the characteristics of the sample-material interaction, have guided the development of a wide range of laser applications in a number of sectors. Nowadays, it is even hard to find a domain of human activity without the use of lasers. Application fields including industry [7][8][9], metrology [10][11], telecommunication [12][13], data transmission [12][14][15], medical [16][17], cultural heritage [1][4][18][19] etc., are well-known. Laser ablation is one of the most imperative irreversible irradiation effects, which can be driven on optically absorbing materials or in their close proximity [20]. As a matter of fact, a certain material sample's original layer or substrate can be uncovered and exposed by the elimination of undesirable layers or incoherent particle distributions in the case of laser cleaning of cultural heritage [21][22]. Fields of laser cleaning application are even wider; it is being used in many industrial needs: sub-micron particles cleaning in microelectronics [17][23], mold cleaning in steel [24], die cleaning in plastic pressure casting [25], paint doffing in the aircraft maintenance [26] and so on. A wide range of difficulties in art conservation have been solved using cutting-edge laser equipment combined with the most advanced scientific approaches and large-scale infrastructure. The recent application fields of lasers in the restoration of artwork objects with artistic and archeological interest are [27][28]:

- a. undesired surface cleaning of artworks, monuments, statues, and artistic cultural heritage,
- b. study of pigment composition and original elements,
- c. elimination of the over paintings and deteriorated varnish layers,
- d. on-site analysis of composition and 3D documentation,
- e. study of the chemical and elemental composition of the material's surface and the layers underneath it,
- f. non-destructive and holographic micro-catching labeling of the artworks, etc.
- g. adaptation of the use of the laser to the cleaning of different types of degrading pathologies (adhered dirt, scabs, craters, fissures/fractures, etc.).
- h. create action protocols for each pathology and each material.

However, laser cleaning in the conservation of artworks was introduced in the early 70s [29][30]; it took many years for this cutting-edge method to impress researchers and experimenters primarily due to the technical limitations of the laser sources, which were readily available at that time. It took a long time for the first laser researchers to achieve success since they had to deal with Ruby and Nd:YAG lasers that had a low pulse repetition

rate, lacked adaptable beam delivery methods, had poor consistency over extended periods of time, and implied expensive experiments [31][32]. Laser technology was limited to laboratory application for more than a decade only due to the conservation and restoration community's apparently adopting a too cautious and careful attitude. Later in the decade of the 1980s, technological improvement in the field of laser cleaning developed dramatically, despite the fact that the costs of experiments were still too expensive for the specific sector of artwork application. It was a critical phase in the survival of the unique approach of laser conservation, which had relatively low productivity in comparison to established chemical and mechanical cleaning processes at the time [33]. In essence, this ground-breaking laser cleaning process enabled systematic investigations to be carried out since the 1990s and refined over time [4][34], contributing to the dissemination of the laser application in archaeological and cultural heritage conservation practice [35][34].

Mechanical or chemical techniques have traditionally accomplished the cleaning of archaeological materials and museum artifacts. Mechanical practices typically introduce an abrasive compound or high-pitched tool to detach undesired layers from the underlying materials by using physical forces. Chemical methods often utilize pH, plummeting oxidizing agents, and electrical charge to solubilize or convert unwanted products on the material surface[36][37][38][39]; thus, any intrusive collection of extraneous material might have a very unfavorable influence occurring and often time-dependent adverse effects [40][41]. Therefore, several heritage conservation investigations revealed that mechanical and chemical cleaning methods may lack adequate precision or control, may even expose the adjacent compounds of the materials, might produce an undesired surface appearance, or could be time-consuming for effective treatments. The use of laser beams for the deteriorated and undesired surface cleaning and safeguarding artworks represents a technological approach complementary to these functional traditional cleaning techniques. The competencies were studied extensively during the last three decades, when lasers became the consistent radiation sources in laboratories.

Nowadays, laser cleaning is a good candidate and has become increasingly popular as a conservation tool for the intervention of archaeological materials (AM) and CH artifacts. In terms of non-invasiveness, gradualness, efficacy, selectivity, self-termination, repeatability, flexibility, and environmental impact, laser cleaning outperforms mechanical and chemical cleaning. It can be applied *in situ* or remotely as a cleaning technique to remove unwanted contaminants from the AM and museum stored artifacts [19][42]. The most imperative characteristics of laser cleaning over the traditional methodologies are [34][43][44]:

- a. laser cleaning is fundamentally a surface treatment that can be tailored for only a thin layer within a few micrometers or less, is directly exploited by absorption of light without damaging the underlying surface, whereas chemical cleaning generally accumulates solvents to inner layers without control,
- b. laser cleaning is more time-efficient in reducing deteriorated layers, more precise & controllable in safeguarding the original appearance and aesthetic value of the materials than traditional cleaning methods, thus enhancing the efficiency of treatment and aiding the overall conservation of the artifact,
- c. selective removal is feasible for high absorption materials (for example, black encrustation) since their ablation threshold is lower than that of low absorption materials (such as light-colored stone) without any problems to preserve historical surface, and
- d. precise control of the treated area and volume due to the limited penetration action of the laser, can be used to remove encrustations with repetitive pulse sequences [45].

Laser cleaning techniques have been the subject of scientific analysis and research interest in artwork conservation. Over the last three decades, quite a number of scientific investigation and research works have been carried out and published in different international journal publications, conference proceedings, and books, concentrating on the effectiveness, selectivity, and success of the laser conservation techniques. Laser cleaning has the potential to revolutionize conservation practice because of its promised benefits over traditional cleaning methods.

The multi-disciplinary and inter-disciplinary research background works for the laser conservation of artworks is to correctly approach the various types of exposed multifaceted problems, which are met on various deteriorated museum stored archaeological materials. The fundamental features of the laser beam are aimed toward investigative applications to scrutinize the archaeological materials, while non-invasive low power beams deliver immediate feedback. Subsequently, the possibility of increasing the laser power and governing selective and controlled ablative properties is the research topic performing the extremely debated application in the most delicate cleaning phase. Appropriate setting of the laser parameters selection could avoid or significantly reduce the side effects that hamper the use of lasers in conservation practice. Recent advances suggest that laser technologies are becoming ever more integrated with traditional cleaning techniques and will likely gain a privileged position within the immediate future.

This doctoral thesis will introduce an advanced laser tool selection methodology for cleaning conservation of archaeological artifacts, hence analyzing the possibilities that the new ultra-short pulse type lasers open in heritage conservation [46]. It also attempts to set the basis for the development of a dynamic, automated or semi-automated laser conservation method for archaeological artifacts. It thus includes some characterization methods for evaluating the quality of the treatment and reducing the risks associated with laser radiation, in order to meet the demanding cleaning challenges in CH. The innovative methodology lies in the evaluation of laser sample interaction following the laser emission parameters and the physicochemical properties of the material, allowing the control of the laser cleaning effective regimes towards an effective and safe cleaning outcomes accordingly.

Laser-assisted cleaning of contaminants, environmental pollutants and deterioration accumulations from the archaeological bones, flints, ceramics, and iron objects are a remarkable success and may highlight the use of this methodology in actual work practice. Several real bone samples, flints, ceramics and iron objects excavated from *Sima de los Huesos*, *Fuente Mudarra La Paredeja*, and *El Portalón de Cueva Mayor* archaeological sites of *Sierra de Atapuerca* -in Burgos (Spain), from prehistoric times- were used in a series of studies to define and refine this laser tool selection methodology, with the goal of ensuring that the original surface, including archaeological details and historic touches, will be preserved. The prospective research and application to enlighten the laser-based intervention have been revealed in this research work. According to their origin and use, the potential of laser cleaning applications in museum stored artifacts and CH material of historical value has also been justified.

The final motivation behind this research is to develop an innovative laser cleaning methodology and a protocol-based laser conservation system, which will successfully be accomplished, and thereafter will be introduced to the everyday conservation practice and presented in this thesis. Finally, a state-of-the-art laser cleaning on the above-mentioned archaeological artifacts, an extensive study on different applicable laser cleaning techniques on all artifacts, and a comparison between the different laser cleaning methodologies and tools will be presented.

1.2 Laser cleaning in conservation

The use of lasers in conservation, has increasingly become a valuable cleaning technique for many conservation professionals across the world, alongside mechanical and chemical

cleaning methods. There is still a growing interest in using lasers to clean archaeological and CH artifacts, even if they have not been widely used yet. The good news is that conservators are starting to adopt laser-based interventions in a substantial quantity. Nonetheless, laser cleaning was brought to the area of art conservation in order to overcome some of the critical issues that these other conventional cleaning methods posed and couldn't fix on their own. Moreover, most other cleaning techniques rely on contact processes, thus becoming abrasive and damaging to the materials they are applied to; laser-based cleaning, on the other hand, is entirely non-contact and non-abrasive, thereby it will only irradiate the material surface layer that the conservator wants to get removed. Surfaces that are rough or have significant ornamental features can benefit considerably from this method.

Laser cleaning works by using a laser beam to irradiate a surface layer, therefore ablating and vaporizing that layer until the necessary depth of ablation has been attained, resulting in a clean surface underneath. The primary goal of laser cleaning in the field of art conservation is to remove an undesired layer without affecting the original surface of the object being cleaned. Obvious advantages of using a laser as a cleaning tool include:

- a.** entirely non-contact and non-abrasive process
- b.** controllable cleaning process with a high degree of accuracy
- c.** noiseless, easy to use, easy to automate, dry and clean
- d.** no waste material is leftover (mostly dust) and no other residue than the ablated material
- e.** more efficient and much safer process
- f.** safe for any type of substrate, even very delicate and subtle surfaces
- g.** potential for hard-to-reach surfaces, no undesirable side effects
- h.** direct response process, the output is immediately visible after the laser treatment
- i.** selective process, a greater focus on a higher quality result
- j.** environmentally friendly process and safe technique to operate (as laser cleaning does not use any chemical solvents or other kinds of consumables)
- k.** comparatively lower operational costs than most other artwork cleaning tools etc.

1.2.1 Laser cleaning fundamentals

A crucial aspect of the conservation process is cleaning. It not only increases the visual value of an artwork or object, but also reveals its true condition to take necessary steps to ensure that it survives to be appreciated by many future generations [47]. Understanding the laser-material interaction is essential for understanding the principles of laser cleaning in conservation and determining the most appropriate laser settings for cleaning a particular CH material.

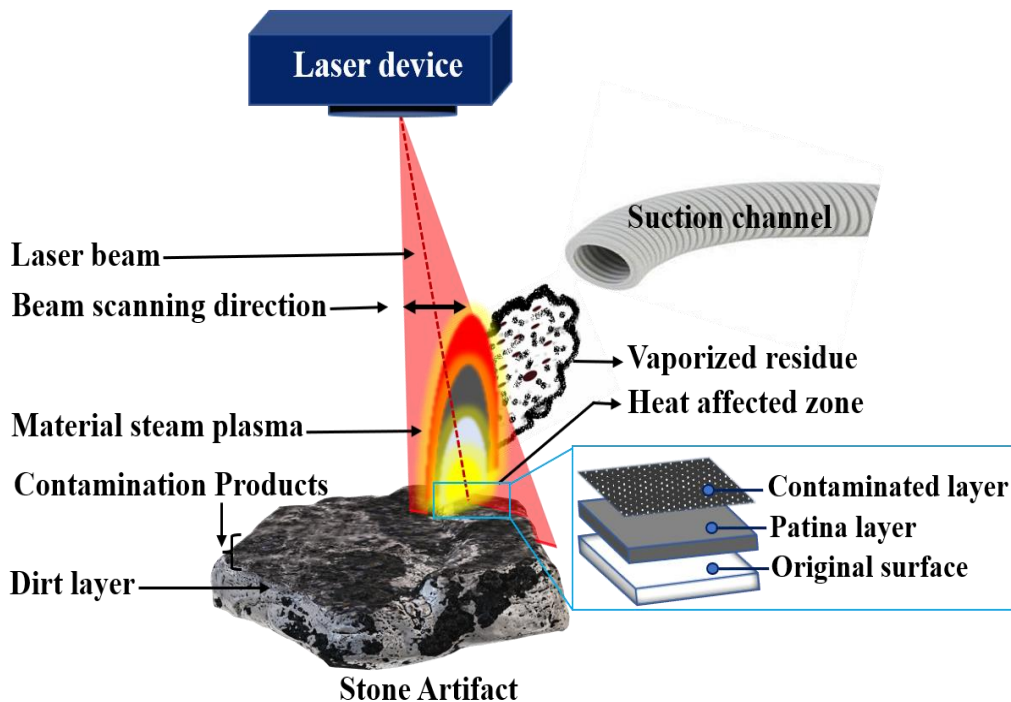


Fig. 1.1: A schematic representation of a typical cleaning process based on laser induced surface desorption, where laser beam scanning is used to selectively remove contaminants. It demonstrates the ideal physical phenomena induced when a laser beam is focused onto a contaminated surface of an archaeological artifact. The resulting effects are associated to the complex processes described for laser ablation[48], which include plasma formation and consequent shockwaves which help remove the contamination layer away.

Laser cleaning is a one of the case of laser ablation [48], in which the desired substrate layer is uncovered by removing superfluous layers of contaminants, encrustations, exposed deteriorations, pollutants, coatings, debris (such as dust, rust, paint, graffiti, oxide staining, etc.), or incoherent particle distributions from the material surface [49]. When focusing on

the material surface using a laser beam, some of its energy is reflected, and the material itself absorbs others. The surface substrate will undergo sublimation or vaporization if the emitted beam energy is higher than the threshold ablation values of the material. Figure 1.1 illustrates the laser cleaning phenomenon induced by a laser beam that focuses on a polluted stone surface while depicting the ideal physical phenomena. Plasma production and subsequent shockwaves [50], which assist removal of contaminants, are associated with complex desorption mechanisms. Ablation happens when the laser Irradiance (usually expressed in W/cm^2) level exceeds a critical threshold determined by the material surface exposed to the laser. Most of the literature uses fluence (emitted energy of a given pulse per unit area of spot size) instead of irradiance. For a fixed pulse duration value, fluence and irradiance are proportional.

1.2.2 Laser cleaning parameters

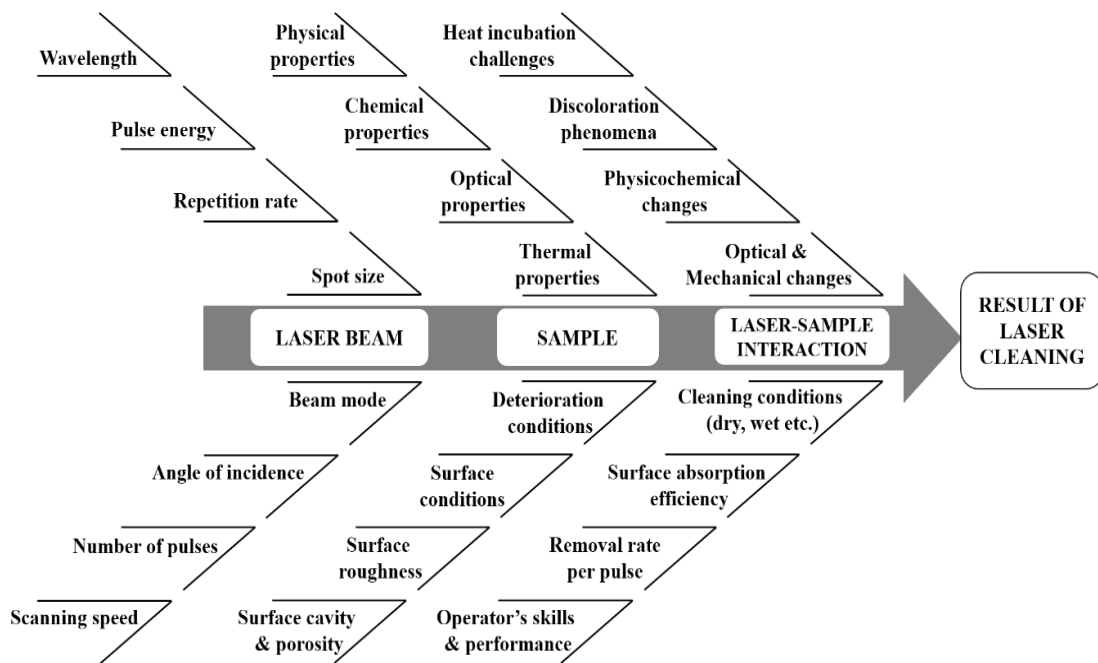


Fig. 1.2: Ishikawa methodology infographic with the main factors affecting the fundamental laser cleaning process. Line scheme of cause and effect result of laser cleaning. (Adapted from [51][52])

A critical step in the cleaning process is identifying the laser irradiation threshold fluences that cause ablation (known as ablation threshold), best cleaning (threshold cleaning), and damage (threshold damage). The ablation threshold is the minimal energy density needed

to accomplish ablation. In contrast, threshold cleaning and threshold damage are terms used to describe the energy density at which the best cleaning is achieved, and damage is visible, respectively. The effects of laser radiation are primarily dependent on the material characteristics, the laser beam parameters and their applying mechanisms, and the interaction between the laser and the material (Fig. 1.2).

Understanding and considering all practical challenges faced during a laser cleaning intervention is important to selecting laser system settings. In actual fact, the desired level of cleaning is achieved by the repeated action of incident laser pulses on a particular material surface, during a period of time chosen by the conservator's observations. Several factors influence whether a suitable outcome is obtained or whether the substrate is damaged during the cleaning procedure (Fig. 1.2). These are intimately related to the irradiance level employed (correlated with the Energy per pulse) and heat accumulation via pulse-to-pulse overlap. The latter may be compensated to some extent by the thermal properties (thermal conduction and diffusivity) of the substrate irradiated.

Proper selection of process parameters is thus essential to achieve satisfactory cleaning results in conservation. Scientific publications suggest that the main parameters that control laser cleaning processes include, on the one hand: i) wavelength [53] and pulse duration [31] (which are characteristics of the equipment that the conservator can't change, generally fixed for any given laser system), and on the other: ii) fluence/irradiance, and repetition rate (the conservator can adjust parameters). The laser irradiance is defined as the laser fluence divided by the pulse duration, where the pulse duration is the total time when one pulse is emitted, and the number of pulses per second is referred to as the pulse repetition rate. Pulse duration ranging from nanoseconds (ns) to picoseconds (ps) have been most commonly used in laser cleaning conservation; practical femtosecond (fs) lasers have been well developed during recent years and are finding increasing applications for cleaning of many types of artifacts, particularly those that appear to be most sensitive to thermal damage.

An incident laser beam has some of its energy absorbed by the surface and transformed to thermal or chemical energy based on its absorptivity at a specific wavelength. The amount of energy absorbed depends mainly on the laser emission wavelength and the characteristics of the material being irradiated. The optimal case is to use a wavelength that is absorbed mainly by the contaminants, but is highly reflected by the substrate. The laser cleaning mechanism is strongly influenced by the laser pulse duration and different beam

emission parameters; those must be appropriately selected to remove contaminants while minimizing damage to the patina layer and substrate underneath [34]. The laser cleaning process can be either a photothermal, photophysical, or a photochemical process, or both [54]. A primary principle of the photothermal approach is that the material is partially ejected or evaporated based on the contrast between dark and light-colored surfaces. It typically happens in the spectrum of visible and infrared laser wavelengths. In the case of the photochemical process, it breaks chemical bonds in the surface material directly might or not generating heat following the pulse duration regimes and the wavelength, which is absorbed nearly equally by dark and light-colored surfaces. It happens while the cleaning is performed in the ultraviolet wavelength range. If both thermal and nonthermal mechanisms are significant in the laser cleaning process, the process referred to as photophysical [54].

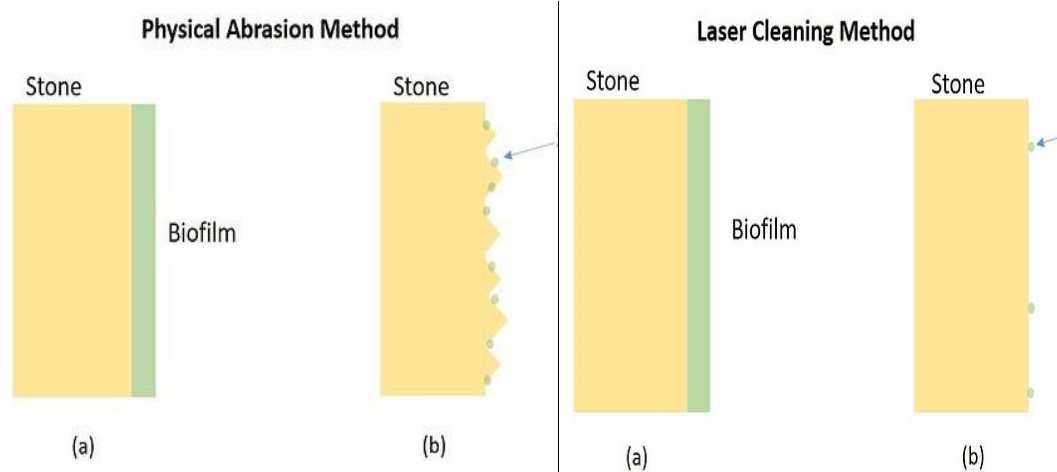
For effective laser cleaning in conservation, ‘self-limiting’ conditions must apply, and specifically the unwanted foreign materials must highly absorb the incident radiation. In an ideal condition, the self-limiting behavior means that the cleaning action automatically stops once the contaminated layer has been removed & the substrate revealed; the exposed substrate will not be damaged by more radiation exposure afterward. However, this is only conceivable in principle when the contaminated layer is thoroughly absorbing and the substrate simultaneously exhibits high reflection [55][56].

1.2.3 How does laser provide value to cleaning?

There have been problems with standard abrasive chemical cleaning procedures and mechanical cleaning for removing varying degrees of degradation brought on by the presence of environmental pollutants [57]. When cleaning with abrasives like bristle brushes or pressurized water, the surface and the open pores of parent materials can be severely damaged [58]. This usually results in accelerated deterioration via corrosion, crystallization and growth of biological organisms after cleaning, which reduces the cleaning process's effectiveness and may question investments in conservation budgets towards surface cleaning of monuments.

Advances achieved in laser technology during the last decade, particularly related to the development of compact, ultrashort pulsed lasers[59], have opened the possibility to undertake some of the most difficult challenges encountered in Cultural Heritage conservation [Refs]. These new lasers can remove most types of surface contaminants even those of biological origin, while providing high pulse repetition rates, which translate into

increased processing speeds. In addition, advancements on laser integration with optomechanical subsystems and user-friendly software control, have significantly simplified their use and may now provide attractive laser cleaning solutions for respectful, efficient conservation of valuable artifacts and parament (Fig 1.3). The growing need for preserving cultural heritage is triggering a rise in the demand for progressively precise cleaning techniques, which feature high contaminant removal selectivity and low environmental impact, as opposed to most commonly used conventional cleaning techniques [60].



Stone with biofilm coating a) before abrasive cleaning and b) after the abrasive cleaning with bristle brushes or pressurized water; illustrates that stone surface becomes rough due to the application of the abrasive method, hence removing material unevenly, aggregate the surface area, thereby sites for biological spores deposit on the stone wall, subsequently boosting their regrowth.

a) Biofilm coated Stone (b) after the laser removal, a moderate and effective removal technique that creates a uniform stone surface, hence reveals a more excellent resistance to biological spore deposit to the surface following cleaning.

Fig. 1.3: Illustration of basic concepts and comparison between physical abrasion method and laser cleaning method, according to ref. [61].

The laser's ability to remove pollutants and deteriorates from material substrates without contact and avoiding damage to patina and substrate layers makes it an ideal alternative tool for many cultural heritage conservation initiatives. Since its first usage in cultural

heritage in the early 1970s, laser cleaning has been successfully used in a wide range of art materials, allowing for a gradual cleaning process that efficiently separates the original surface layers of the material from the degraded ones. With excellent control, selectivity, high accuracy, and other advantages, laser technology may be used to produce value in cleaning historical artifacts with zero or minimal damage. Lasers with pulses as short as femtoseconds are thus presently being developed and tested for cultural heritage cleaning applications, and they are already showing promise in cleaning conservation [62][63].

1.3 Conventional cleaning methods in conservation

Cleaning conservation methods can be considered for both maintenance and active conservation of artifacts. The first step is to decide what should be removed and whether it is essential to remove it; knowing what is involved might assist in making a straightforward choice. Cleaning methods for conservation naturally vary depending on the artifact being cleaned; nevertheless, the unifying factor is that the process should be as non-invasive in nature as possible. Artifact surface cleaning, while beneficial to its appearance, isn't always required or desirable; instead, it's done to protect the artifact's historical and physicochemical integrity. Hence, the conservation community always try to avoid using harsh cleaning processes in favor of museum-approved approaches for carefully removing undesired materials from the artifact's surface.

Archaeological museum stored artifacts present the only information we have about prehistory! As this information necessitates cultural values, artifacts must be conserved for future generations via appropriate conservation and storage, and they can be developed and improved by proper cleaning methods. When it comes to cleaning the surface of an artifact, there are two common traditional approaches used. They're a group of- (i) mechanical cleaning and (ii) chemical cleaning approaches.

1.3.1 Mechanical cleaning in conservation

Hand preparation instruments, such as dental picks, brushes, spatulas, pin vises, and even hammers and chisels, can be used mechanically to prepare archaeological and paleontological specimens for museum storage. Some of these mechanical cleaning instruments are powered by electricity, while others are pneumatically operated by compressed air. Mechanical cleaning equipment falls into a wide variety of classes, each with its own set of benefits and applications [64][65]. Some of them are given as follows:

i. Air abrasive devices

Inflatable pressure propels a spray of grit-like tiny particles out of air abrasive devices that are topped down with sandblasters. Microfossil preparation can benefit from the precision of these tools. Fossil bones and ivory have been cleaned using air abrasion with great effectiveness [66]. Invertebrate fossils discovered in limestone and other hard matrices may also be cleaned up with this technology. In most cases, the air abrasive is only utilized after other mechanical cleaning or hand techniques have removed the bulk of the matrix [67][58].

ii. Miniature air hammers

Air hammers are an excellent instrument for removing complex matrices from fossils and archaeological objects. With a strong tapering stylus, these pneumatic tools can do up to 40000 movements per minute. These technologies have the potential to harm fossils as readily as they may cut through the matrix if used at high speeds. Proper adjustment of air pressure is used to regulate the number of reciprocal motions that the tool makes per unit time, thereby enabling control of matrix removal frequency [68].

iii. Electric etchers or engravers

Pneumatic electric etcher/engravers are essentially little air hammers and are ideal for delicate or fragile samples since they deliver a light touch. These instruments follow the same work function, where a reciprocating stylus is used to remove complex matrix from the artifact's outermost surface. There are different styluses included, each having a specific purpose, such as grinding drills, dental drills, etc. [68].

iv. Pneumatic rotary grinders

Revolving bits are used instead of pounding and vibration to remove the fossil matrix. Specimens can be damaged by extreme force or vibration; therefore, their usage is restricted [65].

v. Electric rotary grinders

Self-contained hand-held grinders powered by electric rotary engines are known as electric rotary grinders (for example - Dremel rotary grinders) [65]. The portable grinders are easy to operate and don't need a lot of effort on the conservators' part. It doesn't matter if they are pneumatic or electric, they are beneficial in the lab, but they are more of a finishing or touch-up tool than a primary matrix removal tool [69].

Although mechanical abrasives are always destructive, the use of a different form of stiff metal brush or other grinding device attached to power tools has been functioning for a longer period of time for archaeological cleaning purposes. Dry brushing with a stiff natural bristle brush and clean water is the only relatively "safe" manual cleaning procedure being used. Stone sculptures with minimal surface soiling are the best candidates for this method, which removes organic growth and loosely bonded dirt [70].

1.3.2 Chemical cleaning in conservation

Cleaning archaeological materials using conventional chemical processes involves applying a substance that reacts with the archaeological material sample and any discolorations that may have occurred on the object's surface. This cleaning strategy typically comprises the direct application of aqueous chemical solutions, or the application of poultices soaked in chemical cleaning solutions, biological cleaning solutions, enzymatic organisms, etc. For decades, chemical cleaning has been primarily performed by the use of chelating agents, most notably salts of Ethylenediamine Tetraacetic Acid – EDTA [71]. The soiling and encrustations of the material are therefore removed laterally with the substance itself. Both alkaline and acid chemicals can be employed for cleaning in a variety of forms, including liquids, gels, and pastes (poultices), depending on the artifacts being cleaned [39][65]. Whereas mechanical cleaning often impinges physical damage, chemical cleaning techniques often leave a permanent imprint on the damaged archaeological materials, either by altering their coloration or leaving residues on the objects themselves. Despite the best efforts made to rinse off the chemicals when applying chemical cleaning, there will always be some residue left behind since the chemicals are washed into the primary structure of the materials they are cleaning. The effects of gravity on rinsed-off chemicals used in cleaning are likely to persist, with more significant concentrations on the lower areas of the material and in the architectural elements that stand out from the material itself. Even though some short-term impacts of chemical cleaning are seen, the long-term consequences of chemical cleaning, which require more attention when it comes to cultural heritage objects in particular, are as follows [70]:

- i.** Changes in the appearance and color of the artifact due to an irreversible bleaching or discoloration process.
- ii.** Unappealing white deposits resulting in the existence of residual deposits (salts) on the surface of artifacts, which crystallize on the latter.
- iii.** Degradation of some natural minerals results in pitting and alters the smoothness of the surface, resulting in a loss of aesthetic detail.

- iv. Surface greening appearance as a consequence of enhanced algae growth.

Most of these material surface modifications are not only aesthetically unpleasant, but some of them can also lead to the degradation of the material. Even though chemical cleaning was performed on stone sculptures and sandstone buildings in Europe some 25-30 years ago, some of these structures now require extensive masonry repairs, despite being chemically cleaned.

1.4 Archeological Sites

1.4.1 Sierra de Atapuerca

The *Sierra de Atapuerca* (Atapuerca mountain range) has become a most significant archaeological region following the discovery of the ‘first hominin’ presence in Europe [72]. It is a rather complex site with numerous limestone caves, situated 12 km east of the city of Burgos, an ancient karstic area of northern Spain [73]. The plentiful bones and stone tools of Europe’s oldest hominins excavated there date back to 0.78 ~1.2 million years [74]. This site has been recognized for the abundant human (genus: *homo*) remains excavated in 1976 [75]. Several fossils of *Homo heidelbergensis* (the Neanderthal predecessor) were also discovered at *Sierra de Atapuerca* [76].

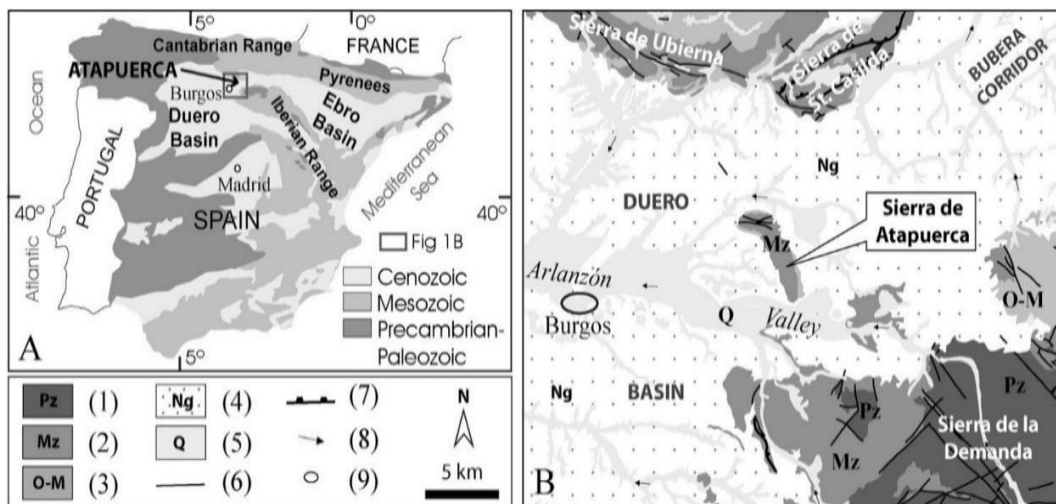


Fig. 1.4: The Iberian (A) and north-east Douro Basin (B) context of the geological setting of *Sierra de Atapuerca*; ‘Pz’ represents Palaeozoic, ‘Mz’ for Mesozoic, ‘O-M’ for Oligocene Lower Miocene; ‘Ng’ for Neogene, ‘Q’ for Quaternary, ‘—’ for faults, ‘—|—’ for thrusts, ‘→’ for drainage direction and ‘O’ for towns [41]

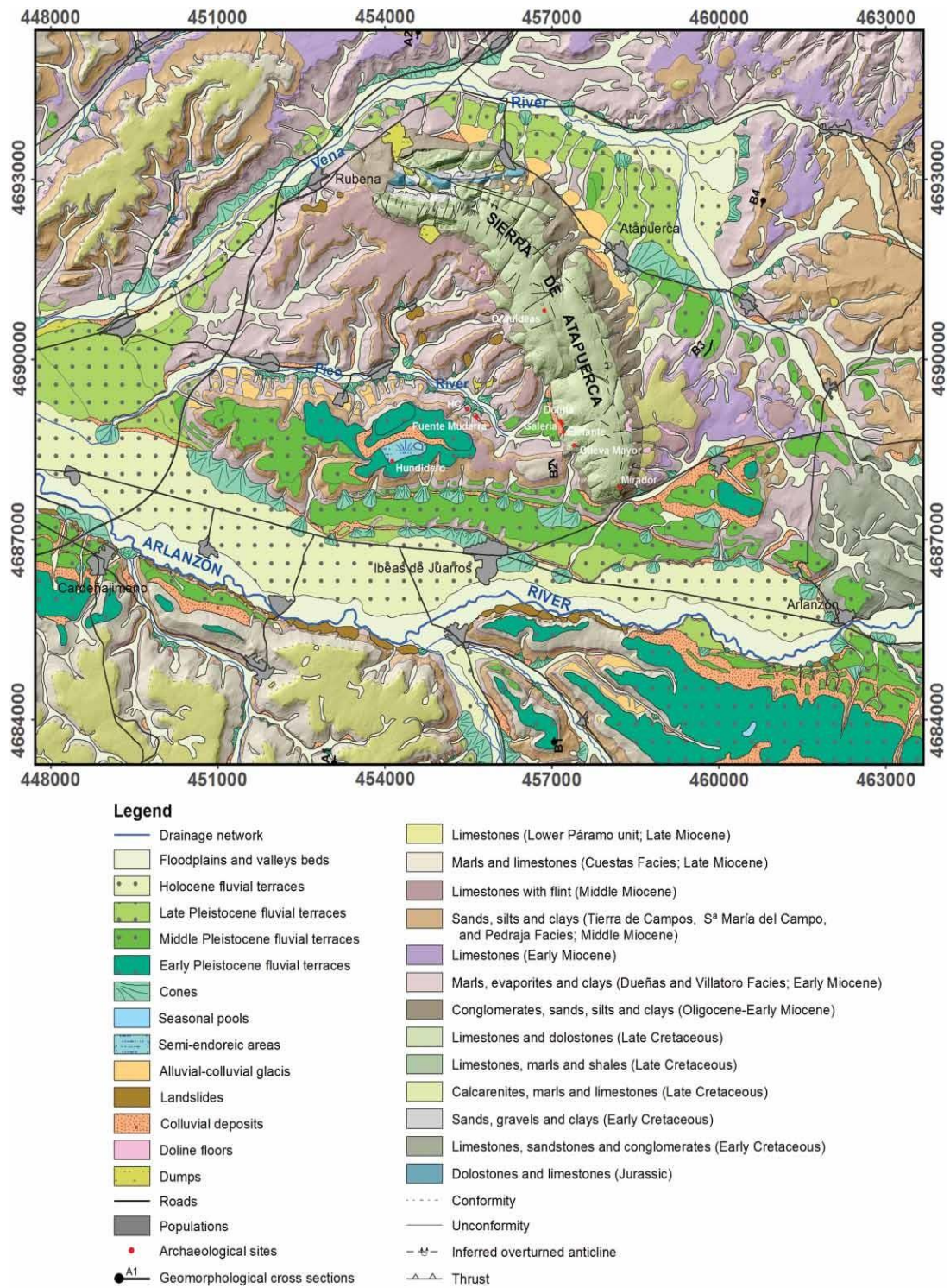


Fig. 1.5: Simplified geological map of Sierra de Atapuerca [82].

In terms of geology, the *Sierra de Atapuerca* is located in the north-western Duero Cenozoic Basin in north-central Spain, between the Cantabrian and Iberian Alpine ranges (Fig. 1.4). It is bordered to the southeast by the *Sierra de la Demanda* (the north Castilian branch of the Iberian Ranges), and to the north by the southern slopes of the Cantabrian Mountains (Fig. 1.4 A) [77][78][79]. It is structurally a part of the Iberian Range, which is configured by the name anticline, and contains Quaternary deposits that are primarily fluvial terraces, valley floors, alluvial fans, floodplains, and colluvial deposits [80][81].

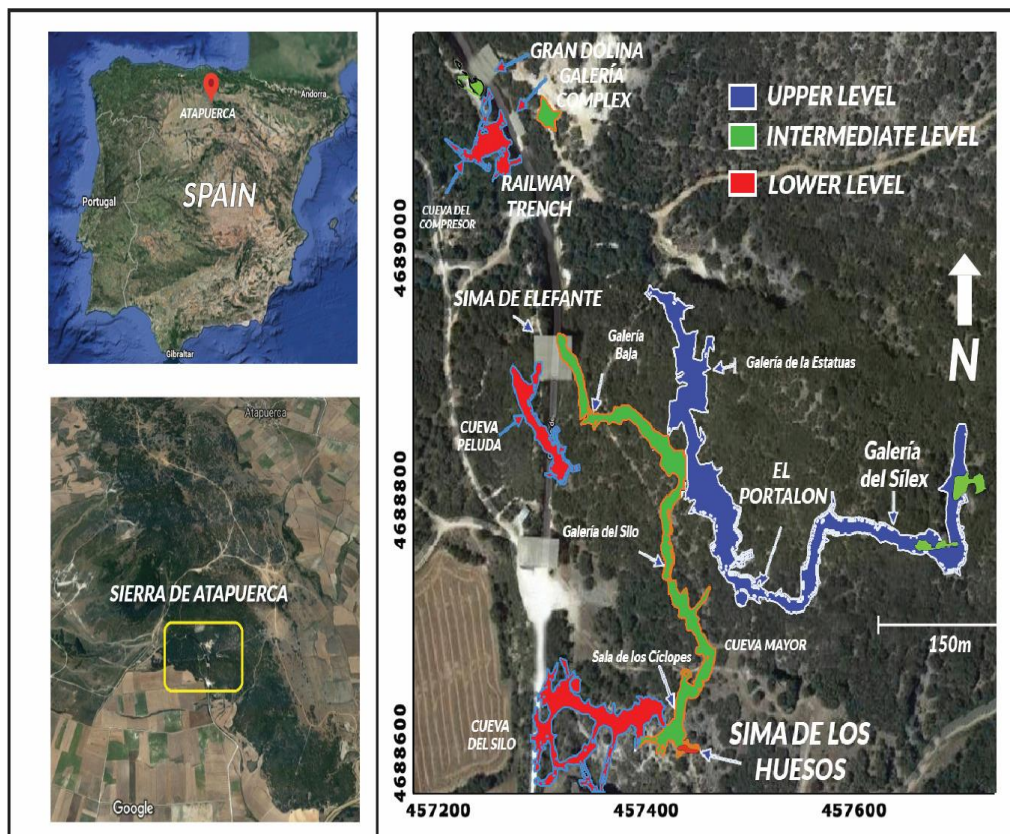


Fig. 1.6: Location map of Atapuerca (Source: Google map). On the right, a karst-based map illustrates the different Atapuerca sites (reproduced from [87][88])

Lithologically, this region comprises sand, gravel, and polygenic Palaeozoic pebbles from the Pleistocene and Holocene eras [83]. River Arlanzon and River Vena of Atapuerca's floodplain lithology is made up of quartzites, unique limestone gravels and cobbles, sand, silt, and clay. With alluvial input and colluvium effect, the valley bottoms of Atapuerca have a seasonal alternation of coarse and fine materials. *Sierra de Atapuerca* sands are mainly composed of fragmented rock (Fig. 1.5) [84][85][86].

The story of Atapuerca's early inhabitants might well be kept hidden forever. But a British firm named the Sierra Company had initiated a railroad construction in the area in 1890. Throughout the construction of the railway trench, workers detached a portion of one mount side. They revealed that the sediment-filled cavern, now well-known as *Gran Dolina*, is a critically significant archaeological site in Europe. It contains human remains dating back about 800,000 years [89]. In the beginning, concentration focused on the *Sierra de Atapuerca* region's geology because of the abundance of limestone there. Though initially, the dark caverns of Sierra exposed countless cave bear teeth and other animal fossils, however, the first human fossil discovered in 1976 was the early human lower jawbone dated to 400,000 years [90][89]. During that time, archaeologists discovered hundreds of ancient human fossils. *Sierra de Atapuerca* surprisingly became one of the most prominent archaeological locations, gradually establishing itself as a focal point of archaeological interest following the residence of Europe's first hominid [56]. The cavern sites of the earliest human livelihood there listed in the chronological order are: 1) Sima del Elefante, 2) Gran Dolina, 3) Galería, 4) Sima de los Huesos (Fig. 1.7), 5) Portalón and 6) Mirador (Fig. 1.6) and the discovered open-air outdoor sites there include 1) Hotel California, 2) Hundidero, 3) Fuente Mudarra, 4) Valle de las Orquídeas and 5) Paredeja along with 27 open-air campsites [81]. The scientific discovery of the Atapuerca site began in 1964, and the *Sierra de Atapuerca* was designated as a World Heritage site by the United Nations Educational, Scientific, and Cultural Organization (UNESCO) in 2000 [93].



Fig. 1.7: Bear rib and phalanx excavated from the *Sima de los Huesos* site, dated back to the Pleistocene era.

1.4.2 Sima de los Huesos

One of the most surprising discoveries at *Sierra de Atapuerca* is a cavern site called *Sima de los Huesos* (the Bones Pit), the most remarkable and significant site. The pit unearthed approx. 166 cave bears from the Middle Pleistocene and approx. 28 individual humans

excavated by more than 6500 bone fragments and more than 500 teeth, thus making this pit one of the biggest collections of earliest hominid fossils in the world. Dating shows that this site's age ranges from at least 300,000 years ago to 600,000 years [91]. Brain sizes of the discovered human fossils identified here are approximately similar to those of the Neanderthals (*Homo neanderthalensis*) and modern humans. Some of the skeletons possess numerous traits unique to Neanderthals but not completely similar to the characteristics of the Neanderthals. There are very few articulated animal and human skeletons; some bones carry tooth marks from when carnivores chewed on them. The archaeological deposits of the site include several large collapsed limestone blocks and deposits of mud combined with a bone-bearing breccia. Extinct species of lion, wildcat, grey wolf, red fox etc., and other known animals have been identified in the pit [92]. Figure 1.6 presents the position of the Atapuerca sites and the karst-based map showing the position of the different cavern sites following the original topography by G.E. Edelweiss ([87][88]). The blue color represents the *upper level*, green the *middle level*, and red the *lower level* of the karst.

1.4.3 Fuente Mudarra

A unique settlement of the Middle Paleolithic era, *Fuente Mudarra* is located three kilometers from Railway Trench in the *Sierra de Atapuerca* and is an open-air site of Neanderthal chronology. It is a unique settlement that records the period from 150000 to 100000 BC [94]. It is situated on the left slope of the river Pico, on a colluvial reservoir on the slope that drives from the high terraces of the Arlanzón until the channel of the Peak, a place from where the valley of the Pico River is controlled, that is believed to have been used by Neanderthal people to hunt and work on their tools. Within the revealed 31 rich Middle Paleolithic lithic outdoor archaeological assemblages of the Sierra de Atapuerca [95], *Fuente Mudarra* has an extreme significance as the Neanderthal stone industry workshop has been found here, which uncovers a workshop of stone tools with raw materials from the area.

Fuente Mudarra is an open-air deposit of 12 m² that has been intervened for four campaigns. From 2012 until today, archaeologists have introduced the four archeological levels ensuing the Neanderthal occupations where stone tools have been identified. Levels 0 and 1 were practically sterilized since they were scrambled greatly by military activities from the base of Castrillo del Val and muddled as for the prior agricultural usage land tail. Levels 2 and 3 enclose the lithic industry, although in small quantities. Level 4 contains a greater concentration of archeological stone tools, whereas level 4b within the

same campaign revealed a change of coloration in the sediment, and a huge percentage of total lithic pieces were recovered here.

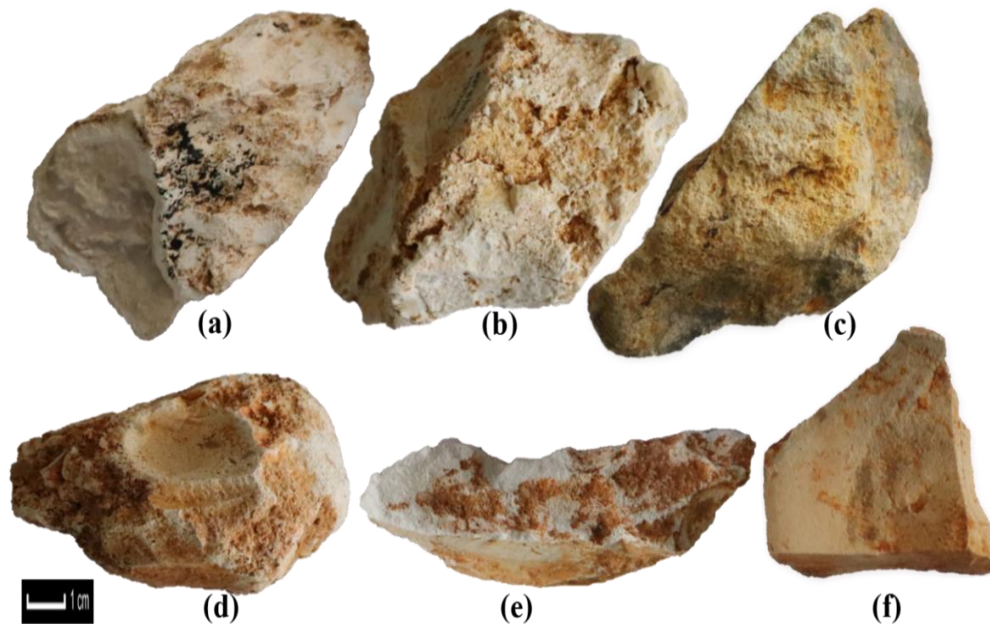


Fig. 1.8: Flint samples excavated from *Fuente Mudarra* (a,b,c) and *La Paredaja* (d,e,f) (Burgos, Spain)

A total of 292 lithic pieces were recovered, including an unspecified bone fragment from the *Fuente Mudarra*. They are nearly on or next to an outgrowth of Neogene flints [81] (Fig. 1.8: a, b, and c). Also, some number of Cretaceous flints there originate from the Orchid Valley, and some pieces of material that have appeared there need to be investigated as they do not seem from the *Fuente Mudarra* [96]. The collections of stone tools were identified to aim at the production of flakes, whereas a high percentage of the denticulate pieces were thought to be part of the retouched flakes; reuse is observed in many parts [97]. The dating of the levels of this deposit is defined from a previous survey which was carried out in 2007 by the Radiochemical Dating Laboratory of the Autonomous University of Madrid, dated thru the Optically Stimulated Luminescence technique (OSL) and obtained the *Fuente Mudarra* in an age of $56,452 \pm 3279$ BP years for level 4 [80].

1.4.4 La Paredaja

The very new archeological site, *La Paredaja*, a cave that has been infilled and collapsed, was discovered during the fieldwork conducted in the summer of 2018. It is located on the

southern slope of the *Sierra de Atapuerca*. The Middle Pleistocene fluvial terraces T5, T8, T9, and T10 of the river *Arlanzón* have been found within a few hundred meters of the site's boundaries. The removal of blocks and cleaning of the sedimentary sequence began in 2019 as part of excavations at this site, which involves 10 meter-thick excavations with 20 meter-thick concealed strata. It has been found that the majority of the artifacts found in *La Paredaja* are lithic tools carved out of Cretaceous flints (Fig. 1.8: d, e and f).

1.4.5 El Portalón de Cueva Mayor

El Portalón de Cueva Mayor is an exceptional Holocene archaeological site located in the *Sierra de Atapuerca*, 15 km from the city of Burgos (Spain) [98]. The site is located at the natural entrance to the karst system of the Atapuerca mountain. The archaeological site contains an archaeo-stratigraphic sequence of more than 10 m covering a chronology of 30 kiloyears from the Upper Pleistocene to the Middle Ages [98]. In the Holocene sequence, stratigraphic units have been documented from all chrono-cultural phases from the Mesolithic to the Middle Ages, with an exceptionally rich archaeological content composed of pottery, lithic and bone industry, personal ornament elements, metallic objects and human, faunal and archaeobotanical remains, among others [98][99][100].

A considerable quantity of ancient archaeological ceramic sherds with diameters ranging from millimeters to 2–3 cm has been unearthed at *El Portalón de Cueva Mayor*, classified as the Chalcolithic and Neolithic stratigraphic levels. The Neolithic pottery originates from a habitational environment, with evident domestic activity, whereas the Chalcolithic remnants came from funeral and stabling contexts, where a huge tumular accumulation of human graves and animal activities were observed [93]. The ornamental decoration and design aspects are generally the major distinction between Neolithic and Chalcolithic pottery but beyond that, no variations are detected between them from the technical point of view [98][101].

CHAPTER: 2

LASER CLEANING IN CULTURAL HERITAGE

CHAPTER TWO

LASER CLEANING IN CULTURAL HERITAGE

Summary: Laser cleaning has been considered amongst the most noteworthy contributions of Physics toward the conservation cleaning treatment of archaeological materials and museum artifacts. It has been introduced and developed following the in-situ material cleaning challenges; nowadays, it is the subject of many published works on stones and iron objects, but still needs more attention and improvements while its application to archaeological bones and ceramics is not widespread. This study reviews the wide range of applications of laser cleaning and the accompanying laser-material interaction regimes in the conservation of these archaeological materials, and focuses on the methodological techniques used to address typical cleaning challenges. It is difficult to determine if one laser cleaning technique is appropriate enough for specific artifacts because these investigations sometimes appear to be inconsistent, implying that the outcomes of laser cleaning are very case-dependent. For optimal laser cleaning, thorough consideration of the physicochemical properties of the materials to be cleaned and their subsequent interactions with the laser must be taken into account while selecting the best laser parameters. The findings here highlight the importance of systematically assessing the cleaning outcomes to develop more effective, operative and safer laser cleaning protocols, and to let conservators inform whether laser cleaning is an option for preserving such artifacts under their care. Moreover, this study provides a useful starting point for conservation experts who wish to pursue further research into the laser cleaning of ancient artifacts. The present work concludes with suggestions for further research that might be carried out in the near future in order to obtain better cleaning for archaeological materials conservation.

2.1 Introduction

The laser, which revolutionized man's use of light, is so ubiquitous and significantly recognized as one of the top leading technological achievements of the 20th century [6]. The domain of laser application is widespread, including many scientific investigations, ranging from medical sciences [102][103] to cultural heritage applications [18][49][104][105][106] [107][108]. Laser-based interventions have increasingly been

applied to the conservation of archaeological and cultural heritage materials, in line with scientific and technological improvements that have been made since the first laser was demonstrated. Laser application as a cleaning tool signifies the most important developments of physics toward artworks conservation. Though the first functional laser was built in the 1960s, real-world implementations in different research areas have taken years to develop [109]. However, the first attempt of using pulsed laser radiation was proposed by Schawlow in 1965, who used a ruby pulsed laser to eradicate a high absorptive black pigmented layer from the paper surface [110]. The first laser cleaning attempt with successful implementation for removing encrustations and deteriorations from stone artifacts was made in 1970 [111]. Later, a high number of research projects for artworks cleaning by laser were introduced by the pioneering efforts of J.F. Asmus and L. Lazzarini in the decades of the 70s, taking into account the aesthetic values of the sample [112][113][114][115]; but the innovative applications in the cultural heritage field started to be extensively applied only three decades later.

Over the last three decades, the increasing application of the laser cleaning method, combined with technological advancements taking into account laser parameters and material characteristics, led to widespread trials and possibilities. The gradual acceptance of laser cleaning as a conservation technique within the science and conservation communities is mirrored in the high number of scientific publications in interdisciplinary journals, literature, books, dedicated conferences etc., mainly concentrating on laser performance, selectivity and subsequent success, comparing the potential advantages to the conventional mechanical and chemical cleaning. It triggered the laser methodology to be included and spread as an encouraging example to effectively solve many challenges faced by the conservation community. The effects of laser cleaning solutions are now simple to monitor and enable conservators to work comfortably in line with the importance of the origin and use of art objects. The increasing need to conserve archaeological materials has led to higher demand for highly selective and gradually accurate cleaning techniques and zero damage or minimal impact following traditional cleaning methods. Although laser cleaning has not been universally embraced as a solution for all sorts of cleaning conservation treatment challenges, it is increasingly recognized as an appreciated environmentally friendly non-contact technique that delivers greater accuracy and control. Since the 90s, different laser systems have been widely used to clean archaeological materials to eliminate encrustations and particulates from material surfaces [116][117]. It has been a significant challenge for multidisciplinary, innovative research development to develop a common language and laser tool selection criteria to efficiently apply lasers in

large-scale conservation practice. Some of the essential fundamental factors to be taken into account in the cleaning of artworks that expedite the conservation issues in order to establish the correct laser tool selection criteria are as follows:

- a. variety of archaeological materials (such as stones, bones, ceramics, metals, paintings, glasses, parchments, papers, etc.) and their material properties (physical, chemical, thermal, optical, etc.)
- b. decay and weathering problems associated with the materials (such as for example in the case of stones: erosion, exfoliation, alveoli formation, blackening, scouring, etc.), deterioration problems (physical factors, chemical factors, biological factors, mechanical factors, etc.) and contamination scenarios (homogeneous, heterogeneous, etc.)
- c. creation of individual characteristic patina layers (a process of encrustation that is intensively based on the environmental factors under which the material was exposed throughout its lifetime, e.g., environmental pollutants, water exposure, sunlight, etc.)
- d. crusts / surface deposits (harsh, insoluble, and thick deposits must be removed without damaging the sensitive mineral substrate, which is very vulnerable to chemical transformations)

Although laser cleaning techniques have been frequently explored on archaeologically significant stones and iron artifacts, only a few case studies of laser cleaning on bones and ceramics have been published thus far. These findings complicate conservators' assessment of whether laser cleaning is a procedure appropriate for all types of archaeological materials. Systematic investigations dedicated to ablation phenomena and interpretation of the basic laser-material interaction processes are still necessary to establish practical protocols for cleaning archaeologically significant delicate and sensitive artifacts, notably bones and ceramics. While at the same time, more insights into the cleaning of stones and iron objects may be beneficial to broaden the application scope. By providing an overview of the different laser systems that have been used on these materials so far, it may be possible to make better decisions about how to employ technology and how to conduct research, rather than just relying on phenomenological descriptions of laser-material interaction dynamics. State-of-the-art laser cleaning of bones, stones, ceramics, and iron artifacts is the subject of this comprehensive review that aims to describe how specific laser parameters affect the laser cleaning outcomes and experimental insights, defining the suitable cleaning settings for laser cleaning as an outcome. Each material is reviewed, and

the problems and outcomes with drawbacks related to laser cleaning are provided. Additionally, this chapter discusses the areas that require further investigation.

2.2 Laser systems used in conservation/restoration

Several enterprises in the conservation sector make use of laser technology for surface cleaning. Laser cleaning has been tested for the conservation of a series of archaeological and cultural heritage materials conservation, particularly making use of the most recent laser technology advances. These pertain not only to the miniaturization and portability of lasers but also to automated laser scanning mechanisms, which may proliferate in the upcoming years and may make a difference in their application on sensitive materials, such as is the case with mineralized Pleistocene bone and unearthened Neogene and Cretaceous flints.

Table 2.1: The mostly used laser systems for cleaning archaeological materials.

Laser name	Type	Wavelength(s)	Pulse duration(s)	Pumping method	Reference(s)
Nd:YAG (Yttrium Aluminum Garnet doped with Neodymium)	Solid-state	1064 nm (fundamental) 532 nm (2 nd harmonic) 355 nm (3 rd harmonic) 266 / 248 nm (4 th harmonic)	200 - 500 μ s (FR) 50 ns - 3 μ s (SFR) 5 - 20 ns (QS) 20 - 120 ns (long QS) 150 - 800 ps 500 fs	Arc lamps or laser diodes	Bones: [106][118][119][120] Stones: [25][121][122][123][124][125][126][127][128][129][130][52][54][68][70] [76] Ceramics:[131][132][133][134] Iron Objects: [135][63][136][137][138][139][140]
Er:YAG (Yttrium Aluminum Garnet doped with Erbium)	Solid state	2940 nm	80 - 250 μ s	Laser diodes or Er-fibers	Stones: [141][142][143] Iron Objects: [63]
Excimer	Gaseous	ArF (193 nm) KrF (248nm) XeBr (282 nm) XeCl (308nm) XeF (351nm)	10 - 30 ns 100 ns	Arc lamps or gas discharge	Bones: [144] Stones: [145] Ceramics: [132]
CO ₂	Gaseous	10600 nm	50-100 ns	Gas discharge	Stones: [146] Iron Objects: [135][147]
Ti: Sapphire	Solid-state	650-1100 nm tunable	100 - 170 fs	Argon laser	Stones: [148] Iron Objects: [63]

It is possible to operate lasers in different modes. Q-Switched (QS) and Short Free Running (SFR) are the most widely used laser modes. The SFR mode generates standard duration pulses at the level of microseconds (μs), while the QS mode generates slightly shorter duration pulses, typically about 10 ns. Several types of pulsed lasers are used in laser ablation; they are typically categorized based on the active medium. Different materials (in the gaseous, liquid, or solid states) can be employed as the active medium, and their different qualities can give rise to distinct features for each kind. It can require active cooling, depending on the optical loss of the medium. Using Q-switching, a technique for generating pulsed output power, a pulsed beam can be obtained, and a large amount of energy can be concentrated on a surface in a short time. In archaeological material conservation, Q-switched pulsed lasers are mostly used, and they need to be categorized as there are several different forms (Table 2.1).

2.3 Laser based interventions on Archaeological Bones

It has been more than three decades since new laser technologies and operating techniques were developed that enabled for selective removal of damaged artifact layers when traditional mechanical and chemical treatments failed in a variety of situations [121][149][150]. Nonetheless, laser cleaning is not being well accepted by conservators/restorers yet when it comes to cleaning archaeologically significant bones, having only been applied in a few cases [106][118][119][120][144]. This is dependent on a number of factors, including: a) the fact that this is not yet accepted as a mature technology from the bone conservation point of view for avoiding damage to delicate and fragile bone surfaces; b) a lack of understanding of the fundamentals of laser material interaction mechanisms, and: c) a scarcity of investigative devices that can provide both, qualitative and quantitative information during the laser cleaning process. When it comes to short-pulse lasers, they weren't accessible until the 1990s, and the lack of uniformity and homogeneity in bone composition [151] and the contamination state of the objects owing to the extended burial duration may also be major factors.

In general, bone tissue is formed of living cells surrounded by a firm matrix consisting of phosphates and other calcium minerals connected together by the protein collagen. In the ivory sample, its collagen is a high concentration of hydroxyapatite, which contributes to its distinctive properties, and Keratin is usually detected there. Regardless of their elemental composition or heterogeneous structure, bones are vulnerable to significant changes in both content and structure over time; these changes can significantly impact

their overall interaction with laser radiation. When bones are exposed to the environment for an extended period of time, they become discolored and dusty as a result of inorganic mineralization weathering, losing their original appearance and aesthetic values [106]. While mechanical and chemical damage to historic patinas can be minimized or avoided, laser cleaning of bone can selectively remove undesired fossilized minerals, dirt, and other contaminants from the bone surface. It is common to employ a detergent wash within a regulated temperature or to apply alcohol or other chemical solvents to the surface of an unearthened bone to clean it. However, laser cleaning is a dry technique that may clean bones with rough and weak surfaces, while respecting the original layer to preserve as much of the surface anatomical information that has been hidden by contaminants.

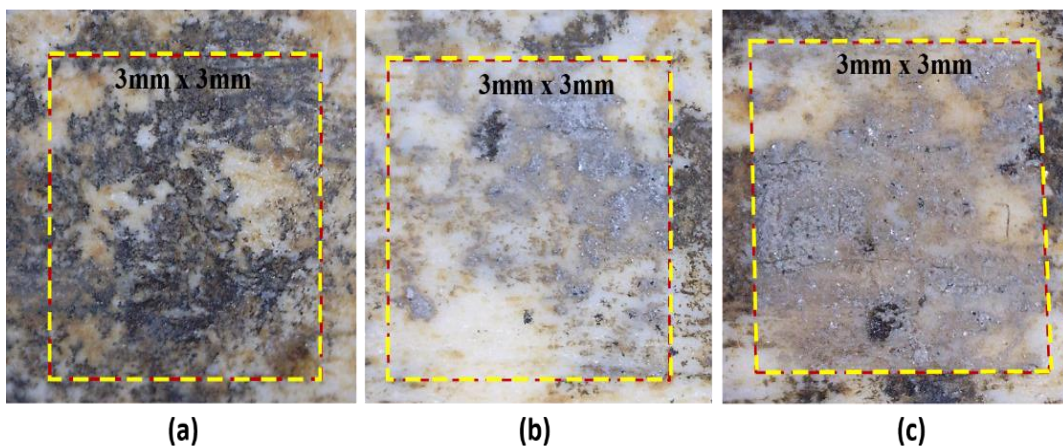


Fig. 2.1: Microscopy images obtained on the Pleistocene bone: ‘a’ represents the mineralized dark-blackish surface, ‘b’ represents the well-cleaned bone surface treated with n-IR 800 ps lasers, and ‘c’ represents the laser damaged surface where melting is evident (reproduced from [106]).

Laser based interventions generate varied impacts on the surface of archaeological bones when they are cleaned with lasers, according to the investigations that have been conducted [106][118][119][120][144]. Table 2.2 lists the laser parameters, the problems that needed laser treatment, and the outcomes of different bone cleaning investigations. Looking for the safest laser to clean archaeological bones is a challenge; the green laser emission at 532 nm and the n-IR emission at 1064 nm have been found comparatively effective, while the ultraviolet laser (355nm) with ns pulse duration has been found to be the most destructive. In one case, it has also been observed that ArF laser emission at 193 nm provides an expected good cleaning [144]. Although the Nd:YAG system can produce the fourth harmonic at 266 nm and the fifth harmonic at 213 nm, researchers never went for these

wavelength investigations owing to the findings achieved with the third harmonic. Laser irradiation emission at 355 nm induced discoloration, a rise in roughness, a loss of gloss on the treated surfaces, and the lowest damage threshold values of the laser fluence. The presence of patina and encrustation heterogeneity in bone samples had a significant impact on the interaction of laser radiation that needs to be emphasized. Ivory cleaning by laser is better when cleaned with the fundamental Nd:YAG laser wavelength at 1064 nm. The cleaning threshold of all three laser wavelengths was considerably lowered when the lasers were operated at a high repetition rate. Most of the authors agreed that the findings reported in their manuscripts should be evaluated in terms of broadly defined cleaning protocols (not to be interpreted as the absolute values) and used as recommendations for future laser conservation of archaeological bone artifacts.

Table 2.2: List of the results obtained on archaeological bones cleaning using different laser systems.

Archaeological bones cleaning by laser							
Laser	Wavelength	Pulse duration	Cleaning fluence (Jcm ⁻²)	Problem(s)	Outcomes(s) / side effect(s) / discussion	Reference(s)	
Nd: YAG	1064 nm	5-7 ns	5	Bone covered with calcareous layers and hard gray-white encrustation	The stain moves or is vaporized as a result of thermal expansion.	[119]	
		7 ns	>4.5	Craneous covered with dirt (i.e., particles, grease and stacked earth)	Damage threshold fluence identified.	[118]	
		8 ns	2	Grey inorganic encrustation and organic aliphatic chemicals at the substrate of the ivory jug	No visible damage when cleaned with a laser to the primary ivory substrate.	[151]	
		15 ns	3.2	White bovine rib with encrustations	No changes in color or texture; effective cleaning.	[120]	
		15 ns	3.5	Thick encrustation on the brown bovine tibia bone patina	Safe cleaning; no visible damage with the naked eye.	[120]	
		15 ns	5.7	Sample made of ivory	The microscope reveals subtler shifts in color and texture.	[120]	
		800 ps	> 0.16	Hard blackish encrustations, greyish contaminants, atmospheric soil dust, and weathering patterns on bone	Laser irradiation appears safe; consequently, bone surface pollutants created by mineralization may be cleaned effectively and satisfactorily in the method described.	[106]	
	532 nm	15 ns	5	White bovine rib with encrustations	Laser fluence was found to be within acceptable limits.	[120]	
		15 ns	>2	Thick encrustation on the brown bovine tibia bone patina	Safe cleaning.	[120]	
		15 ns	3.5	Sample made of ivory	Changes in color and loss of gloss were detected on the surface.	[120]	
	355 nm	15 ns	1.5	White bovine rib with encrustations	In the shape of a halo surrounding the laser spot on the sample surface, and changes in surface color (yellowing) was noticed.	[120]	
		15 ns	>1	Bovine rib sample covered with brown patina	Even though the energy density was so low that radiation did not damage the surface, dark brown spots could be seen.	[120]	
		15 ns	>0.9	Sample made of ivory	Yellowing and tarnishing observed in surface after laser.	[120]	
	Excimer	ArF (193 nm)	-	10	Surface layers of dirt on ancient bones and teeth	A very smooth and intact surface was observed after an acute removal of dirt without destroying the value of ancient tissue.	[144]

2.4 Laser based interventions on Stones

Laser stone cleaning has become increasingly noticeable due to the limitations of traditional cleaning techniques, which are unable to completely clean the targeted stone surface without causing micro damage or alteration. Though sometimes a certain level of damage is very microscopic, it will lead to a more likely surface deterioration in the future. The laser is selected with the needed specifications to achieve great accuracy and selectivity while separating the black crust / soiling from the light-colored substrate without causing unintended damage. First suggested in the 1970s [109], the notion of employing pulsed laser radiation to remove encrustations and damaged layers from stone artwork as a light eraser extends back to the beginnings of laser technology [110]. As a result of its high cost and inability to move for *in situ* cleaning treatment, this early laser system method was only used inside the laboratory until the 1990s [112][113][114]. Many conservators were concerned about the probable adverse effects of laser irradiation on stones before this decade, but this fear has waned as a result of more in-depth research on laser-stone interactions. Using fluence levels set by the intrinsic properties of the laser system and treated stones, it was possible to distinguish between removing strata and disclosing the layers underneath. Since then, many studies have been conducted to improve cleaning effectiveness and efficiency while also addressing the negative aspects of the procedure.

Nowadays, conservators perform a variety of laboratory or in-situ experiments, contrasting lasers with other traditional approaches, to verify the cleaning efficiency of the laser [79]. Several fundamental investigations were undertaken in a variety of research projects, including phenomenological descriptions [31] of the impacts of radiation and diagnostic measures of the material removal processes, before and after cleaning studies on the well-known problem of urban pollution-induced black crusts [152][153]. The scientific publications have confirmed that QS Nd:YAG lasers at IR wavelengths (1064 nm) with typically 5-10 ns pulse duration may be considered as good cleaning tools for eliminating dark-colored over layers from light-colored substrates mainly on artworks of stone [154][104][155]. These lasers indeed provoke very short pulses of heat. The short pulse length is important as it prevents heat from penetrating the stone surface under the dirt. This type of laser is in this particular case ideal, because most soiling layers absorb much more than the underlying substrate at this n-IR wavelength. This means that if cleaning is done under safe limits, more bursts of pulses would have little effect on the surface until the dirt has been eliminated since insufficient energy is consumed to do further damage. Also, the Nd:YAG laser is highly effective, simple to manage and reasonably lightweight.

Infrared photothermal mechanisms appear adequate to remove undesirable contaminants. Their efficacy is attributed, however, to their self-limiting nature, since the majority of encrustations commonly found on stonework absorb in this wavelength regime at a level significantly higher than the stone substrate itself [104][156]. The usage of IR laser beams to remove contaminants from stone surfaces sometimes would have produced a distinct color effect [157], such as a yellowish appearance [31][56]. Many conservators argued that this yellowing for substrates is mainly found in marble [56] and other stones [158]. Laser yellowing remains a very complex issue, and many reasons have been identified for why lasers produce the yellowing appearance [159]. In the mid-decades of the 90s, multiple scholars had affirmed that different underlying yellow layers had been discovered in laser cleaning operations. The most challenging part was figuring out whether or not there were any yellow layers beneath the dirt and grime that had been removed by laser cleaning. In addition, soiling leftovers may be responsible for yellowing. Microscopic examination indicated the presence of iron compounds on laser cleaned surfaces, as well as providing evidence for carbon residues, microbial crust contamination, organic soluble contamination, etc. [160][161][56].

Several hypotheses were put forward in order to explain the cause of laser-induced yellowing. One of the most accepted one was that the yellowing was caused by light scattering from voids and irregularities of the surface or particulates [161][162]. Later, no signs of any exposure have been found on yellowing which could be a reason for damage to the stone. There was also evidence of a laser yellow organic compound steeped with an epigenetic gypsum-rich matrix of the pollution crust layer under the black crusts [163]. Many authors believe that yellowing is caused by inadequate removal of pigmented stratum and/or diffusion of organic substances over the artwork's outermost layers, this being supported by laboratory findings [164][165].

The issue of discoloration has been widely researched, and several publications have focused on the subject [157][160][166]. Laser cleaning parameters have also been proven to play a role in the yellowing issue. Implementation of laser cleaning technologies is also an addition in minimizing damage and unintended alteration to the stone substrates. Apparently, laser wavelength and pulse duration plays an essential role in yellowing discoloration issues [31][153][156][167]. The yellowing usually is more noticeable at 1064 nm and, thus, less noticeable at the 2nd harmonic of 532 nm and the third harmonic of 355 nm [168]. A recent study in various calcareous substrates has shown that the rise in laser yellowing is due to soiling strength and thus supports the opinion that the primary cause of laser yellowing could be soiling residues [164]. Though no yellowish discoloration is

observed upon ultraviolet (UV) irradiation, in contrast, the use of UV radiation of 355 nm wavelength to treat contamination and pollution crusts has often reported discoloration towards gray [56][169][170]. The entire contamination or pollution crust is gradually eliminated at this wavelength regime based on the ‘layer-to-layer’ ablation mechanism. It is noteworthy that high fluence values are necessary for successful material removal in this regime, resulting in alteration or damage of the substrate [169][171].

The removal and suppression of biological growths, known as biodeterioration, as well as bio- colonization might be another issue with stone conservation that necessitates further efforts. Several authors studied the use of laser irradiation to remove biodeteriorations from stone surfaces under controlled conditions [122][172][173]. A variety of biological growths were also subjected to *in vitro* irradiation tests [145][174][175]. Because of the high operational fluences required to remove organic pollutants firmly fused to the stone substrate, laser cleaning has been shown to be detrimental in some situations. The low ablation efficiency of the operating laser was also to blame for its limitation. An in-depth analysis of the cleaning sample’s physicochemical properties showed that the high-temperature incubation, which conservators are currently working to resolve with today’s laser system advancements, limits the cleaning process efficacy. Table 2.3 summarizes the findings of laser cleaning of archaeological stones.

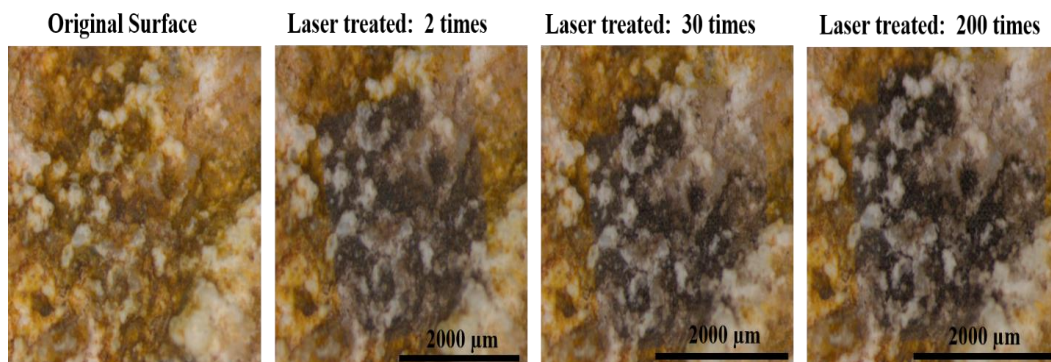


Fig. 2.2: Microscopy images obtained on the Neogene Flint; the UV radiation of 355 nm wavelength to treat pollution crusts has reported satisfactory removal of contaminants (fluence is 0.95 Jcm^{-2}), but discolored in gray, have been observed at this thesis investigation.

The darkening, soiling, chromatic alterations, and formation of black crusts that occur as a consequence of stone materials being exposed to pollutants should be avoided, and cleaning is necessary for aesthetic and conservation reasons. The short-pulsed laser provides

significant advantages over standard mechanical and chemical cleaning processes for deteriorating stones. Laser cleaning has been popular among conservators for a range of stone cleaning procedures because of its non-contact, selective nature, and inclination to self-limit. Nd:YAG QS micro- and nanosecond near-IR pulsed laser cleaning has been the most often employed laser technology for various stone types and *in situ* conservation applications last decades (Table 2.3). It has been observed well to use wavelengths other than the fundamental 1064 nm for specialized cleaning treatments due to the high absorptivity of certain stone types (especially in marble). It suggests that the Nd:YAG laser can be used at 3rd and 4th harmonics. In some cases, the difference in absorption coefficients between encrustation and the stone substrate is insufficient to produce meaningful changes in ablation thresholds. To avoid discoloration and address the issues mentioned above, some authors experimented with the sequential (SQ) use of IR and UV laser (i.e., IR→UV), which did not produce a satisfactory result when discoloration was caused by the IR laser irradiation first; though the discoloration could be removed to some extent, the observed surface morphology appeared a lot more uneven than expected [156].

Similarly, when an IR beam was used to remedy the impact of UV irradiation (i.e., UV→IR), SQ usage was shown to be insufficient for encrustation removal. However, when the final color, surface morphology, and homogeneity of the cleaned regions are considered, synchronous (SN) application of IR and UV laser in spatial and temporal overlapping appeared to provide the expected good cleaning surface [156]. However, there hasn't been much emphasis paid to clean using recently developed ultrashort fs pulsed lasers for *in situ* stone conservation applications. This might be a breakthrough for this sort of material conservation due to controlling the photothermal and photochemical effects that are usually triggered by short-pulsed lasers. On another note, the issue of excessive heat accumulation might also be alleviated by using the safe cleaning settings provided by fs lasers.

Table 2.3: List of the results obtained on archaeological stones cleaning using different laser systems.

Archaeological stones cleaning by laser						
Laser	Wavelength	Pulse duration	Cleaning Fluence (Jcm ⁻²)	Problem(s)	Outcome(s) / side effect(s) / discussion	Reference(s)
		5 ns	2	Lichen, algae, and fungi on the surface of dolostone	Cleaned fungus, algae, lichen, and endolithic mycobionts; their survival is diminished by photosynthetic damage.	[174]
		5 ns	0.6	Thick encrustation on Hontoria limestone	All forms of pollution crust were effectively removed; however, yellow discoloration was evident in all cases.	[159][160]
		6 ns	2	Naturally developed biofilm on Vilachán granite	No discoloration, but because of the dark hue of the remnants, a second laser scan may increase the cleaning efficiency.	[123]
		6ns	2 - 5	Dark cement crusts on the selenite (mineral gypsum) surfaces	Removed the hard/thick cement crusts efficiently; no change in the crystalline phase, and the natural patination layer remains intact.	[124]
		6 - 10 ns	20.16	Sulphated black crust on building granites	Not wholly removed the crust; only the black color (carbonaceous particles) has been totally eliminated from the crust.	[176]
		7 ns	0.5	Microbial encrustation on marble surface	The extensive fungus and lichen network could not be removed; causing a dramatic color change from originally white to yellow.	[56]
		8 ns	2.3	Stones inoculated with bacteria, yeast, and fungus	Ineffective; stone mineral framework melts even at very low energies, with slight discoloration on the surfaces.	[172]
		15 ns	2.5	Crustose lichens on dolomite stone	Lichen thalli and endolithic microbe damage to the surface are effectively removed.	[173]
		15 ns	0.8	Soiling on Pentelic marble	Removed all sorts of pollutant crust; yellow discoloration was observed in all cases.	[160]

Chapter Two: Laser Cleaning in Cultural Heritage

Nd: YAG	1064 nm	20 ns	1 - 5	Grey shade on white marble	Micro-explosion-like mechanical effect was caused by the impact.	[125]
		few ns	0.8	Pollution crusts on the Athens Acropolis monuments and sculptures	Synchronous use of IR and UV lasers with 0.8 and 0.6 Jcm ⁻² was shown to be effective; IR beam to remove relatively thick crusts, while using UV preferred ablation to remove thinner soiling layers.	[156]
		20 μs	2	Black crust on Pliocene sandstone	Removed degradation products in a controlled manner, preventing any unwanted side effects.	[126]
		20 μs	1 - 5	Grey shade on white marble	Thermal action causes melting & dispersion of particles on surface.	[125]
		20 μs	0.6 - 1.3	Grey layer & black crust on limestone	A thorough cleaning was nearly hard to achieve.	[127]
		20 μs	3	Black crusts and altered stone surfaces of monuments	Effective and fully preserve the original surface; induce a strong plasma-mediated photomechanical process for stone cleaning.	[121][128] [129]
		30 μs	2	Black crusts on complex decorated stone surfaces	The façade's marble, serpentine, and other stone kinds had been cleaned well.	[177]
		40 - 120 μs	4 - 8	Colonization of dark brownish colored lichen on Carrara marble artifacts	Laser did not affect the stone substrate; however, irradiation left biological fragments on the stone surface.	[122]
		60 - 120 μs	1	Pollutants on façade, statues and sculpture	A solid balance was presented between portability, convenience, dependability, and cleaning efficacy.	[177]
	532 nm	6 ns	2	Sub-aerial biofilm on Vilachán granite	Induced the highest color modifications.	[123]
		6 ns	0.37 - 1.25	Different types of building stone	Cleaned whitish limestones without perceptible color changes, whereas reddish stones would suffer strong color variations.	[178]
		7 ns	1.1	Black encrustation on stones	Incapable of removing the black encrustation completely without leaving remains; the surface color altered considerably.	[56]
		10 ns	0.2 - 5	A superficial dark grey to black crust on historical limestone buildings	Laser surface treatment retains the stone's unique patina, but it also leaves the surface smooth.	[130]
		10 ns	1 - 1.4	Colonization on marble artifacts	Lichen satisfactorily removed from the Carrara marble surface.	[122]

Chapter Two: Laser Cleaning in Cultural Heritage

	355 nm	4 ns	0.08 - 0.35	Basaltic stone inoculated with bacteria, yeast, fungus and lichens	Efficient removal with the threshold cleaning fluence of 0.18 for bacteria, 0.08 for yeast, 0.34 for fungus, and 0.35 Jcm ⁻² for lichens.	[172]
		5 ns	0.3	Thick encrustation on Hontoria limestone	Only the thinnest soiling layers could be cleaned in part, and a graying of the hue was seen.	[160]
		6 ns	2	Sub-aerial biofilm on granite	No noticeable surface alterations; burnt organic residues observed.	[123]
		6ns	0.5 - 8.5	Dark cement crusts on selenite surface	Unsuitable cleaning.	[124]
		7 ns	0.5	Biogenically encrusted marble	Showed promising results; effective in ablating the superficial crust.	[56]
		15 ns	0.35	Soiling on Pentelic marble	Ineffective; partial cleaning with thinner soiling layers; grey discoloration was observed.	[160]
		15 ns	0.5	Crustose lichens on dolomite stone	Lichen thalli & endolithic microbe damage are effectively removed.	[173]
Nd: YVO ₄	355 nm	25 ns	0.14 & 0.21	Extensively colonized lichens on granite	Not capable of extracting lichens completely, and provoked mineral damages, mainly on biotite.	[175][179]
		25 ns	0.1019	Biological crusts from granite surfaces	A flattening of the granite surface is noticed as a result of the melting of rock-forming materials.	[148]
Er: YAG	2940 nm	250 μs	0.318	Lichens colonization on stone	Lichen cellular structure is destroyed and cleaned.	[141][142]
		100 μs	1.4 -1.6	Cemented dust on limestone	Removal of soiling compounds was successfully achieved.	[143]
Excimer	KrF (248 nm)	-	0.56	Black crusts, soil-dust and biological deposits on Pentelic marble	While it is effective at removing small compact crusts, soil dusts, and biological encrustations, it is insufficient for thick black crusts.	[145]
	XeCl (308 nm)	-	0.89	Pentelic marble with black crusts, soil-dust, and biological deposits	Effective and efficient cleaning; acceptable removal of thick dendritic crusts.	[145]
CO ₂	10.6 μm	100 ns	1 - 1.5	Black deposit on grey marble	Effective cleaning; no discoloration.	[146]
Ti: Sapphire	790 nm	120 fs	38.197	Biological crusts from granite surfaces	Perform well in removing biological crusts while removal efficiency was high.	[148]
	395 nm	130 fs	16.552	Granite surfaces with biological crusts	Excellent performance in the removal of biocrust from granite.	[148]

2.5 Laser based interventions on archaeological Ceramic Materials

Ceramics are objects of art that provide a wealth of information about procurement of raw materials and production technologies in human history and culture. Ancient civilizations used clay and other earth materials to make a variety of pottery and ceramic objects, which are then fired at high temperatures to harden and preserve their form. Archaeological excavations often turn up vast numbers of potteries and ceramics, making them important for understanding a site's history from both an archaeological and anthropological perspective. When analyzing historical events from a material's perspective, it is vital to study pottery and other ceramic materials [180]. Excavated pottery or ceramic artifacts from archaeological sites are typically covered with a variety of soil contaminants, organic stains, hard deposits and gray-white encrustations, which have altered their original chemical composition and aesthetic appearance [181][182][39]. The surface is coated with encrustations and other stains as a consequence of their burial for extended periods. The presence of dirt on archaeological ceramic materials is a significant source of degradation, thus cleaning ceramic artifacts is frequently an essential step in the stabilization process [179].

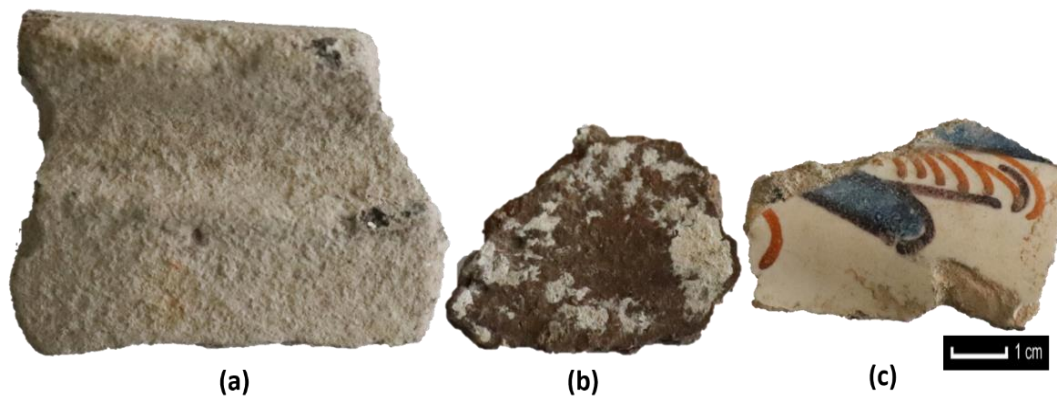


Fig. 2.3: Representative images of 3 different archaeological ceramic materials with diverse cleaning problems, subjected to this thesis investigation: (a) big concreted pottery galbo sherd with hard cement type concretions, (b) fragment of archaeological pottery with soft whitish colored mineralogical contaminants and (c) colored ceramic sherd with soil deposits.

In essence, a ceramic tile is an integral part of artistic heritage, made of a coarser clay with a lesser proportion of fine kaolin clay [183]. It is fired at lower temperatures and can be slightly more prone to water penetration. Still, this characteristic is reduced to a minimum

if the ceramic tile is coated with a protective glaze. There are a number of factors that have contributed to the degradation of this valuable ancient tile legacy. These include exposure to weathering and pollution as well as mechanical stresses and, in some cases, poor tile fastening. The result has been a deterioration in the quality of the artwork. Environmental factors can cause tile degradation: the growth of fungus and bacteria, the deposition of dirt on the tile surface, and the crystallization of salts in the tile body, which can result in fracture [133]. Despite the fact that standard mechanical and chemical cleaning methods have been utilized for cleaning this sort of objects for many years, similar to archaeological bones cleaning, there have only been a very few case studies where laser cleaning has been evaluated for ceramic materials conservation purposes [131][132][133].

Table 2.4 lists the results obtained on archaeological ceramic materials cleaning using different laser systems. Laser-assisted removal of encrustations from pottery sherds and glazed ceramics is most successful when the laser and energy density are chosen carefully. Even at high energy fluence, the excimer laser (248nm) could not entirely remove the last layer of dirt from ceramics and pottery. While the fundamental wavelength of Nd:YAG laser has a high cleaning rate of black deposits from the surface of artifacts, it also has several drawbacks to consider while cleaning these items. Surface yellowing is commonly noticed, and attempts to erase this coloration by increasing the laser power resulted in damage to the artifact's surface texture. For instance, fusing, shattering, or explosion occurs due to the extreme temperature effect and mechanical shockwaves that generate enormous local stresses at the substrate-underlying surface contact. The 2nd (532 nm) and 3rd (355 nm) harmonics of the Nd:YAG laser have been found comparably better for these types of archaeological artifacts, while the fundamental emission (1064 nm) was found as comparatively unsuitable, and the 4th harmonic seemed impractical due to its much lower material removal rates. When the 2nd and 3rd harmonic laser wavelengths were applied on pottery/ceramics, no surface damage or undesirable color change was detected, and dirt seemed to be removed entirely. Still, it was dependent on encrustation and dirt types.

Table 2.4: List of results reported in the literature on archaeological ceramic materials cleaning using different laser systems.

Archaeological ceramic materials cleaned by laser						
Laser	Wave-length	Pulse duration	Cleaning Fluence (Jcm ⁻²)	Problem(s)	Outcome(s) / side effect(s) / discussion	Reference(s)
Nd:YAG	1064 nm	-	1.5 - 9	Pottery coated with hard gray-white encrustation	High irradiation for crust removal and minimal utilization for ceramics; excellent cleaning without damage or color change.	[131]
		-	0.49	Pottery coated with soot mixed with soil residues	The surface appeared very homogeneous and clear after cleaning.	[131]
		-	0.6	Pottery coated with black soot	Better cleaning results were obtained.	[131]
		-	1	Green & blue-glazed outdoor ceramic covered with a black layer of pollutant residues	Although the black encrustation was successfully removed, a little yellowish variation in color was observed.	[132]
		6 ns	0.7	Titles covered with the dirty glazed (blue/ white-colored) surface	Discoloration observed; caused damage to the underlying surface; not able to remove all the superficial dirt.	[133]
		-	1.3	Medieval pottery mug covered by a thin, strong and brittle sinter layer	Moisturizing the surface enhanced cleaning results and cleaning rate; no laser-induced surface side effects were found.	[134]
		-	1.1	A glazed Roman period pot with a lime sinter layer	After laser irradiation, the glaze's glossy appearance was lost.	[134]
		10ns	1.6 – 1.9	Fungi contaminants on ceramic	Most efficient for removing fungi from ceramic surface.	[184]
	532 nm	6 ns	0.2	Titles with the dirty glazed (blue/white-colored) surface	Most effective cleaning; efficiently clean the dirty glazed surface.	[133]
	355 nm	-	0.6 - 0.9	Black layer of pollution residues covers outdoor ceramic in green and blue glazes	There was no damage to the surface or undesired color; the dirt removal seemed complete.	[132]
266 nm	6 ns	0.1	Titles with the dirty glazed (blue/white-colored) surface	The cleaning operation was unsuitable and impractical due to the low material removal rate.	[133]	
Excimer	KrF (248 nm)	-	0.7 – 1.6	Green-glaze and blue-glaze outdoor ceramic covered with a black layer of pollutant residues	The cleansed surface turned yellow because the last layer of debris formed by tiny particles was not entirely removed.	[132]

2.6 Laser based interventions on archaeological Iron Objects

The most typical cause of deterioration in ancient iron artifacts is chemical alteration, not physical depreciation. Most iron artifacts from antiquity are brittle and prone to falling apart when handled. Corrosion occurs when chemicals from various environmental sources combine with iron objects to generate more stable compounds visible as weathering and degradation. The iron objects are replaced by corrosion products (Table 2.5), altering the artifact's physical attributes. When it comes to corrosion products, they are frequently chemically identical to the iron's source material.

Corroded archaeological iron objects are generally fragile and flaky. As a result, corrosion products' chemical and physical characteristics might vary significantly even within a single sample of corrosion products. Many elements influence the results of any cleaning practice; therefore, it is very significant to physicochemically characterize any iron artifact before cleaning to avoid unanticipated damage to the object being cleaned. Laser cleaning results are highly dependent on the material's surface properties. For example, surface roughness has an impact on absorptivity. Rough surfaces absorb more energy compared to smooth ones. It is challenging to clean very rough surfaces with cavities; hence using low-energy pulses and irradiating from many angles can help alleviate this issue. Laser cleaning outcomes may be affected by a variety of circumstances, and even the same laser might provide varied results depending on the material that is being used. Surface structure, color, and porosity have an impact on the cleaning procedure. Additionally, operating parameters must be changed when the thickness of a deposited layer to be cleaned changes. When selecting a laser for surface cleaning prior to the conservation procedure, adequate information on the physicochemical characterization of the iron materials to be treated is essential.

Conservation of iron objects, particularly archaeological iron artifacts, is important to halt degradation. Cleaning, repairing, stabilization, and surface treatment are part of conventional conservation treatment. Iron artifacts require a significant amount of proper cleaning as part of the artifact stabilization process, which is one of the most vital stages in their restoration. Apart from eliminating a possible cause of damage, cleaning an object thoroughly eradicates pollutants. Artifact cleaning processes are the most problematic to control, and the outcomes might be essential for the long-term safeguarding of the object. Additionally, cleaning can be used to prepare a surface for subsequent treatments like coating or rejoining damaged portions. Shattered fragments of an artifact are usually reassembled with the use of various types of adhesives for showcasing to the museum

visitors as a part of repairing. To maintain the stabilization of an iron artifact, it is necessary to eliminate as many corrosion sources as possible. Surface treatment has been considered the final step in restoring iron objects. In this case, the conservators have mostly chosen a protective surface coating that can be placed on the artifact to provide further protection.

Table 2.5: Corrosion products which are usually found in the different heavily corroded archaeological iron objects.

Corrosion products	Chemical name of compounds	Chemical formula	Shades on the iron object surface	Reference(s)
Magnetite	Iron (II, III) oxide	Fe ₃ O ₄	Blackish	[185][186][187][188][189][190][191][192][19][137]
Hematite	Iron (III) oxide	α-Fe ₂ O ₃	Bright reddish	[185][191][19][138]
Maghemite	Iron (III) oxide	γ-Fe ₂ O ₃	Dark brownish	[188]
Limonite	Iron (III)oxyhydroxide	FeOOH	Yellowish-Brownish/Orangish	[185]
Goethite	Iron (III)oxyhydroxide	α-FeOOH	Reddish /Brownish / Yellowish	[63][185][193][194][186][188][189][190][191]
Akaganeite	Iron (III)oxyhydroxide	β-FeOOH	Orangish / Red-brownish	[63][185][188][193][194][186][195][189][196]
Lepidocrocite	Iron (III)oxyhydroxide	γ-FeOOH	Orangish / Reddish	[185][193][194][189][191]
Rozenite	Iron sulphate tetrahydrate	FeSO ₄ ·4H ₂ O	Greenish	[185][197]
Siderotil	Iron sulphate pentahydrate	FeSO ₄ ·5H ₂ O	Whitish	[185][197]
Melanterite	Iron sulphate heptahydrate	FeSO ₄ ·7H ₂ O	Bluish-greenish	[185][188]
Siderite	Iron (II) carbonate	FeCO ₃	Greyish/Yellowish /Brownish	[185]
Pyrite	Iron (II) disulfide	FeS ₂	Yellowish	[185][197]
Butlerite	Iron hydroxide sulphate dihydrate	Fe(OH)SO ₄ ·2H ₂ O	Orangish	[185][197]
Natrojarosite	Iron sodium hydroxide sulphate	Fe ₃ Na(OH) ₆ (SO ₄) ₂	Bluish/Yellow-Brownish	[185][138][197]
Jarosite	Iron potassium hydroxide sulphate	Fe ₃ K(OH) ₆ (SO ₄) ₂	Yellow-Brownish	[185]
Vivianite	Iron (II)orthophosphate	Fe ₃ (PO ₄) ₂ ·8H ₂ O	Whitish/Bluish	[185]

Figure 2.4 shows a typical corroded iron object, which is contains a variety of corrosion products and contaminants from the environment, subjected to this thesis work.



Fig. 2.4: A typical corroded archaeological iron object found in *Sierra de Atapuerca* (Spain)

When archaeological iron objects are buried, they are often shielded by an extremely thick crust layer that contains soil deposits from the earth and iron corrosion products, the most frequent of which are goethite (α -FeOOH) and magnetite (Fe_3O_4). They generally have developed over the time the iron objects were buried [19]. The conservators are working to eliminate the majority of these pollutants and unveil the original artifact's surface that is being conserved and restored. The plasma generated during laser cleaning intervention absorbs the majority of the energy contained in the laser irradiation pulses, resulting in a reduction in the cleaning efficiency. It is also necessary to exercise caution if it is to be avoided those issues with surface dryness and coloring of the rust arise and they must be avoided. There is also the possibility that any iron oxide that forms would melt, causing irreversible damage. Such issues can be avoided by thoroughly analyzing the implemented fluence values and the parameters applied to clean the specific iron objects. This process makes it possible to treat archaeological iron artifacts with a better inherent value after the procedure has been mastered. However, various laser systems have different effects on iron artifacts when cleaning them. For example, the TEA CO_2 laser outperforms the Nd:YAG when eliminating organic contaminants off iron artifact surfaces. But high mid-infrared beam reflection is one of iron's unique features. It is theoretically possible to expose iron objects to high mid-infrared laser beam power levels without damaging them. At high enough fluences, TEA CO_2 laser pulses can damage surfaces even when employed in typical cleaning procedures [162][198]. Laser emission at longer wavelengths for iron object cleaning to remove corrosion products may only partially remove the corrosion layers, as observed by some case studies [135][63]. Although the effects of using wetting agents (i.e., irradiation conditions) were not in the scope of this paper, it has been observed that the QS Nd:YAG laser at the different wavelengths (preferably, 1064 and 532 nm) with a wide range of wetting agents failed to remove corrosion completely from archaeological iron materials [135][63].

Most investigators evaluated the feasibility of laser-based interventions on archaeological iron artifacts and noted the occurrence of darkening on the iron surface [63][139][199]. The primary source of darkening was the transition of yellowish-brownish goethite (FeOOH) into blackish magnetite (Fe_3O_4), the principal component of iron corrosion; this happened at all wavelengths and pulse durations investigated. However, rust and corrosion removal proved both time-consuming and impractical in this instance. Many studies suggested that the coating of magnetite that appears on the surface of iron items as a consequence of irradiation (i.e., darkening) might help preserve them for the long term, even if darkening has a significant impact on the appearance of laser-cleaned iron objects [135][19][200]. It is because magnetite is a very stable oxide that can safeguard the underlying iron from additional corrosion caused by the environment. Moreover, using laser cleaning to eliminate rust while simultaneously increasing the corrosion resistance of iron objects is a common industrial practice nowadays [101]. Because weathering in ancient iron artifacts is ongoing and demands extremely low relative humidity to be stopped, laser irradiation has not been employed extensively in conservation so far; thus, further work is necessary. Table 2.6 summarizes the laser cleaning studies on different archaeological iron objects.

Table 2.6: A list of published results on the cleaning of archaeological iron artifacts using different laser systems.

Archaeological iron objects cleaned by laser						
Laser	Wave-length	Pulse duration	Cleaning Fluence (Jcm^{-2})	Problem(s)	Outcomes / side effect(s) / discussion	Reference(s)
Nd:YAG	1064 nm	40 - 120 μs	8	Deeply corroded Roman sword	Phase transition is detected; this results in the passivation and consolidation of the surface of a badly corroded Roman sword, which remains corrosion-free after 15 years.	[137]
		8 ns	0.4–1.5	Corroded iron objects with soil particles	Not adequate for layer-by-layer rust removal.	[63]
		8 ns	0.175	Corroded iron alloy armor	Damage and melting to the underlying metal.	[136]
		8 ns	2.6	Ironwork in fine-grained white silica sand with various ground conditions	Not effective; partial removal of corrosion; darkening phenomena observed.	[139]
		8 ns	0.14	Corroded iron artifacts	Chemical or mechanical cleaning is ineffective; laser irradiation specifically eliminates selective corrosion products.	[147]
		8 ns	1.4	Corroded iron objects subjected to natural weathering	Removed corrosion layer; the surface morphology seems harsher and is more susceptible to attack by external factors.	[137]
		~ 10 ns	0.4 - 2	Corroded nails and hand tools	This method cannot remove corrosion (burial encrustation and rust); melting and darkening have been detected.	[135]
		120 ns	1.5	Iron samples subjected to natural weathering in outdoor conditions	There was localized micro melting and partial alteration of the remnant mineral regions on the surface.	[137]
		150 ps	0.17	Corroded iron object	Effective removal; no darkening and melting observed.	[140]
	150 ps	1	Corroded archaeological iron objects	Not removing the crust of corrosion good; color changes.	[138]	
	532 nm	8 ns	0.09	Corroded iron alloy European scale armor	Reduced the corrosive effects of ferrous metals while protecting the alloy below.	[136]
		~ 10 ns	0.4 - 2	Corroded nails and hand tools	Corrosion removal was not fully possible; darkening observed.	[135]
	Er:YAG	2940 nm	100 μs	0.1–1.7	Corroded iron belt pad	Partially removed corrosion (goethite and lepidocrocite).
CO ₂	10.6 μm	100 ns	8	Corroded nails and hand tools	Partial removal (burial encrustation and iron oxides) achieved.	[135]
		10 μs	0.19 to 0.66	Corroded iron artifacts	Selectively eliminated corrosion products; however, it was not as successful as chemical or mechanical cleaning.	[147]
Ti: Sapphire	800 nm	100 fs	1.3–11.5	Corroded iron belt pad with soil particles & organic materials	Effective corrosion removal (goethite and lepidocrocite), but very slow and inconvenient.	[63]

2.7 Discussion

Researchers tried out the different laser cleaning options for different categories of dirt (pollutants, contaminants, dust, staining, encrustations, etc.) on several types of archaeological materials (bones, stones, ceramics, and iron objects) under the impact of different types of lasers (Nd:YAG fundamental, 2nd, 3rd and 4th harmonic, Nd:YVO₄, Er:YAG, excimer, CO₂ and Ti:Sapphire), that were commercially available. A debate is still going on about how effective laser cleaning is! Each type of contamination and material's performance varies according to the type of equipment employed and the laser's wavelength and pulse duration. Laser cleaning outcomes are highly dependent on the laser beam, sample, and laser-sample interaction. For example, some findings were encouraging for one type of laser system while others were discouraging for another type of laser system, even using the same sample, contaminations, and fluence values. On the other side, spectacular outcomes can be obtained with a different type of laser system when applying similar samples and similar types of dirt with different fluence values. Therefore, irradiance (laser pulse peak power density) [201] values might be taken as an essential reference in the future, instead of fluence (pulse energy density) for laser threshold cleaning purposes, since it is independent of different laser devices and emission characteristics (it particularly incorporates pulse duration); thus it may serve as a more universal reference for a potential variety of laser irradiation treatments. Nevertheless, although irradiance levels influence the processes of incubation and energy accumulation, involved specially in thermomechanical damage, the latter phenomena must be carefully considered in relation to the effects of pulse-to-pulse overlap with respect to their spatial and time distribution.

The findings of some of these studies were promising, while some laser treatments proved highly detrimental to the preservation of the objects. Several observations prompt researchers to conduct microscopic and spectroscopic research to understand occurrences better. When Nd:YAG lasers are used at their fundamental wavelength, the heat action causes cracking and melting of archaeological materials, which may be prevented with precise fluence control. However, a change in coloring has the worst negative impact on the samples' original look and aesthetic value. Most authors studied the causes or at least the material on which these occurrences developed while analyzing these unsuccessful laser interventions. Color changes and heat incubations were observed mainly on some materials based on the wavelengths employed. The infrared Nd:YAG laser produces a yellowish/greyish surface alteration for stone and iron artifacts. If patina may be discovered on stone and bone as the main reason for being discolored, the same rationale does not apply to ceramics or iron objects, where aging does not induce yellowing. It appears that

this discoloration is not generated by a change in the substance, but rather a coating of foreign materials/dirt that has been redeposited or is still deposited on the surface of the material.

As numerous authors have mentioned, the advanced sophisticated techniques and different methodical approaches have not yet been able to identify the leading cause of discoloration upon laser cleaning. Even it is mentionable from the findings of this manuscript that recently developed ultrafast laser systems have not been applied widely enough to identify the best possible outcomes. Femtosecond laser pulses fundamentally change laser-material interaction processes because of their ultrashort irradiation durations and high intensity [105]. They can generate a powerful plasma capable of ablating certain target materials from a specific target materials substrate region, which may have consequences for cleaning complex artifacts, such as fragile bone surfaces. Thermal damage (microcracks and heat-affected zone) is also considerably decreased because of the low heat conduction via lattices during the fs period due to the high intensity. The fs laser ablation method is deterministic and reproducible, practically allowing for cleaning any archaeological artifacts with any contaminants. Due to their high controllability and ability to be applied selectively, newly emerged ultrafast laser systems could be used in the future to achieve more effective and safer cleaning of archaeological artifacts and safeguard their surface details.

Further cleaning with a different type of laser, such as a 2nd harmonic Nd:YAG, can eliminate discoloration concerns and restore the artifact's natural look. To prevent such undesirable coloring, the application of IR and UV laser irradiation in sequential and synchronous mode may be worth considering in the future, as they can aid in achieving the ideal success rate for laser cleaning [156]. Infrared Nd:YAG laser cleaning removed pollution encrustation perfectly from stone substrates with an extreme yellowing appearance, leaving behind no visible surface damage, hence the application of third harmonic Nd:YAG assisted in entirely removing the yellowing discoloration, leaving a surface that is perhaps too white when compared to typical cleaning procedures. It is particularly noticeable on stone substrates with pollution encrustations [160]. Another thing to consider is the possibility that a photochemical change might explain the color variations seen on a few ceramic materials, which often include a greying or blackening. When the laser irradiates iron objects, the metallic oxides in the artifacts also change color. A valence state shift (oxidation or reduction) of the iron object compositions might be the cause of this color change. Further research is needed into how laser-assisted cleaning affects

archaeological materials, what kinds of lasers are most suited to remove dirt layers, and how various operational parameters may be optimized.

2.8 Conclusions

Archaeological materials were generally observed not to be successfully cleaned and intervened until the 90s with the laser as expected by the conservators-restorers. In most cases, removing dirt and contaminants was not self-limiting, and thermal side effects such as darkening and micro-melting could not be avoided due to the drawbacks of the pulsed laser system's availability. For archaeological bones and stones, good results were usually obtained with the newly emerged ultrashort laser pulse (<sub-ns) system compared with the long-pulsed laser systems reducing thermal side effects. In recent years, archaeological material cleaning using ultrafast fs laser pulses appears to be a growing and promising technique. Further intervention on the laser-sample interaction by fs ultrafast laser on varied laser pulse durations and emission wavelengths is necessary for future conservation practice.

Thinner soiling layers on the stone surface are best treated with UV-favored ablation, whereas thicker and more inhomogeneous crusts are best treated with an IR laser beam (which is well absorbed by the majority of the crust). In order to better understand the substrate damage related to the laser cleaning application, further study into the mechanism of laser-material interaction, specifically absorption and relaxation, is required. Additionally, the long-term burying of archaeological materials in an interior setting (such as flints) alters the material's chromatic and visual appearance; no laser application has been found on those so far, which may have immediate attention in order to handle by laser cleaning.

In the case of archaeological iron objects, lasers were only able to partially remove corrosion; therefore, wetting agents might be essential in order to get the best potential results in cleaning. The darkening of the iron surface was linked to the change of goethite to magnetite, although this was not the only explanation. However, some authors suggest that the magnetite coating on the surface of iron objects protects the underlying iron from further corrosion and should be regarded as helpful for their long-term preservation. There should be in-depth discussion and further investigation of this topic using the latest laser technology among the broader conservation community as this is an intriguing proposal.

According to published reports, cleaning ceramic and iron objects using lasers has had some success. It was found that the presence of organic material directly under the patina layer negatively impacted the results of laser cleaning. Heat incubation [107] produced damage to the substrate layer as a result of laser-sample interaction. Several unique case studies revealed that the Nd:YAG laser performed well with no biological stuff beneath it when cleaning biodeteriorations. There is still more work to be done to determine whether or not the laser system can be used to clean other sorts of archaeological artifacts, despite the fact that a case study showed effective cleaning of archaeological material. Even though it's likely to be harmful, this has to be investigated further.

CHAPTER: 3

EXPERIMENTAL TECHNIQUES

CHAPTER THREE

EXPERIMENTAL TECHNIQUES

Summary: This chapter summarizes the experimental information of five different laser techniques that have been employed throughout this thesis investigation: femtosecond (fs) and sub-nanosecond pulsed laser technology with an emission wavelength in the n-IR regimes (1030nm, 1064 nm), visible green regime (515nm) and Ultraviolet (343nm, 355nm) regimes. The burst pulse and laser beam scan mode have also been discussed, along with the irradiation parameters utilized to define the laser cleaning protocol. Material characterization techniques, namely Optical Microscopy (OM), Infrared (IR) Thermal Cameras, Scanning Electron Microscopy with Energy Dispersive X-ray Spectrometry (SEM-EDS), X-ray Photoelectron Spectroscopy (XPS), Fourier Transform Infrared Spectroscopy (FTIR), and X-ray Diffractometry (XRD) also summarized those had been employed in different case studies throughout the different chapter of this thesis.

3.1 Laser systems and parameters

A total of five distinct laser systems have been used in this thesis for laser interventions, three of which were ultrafast fs pulsed lasers, while the other two were sub-ns pulsed lasers.

3.1.1 Ultrafast femtosecond (fs) lasers

The ultrafast fs laser system was employed for a series of irradiation tests to ascertain the effect of the different laser emission parameters on the artifacts' contamination and substrate. The irradiation was carried out utilizing a Carbide model (CB3-40W+CBM03-2H-3H, Light Conversion, Lithuania) diode pumped Yb:KGW solid-state fs laser, with a linearly polarized output, is coupled with a galvanometric mirror configuration (Direct Machining Control, UAB, Lithuania). This laser system provides three different harmonics: n-IR laser irradiation at a fundamental wavelength of 1030 nm, visible green laser irradiation at the 2nd harmonic of 515 nm and UV laser emission at the 3rd harmonic of 343nm. This laser technology is provided with a pulse on demand mechanism, known as a pulse peak divider (PPD). The pulse frequency can be adjusted between 1 Hz and 1 MHz,

using an appropriate resonator frequency and PPD value. Figure 3.1 shows a scheme of the usual working procedure with this laser.

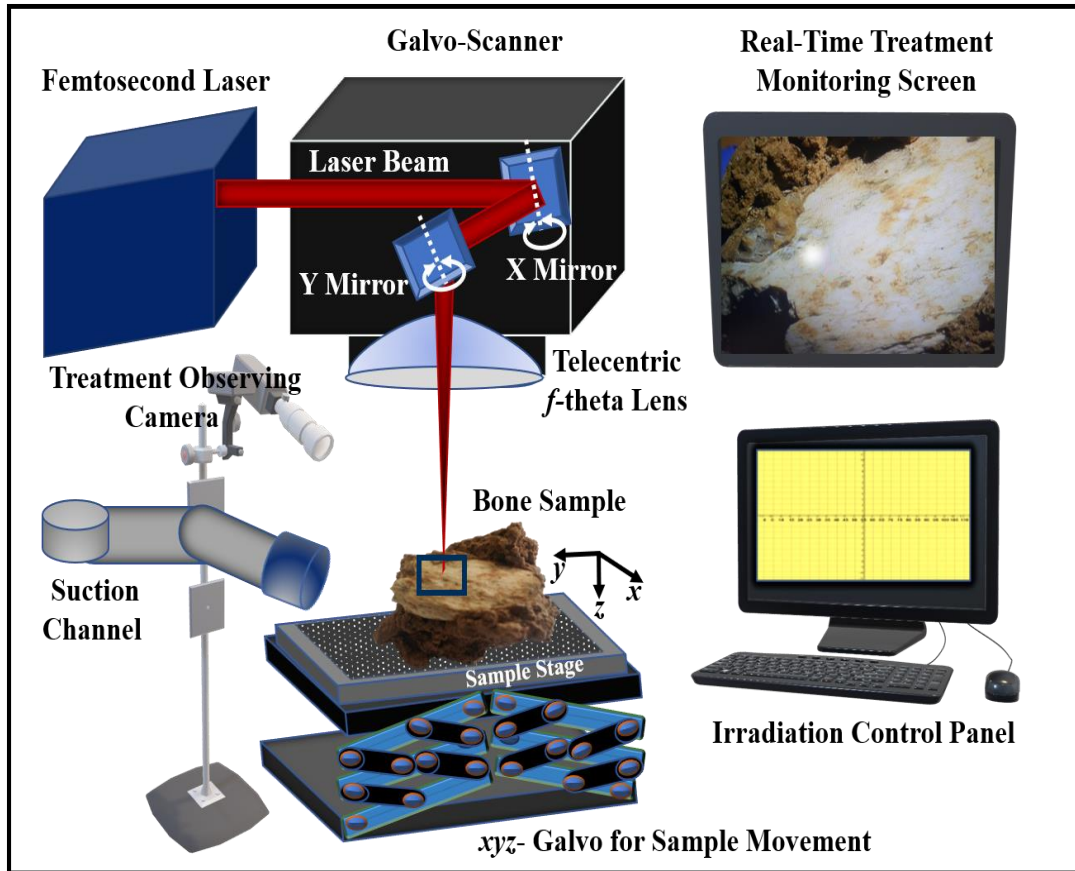


Fig. 3.1: Illustration of the principal arrangement of the experimental setup where fs laser beam directed through XY-mirrors controlled by galvo-scanner and later telecentric f -theta lens to sample stage following xyz - coordinate system. The suction channel is for collecting debris after laser cleaning, and the treatment observing camera aid to watch the real-time treatment by a wall-mounted monitoring screen. The computer is employed for controlling different irradiation parameters by using CAD-type software.

The three distinct fs radiations were used in this thesis, and their typical emission characteristics are shown in Table 3.1. The root-mean-square variation in pulse-to-pulse energy stability over 24 hours for all three laser systems is less than 0.5 percent.

Table 3.1: Characteristic emission of three different fs lasers and two different sub-ns lasers employed for the present study. Values are specified for the pulse emission wavelength λ , pulse duration (τ), average power (P), pulse repetition rate (f), maximum pulse energy E_p , and beam diameter D_b at full-width half-maximum (FWHM) [202], applying the $1/e^2$ criterion for a Gaussian beam distribution.

Laser(s) → ↓ Parameter(s)	Femtosecond n-IR	Femtosecond Visible Green	Femtosecond UV	Sub-nanosecond n-IR	Sub-nanosecond UV
Wavelength λ	1030 nm \pm 10 nm	515 nm \pm 3 nm	343 nm \pm 3 nm	1064 nm	355 nm
Pulse duration τ	228 fs	249 fs	238 fs	800 ps	300 ps
Average power P	40 W	20 W	9.33 W	8 W	3 W
Resonator pulse repetition rate f	200 kHz – 1 MHz	200 kHz – 1 MHz	200 kHz – 1 MHz	200 – 800 kHz	200 – 800 kHz
Maximum pulse energy E_p	200 μ J	100 μ J	46.6 μ J	40 μ J	15 μ J
Beam diameter D_b	100 μ m	50 μ m	30 μ m	79 μ m	31.4 μ m

3.1.2 Sub-nanosecond (sub-ns) lasers

The two different sub-ns pulsed lasers utilized in this thesis work are as follows:

- i. A sub-ns near-infrared (n-IR) laser (PowerLine Pico 10-1064, ROFIN-SINAR Laser GmbH, Germany) irradiating at fundamental harmonic with the wavelength of 1064 nm, a pulse duration of 800 ps, a maximum output power of 8W, and a maximum output pulse energy of 40 μ J, coupled with a galvanometer mirror system. The pulse repetition rate can be selected from 200 kHz to 800 kHz for this laser system. The laser system is entirely compact and air-cooled.
- ii. A sub-ns UV laser (PowerLine Pico 10-355, ROFIN-SINAR Laser GmbH, Germany) coupled with a galvanometer mirror system, irradiating at fundamental harmonic with the wavelength of 355 nm, a pulse duration of 300 ps, a maximum output power of 3W, and a maximum output pulse energy of 15 μ J. The pulse repetition rate can be selected from 200 kHz to 800 kHz. The laser system is also air-cooled and entirely compact.

The characteristic emission information of both sub-ns lasers subjected to this study is presented in Table 3.1.

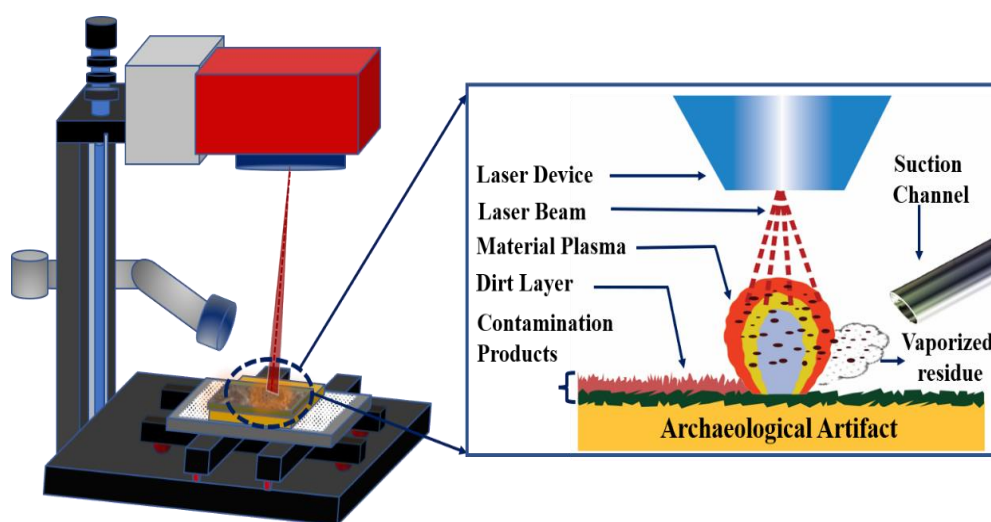


Fig. 3.2: Illustration of the sub-ns laser cleaning apparatus used for the present study (left), where the laser x-y scanner head is shown above the archaeological artifact sample and a fume extraction device. The right inset illustrates the ideal sample behavior under laser irradiation, where the contaminant layer is removed, while the protective patina (green) is preserved.

Figure 3.2 depicts the sub-ns laser setup utilized in this thesis study. Additionally, it gives a simplified illustration of the ideal physical processes that occur when a laser beam is focused on an archaeological artifact that has been contaminated. Plasma generation and subsequent shockwaves aid in removing the contaminated layer as a result of laser ablation [48]. The right inset of the Fig. 3.2 provides a visual representation of these intricate occurrences. When using a laser with a fixed pulse width, selecting an adequate power output and pulse repetition rate permits the removal of contaminants while simultaneously preventing damage to the patina layer and the substrate underneath it [27].

3.2 Laser pulse scanning modes

Two different scanning approach has been applied to this research. They are as follows:

3.2.1 Burst pulse mode

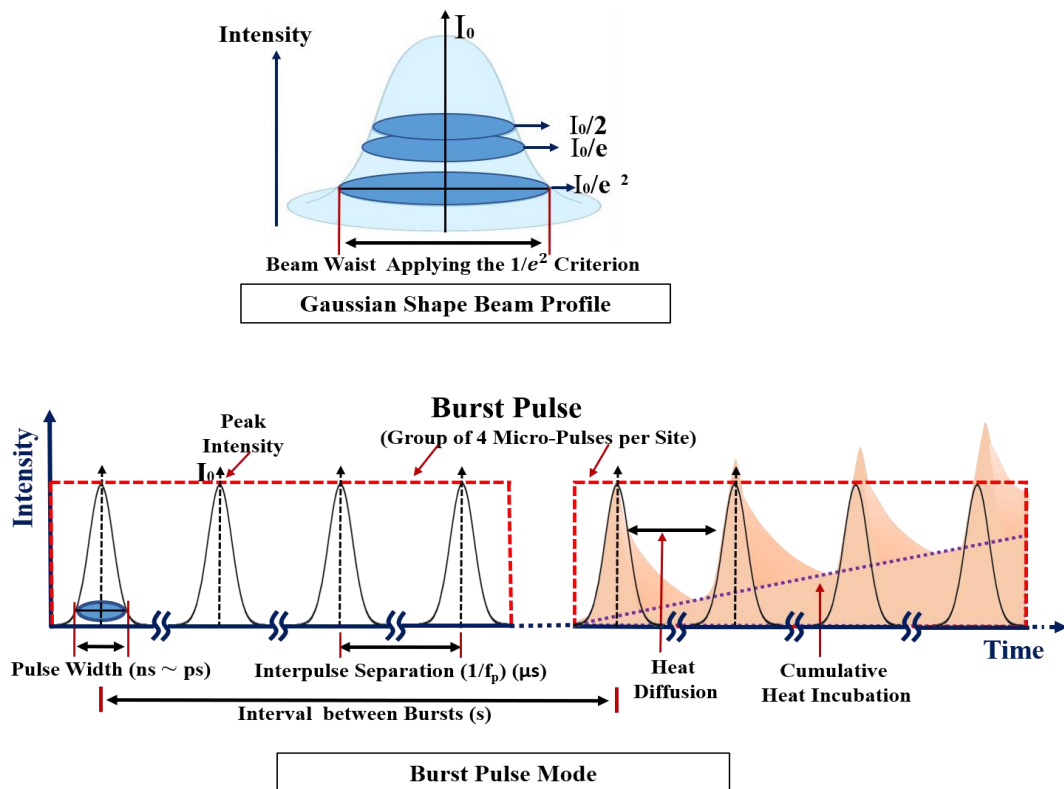


Fig. 3.3: Schematic representation of the burst pulse mode method of laser. The upper inset depicts the connection between laser intensity and various definitions of beam waist for a Gaussian beam profile, emphasizing the $1/e^2$ criteria utilized in this investigation [202]. The lower inset

illustrations depict the laser output intensity at a specific place as a function of time for the burst pulse mode used to control thermal damage [203][204]. On the left, the lower inset visually depicts the pulse width and pulse-to-pulse (interpulse) spacing. On the right, it illustrates how thermal incubation occurs during the subsequent pulse irradiation procedure; indicated between bursts is a somewhat longer time interval that depends on the geometry chosen for the laser treatment.

To selectively irradiate the samples' surface around specified localized locations, a burst pulse mode approach (Fig. 3.3) [106][51] offered by the computer CAD-like program controlling the laser output and integrated galvanometer mirror scanning head was utilized. In burst mode, the laser performs spot-by-spot scanning, with the scanning settings adjustable. In each preselected point on the sample surface, a laser system designed to operate in burst mode generates a burst (i.e., a series of a defined number of pulses) with a high intra-burst repetition rate. A single burst is visible at a specific position, where this specific mode allows for the irradiation of specific areas while controlling the laser emission parameters, the distance between burst positions, the energy of each individual burst pulse, and the number of pulses in a burst repeated over the same irradiated position (Fig. 3.3, lower inset). The latter controls thermal incubation, or the buildup of energy input as a function of time into a specific region of the sample.

In the top inset of Fig. 3.3, the relationship between laser intensity and beam energy distribution is depicted to assist explain how beam waist is established here. The bottom inset depicts the burst pulse mode employed in this investigation, in which successive groups (bursts) of pulses irradiate the material surface at a defined location and under precise circumstances to prevent thermally damaging the substrate while eliminating contaminants. It permits the surface to sufficiently cool between burst pulse sequences [106].

3.2.2 Continuous beam scanning mode

The continuous beam scanning approach (Fig. 3.4) [205], which was enabled by the computer-aided design (CAD)-like software, that controlled the laser output and incorporated galvanometer mirror scanner applied to selectively irradiate the specified localized sample surface. In beam scan mode, a beam is scanned over the surface of a fixed sample, so that the beam scan speed and line-to-line distance must be specified in the CAD-like software end. The distance among the beam scan in transverse line (i.e., distance between pulses) is controllable by fine-tuning the laser beam scanning velocity; the whole

line length and the beam movement velocity over the sample controlled by the XY-Galvanometer scanner. Analyses of mechanical damage, physicochemical changes and heat buildup in the substrate studied the effect of laser beam scanning mode on the efficiency of material removal. While in the beam scanning mode, the investigated parameters cover the varied scanning speed, i.e., the amount of laser spot overlap in a single line scan, focus position and overlapped line number.

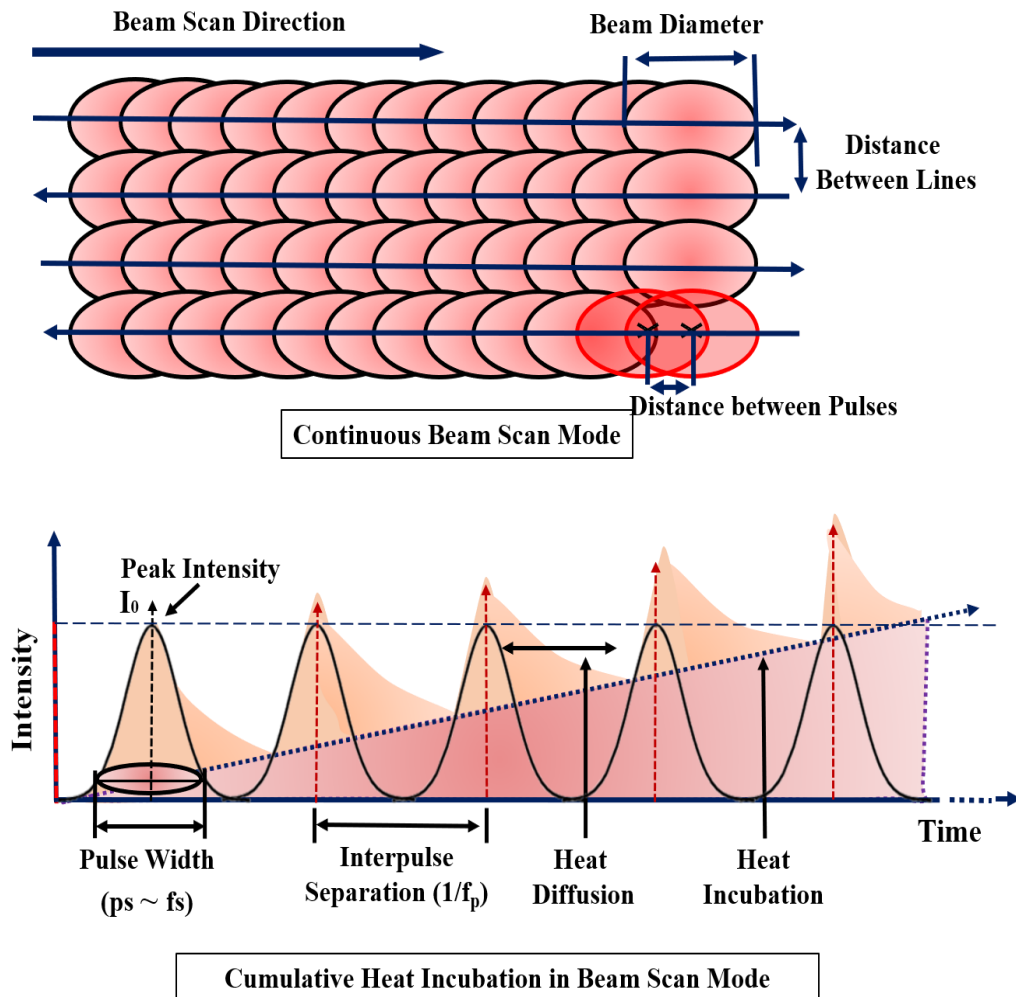


Fig. 3.4: Schematic representation of laser beam scan mode method. The upper inset illustrates the laser beam scanning pulses utilized in this investigation. The lower inset drawing depicts the laser intensity output as a function of time for the beam scan mode employed in a given position, where cumulative heat incubation is presented. It graphically illustrates the pulse width and pulse-to-pulse (interpulse) separation, as well as how thermal incubation takes place along the consecutive pulse irradiation process.

The beam scan mode utilized in this study is depicted in Fig. 3.4. The top image shows a scheme of the laser beam scanning pulse mode. The lower inset illustrates the beam scan mode employed in this work, in which pulses are scanned across the material surface at a specified position in a given time, and under specific circumstances to minimize thermal damage to the substrate while eliminating contaminants.

3.3 Irradiation parameters that utilized to define the laser cleaning protocol

In the case of the Gaussian laser beam profile, the definition of the beam spot size is based on the distance (radius) from the $(\frac{1}{e^2})$ point to the centre point of maximum irradiance [202]. According to ISO 21254-1:2011 standard, the effective area of a laser spot (A_{spot}) is an essential metric used to define the damage threshold of optical materials [206], which can be calculated as:

$$A_{spot} = \pi r_0^2$$

An expression of the nominal power (P) emission over time expressed in Watts, i.e., total amount of laser energy delivered divided by the duration of the laser exposure. On the other hand, a measurement of the total amount of time that a pulse is emitted, known as pulse duration (τ), also called pulse width or pulse length; whereas the number of laser pulses per second of the laser that reach the sample surface, known as the repetition rate, or effective frequency (f_p), usually expressed in Hertz (Hz).

It is worth mentioning that two different types of laser systems (i.e., sub-ns and fs lasers) have been utilized in this thesis came up with two different types of emission characteristics, including the generation of frequency (f_p). In the case of the sub-ns lasers, the frequency is the resonator frequency which directly applied to the cleaning process; on the other side, the resonating frequency is not the final frequency for the case of fs laser; it is the effective frequency after applying the PPD which applied on the cleaning process. In all the cases, energy per pulse (E_{pulse}) is fixed by the resonator frequency. For instance, in the case of the fs laser, it is possible to select a resonator frequency of 200 kHz, but PPD suppresses a percentage of pulses to reduce the effective pulse repetition rate or frequency to values that can be on the order of 1 kHz to 200 kHz. The PPD index changes the output frequency, but never the E_{pulse} and, consequently, neither the peak power.

The scanning system of a laser technology determines the maximum scan speed (v_{laser}) that may be achieved by the system. The speed is expressed in metrics per second. It gives an

account of the rate at which both mirrors of the scanning system may move, as well as the rate at which they can deflect the beam. The actual scan angle has a direct impact on the device's maximum scanning speed. Generally, the higher the scan speed, the better the quality and uniformity of the laser beam.

Distance between scan lines (δ_{lines}) and the length of the line scanned by the laser, denoted as l_{line} are another two parameters that have to be controlled in the definition of the scanning protocol.

3.3.1 Irradiance for a single laser pulse

The overall optical energy content of a pulse is referred to as the 'pulse energy', which is just the integral of the optical power over the pulse's duration. On the other hand, pulse energy is produced by temporally integrating the power.

$$E_{pulse} (Or, E_p) = \frac{P}{f_p}$$

When it comes to laser pulse peak power, the following equation expresses how pulse energy and pulse duration interact:

$$P_{peak} = \frac{E_{pulse}}{\tau}$$

Therefore, the fluence (F_{pulse}) is defined as the energy in a pulse divided by the area in which it illuminates:

$$F_{pulse} = \frac{E_{pulse}}{A_{spot}}$$

The irradiance (I_{pulse}) is calculated by dividing the power by the surface area it illuminates. This is an important attribute to understand since it provides information on the pulse's overall energy and its spatial and temporal distribution [207]. The laser light may then be utilised to see how a certain substance responds.

$$I_{pulse} = \frac{E_{pulse}}{\tau A_{spot}} = \frac{F_{pulse}}{\tau}$$

The equation shows the average value of the laser irradiance in time and space within each pulse. Fluence and irradiance value are proportional if we do not modify the pulse duration.

3.3.2 Energy distribution of the Gaussian laser beam profile

Irradiation on the samples, in both fs and sub-ns laser sources, was performed in ambient air in this thesis. The beam impinged perpendicularly onto the target surface, placed on a xy- laser scanner translation stage, z-axis was perpendicular to the sample surface, which was controlled manually by moving the xy- stage using a movement screw. The waist diameter of the laser beam ($1/e^2$ criterium for a Gaussian beam distribution) in all laser systems was approximately deduced following the D^2 -method proposed by Liu [202] (Fig. 3.5).

Liu's method is a simple and straightforward experimental technique for determining the fluence ablation threshold based on measurements of the sizes of induced alterations at different irradiation energy, without considering the beam profile. This approach is based on the assumption of a Gaussian laser beam profile, where F_{pulse} and I_{pulse} are the average values; it is essential to keep in mind that the value in the center of the spot is twice as high as the value on average [208]. The distribution of energy in the beam may be written down mathematically as follows:

$$F(r) = F_0 \exp\left[-2\left(\frac{r}{r_0}\right)^2\right] = 2 F_{pulse} \exp\left[-2\left(\frac{r}{r_0}\right)^2\right]$$

where $F(r)$ represents the local fluence at a certain radial point, F_0 represents the peak fluence value, and $2r_0$ represents the beam spot diameter at $\frac{1}{e^2}$ criterium of the peak value [208].

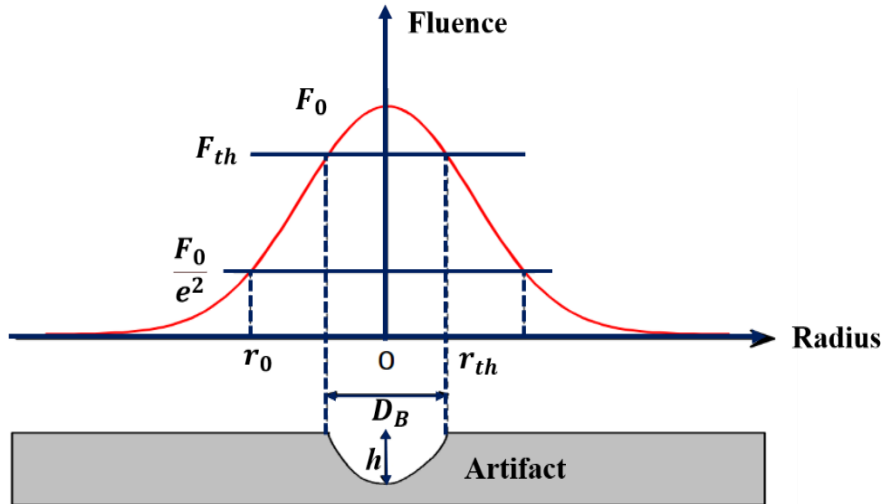


Fig.3.5: Principles of laser ablation with $\frac{1}{e^2}$ criterium for a Gaussian beam distribution profile.

Due to the variations in experimental setups and irradiation techniques, the energy distribution throughout the target surface was calculated in all laser systems to compare the different laser domains. To do this, it was essential to estimate the pulse overlap in both the 'x' (horizontal scanning direction overlap) and 'y' (lateral overlap between adjacent laser trajectories) directions, as well as the cumulative energy deposited by a Gaussian beam running over the surface in the manner seen in the top image in Fig.3.4.

It is essential to keep in mind that the laser emission parameters are being taken into consideration in these calculations. In general, we should consider the values of the energy absorbed by the surface of the material. This might provide an explanation for some of the impacts that we have seen, such as the fact that the laser treatments change depending on the incidence angle that is used.

3.3.3 Irradiance for burst pulse mode

In burst pulse mode, we apply a set number of pulses N to the same location rather than shifting the sample. The time between two pulses: $\Delta t_{pulses}=1/f_p$; hence, the cumulative fluence is considered as:

$$F_{total} = N F_{pulse}$$

But the surface absorption shifts during the burst pulse procedure, and as a direct result, the effects of each unique pulse are distinct at every stage of the treatment. On the other hand, the value of total F_{pulse} by itself is not a useful parameter in the burst pulse method that may be utilised to specify a particular treatment because the time required to apply these N pulses is also relevant. The final effect is entirely different following the number of pulses in a burst and their application mechanism.

3.3.4 Irradiance for beam scan mode [209]

Laser treatments are often required to be carried out throughout a region or the complete surface. Laser beam scanning the surface of the sample while the laser is coupled to a galvanometric mirror system is one of the most widely used methods. In beam scanning, the surface is scanned with successive lines that are separated by a distance (δ_{lines}), but the irradiated target stays in the same place during the process, considered to be fixed. In this instance, the laser is scanning a single line that is lengthwise l_{line} , that verifies $l_{line} \gg r_0$ along the x-axis.

The laser beam spot can scan the specified surface either line by line in the same direction (this type of scanning is referred to as unidirectional scanning), or it can meander around the surface, alternating the direction it started in with the opposite direction (meandering bidirectional). It is essential to determine which method is most effective for scanning the surface, while also taking into consideration other characteristics such as the scanning speed or repetition rate, as well as the acceleration and deceleration of the galvanometric mirrors. Because incubation processes can cause temperature changes between the beginning and end of each line, unidirectional beam scanning can cause these temperature disparities, which in turn result in distinct surface alterations along the line. However, the bidirectional scanning method causes incubation at both ends of the line. This is due to the fact that the beginning of each line is located closer to the end of the line that came before it.

The laser follows a line initially when doing beam scanning. The spacing between the centres of two successive pulses is critical in this approach. This indicates the area in which two pulses cross over one another. There is a $\frac{1}{f_p}$ interval between two pulses. In this line, the ratio between scanning speed (v_{laser}), and pulse repetition rate (f_p) gives the distance between the centre of two consecutive pulses:

$$\delta_{pulses} = \frac{v_{laser}}{f_p}$$

Due to its Gaussian profile, this distance determines how the beam's energy is distributed throughout its path of travel. For varied δ_{pulses}/r_0 ratios, the fluence distributions are illustrated in Fig. 3.6, with r_0 being the beam spot radius. The energy distribution along the scanned line can be considered uniform along the x-axis when $\delta_{pulses} / r_0 < 0.9$. That difference is less than 0.2 % if the threshold is set at 0.8. A Gaussian distribution may also be seen along the y- axis, which is the perpendicular direction.

In this thesis work, the treatments that have been experimented are always with $\delta_{pulses} / r_0 < 0.75$, or equivalent. Hence, the maximum speed that can be used to obtain a uniform treatment is:

$$(v_{laser})_{max} = 0.75 f_p r_0$$

When processing parameters are used to achieve uniform energy distribution in the homogeneous region, the maximum accumulated energy fluence that is reached at the centre of the scanned line can be calculated using the following expression:

$$F_{centre1D} = 1.588 \frac{\pi r_0}{2 \delta_{pulses}} F_{pulse}$$

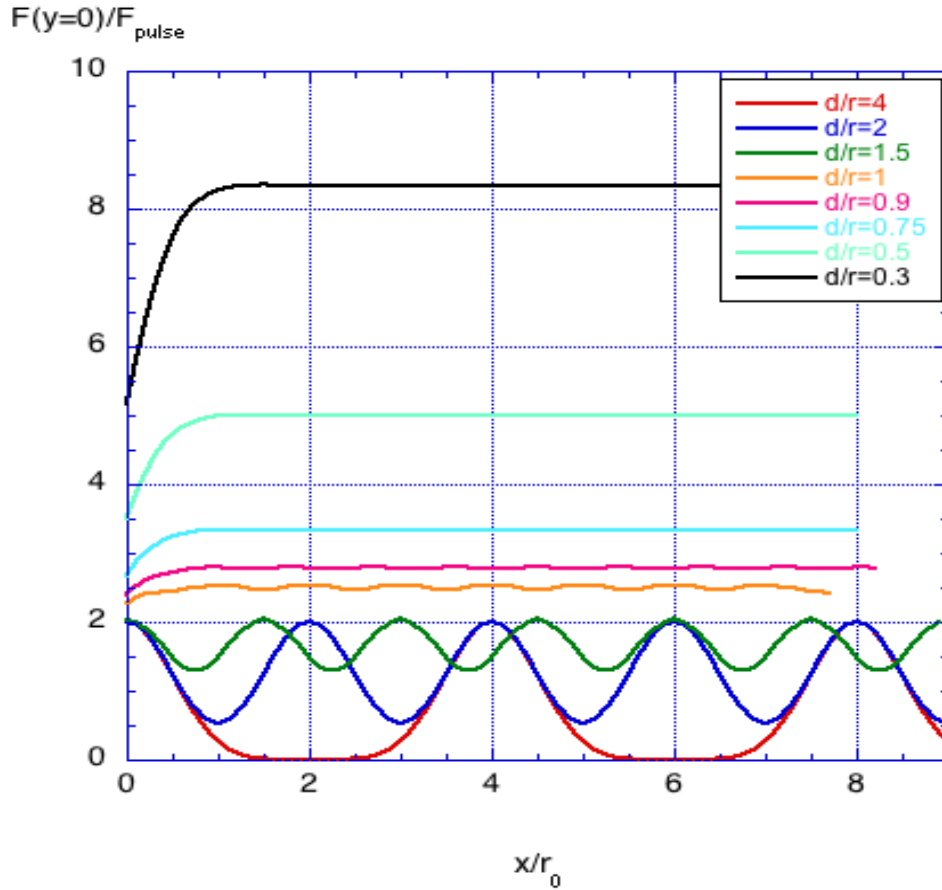


Fig 3.6: Uniform energy distribution along the scanning direction in the center of the laser processed line depending on the ratio of δ_{pulses}/r_0 [209]

Considering the overlapping between two consecutive pulses, it is possible to determine N_{eff1D} , the effective number of pulses, defined as the ratio between the accumulated energy fluence in a line, F_{1D} , and F_{pulse} . Taking into consideration how many pulses are generated in a certain processing time period, and that the beam spans a rectangle with an area of $(2 r_0) (v_{laser} \Delta t)$. The following is the typical fluence along the line:

$$F_{1D} = \frac{N E_{pulse}}{2 r_0 v \Delta t} = \frac{f_p E_{pulse}}{2 r_0 v} = \frac{f_p \pi r_0 E_{pulse}}{2 v \pi r_0^2} = \frac{f_p \pi r_0 E_{pulse}}{2 v \pi r_0^2} = N_{eff1D} F_{pulse}$$

$$\Rightarrow F_{1D} = N_{eff1D} F_{pulse}$$

Therefore,

$$N_{eff1D} = \frac{f_p \pi r_0}{2 v} = \frac{\pi r_0}{2 \delta_{pulses}}$$

Fluence distribution in the perpendicular direction is similarly Gaussian, and may be calculated as follows:

$$F(y) = F_{centre1D} \exp \left[-2 \left(\frac{y}{r_0} \right)^2 \right] = 1.588 \frac{\pi r_0}{2 \delta_{pulses}} F_{pulse} \exp \left[-2 \left(\frac{y}{r_0} \right)^2 \right]$$

Scanning in a direction that is perpendicular to the original direction causes overlapping of the Gaussian fluence distributions. Performing a similar analysis in this 2D scanning procedure, in order to determine whether or not the energy distribution is uniform, check to see whether δ_{pulses} / r_0 is less than 0.9. It is reasonable to assume a uniform energy distribution over the surface as a result of the overlapping requirements mentioned here.

N_{eff2D} , the effective number of pulses in this 2D configuration, can be calculated by keeping in mind that the number of pulses needed to cover a given processed area can be approached by $(N_1 \delta_{pulses}) (N_2 \delta_{lines})$, and that the total energy deposited by the laser in this area is $N_1 N_2 E_{pulse}$. The effective number of pulses in 2D can be calculated as [209]:

$$F_{2D} = \frac{N_1 N_2 E_{pulse}}{Area} = \frac{N_1 N_2 E_{pulse}}{N_1 \delta_{pulses} N_2 \delta_{lines}} = \frac{\pi r_0^2 E_{pulse}}{\delta_{pulses} \delta_{lines} \pi r_0^2} = N_{eff2D} F_{pulse}$$

$$\Rightarrow F_{2D} = N_{eff2D} F_{pulse}$$

N_{eff2D} , the effective number of pulses in this 2D configuration can be calculated finally as:

$$N_{eff2D} = \frac{\pi r_0^2}{\delta_{pulses} \delta_{lines}}$$

The single pulse's features also have an impact. Controlling l_{line} and v_{laser} enables the distance between line scanning (δ_{lines}) parameter to be fixed. In the case of a unidirectional setup, this is the correct approach; but in the bidirectional option, this is rather more complicated.

In this theoretical calculation, we have only considered the energy of the laser emission, but other parameters such as the material surface absorption or the incident angle can modify the effective amount of beam energy that is involved in the cleaning process.

3.3.5 Irradiance value as the standard for the calculation

Irradiance [201] and fluence are not always proportional in this thesis due to the usage of different distinct laser systems. Since irradiance values are independent of different laser devices and emission parameters characteristics (particularly wavelength and pulse duration), it has been taken as a fundamental reference in this study for direct and cumulative (thermal buildup) damage, thus a universal reference for a potential variety of laser irradiation treatments [106].

3.4 Surface characterization techniques

Sample characterization procedures must be tailored to the unique challenges of analyzing CH and AM, which may at times be different from those encountered in a regular conventional laboratory. The most important difficulties are connected to the type of artifact and the procedure that must be used, so that the CH or AM artifacts can be preserved and a number of historical/archaeological questions can be answered.

CH/AM artifacts are studied using analytical techniques commonly utilized in other domains to analyze organic and inorganic materials. Once the selected samples are in the lab, the sampling strategy must be addressed and considered: it can impact the scale of interpretation and limit or extend the methodologies and techniques used to study artifacts. Characterization techniques can give information irrespective of CH or archaeological context, shape, and stylistic elements used to define objects. Based on artifacts availability and research goals, this research work has focused on applying and validating state-of-the-art non-destructive approaches. When characterizing CH materials, standard optical measuring methods (such as spectrometry, classical and confocal optical microscopy, etc.) are often used in conjunction with other diagnostic approaches. Optical microscopy's role

in this laser-based archaeological materials intervention is enhanced by identifying and mapping examined materials' surfaces, evaluating multispectral imaging before and after laser cleaning, and visualizing top-surface layers. The sensitivity, adaptability, and analytical approach of well-known physicochemical characterization techniques have led to the development of spectroscopic techniques that excel in precise diagnostics of the materials and provide information on the chemical composition of the materials being studied.

Scanning Electron Microscopy (SEM) with Energy Dispersive Spectrometry (EDX) is the most common and popular characterization technique, exploiting the interaction of electron beams with matter to provide surface morphology, microstructure and qualitative elemental analysis at the nm- μ m scale. X-ray Diffraction and Fluorescence are used to study materials' physicochemical and crystallographic surface changes and elemental compositions. An exceptionally reliable and well-known fingerprinting technology, Fourier Transform Infrared Spectroscopy (FTIR), can mainly identify organic functional groups and it does not provide quantitative information. On the other hand, X-ray Photoelectron Spectroscopy (XPS) has been used to obtain quantitative elemental analysis and to identify crystalline and amorphous phases on surfaces, respectively.

To determine the laser tool selection criteria for cleaning conservation of archaeological materials and museum stored artifacts, several physicochemical characterization techniques were used in this study. The following are the details:

3.4.1 Technical Photography

To document and evaluate the surface morphology, contamination, and degradation status of cultural heritage artifacts, in addition to optical microscope study, technical photography is typically the initial step. Aspects of a material's surface, contamination and encrustation condition thoroughly inspected by using a Canon EOS 200D digital camera in order to capture and analyses the general surface morphological characteristics of the different archaeological materials, subjected to this study.

3.4.2 Optical Microscopy (OM)

In every experiment in this thesis, a handheld microscope (Dino-Lite Edge) with a maximum magnification of 230x was used to examine the ceramic surface 'before and after' the laser treatment (Fig. 3.7a). The final image is acquired using the Dino Capture

2.0 operating software, which is connected to the computer through a USB cable and illuminated by LED lighting.

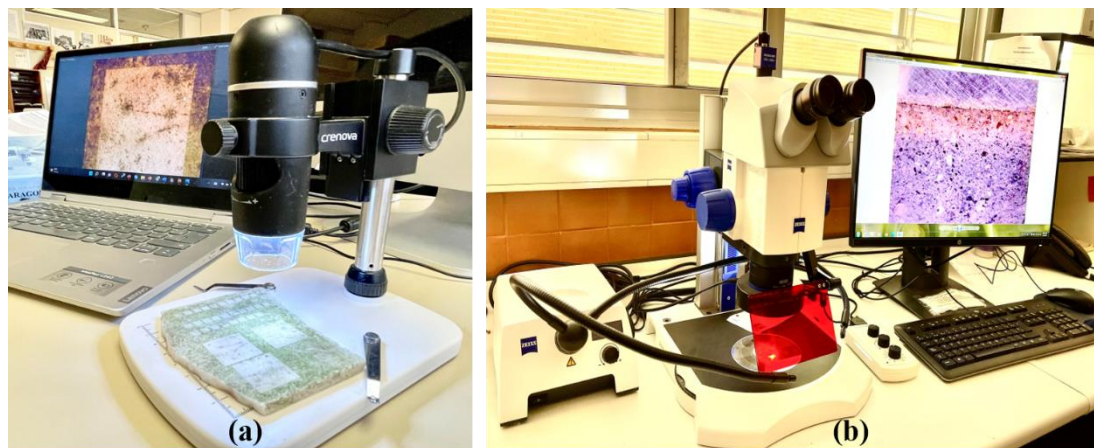


Fig. 3.7: Optical microscopy utilized in this thesis: (a) Dino-Lite Edge microscope: Instituto de Nanociencia y Materiales de Aragón (CSIC - University of Zaragoza), and (b) Zeiss Imager microscope: Servicio General de Apoyo a la Investigación, University of Zaragoza (Spain).

An optical microscope was used to examine some samples using a Zeiss Imager microscope equipped with an AxioCam camera after it had been cross-sectioned and polished with the discs of various granulations on a grinder–polisher (Fig. 3.7b). The imaging investigations were performed in a dark field using reflection at a magnification of 50.

3.4.3 Scanning Electron Microscopy with Energy Dispersive X-ray Spectrometry (SEM-EDS)

The elemental composition, surface physicochemical characteristics and microstructure of the bone sample surface were studied both of ‘before and after’ the laser treatment. In order to understand the bone sample and diagenesis affects, bone cross-section had been explored. Here in this regard, Environmental Scanning Electron Microscopy (ESEM) titled Quanta FEG250 was employed for high-resolution imaging, and EDS was used to evaluate the elemental composition semi-quantitatively at 10 kV electron acceleration voltages, while all obtained values were standardized to a non-laser treated portion of the same area of sample (Fig. 3.8b).

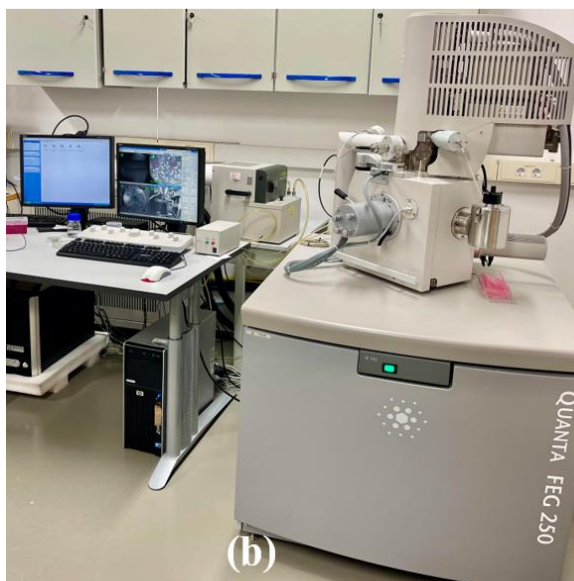
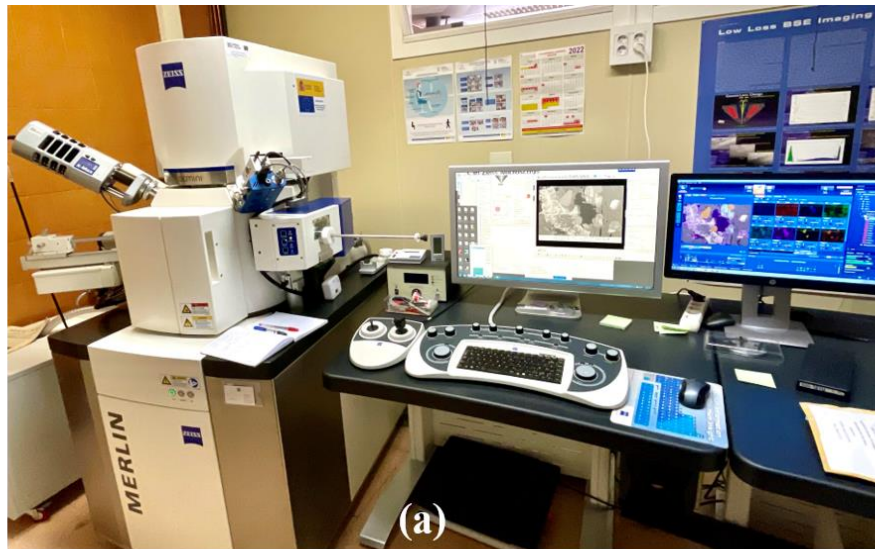


Fig. 3.8: SEM-EDX equipment utilized for surface characterization: (a) Servicio General de Apoyo a la Investigación, University of Zaragoza (Spain), (b) Laboratorio de Microscopías Avanzadas, University of Zaragoza (Spain), and (c) HERCULES Laboratory, University of Évora (Portugal).

Additionally, improved resolution inspections on polished cross-sections of the bone sample were conducted utilizing a Field-Emission Scanning Electron Microscopy (FE-SEM), titled Carl Zeiss MERLIN, equipped with secondary electrons (SE) and in-lens

detectors. The chemical composition was measured semi-quantitatively in this instance using EDS (INCA350 Oxford Instruments) at 15 kV (Fig. 3.8a).

A few selected samples were also investigated to highlight the structural characteristics and the elemental composition by using the HITACHI S3700N SEM system (Fig. 3.8c), which is interfaced with a QUANTAX EDS microanalysis system and equipped with a Bruker AXS 5010XFlash 5010 Silicon Drift Detector (129 eV Spectral Resolution at FWHM/Mn $K\alpha$). At 20 kV accelerating voltage, ~10 mm working distance and 90~120 μ A emission current, the EDS conditions were set for backscattered electron mode (BSEM). Bruker Esprit 1.9 software has been used for the investigation of the spectra.

3.4.4 X-ray Photoelectron Spectroscopy (XPS)

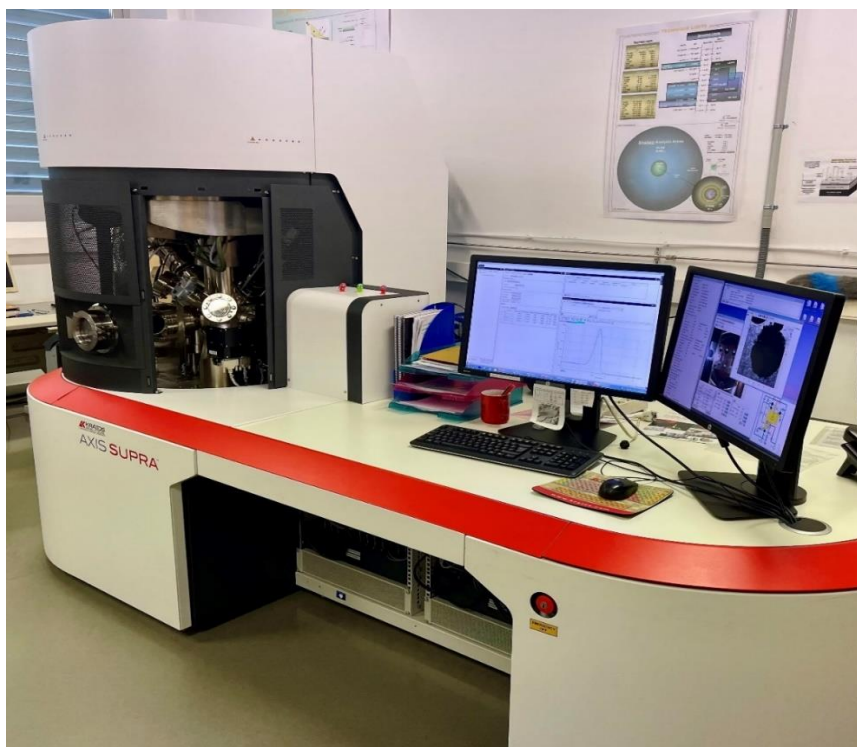


Fig. 3.9: XPS characterization technique utilized for bone surface characterization; Laboratorio de Microscopías Avanzadas, University of Zaragoza (Spain)

An X-ray photoelectron spectrometer (Kratos AXIS Supra XPS, monochromatic Al $K\alpha$ X-ray source with 225W: 8 mA/15kV energy) was used to study the outermost bone surface

chemical composition (Fig. 3.9). A base pressure of $\sim 10^{-9}$ Torr and an area size of $700 \mu\text{m} \times 300 \mu\text{m}$ were used to gather the photoelectron signal for the complete survey spectrum. The pass energy value per step employed was – i) Wide: 160 eV / 1000 meV and ii) Regions: 20 eV / 100 meV. All samples were investigated by means of a combined electron and argon ion gun neutralizer system (Ar+ 500eV) to diminish sample charging effects. In general, XPS provides information on the atomic concentration of the elements present on the topmost surface of the sample. For this study, XPS characterization was used to quantitatively determine the chemical composition at the surface of the sample. A total of 8 distinct areas of the bone sample were analyzed by XPS; typical depth of the analysis is about 5 nm (3-10 nm). General survey-scan and selected regions of interest spectra were collected in Hybrid-slot lens mode, which corresponds to a spot analysis area of approx. $700 \mu\text{m} \times 300 \mu\text{m}$. The sample was analyzed “as received” and after 300 seconds Ar+ ion etching.

3.4.5 X-ray Diffraction (XRD)

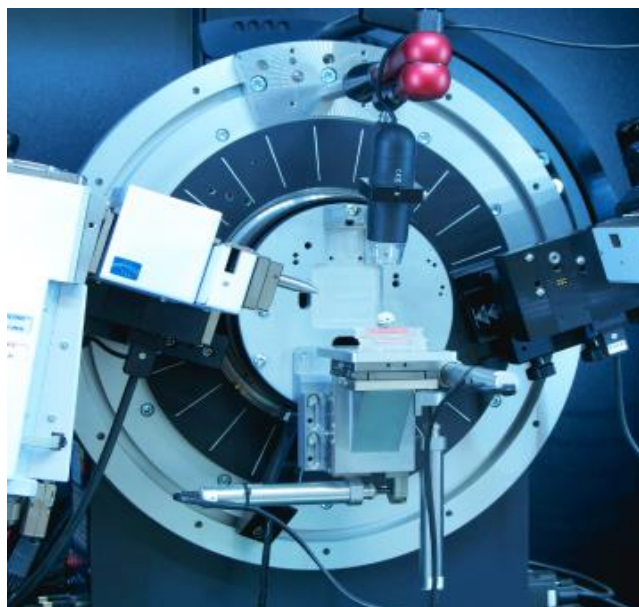


Fig 3.10: The DAVINCI design Bruker AXS D8 Discover X-ray Diffractometer.
© HERCULES Laboratory, University of Évora, Portugal.

The DAVINCI design Bruker AXS D8 Discover X-ray Diffractometer (XRD) was used to determine the crystalline phases in bone samples before and after laser cleaning (Fig. 3.10).

It has a Cu K α source and a Lynxeye 1-dimensional detector working at 40 kV and 40 mA. Scans were conducted from 3 to 75° 2 θ , with 0.05 2 θ step and a time step size of 1 s/step. All XRD spectra were interpreted using the Diffract-EVA software package (BRUKER/AXS GmbH, Germany) in conjunction with the PDF-2 mineralogical database.

3.4.6 Fourier Transform Infrared Spectroscopy (FTIR)



Fig. 3.11: Fourier Transform Infrared Spectroscopy utilized in this thesis investigation.
© HERCULES Laboratory, University of Évora, Portugal.

Since it enabled for in-situ and non-destructive investigation, it was decided to analyze the bone samples in ATR mode. When working in ATR mode, the FTIR spectra were acquired with a single reflection diamond ATR module and a Bruker Alpha spectrometer, which was used to acquire the data (Fig. 3.11). The studies were carried out at room temperature and with the surrounding humidity. Background measurements were taken prior to bone sample analysis in order to decrease the impact of carbon dioxide and water vapor on the results. The bone surface was in direct contact with the diamond crystal, which was positioned on the surface of the sample holder, and it was exposed to pressure as a result of this contact. The spectra obtained in the absorbance mode with 128 scans and a spectral resolution of 4 cm⁻¹, and they were acquired in the range of 4000 to 375 cm⁻¹. The OPUS/Mentor program (version 6.5) used to record and analyzed the spectra. Identification

of bone composition was accomplished by comparing the major characteristics of the acquired spectra between untreated and laser treated surface, as well as to those of articles that have worked with comparable methods and materials.

3.4.7 Infrared (IR) Thermal Camera

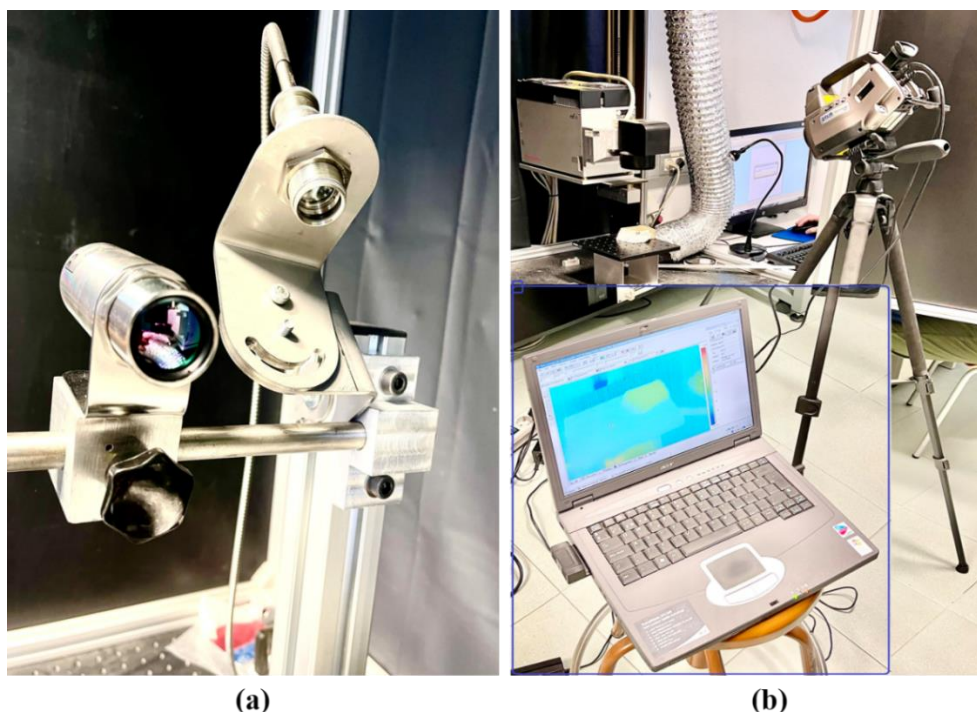


Fig 3.12: IR Thermal Cameras utilized in this thesis investigation: (a) Optris Xi 400, and (b) Thermo Cam P25; Instituto de Nanociencia y Materiales de Aragón (CSIC - University of Zaragoza), Spain

The real-time thermal incubation of artifacts surface when cleaned with laser, monitored and captured by using the newly developed Optris Xi 400 (Optris GmbH, Germany) combines the benefits of a robust, compact pyrometer and an advanced IR camera (Fig. 3.12a). The 80 Hz frame rate and 8 – 14 μm spectral range allow for monitoring fast thermal processes, even including a line-scan function. The spot finder IR camera has an optical resolution of 382 x 288 pixels and comes with an extensive ready-to-use package, including a versatile image processing software. This thermal camera provides the option for three different temperature measurement ranges: 20 - 100 $^{\circ}\text{C}$; 0 - 250 $^{\circ}\text{C}$, and 150 - 900 $^{\circ}\text{C}$. The system accuracy is ± 2 $^{\circ}\text{C}$ or ± 2 %, whichever is greater.

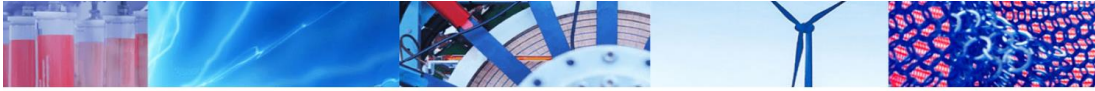
Additionally, another thermal camera (Thermo Cam P25, Teledyne FLIR Systems, USA) was used to monitor the average temperature rise in the bone surface during laser treatments (Fig. 3.12b). This thermal camera's spatial and temporal resolution enables reliable determination of average temperatures. Although the temperature at the laser spot incident on the bone surface can rise significantly within a short period of time, the average bone surface temperature around the irradiated area is maintained near room temperature, as long as heat accumulation is not significant.

CHAPTER: 4

SUB-NS-PULSED LASER CLEANING

CHAPTER FOUR
SUB-NS-PULSED LASER CLEANING OF AN
ARCHAEOLOGICAL BONE FROM THE *SIERRA DE*
***ATAPUERCA*, SPAIN: A CASE STUDY**


Summary: One of the primary objectives of this PhD thesis was to develop a protocol for cleaning archaeologically significant art objects by using sub-ns pulsed laser in emission at n-IR wavelength. The results from this study were published in the Nov 2021 issue of a peer reviewed journal (SN Applied Sciences). This study demonstrated the potential of sub-ns-pulsed lasers in burst pulse operating mode. It paved the way to safer laser cleaning procedures which may apply for the operative and efficient conservation of archaeological bone artifacts. Based on the results from this study, we have developed and designed our next study where we aimed to introduce and explore the ultrafast lasers in different emission wavelengths (UV, Visible Green and N-IR), using both, the burst pulse and beam scan modes, in order to revealed the best cleaning protocol and laser-based intervention for CH materials and museum stored artifacts. In this section (pages 80- 97), we have included this published article as Chapter 4 of this thesis, keeping the text as published. In order to be consistent, however, bibliography and style formats were adjusted to those chosen for this thesis.



Research Article

Sub-ns-pulsed laser cleaning of an archaeological bone from the *Sierra de Atapuerca*, Spain: a case study



Md. Ashiqur Rahman^{1,3,6}  · German F. de la Fuente¹ · José Miguel Carretero² · Evan Maina Maingi^{1,3,5} · M^a Pilar Alonso Abad³ · Rodrigo Alonso Alcalde⁴ · Rémy Chapoulié⁵ · Nick Schiavon⁶ · Luis A. Angurel¹

Received: 10 March 2021 / Accepted: 27 October 2021

Published online: 13 November 2021

© The Author(s) 2021 [OPEN](#)

Abstract

Controlled laser irradiation parameters using recently developed sub-nanosecond pulsed laser technology with emission wavelength in the near Infrared regime (1064 nm) have been assessed on a Pleistocene bone from the archaeological

Abstract: *Controlled laser irradiation parameters using recently developed sub-nanosecond pulsed laser technology with emission wavelength in the near Infrared regime (1064 nm) have been assessed on a Pleistocene bone from the archaeological site of Sierra de Atapuerca, Spain. Burst pulse mode was employed to explore contaminant removal efficiency, while at the same time, assessing the degree of damage produced to the underlying original substrate surface. The surface morphology and composition of the deteriorated bone have been characterized, along with the effects of laser irradiation at 1064 nm, using Optical Microscopy (OM), Scanning Electron Microscopy – with Energy Dispersive X-ray Spectrometry (SEM-EDS), and X-ray Photoelectron Spectroscopy (XPS). The most effective laser cleaning parameters in burst mode have been identified in order to optimize the emission parameters of the laser, thus localizing its interaction within the outermost layers of contaminants and degradation products, avoiding damage to the underlying original bone surface. Hence, threshold cleaning and substrate damage values have been determined for this new sub-ns laser, paving the way to safer laser cleaning procedures that may practical for the effective conservation of bone archaeological artifacts.*

Keywords: sub-ns laser; cleaning; archaeological bone; Sierra de Atapuerca; Cultural Heritage;

4.1 Introduction

The *Sierra de Atapuerca* mountain range has become one of the most famous archaeological regions of the world following the discovery of the ‘first hominin’ presence

in Europe [72] [72][210]. From a geomorphological point of view, it is a rather complex site characterized by the presence of numerous limestone caves and located in an ancient karstic area of northern Spain, 12 km east of the city of Burgos. The plentiful bones and stone tools of Europe's oldest hominins excavated there date back to 0.78 ~1.2 million years [74]. Geologically, *Sierra de Atapuerca* belongs to the Iberian Mountain Range, with Quaternary deposits mostly found in valleys, fluvial terraces, floodplains, alluvial fans and colluvial deposits [80]. One of the most surprising discoveries at *Sierra de Atapuerca* is a cavern site named *Sima de los Huesos* (the Bones Pit). The pit contained the remains of approx. 166 cave bears from the Middle Pleistocene and approx. 28 individual humans with a total of more than 6500 human bone fragments and more than 500 teeth recovered, making this pit one of the biggest collections of earliest hominid fossil remains in the world. Dating analysis suggests the age of the site to range from at least 0.3 to 0.6 million years [91][92].

Bone degradation processes are referred to as bone diagenesis [211]. Bones are mainly composed of organic molecules (i.e., proteins and fats) and inorganic minerals. They are the compound tissue that is made up of three main parts: a) mineral that comprises hydroxyapatite $\text{Ca}_{10}(\text{PO}_4)_6(\text{OH})_2$, b) protein that mainly comprises collagen, and c) ground substance (an amorphous gel-like substance in the tissue) which is made of other organic compounds [212][213]. After demise, most of the organic collagen are eventually metabolized by the action of bacterial enzymes, which is the first step of bone diagenesis. Bacterial enzymes break down the organic collagen into peptides, and these peptides are reduced to their elemental amino acids, which are normally leached away by the groundwater. As soon as the organic collagen has been removed from bone, the precipitated crystalline hydroxyapatite starts to be degraded by the inorganic weathering processes, with leaching of ions such as calcium (Ca), iron (Fe), aluminum (Al), potassium (K) and manganese (Mn). The collagen and hydroxyapatite are bound together by strong protein-mineral bonds, providing the bones with their strength and durability which will gradually be conceded and lead to a general deteriorated structure. Continuous deterioration will subsequently take place, until full physical break down, decalcification, and bone dissolution occurs [214]. Additionally, burial soils contain mostly insoluble inorganic phosphorus (P) complexes [215], frequently with Fe, Ca and Al. Thus, limited phosphorus leaching is expected, although it relies on the hydrogeology of the buried archaeological soils [216][217], as well as soil microorganisms (like *Penicillium*) to solubilize insoluble inorganic complexes [215]. On an interment level, the bone is outlined with black stains by the phenomenon of burial silhouette, which has an intriguing link with evidence of burial

hydrogeology settings. It has been noted that in sandy and gravelly acidic soils, the organic phosphorus complexes attract other soil metals, most notably manganese, resulting in black stains on the bone surfaces [218].

The most noteworthy point is the degree of bone degradation which is highly dependent on its surrounding environment. In the presence of soil, bone contamination is usually influenced by both physical (such as water, moisture, relative humidity, temperature, soil type, and pH), as well as biotic agents (i.e., fauna and flora) [219][220]. Water infiltrating down on the nearby environment of bone, normally through the soil above, causes dissolution of its mineral content and leaching out of the bone. In general, the minerals that precipitate are iron and manganese oxides and hydroxides, as well as carbonates (including calcite) and silica. Bone mineralization within the soil results in the gradual addition of inorganic minerals dissolved in groundwater. With time, the diagenetic processes cause the bones to increasingly harden towards a rock-like object. In exceptionally rare cases, soft tissues of bones can also become mineralized [212][221].

The conservation of archaeological materials and museum stored objects have, during the last decades, been considered a significant challenge for innovative science and multidisciplinary research development. In this sense, modern intervention tools and characterization methods may play an essential role to successfully solve many conservation challenges presently faced by the cultural heritage conservation and restoration community [18][222]. Conventional conservation techniques for Cultural Heritage (CH) materials usually include chemical and mechanical cleaning methods that have been employed for centuries. In contrast, laser cleaning techniques may be included as an outstanding and encouraging example of how relatively recent technological advances may be applied to improve conservation methods for CH materials [4][172][157].

Although laser cleaning in the conservation of CH materials began in the early 1970s [29][30], it took several decades for its wide use due to severe technological limitations. The first laser system used for conservation operated with Ruby and Nd: YAG lasers, with a low pulse repetition rate, a lack of flexible beam distribution mechanisms, very poor consistency for long-term operations, and high experimental costs [31][32]. The technical development for laser cleaning improved dramatically later in the 1980s, but the experimental costs were still out of proportion for use in the CH sector. It was a crucial period for the novel approach of laser conservation to survive with relatively low productivity, when compared to traditional mechanical and chemical cleaning techniques

[33]. The availability of new laser technologies enabled systematic investigations on extensive applications after the 1990s, triggering dissemination of the laser methodology in CH conservation practice [223][34].

The laser cleaning approach has been successfully applied for almost three decades, however, on a variety of archaeological materials with diverse types of contamination and/or deterioration. Laser cleaning of archaeological mineralized bone has not gained much attention yet from the conservation and restoration community, as very few case studies have been reported so far [21][224][225]. The main reason behind this may be related to the absence of adequate pulse lasers which may avoid damage to sensitive/fragile surfaces. Bones are neither uniform in their composition nor the deterioration and mineralization occurring in bones are homogeneous. Furthermore, reducing the risk of damage to the original bone substrate surface appears as a crucial challenge. To solve the latter, it will be necessary to establish which parameters lead to a distinct laser interaction with the contaminant layers vs. the original bone substrate surface.

Thus, if properly applied, laser cleaning of bone can minimize and avoid both mechanical and chemical disruption of historic patinas, while selectively eliminating contaminating agents (i.e., unwanted fossilized minerals, soil etc.) in archaeological bones. The traditional cleaning method applied on an excavated bone is mostly based on the use of a neutral detergent wash under controlled temperature, or the application of alcohol or other chemical solvents that so often alter the bone surface. In contrast, laser cleaning is a dry method where bone parts with rough surfaces and weakened regions can be, in principle, cleaned without altering their original surfaces.

In essence, archaeological bones are quite vulnerable to contaminants. They get discolored over the years due to inorganic mineralization weathering, and may appear dusty (exposed up with encrustations, blackish contaminants and dust), thus losing their original appearance and aesthetic value. The objective of the present work is to make use of new sub-nanosecond (sub-ns) pulsed laser technology [226] to ascertain its potential use in removing contaminants from Pleistocene bone sample surfaces found in *Sierra de Atapuerca*, while respecting the original patina on the substrate surface to preserve as best as possible the surface anatomical details obscured by contamination. The reason for using a sub-ns laser is to avoid excessive heating of the irradiated substrate. On the one hand, this laser is compact and air-cooled and offers several advantages with respect to the substantially more expensive femtosecond (fs) lasers. On the other, it is expected to

significantly reduce thermal incubation [227][228][229][230] with respect to competing ns pulsed lasers, most commonly employed for surface cleaning.

4.2 Materials and methods

4.2.1 Materials

One Pleistocene bear bone from *Sima de los Huesos* was selected for the present study. It is described physically as a 6.3 cm long x 0.9-1.2 cm wide x 0.35-0.7 cm thick rib sample excavated in 1986 as soiled material, dating back to 430,000 years. Some part of this bone exhibits various shades of grayish discoloration different from the natural whitish-yellowish color typical with fossilized bones, presumably due to Fe staining. It was inhomogeneously covered with hard blackish encrustations, greyish contaminants and atmospheric soil dust, as well as with weathering patterns suggested to be caused by manganese (Mn) mineralization effects [218][231][232][233]. Dust on the bone surface was previously removed by a standard mechanical procedure; front and side-view photographs of the bone sample are shown in Fig. 4.1. A particular objective of this study is to remove this bone's hard-blackish stains from its outmost layer without altering its original surface.



Fig. 4.1: Front (upper photograph) and back surface (lower photograph) views of a bear rib (shaft) bone excavated at the *Sima de los Huesos* site at *Sierra de Atapuerca* (Burgos, Spain).

4.2.2 Experimental

4.2.2.1 Laser irradiation of Pleistocene bone

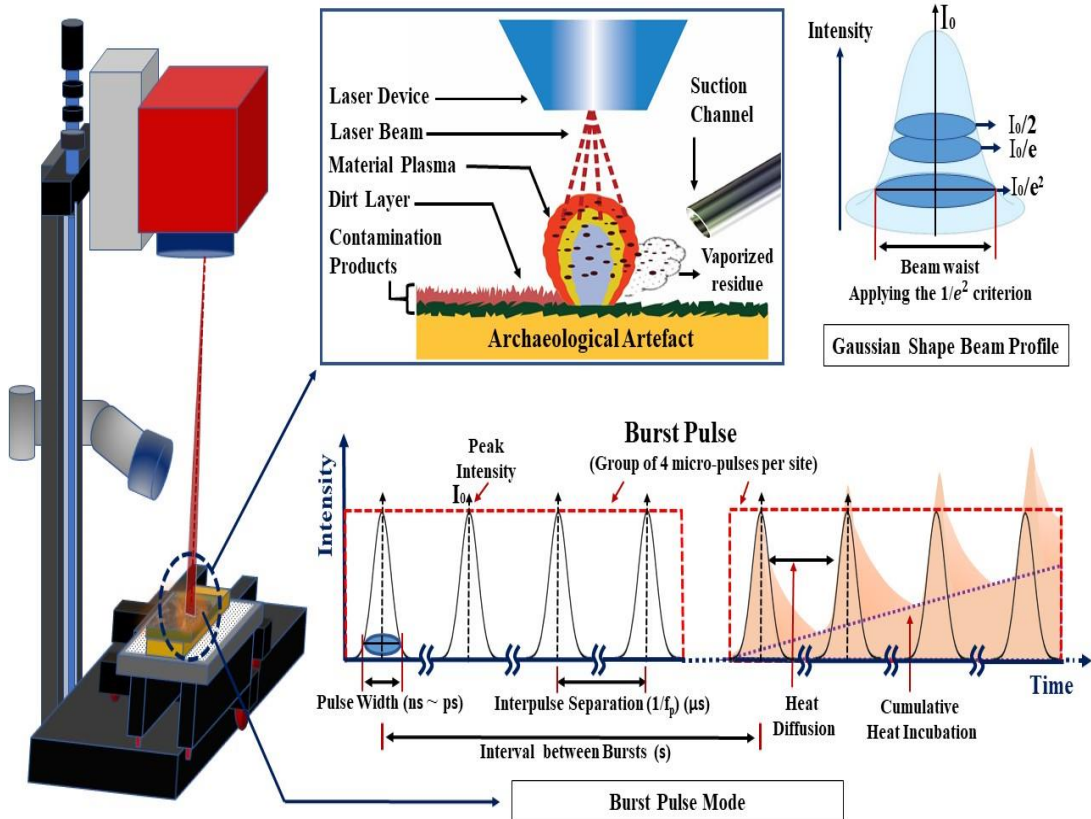


Fig. 4.2: Illustration of the laser cleaning apparatus used for the present study (left), where the laser x-y scanner head is shown above the archaeological artifact sample and a fume extraction device. The upper center inset illustrates the ideal sample behavior under laser irradiation, where the contaminant layer is removed, while the protective patina (green) is preserved. The upper right inset represents the relationship between laser intensity and different definitions of beam waist related to a Gaussian beam profile, highlighting the $1/e^2$ criterion used in this study [202]. The lower inset drawings represent the laser intensity output in a given position as a function of time for the burst pulse mode employed to control thermal damage [203][204]. The lower inset graphically illustrates the pulse width ($\tau_p = 800$ ps) and pulse-to-pulse (interpulse) separation (ca. $2 \mu\text{s}$) on the left side. On the right side it provides an illustration of how thermal incubation takes place along the consecutive pulse irradiation process. Between bursts, a much larger time interval that depends on the particular geometry selected to make the laser treatment (ca. 0.4 s) is indicated.

Figure 4.2 provides an illustration of the laser apparatus used to carry out this study. It also includes a simplified representation of the ideal physical phenomena induced when a laser beam is focused onto a contaminated surface of an archaeological artifact. The resulting effects are associated to the complex processes described for laser ablation [48], which include plasma formation and consequent shockwaves which help remove the contamination layer away. These complex phenomena are illustrated in the upper center inset of Fig. 4.2. For the fixed pulse width laser used in this study, selection of appropriate power output and pulse repetition rate enables contaminant removal while avoiding damage to the patina layer and substrate below it [27]. The relationship between laser intensity and beam energy distribution is represented in the upper right inset of Fig. 4.2 in order to help visualize how beam waist is defined here. Finally, the lower inset represents the burst pulse mode used in this study, where consecutive groups (bursts) of pulses irradiate the material surface at a given position under specific conditions to avoid causing thermal damage to the substrate, while removing contaminants. It is important to have in mind that the interval between bursts (usually ranging between 100 ms and 1 s) is much longer than the interpulse separation (ca. 2 μ s) and the pulse width (800 ps). It allows the irradiated surface to cool sufficiently between burst sequences.

Laser irradiation experiments were performed using a computer-controlled galvanometer-scanner-equipped sub-ns pulsed near Infrared (n-IR) laser. This was manufactured by Rofin (Munich) and its essential emission characteristics are summarized in Table 4.1. Most important consideration is given to wavelength (λ), pulse width (τ_p), pulse repetition rate or frequency (f_p) and nominal power (P_{max}). The output laser beam follows a circular gaussian energy distribution mode.

Table 4.1: Characteristic emission of the sub-ns laser employed for the present study. Values are given for the nominal (maximum) output power (P_{max}), emission wavelength (λ), pulse width (τ_p), pulse repetition rate (f_p) and beam waist applying the $1/e^2$ criterion (D_b) for a gaussian beam distribution (Fig. 4.2).

Laser type	P_{max} (W)	λ (nm)	τ_p (ps)	f_p (kHz)	D_b (μ m)
n-IR	8	1064	800	200-800	80

A burst pulse mode method (Fig. 4.2) [51] provided by the computer CAD-like software controlling the laser output and integrated galvanometer mirror scanner head, was used to selectively irradiate the samples' surface around specific localized areas. In burst mode, the

laser does a spot-by-spot scanning process, where the scanning parameters can be adjusted. A laser system configured to operate in burst mode generates a burst (i.e., a sequence of a defined number of pulses) with a high intra-burst repetition rate in each preselected position on the sample surface. A single burst is evident at a particular position, where this specific mode enables irradiation of selected areas controlling the laser emission parameters, the distance between burst positions, the energy of each individual burst pulses, and the number of pulses in a burst repeated over the same irradiated position (Fig. 4.2, lower inset). The latter exerts control over thermal incubation, that is, accumulation of energy input as a function of time into a given area of the sample. In this laser system, irradiance (average power density of a given laser pulse) [201] and fluence (pulse energy density) values are proportional. In this work, irradiance values have been taken as a basic reference, for direct and accumulated (thermal incubation) damage, since it is independent of different laser devices and emission characteristics (particularly pulse duration).

4.2.2.2 Characterization

Surface morphology, elemental composition and microstructure were characterized before and after laser treatment of the samples, both on their surface and cross-section. Environmental Scanning Electron Microscopy (ESEM) (Quanta FEG-250) was used for high-resolution imaging while elemental composition was semi-quantitatively determined by EDS. In addition, improved resolution studies were carried out on polished cross-sections of the bone sample using field-emission SEM (FE-SEM, Carl Zeiss MERLIN) comprising secondary electrons (SE) and in-lens detectors. Chemical composition was semi-quantitatively determined in this case by EDS (INCA350 Oxford Instruments) using electron acceleration voltage of 15 kV.

An X-ray photoelectron spectrometer (Kratos AXIS Supra XPS, monochromatic Al K α X-ray source with 225W: 8 mA/15kV energy) was used to study the outermost bone surface chemical composition. A base pressure of $\sim 10^{-9}$ Torr and an area size of 700 μm x 300 μm were used to gather the photoelectron signal for the complete survey spectrum. The pass energy value per step employed was – i) Wide: 160 eV / 1000 meV and ii) Regions: 20 eV / 100 meV. All samples were investigated by means of a combined electron and argon ion gun neutralizer system (Ar+ 500eV) to diminish sample charging effects. In general, XPS provides information on the atomic concentration of the elements present on the topmost surface of the sample. For this study, XPS characterization was used to quantitatively determine the chemical composition at the surface of the sample. A total of 8 distinct areas of the bone sample were analyzed; typical depth of the analysis is about 5 nm (3-10 nm).

General survey-scan and selected regions of interest spectra were collected in Hybrid-slot lens mode, which corresponds to a spot analysis area of approx. 700 μm x 300 μm . The sample was analyzed “as received” and after 300 seconds Ar⁺ ion etching.

In order to observe the surfaces of bone before and after the laser treatment, a portable microscope (Dino-Lite Edge) with a maximum magnification capacity of 230x was employed. It was fitted with an LED lighting accessory and linked via USB cable to a computer using Dino Capture 2.0 operating software.

4.3 Results and discussion

Undesired contaminant removal from the above-described bone surface requires laser emission conditions which may ideally cause a considerable difference in absorption between the contaminants and the bone substrate itself. The most relevant parameters under consideration for this task are summarized in Table 4.2. Among these, the nominal output power (P_{max}), f_p , τ_p and D_b determine the resultant irradiance (I_L) values; i.e. $I_L = \frac{4P}{\pi f_p \tau_p D_b^2}$

. On the other hand, thermal incubation is also determined by the above processing parameters, but determined directly by the number of incident pulses within a given area of the surface in a given time, combined with the degree of overlap between consecutive pulses [234][235][236]. A combination of irradiance and incubation values determines the degree of interaction between the laser and the substrate, and thus the degree of damage to the latter [237]. Very small areas were thus irradiated throughout the different regions within the bone surface and initially explored and examined by confocal and electron microscopy, where melting evidence and microstructure changes were properly assessed. Determined cleaning and damage threshold values are based on multiple observations and experiments carried out over representatively different surface finish sites within the bone. From these observations it was concluded that irradiance levels below 0.20 GW cm^{-2} guarantee that damage of the bone is avoided. These also suggested that damage to the substrate surface was produced at an irradiance value of 0.22 GW cm^{-2} . Accordingly, and considering a safety margin, irradiance values below 0.20 GW cm^{-2} apparently do not cause damage and were thus selected for further cleaning studies. The incubation level was kept constant for all of these initial experiments, as gathered from the number of pulses (N_p) applied in burst mode, as specified in Table 4.2. Irradiation was focused on the dark contaminated areas of the sample shown in Fig. 4.1.

Table 4.2: Experimental parameters used for the initial assessment of the laser interaction with archaeological bone studied and reported here. The laser fluence F_L is the emitted energy of a given pulse per unit area of spot size, the irradiance I_L is the laser fluence per pulse duration, the pulse repetition rate f_p is the number of pulses per second, the pulse energy E_p is determined by dividing the output power by the pulse repetition rate, and the effective pulse number N_p is the number of pulses received in any specific position of the surface in burst mode (fixed at 25). Distance between two positions was fixed at 20 μm .

Region ID	P (W)	f_p (kHz)	Pulse Energy (J)	F_L (J/cm ²)	I_L (GW/cm ²)	Observations
1	7.24	300	2.41×10^{-5}	0.48	0.60	Damage due to high incubation, thus melting and cracks generated on the surface (Fig. 4.6: L_W)
2	6.77	500	1.35×10^{-5}	0.26	0.33	Damage, thus melting and cracks generated (Fig. 4.6: L_G)
3	6.29	600	1.05×10^{-5}	0.22	0.28	Damage, thus melting and cracks generated
4	5.34	600	8.9×10^{-6}	0.17	0.22	Damage, thus melting and cracks generated (Fig. 4.3: g & h)
5	5.34	700	7.63×10^{-6}	0.15	0.19	No damage appears, hard blackish encrustations mostly cleaned (Fig. 4.3: e & f, and Fig. 4.6: G_1)
6	6.29	800	7.86×10^{-6}	0.16	0.20	No damage appears, hard blackish encrustations mostly cleaned
7	4.39	600	7.32×10^{-6}	0.14	0.18	No damage appears, hard blackish encrustations mostly cleaned

A “cleaning” threshold irradiance I_L for n-IR burst mode irradiation with emission at 1064 nm was thus determined with the aim of eliminating the dark blackish colored over-layers from the light whitish colored substrate. In various areas, multiple laser irradiation treatments were performed on the bone surface, which, in all cases, underwent prior soft brush mechanical cleaning to remove loose dirt. Below this I_L cleaning threshold value, no contaminant removal was appreciated.

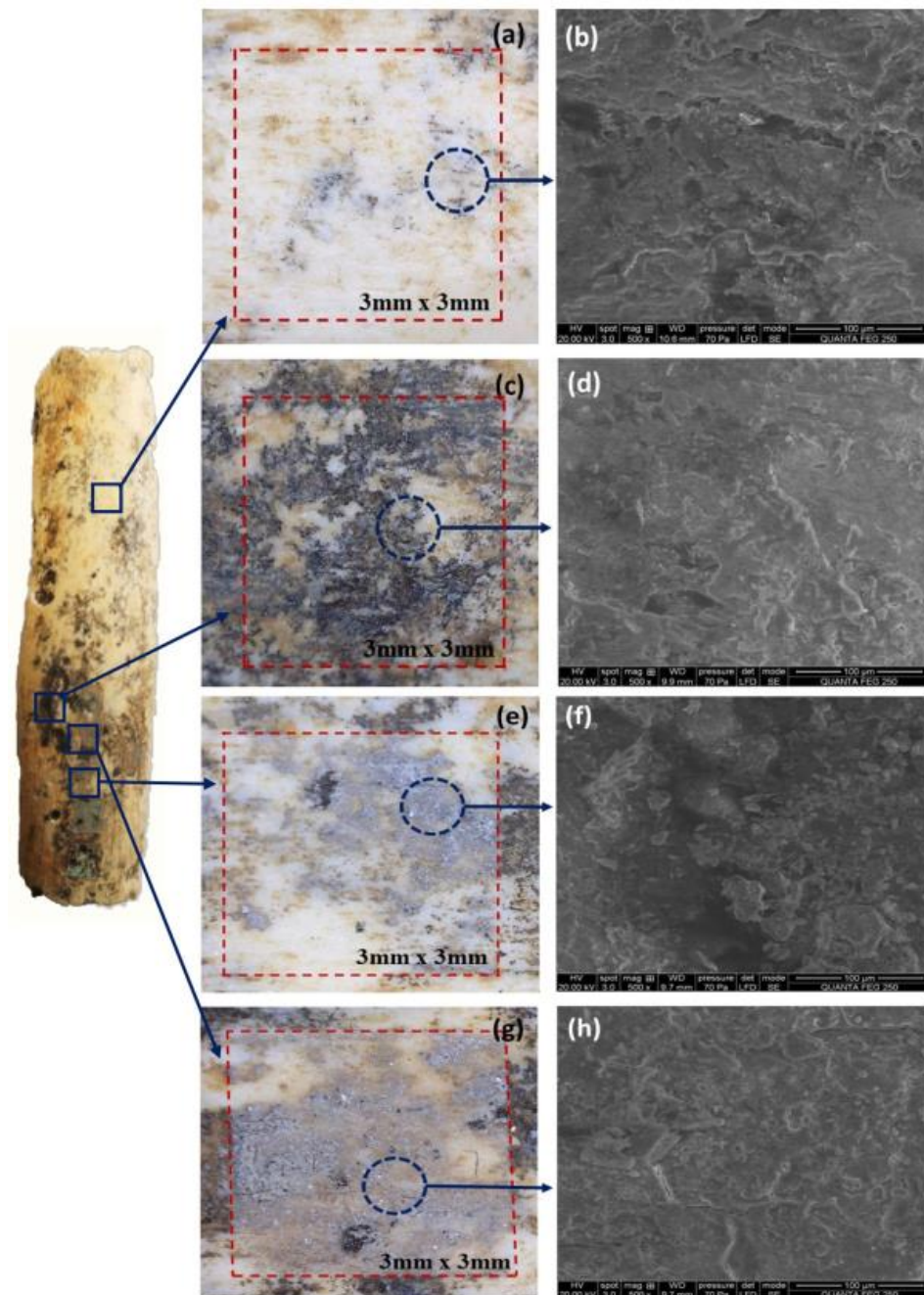
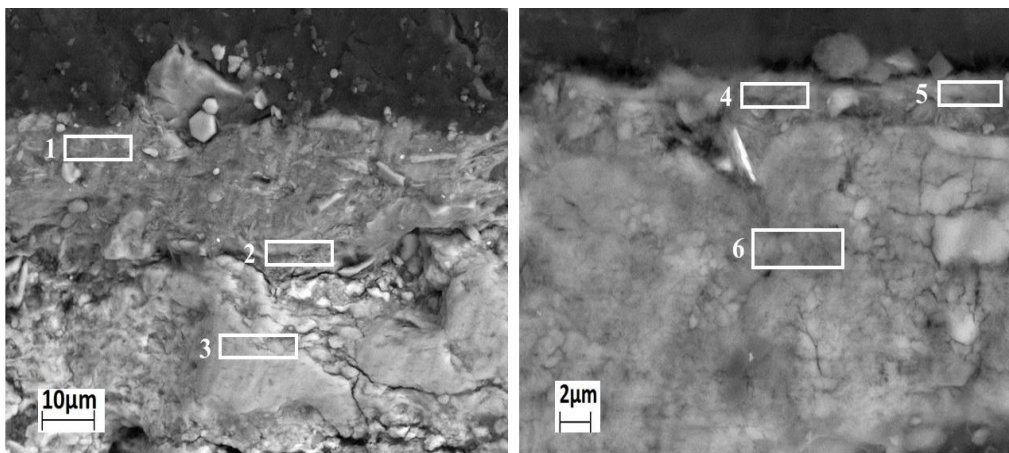


Fig. 4.3: Optical microscopy and SEM images obtained on the Pleistocene bone sample subjected to this study: ‘a and b’ correspond to the non-treated whitish original surface; ‘c and d’ to the original Mn mineralized blackish dark surface; ‘e and f’ to the n-IR laser-treated bone surface (Table 4.2: Region ID - 5); ‘g and h’ to the laser treated surface where melting is evident (Table 4.2: Region ID - 4).

The irradiance values applied for the above experiments thus ranged from ~ 0.18 to ~ 0.6 GW cm⁻² by changing the laser system's power output. Further irradiation of selected regions in the bone sample were carried out between the lowest power value of 4.39 W and 7.24 W, where the highest non-damaging irradiance values were achieved (Table 4.2: Regions ID- 5,6,7). Several regions were handled, covering 3 mm square areas each, under the same irradiance conditions while leaving a particular area as the reference for the proper cleaning procedure. It takes approximately 0.95 – 1.2 seconds to clean the 3 mm square region with typical processing parameters.



Spectrum (%At)	O	Ca	Al	Si	P	Mn	Fe	K	Na	Mg	Cl	Total
1	56.2	8.98	8.82	14.8	4.90	0.49	2.36	1.92	0.23	0.99	0.31	100
2	40.4	12.3	9.54	17.3	2.89	8.12	5.95	3.51	--	--	--	100
3	65.9	20.9	0.19	0.22	11.8	--	0.19	0.15	0.48	--	0.17	100
4	63.4	3.95	8.40	14.8	2.64	2.13	2.02	1.36	--	0.83	0.39	100
5	65.3	2.00	11.07	14.4	1.42	2.10	1.21	1.49	--	0.73	0.30	100
6	65.5	20.3	0.29	0.40	11.7	0.70	0.25	--	0.53	--	0.35	100

Fig. 4.4: Non-irradiated bone cross-sections observed on micrographs obtained by FE-SEM under different magnification. EDS analyses performed on the indicated areas are summarized in the Table below. The presence and distribution of Ca and P, essential components of bone, is confirmed and observed to increase significantly below a depth of ca. 6 µm. Contaminants are thus restricted to the outermost layers of several µm. Mn is detected to a depth of ca. 25 µm and follows a similar trend as Fe. Al and Si confirm that the bone has been in contact with clay, as their presence is found significantly reduced below a depth of ca. 8-10 µm.

Figure 4.3 presents optical micrographs of the actual area of the bone previously cleaned by conventional mechanical methods. A blackish mineralized region with hard greyish encrustations is also shown, along with laser cleaned regions, all accompanied by the corresponding SEM images for the same areas. As the pulses exhibit a gaussian spatial beam profile, the maximum, non-damaging laser irradiance I_L on the sample surface determined for dark mineralized area contaminant removal is $\sim 0.20 \text{ GW cm}^{-2}$ (Table 4.2). The dark blackish and greyish contamination crusts often resulted in surface discoloration into a brownish color, but SEM-EDS and XPS characterization studies suggest that laser cleaning did not cause any compositional changes under these conditions. It is suggested that the thermal dissociation of the Mn and Fe compounds combined may be the reason for a minimal brownish alteration. Similar results for different area treatment revealed that, at I_L values slightly above the ablation threshold, the mineralization is not fully removed and a very thin layer of matrix material can still be present on the mineralized area of the surface (Fig. 4.3e).

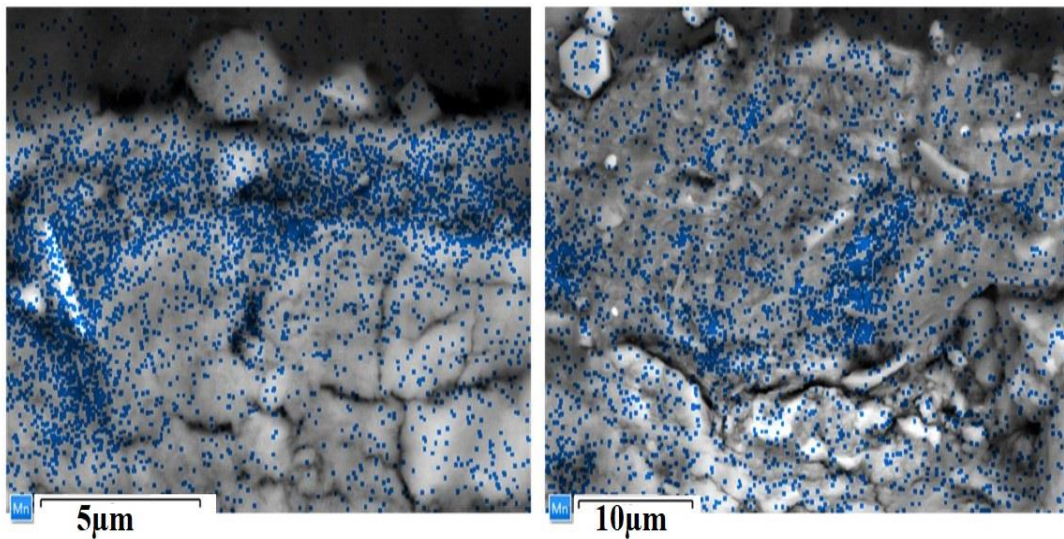


Fig. 4.5: Non-irradiated bone cross-section observed under FE-SEM and the corresponding EDS map analysis for Mn (2 different areas of interest presented).

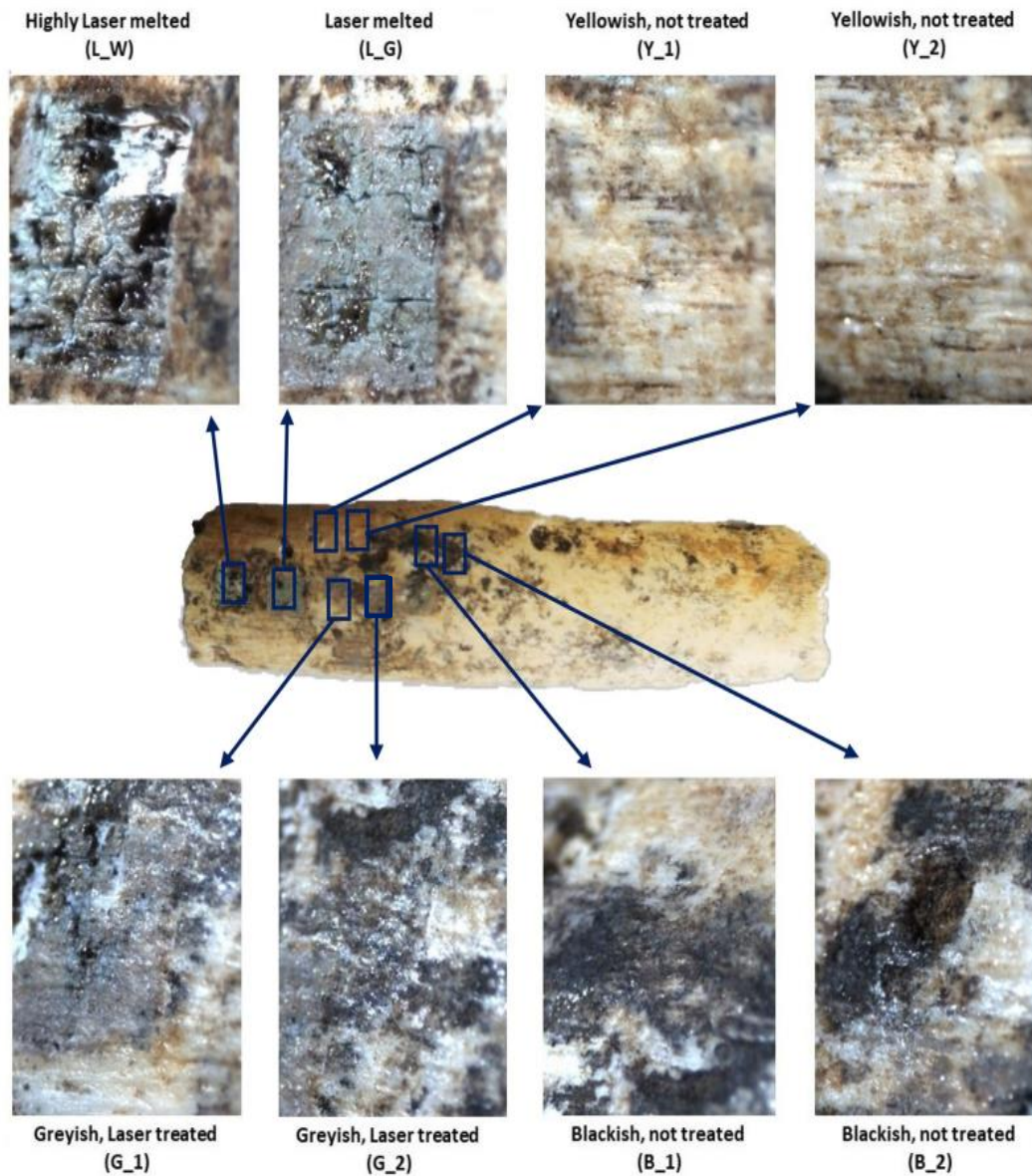


Fig. 4.6: Optical micrographs of the different laser treated and non-treated bone areas where laser induced phenomena and original surface conditions are indicated.

In both mappings and area analysis by SEM-EDS, the laser-cleaned region also suggests the presence of a significant amount of Mn. This is not surprising, in view of previous studies confirming that Mn may be part of the bone itself [238]. The cross-section of the bone sample was thus studied by FE-SEM to further explore the presence of Mn and other representative elements within the bone, and to semi-quantitatively determine its chemical

composition by EDS (Fig. 4.4 and Fig. 4.5). Thus, the presence and distribution of Ca and P, essential components of bone, is confirmed and observed to increase significantly below a depth of ca. 6 μm . Mn is detected to a depth of ca. 25 μm and follows a similar cross-section distribution trend as Fe, thus it is consistent with its incorporation through a mineralization process. In addition, the cross section elemental analysis map distributions shown in Fig. 4.5 may be consistent with its possible presence as an original bone component. Furthermore, Al and Si confirm that the bone has been in contact with clay, as their presence is found significantly reduced below a depth of ca. 8-10 μm . These measurements are thus consistent with the essential fact that the presence of contaminants appears restricted to the outermost layers (several μm) of the bone artifact. On the other hand, the mechanical breakdown or chemical degradation of the bone surface, to the degree that the bone has been buried for a long period, allowed the precipitation of Mn and Fe compounds to a visible depth; hence their mineralization produces blackish encrustations and greyish stains on the artifact's outermost layer (Fig. 4.3c).

XPS analyses were consistent with those obtained by EDS and were used to determine the effect of laser irradiation and damage on elemental composition at the outermost surface. Thus, after a high irradiance treatment which resulted in severe melting of the bone surface (Fig. 4.6: L_W, L_G; Table 4.2: Regions ID – 1, 2; Table 4.3: L_W, L_G) the Mn content was observed to increase after surface ion etching, while that of Fe decreased (Table 4.3: Y_1 vs. G_1). Therefore, while high irradiance level laser treatments showed that the bone samples were fully melted due to the large level of heat accumulation (thermal incubation), it was possible to physically observe the variations in surface aspect as a function of the irradiance. These included drastic changes with respect to the original texture, morphology and color of the bone sample (Fig. 4.6: L_W, L_G; Table 4.2: Regions ID – 1, 2). In addition, Fig. 4.6: G_1 confirms that Mn and Fe are still present in appreciable amounts within the greyish area irradiated at 0.19 GW cm^{-2} (Table 4.2: Region ID – 5; Table 4.3: G_1).

Table 4.3 shows the XPS survey and analysis data for the areas specified on the optical micrographs of Fig. 4.6. Results have been quantified for the detected elements using the C 1s binding energy spectrum as reference both, before and after 300s of Ar⁺ ion etching. The Ca/P atomic ratio reflects a consistent composition related to the essential Ca hydroxyapatite structure of bone, found to allow for significant compositional variations in archaeological fossilized bones [239][240][241] Fluorine may also be expected in fossil bones and has been related particularly with water intake [241], thus it varies depending on

the site at which the fossils are found. Elements like Si, Al, S, Fe, Mn, Na and N may be associated with the burial environment, as they are related to aluminosilicates (such as feldspars, for example), nitrates, sulfates etc., generally found as components of soil in the *Sierra de Atapuerca* archaeological site [242].

Table 4.3: Relative surface concentration of elements (atomic %) detected by XPS on the archaeological bone sample before (000s) and after (300s) 300s Ar⁺ ion etching.

Sample	Laser	Ca %	P %	Si %	Al %	S %	Fe %	Mn %	Na %	N %	F %
L_W/000s	Treated	7.75	2.76	3.64	2.12	1.19	0.75	0.38	1.97	---	0.49
L_W/300s	Treated	8.86	2.61	3.79	2.11	1.49	0.95	---	1.77	---	0.35
L_G/000s	Treated	5.67	2.83	5.94	3.96	0.57	1.41	0.36	1.06	---	0.39
L_G/300s	Treated	6.74	3.35	5.96	3.98	---	1.53	0.44	1.09	---	0.29
Y_1/000s	Non-treated	3.72	1.75	4.14	2.11	---	0.65	---	0.14	0.81	0.46
Y_1/300s	Non-treated	3.89	1.58	4.38	1.89	---	0.67	---	---	0.45	---
G_1/000s	Treated	3.60	1.83	2.74	1.66	0.37	0.55	0.46	0.59	---	---
G_1/300s	Treated	4.40	2.17	3.16	1.84	---	0.42	0.53	0.50	---	---
B_1/000s	Non-treated	4.93	2.85	1.51	1.19	0.18	0.28	---	---	0.56	0.49
B_1/300s	Non-treated	5.49	2.99	1.78	0.84	0.32	0.50	0.39	---	---	---

The several nm etchings performed for this XPS study suggest that in some of the areas where Mn is found, its presence increases slightly as the analysis is performed inwards from the outermost surface. This corresponds roughly to less than 10 nm, so it is not representative for the bulk sample. Nevertheless, it is consistent with the presence of contaminants containing S and F at the outermost surface of the samples. It is more

appropriate here, however, to compare original areas of the bone with those affected by the laser irradiation. This is the case for Y_1 and G_1 areas, whose compositions are shown in Table 4.3. For example, a decrease in Ca, Si, Al and Fe content is accompanied by an increase in P and Na upon laser irradiation, consistent with the removal of aluminosilicates and iron-containing compounds expected to be present in the soil found in the site [56]. In addition, the fact that P and Na content increases after laser irradiation may be indicative of their stabilization via melting, inevitably causing damage to the surface. This is consistent with the surface aspect observed on samples L_W and L_G in Fig. 4.6, within the dark area affected by the laser. Furthermore, the dark color observed in the latter contain Fe and Mn, which are known to exhibit such color once their compounds have solidified from a melt [243]. Mn signals were also observed by SEM-EDS analysis, as discussed above, and its presence was confirmed at and near the surface of the sample by XPS. It seems thus reasonable to assume that the presence of Mn may originate not only on mineralization, but also on the original bone itself.

Regarding laser irradiation of the archaeological bone sample, this work has established a damage threshold in terms of the irradiance value. There is a need, however, to explore more in detail the relationship between irradiance and thermal incubation, in order to approach future laser conservation work from an optimum understanding of parameters which may assure respectful intervention of these types of artifacts.

4.4 Conclusions

This work explored the interaction of an 800 ps (sub-ns) pulsed near IR laser, with emission at 1064 nm, with the contamination and deteriorated layers present in an archaeological Pleistocene bear bone sample of *Sierra de Atapuerca*, which has undergone severe weathering throughout ages. The laser was operated in burst mode, and laser parameters which avoid damaging the surface of the bone sample were identified. A laser irradiance of 0.20 GW cm^{-2} was determined as the threshold damage value for these types of samples when working in burst mode. Below this value, the laser irradiation of Pleistocene bone appears safe and may lead the way to an efficient and satisfactory cleaning of its surface contaminants. SEM-EDS and XPS characterization studies comparing both, as-received and laser irradiated samples, enabled to conclude that contaminants containing mainly mineralogical clay components had been removed from the surface of the bone artifact. The presence of alumino-silicates was mainly found, for example, at its surface and was reduced significantly as the presence of Ca and P increased towards the sample's interior and upon laser irradiation. Furthermore, there are no significant compositional changes on

the bulk of the archaeological samples during irradiation. Their surface becomes darkened, however, upon laser irradiation above the damage threshold, apparently due to the presence of Fe and Mn within the resolidified surface. These may be present in the artifact for different reasons. Fe compounds may stem from the soil, while Mn could also be originating as a component of the bone itself, as it is particularly found in sufficient content within the sample cross-section and far from its surface.

CHAPTER: 5

IMPACT OF WAVELENGTH & PULSE DURATION

CHAPTER FIVE

IMPACT OF WAVELENGTH & PULSE DURATION

***Summary:** The impact of wavelength and pulse duration in laser cleaning of hard blackish contaminants crust from archaeologically significant Pleistocene bone is investigated in this chapter. The aim is to define practical cleaning procedures and determine better laser parameters for cleaning archaeological bone from Sima de los Huesos (Spain) based on conservation and restoration perspectives. Bone surface cleaning was performed utilizing two newly developed Q-switched Nd:YAG lasers: sub-nanosecond pulsed lasers with emission wavelengths at 355 nm and 1064 nm, respectively, and an Yb:KGW femtosecond pulsed laser with emission wavelength in the third harmonic at 343 nm. In all experiments, the laser beam scanning mode was applied to measure cleaning efficiency in removing contaminants and degradation products while assessing the underlying substrate surface damage. Wavelength-dependent absorption, pulse repetition rate and materials thermal properties are among the parameters considered to evaluate the potential that these types of lasers offer towards an increased cleaning efficiency of degraded bone surface. As a result, the effects of three laser irradiation systems and the bone surface morphology & composition were studied and compared using Optical Microscopy, Scanning Electron Microscopy – with Energy Dispersive X-ray Spectrometry (SEM-EDS), Thermal Camera, Fourier Transform Infrared Spectroscopy (FTIR) and X-ray Photoelectron Spectroscopy (XPS). The results indicate that femtosecond laser irradiation is significantly safer and more efficient at cleaning than sub-nanosecond laser irradiation, owing to the controllability of laser irradiation parameters, which allow for a systematic and accurate parameter description of an actual laser cleaning intervention.*

5.1 Background of the study

5.1.1 Laser parameters in artifacts cleaning

Cultural heritage (CH) conservation includes removing present deterioration conditions and preventing future deterioration as efficiently as possible. Given the wide diversity of materials, surface textures, and deterioration processes found in CH objects, the appropriateness of any conservation approach should be thoroughly examined and verified for each kind. Removing contaminants from artifacts without affecting the outermost

substrate is an essential prerequisite for the conservation process. For the last few decades, cleaning AM and museum stored artifacts using laser ablation has become a particularly appealing alternative approach and is currently fine-tuned to succeed in artifacts cleaning [1][111][223][244]. It has been used on a wide range of archaeological materials, including stones, ceramics, paintings, metals, monuments, bones, built heritages, textiles, and so on [115][245][246][19][108][172][247]. It is considered that laser cleaning techniques will have significant influence on cleaning operations in the near future and has emerged as a viable alternative to conventional mechanical and chemical methods for removing contaminants and deteriorating agents from artifacts.

A laser cleaning approach is based on the selective ablation of degradation and pollutant products from surfaces, and it has the added benefit of being non-contact, chemical-free and environmentally friendly. Several parameters of laser systems, including their wavelength [248], pulse duration, peak power etc. are entirely controllable from the user end [249]. In general, these settings can be tweaked to remove contaminated and degraded layers as efficiently as achievable, while causing no alteration or, in the worst of cases, non-visible limited alterations on the original sample substrate surface [250]. The selectivity and graduality on precise removal of contaminants are the most known advantages of this technique. Additionally, automation of laser cleaning is an attractive alternative that is still being investigated [136][18][4][156].

5.1.1.1 Influence of wavelengths

Studies on the laser cleaning of contaminated surfaces usually investigate and characterize the impacts of variations in laser wavelength on contaminants removal and original substrate preservation [136][251]. Considering the wide range of contaminant compositions and laser parameters, it's not unexpected that most research on laser cleaning of delicate and sensitive artifact surfaces do not provide complete agreement on the optimal criteria. Numerous studies have demonstrated increased contaminant removal when emitting in the Ultraviolet (UV) regime, whereas others favor emission in the near Infrared (n-IR) regime, while yet others find no discernible difference. Laser parameter optimization hypotheses assert that the irradiance value of the laser beam, the absorptivity of the materials, and the thermal conductivity of the layer being removed are all crucial in the safe and successful removal of contaminated layers, and all of these have a direct relation with the proper selection of the wavelength.

5.1.1.2 Influence of pulse durations

The pulse duration is an important parameter that influences laser cleaning. Archaeologically significant material has been cleaned using lasers with pulse durations ranging from microseconds (μs) down to femtoseconds (fs) [252][253][254][255][256]. For cleaning purposes, it has been revealed that heat incubation for shorter pulses on artifacts does not generate as much into the substrate as compared to longer pulse duration [234][257]. Lasers with short and ultra-short pulse durations enable high-precision laser intervention in this field. When compared to nanosecond (ns) laser pulses, lasers with pulse duration in the sub-nanosecond (sub-ns) to femtosecond (fs) range exhibit a substantial improvement in cleaning quality for a variety of materials [258].

New ultrashort pulse (<sub-ns) laser system has been developed in recent years as a new, precise and promising scientific tool for eliminating material from any surface [259]. The usefulness of this technique for cleaning different cultural heritage materials has been examined in the field of heritage conservation [260][105]. One of the most remarkable characteristics of ultrashort laser pulses is their strong nonlinear interaction with matter, which makes them an appealing alternative to nanosecond pulsed lasers [261][262]. The comparatively low thermal load generated by ultrashort laser pulses on the substrate reduces any collateral impact caused by heat accumulation [227], such as burning, cracking, chemical changes, and so on. At the same time, the nonlinear nature of the interaction allows for the removal of layers of material on a nanometric scale with significantly higher accuracy and control [257].

On the other hand, ultrafast fs laser cleaning is a surface functionalization process in which a surface is treated with a sequence of concentrated fs laser pulses, resulting in micro and nanoscale surface ablation [105][263]. When a fs laser pulse interacts with a material, energy is transferred first to the electrons within the material. When describing how energy is transmitted inside a material through phonon energy transfer from heated electrons to vibrations inside the material lattice, the two-temperature model (TTM) is commonly used in the literature. [264]. The effect of fs laser pulses has been studied on a range of different archaeological materials [265][105]; fs technique takes advantage of time-dependent energy coupling dynamics (known as laser induced plasma dynamics) of materials to couple enough energy into the material at the surface in order to intervene outermost layers depending on the material being cleaned [266][267]. It is well accepted that a fs laser pulse is important to minimize overheating and the possibility of micro melting of the treated substrate. In comparison to ns pulsed lasers, which are most widely used for surface

cleaning, it is predicted to considerably minimize severe thermal incubation [268][201][235][236].

5.1.1.3 Other parameters

In essence, the advancement in laser cleaning approach and large scale applications in the cultural heritage materials have allowed for improvements in pulse repetition frequency (i.e., from low to high) [269], flexibility of beam distribution mechanisms [224][270], consistency for long-term operations and experimental costs [271][272][273]. Laser cleaning of archeological artifacts has increased considerably, taking advantage of their controllability, accuracy, scalability, simplicity and working capacity in all material types [274][275][276][157]. However, laser techniques have been investigated for bone in biomedical science applications since 1964, specifically for hard-tissue cutting and dentin removal deprived of entirely satisfying the targeted expectations [277][278]. Despite the fact that laser cleaning has been used successfully on a wide range of archaeological objects with various forms of pollution and/or degradation for more than three decades, conservators have paid little attention to laser cleaning of archaeological mineralized bone, as there haven't been many case studies published on the subject [225][224][21]. The major cause for this might be a lack of suitable pulse lasers that protect delicate and fragile surfaces from cleaning instrument-produced damages. It's possible that the inconsistent composition and pace of bone breakdown and mineralization is another major reason why laser bone cleaning of archaeological significance has received so little study. Additionally, it is necessary to minimize the danger of damaging the original bone substrate surface while using a laser to clean. In order to do this, it is required to identify the parameters that control laser contact with contaminant layers rather than the core bone substrate surface.

5.1.2 Archaeological bone diagenesis

For having a successful laser intervention on archaeological bone, understanding bone diagenesis is essential because bone may act as "windows" into past lifeways, environments, and evolutionary histories [279]. In general, bone is a composite substance composed of organic, inorganic and water constituents [280]. All the latter are inextricably linked to create a single mineralized collagen fibril structural unit [281]. The proportion amount of organic and mineral components in bone, as well as their spatial organization (i.e., porosity, orientation, microstructure etc), all affect its mechanical properties and bone diagenesis [282]. Pre-death bone tissue properties are affected by a wide range of intrinsic and extrinsic factors (such as diet, mineral turnover, age, health status etc.), while post-

death bone undergoes numerous changes that are directly related to the time period how long it's been since death and the burial conditions (such as soil conditions, water, temperature, pH levels etc.) in which it was interred [283][284]. At the beginning of post-death, structural collagen is decomposed, and the proteins of collagen can be replaced fully or partially by inorganic precipitates [285]. When the collagen matrix decomposes, inorganic weathering mechanisms begin to erode the precipitated crystalline hydroxyapatite (HA), causing ions such as Ca, P, Fe, Al, K, Mn etc. to leach out. Some of the CO_3^{2-} groups in the carbonate-hydroxyapatite (CHA) dissolve spontaneously, transforming it into a more stable thermodynamic phase of CHA with a crystal habit remarkably similar to that of HA [286][287]. Strong protein-mineral interactions bind collagen and HA together, giving bones their tensile strength and durability, which are eventually lost following the bones age and diagenesis process. Deterioration continues until the full bodily breakdown, decalcification, and bone disintegration have occurred in bone [214].

Bone contamination can be physical or chemical in the burial ground. Bone tissue's porous nature makes it vulnerable to invasion. The presence of a number of physical and chemical pollutants in ancient bone has been revealed [288]. Contaminants might have entered the bone in one of two ways: either by precipitation from nearby groundwater or physical integration, (Calcium, as an example, may be added into groundwater by the precipitation of calcium carbonate), or inclusions (such as quartz can be found in bone as solid grains).

Phosphorus (P) is essential in the processes of bone diagenesis. It has been stored in many forms at various bodily components; it has been found in proteins composed of nucleic acids and coenzymes, sugar phosphates, and fats of the brain and spinal cord, known as phospholipids. During diagenesis, P leaching happens in its orthophosphates oxidized form—but neither follows simple pathways nor remains in its basic elemental form. Even though oxidized orthophosphates are the most thermodynamically stable and hence transportable forms of phosphorus, they appear to be closely regulated by modest soil acidity in the pH 6–7 range [289]. On the other hand, phosphorus becomes insoluble at pH levels over 7, and is definitely insoluble at pH levels below 5 [290].

Phosphorus exists mostly in burial soils as insoluble inorganic compounds [215], usually in combination with Fe, Ca, Mg and Al. As a consequence, minimal phosphorus leached is generally predicted, but depends very much on the hydrogeology setting of the buried archaeological soils [217] [216]. Soil microbes (Penicillium, Mycobacterium,

Pseudomonas, *Micrococcus*, *Aspergillus*, *Flavobacterium* etc.) also help P transformations from insoluble inorganic complexes to be solubilized, removed from minerals and incorporate into the new protoplasm forms [279]. Moreover, in the mechanism of P absorption by metal oxides (specifically those of Fe and Mn), it might be possible that P leaching is constantly recycled and/or a net migration off-site within some portions of the archaeological soil ensuing the suitable geological settings [291][292]. Furthermore, the bone is outlined with dark stains on a burial level by the phenomena of burial silhouette, which has an intriguing relationship with evidence of burial. It has been emphasized that in sandy and gravelly acidic soils, the organic P complexes further attract other soil metals, particularly Mn, which results in black stains on the bone surfaces [218]. Due to constant recycling of P leaching and inorganic mineralization weathering, it might be possible that hard blackish and minor yellowish stains and thus encrustations may have appeared at the outermost bone layer, following the minerals that are precipitating with Fe and Mn oxides and hydroxides, carbonates and silica [221] [212].

5.1.3 Objectives of the chapter

This present work extensively studied the laser bone interaction of different wavelength-dependent sub-ns and ultrafast fs laser techniques as the best possible alternative to conventional cleaning techniques. Hence, the final result has been taken into account by comparing the topography, structure, and composition of archaeological Pleistocene bone surface 'as received with black encrustations' and 'processed with various laser irradiations'. Another objective was to evaluate the usefulness of new sub-ns and fs pulsed laser technologies for removing blackish – yellowish encrustations from Pleistocene bone surface, excavated in archeologically significant *Sima de los Huesos* site at *Sierra de Atapuerca* (Burgos Spain) [72][92][91], while safeguarding the original patina on the substrate surface, in order to preserve as much as possible the surface anatomical details obscured by bone deterioration and contamination. The bone sample was treated by 800 picosecond (ps) ultrashort pulse laser technology with an emission wavelength in the n-IR regime (1064 nm), a 300ps ultrashort pulse laser with an emission wavelength in the UV regime (355nm), and a 238fs ultrafast pulse laser irradiation with an emission wavelength in the UV regime (343nm). The cleaning experiments were assessed in terms of the rate of removal of the hard blackish encrustation and the resulting damage to the bone-forming minerals. Optical Microscopy, Fourier Transform Infrared Spectroscopy (FTIR) in Attenuated Total Reflection mode (ATR-FTIR), X-ray Photoelectron Spectroscopy (XPS), and Scanning Electron Microscopy with Energy Dispersive X-ray Spectroscopy (SEM-EDS) were used to evaluate the removal rate and efficiency of the laser system.

Additionally, optical and SEM photographs used to assess the induced damage of the outermost bone surface.

5.2 Materials and methods

5.2.1 Pleistocene bone

Three Pleistocene bone pieces from a single bear rib bone were selected for this study. They are physically defined as follows: i) 2.6 cm long x 1.2–1.4 cm wide x 0.7–0.85 cm thick (Fig. 5.1a), ii) 1.9 cm long x 0.6 cm wide x 0.2 cm thick (Fig. 5.1b) and iii) 2.5 cm long x 0.7–1.0 cm wide x 0.4 cm thick (Fig. 5.1c). This 430,000-year-old rib bone was excavated in 1986 as soiled material with atmospheric dust on its surface. It had been previously cleaned mechanically with a soft brush, in order to remove any loose debris as a preliminary step towards conservation. Large areas of these bone artifacts exhibit varied shades of hard blackish-yellowish stains and encrustations unevenly distributed, in contrast to the normal whitish-yellowish color associated with fossilized bones, which most likely arise from weathering patterns attributed to Fe staining and Mn mineralization effects [232][233][232]. The purpose of the present study is to clean the hard-blackish-yellowish stains and encrustations from the outermost layer of this bone without changing its natural appearance.

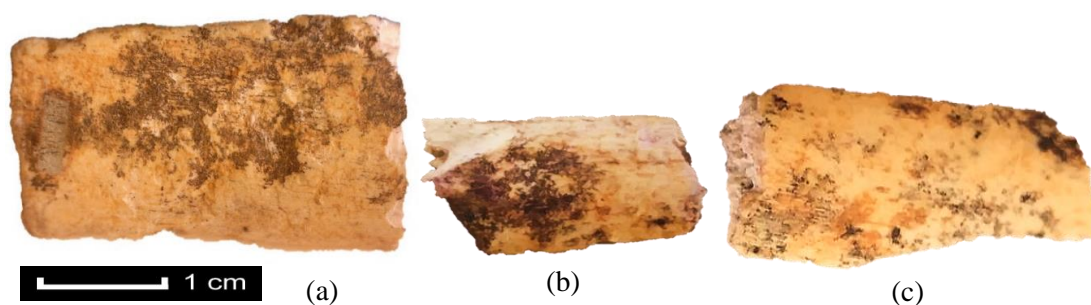


Fig. 5.1: Front side photograph views of the bear rib (shaft) bone fragments excavated at the *Sima de los Huesos* archaeological site at *Sierra de Atapuerca* (Burgos, Spain)

5.2.2 Laser cleaning systems and parameters

Two sub-ns and one fs laser systems employed to this investigation. Table 5.1 presents the emission characteristics of all the three laser systems.

Table 5.1: Characteristic emission of the sub-ns and fs laser employed for the present study. Values are given for the pulse emission wavelength λ , average power (P), pulse width (τ), pulse repetition rate (f), maximum pulse energy E_p , scan speed V , distance between adjacent laser passes d and beam waist (D_b) applying the $1/e^2$ criterion for a Gaussian beam distribution.

	Femtosecond (fs) Laser	Sub-nanosecond Laser	Sub- nanosecond Laser
Wavelength λ	343 nm	1064 nm	355 nm
Pulse duration τ	238 fs	800 ps	300 ps
Pulse repetition rate f	200 kHz – 1 MHz	200 – 800 kHz	200 – 800 kHz
Average power P	9.33 W	8 W	3 W
Maximum pulse energy E_p	46.6 μ J	40 μ J	15 μ J
Beam diameter D_b	30 μ m	80 μ m	31.4 μ m
Distance between adjacent laser passes d	15 μ m	20 μ m	20 μ m

In this study, laser beam scanning approach has been experimented to all the laser treatments test. The laser beam scans the surface at a predetermined rate (i.e., 150 mm/s for fs laser and 3000 to 7000 mm/s for ps laser), while also regulating the spacing between consecutive scan lines (i.e., 15 μ m for fs laser and 20 μ m for ps laser). Continuous beam surface scanning is faster than burst scanning because the laser does not need to stop between pulses [106].

A series of initial explorative experiments were conducted using both fs and sub-ns laser sources to determine the most appropriate parameters for the removal of contaminants and degradation products, taking into consideration prior research on ancient bones [224][225][21]. The target was uniformly irradiated with the sub-ns laser across a region of 2 mm² each by beam scanning mode along parallel lines in the X direction. In contrast, fs laser irradiation of a similar area was carried out by scanning the beam along parallel X-axis lines and then perpendicularly crossing Y-axis lines (i.e., cross: 0° and 90°). Bidirectional hatching (line filling) with no outline mode was applied in all cases. Visual inspection and optical microscopy were used to assess the preliminary test results. The irradiation parameters used for this investigation were those that resulted in the cleanest

possible bone surface (under optical and scanning electron microscopy) with zero or minimal noticeable encrustation leftovers and no apparent damage to the bone's outermost layers. Thermal incubation, or the accumulation of energy input over time into a specific region of the sample, is controlled from the user end by changing different parameters. Irradiance and fluence are not proportional in this study because three distinct laser systems are employed with significantly different pulse duration.

5.3 Results and discussion

The irradiance thresholds I_{pulse} were determined by dividing the pulse energy delivered on the target by pulse duration τ of specific unit area; while the pulse energy E_p is the energy emitted by the laser (P) divided by the pulse repetition frequency (number of pulses emitted per second) (f). On the other hand, fluence F_{pulse} is the energy per unit area per pulse. Hence, it is important to note that if the pulse duration is not changed, fluence and irradiance values are proportional. In addition, nominal power refers to the maximum power output of the laser, P is the power level chosen for each emission condition, which is selected by establishing a pump power level, A in ps lasers, and attenuation level $\%P$ in the fs laser.

In the beam scan mode, the laser scans one line with a predefined length along the X-axis. Apparently, the sample is considered to be in a fixed position and the distance between lines has been fixed manually in the computer program. The distance between the centers of the two-consecutive spots defines the area that overlaps between the two pulses. The elapsed time between two pulses is $1/f$, while the distance between two spot centers is $d=V/f$. It is possible to obtain a uniform energy distribution along the scanning direction throughout the target surface by conveniently establishing the distance between lines and spots and vice-versa.

The 'ablation threshold', 'cleaning threshold' and 'damage threshold' of laser irradiation for the specific Pleistocene bone cleaning is determined employing all three different wavelengths in terms of irradiance value here in this study. Beam scan irradiation mode was performed in order to indicate the irradiance onset that results in the assessment of the irradiated surface following encrustation removal efficiency. All of the irradiation was performed without making any wetting of the bone surface. The damage threshold of bone is defined by the irradiance at which physicochemical changes, such as melting, color changes, cracking, spallation and extraction etc. become visible under the optical microscope and SEM observation. Special attention was focused on the possible damage

to the bone composition, specifically regarding the Ca/P compositional ratio, which might be possible with the highest susceptibility to the laser beam, due to bone optical absorption properties [293]. While determining the damage thresholds for the operating irradiance ranges was rather easy, determining the start of contaminant removal (cleaning threshold) is unquestionably more complex. It is possible that some areas of the final surface were locally irradiated more than once rather than just one in order to fine-tune the removal of the contaminant from the surface. As a result, it is necessary to finalize the good cleaning threshold values for the blackish to yellowish encrustations for each laser systems.

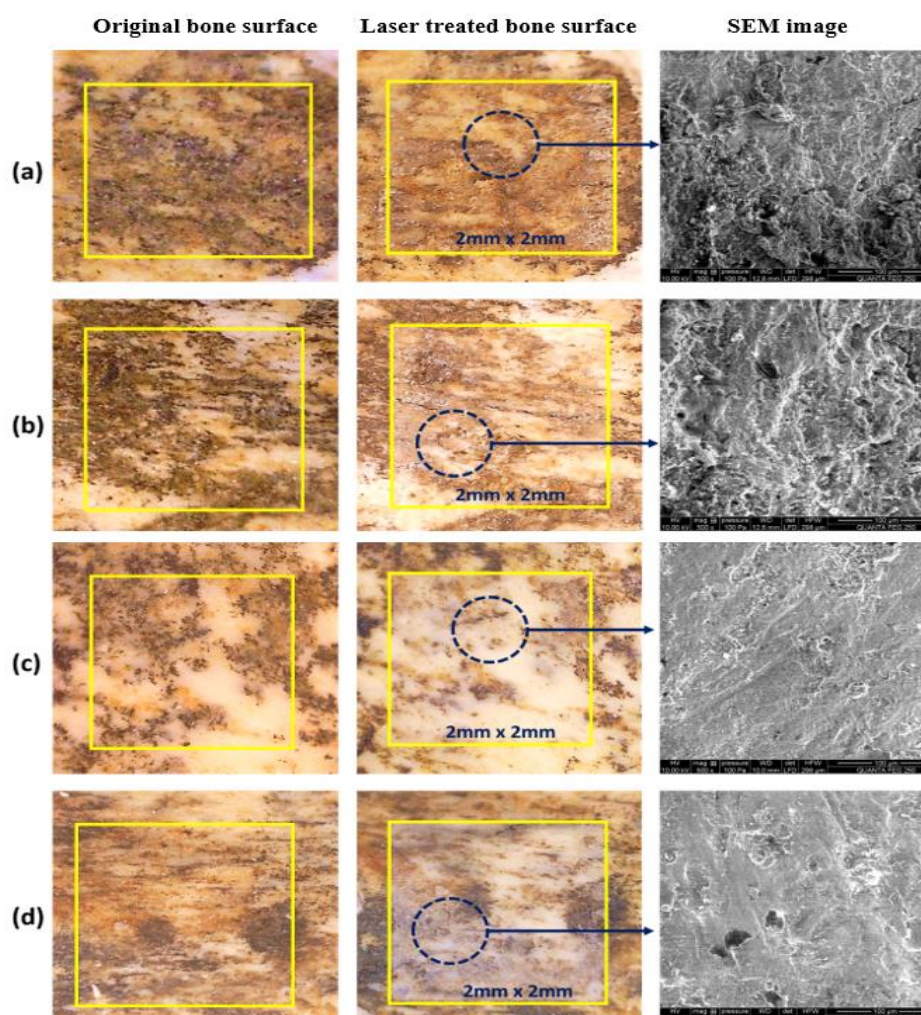


Fig. 5.2: Optical microscopy images of the original bone region (left), laser beam scan mode treated bone region (middle), and corresponding SEM images of the laser cleaned area. Fig ‘a and b’ presents the sub-ns n-IR laser treatment while ‘c and d’ shows the outcomes of sub-ns UV laser treatment.

Table 5.2: The sub-ns laser interaction with Pleistocene bone was studied and reported on using different experimental parameters for the assessments.

Laser	Area	P (W)	f (kHz)	Ep (J)	V (mm/s)	FL (J/cm ²)	IL (GW/cm ²)	Observations
Sub-ns n-IR (1064nm) 800ps Laser	1	7.24	700	1.03x10 ⁻⁵	7000	0.20	0.25	Very little cleaning (Fig. 5.3).
	2	7.24	600	1.21x10 ⁻⁵	6000	0.24	0.30	Cleaning efficiency is not good. (Fig. 5.2a, and 5.3)
	3	7.24	500	1.45x10 ⁻⁵	5000	0.28	0.36	Cleaning efficiency is not good (Fig. 5.3).
	4	7.24	400	1.81x10 ⁻⁵	4000	0.36	0.45	Micro-cracks and melting observed (Fig. 5.2b and 5.3).
	5	6.29	400	1.57x10 ⁻⁵	4000	0.31	0.39	Cleaning efficiency is not good (Fig. 5.3)
Sub-ns UV (355 nm) 300ps Laser	1	0.58	300	1.93x10 ⁻⁶	3000	0.25	0.83	Cleaning efficiency is not much appreciable.
	2	0.49	500	9.80x10 ⁻⁷	5000	0.12	0.42	No noticeable cleaning.
	3	0.66	400	1.65x10 ⁻⁶	4000	0.21	0.71	Cleaning efficiency is not good.
	4	0.90	300	1.65x10 ⁻⁶	3000	0.38	1.29	Structural damage, color changes and melt observed. (Fig. 5.2d)
	5	1.02	400	2.55x10 ⁻⁶	4000	0.32	1.09	Good cleaning. (Fig. 5.2c)

The degree of interaction between the laser and the bone substrate, and therefore the degree of damage to the latter, is determined by a combination of irradiance and incubation values [51]. In order to adequately analyze melting evidence, and color and microstructural changes, small portions of the surface were irradiated throughout the various regions of the bone and initially investigated and respectively examined by optical and electron microscopy. The cleaning and damage threshold values that have thus been determined are based on many experiments and observations. Observations of sub-ns n-IR laser cleaning led to the conclusion that irradiation levels less than $\approx 0.40 \text{ GW cm}^{-2}$ ensure that bone damage is avoided. Additionally, these results indicated that damage to the substrate surface occurred at an irradiation of 0.45 GW cm^{-2} (Fig. 5.2 and 5.3: Area 4) As a result and with a safety margin in mind, irradiation values less than 0.40 GW cm^{-2} appear to cause no harm and were so chosen for future cleaning investigations.

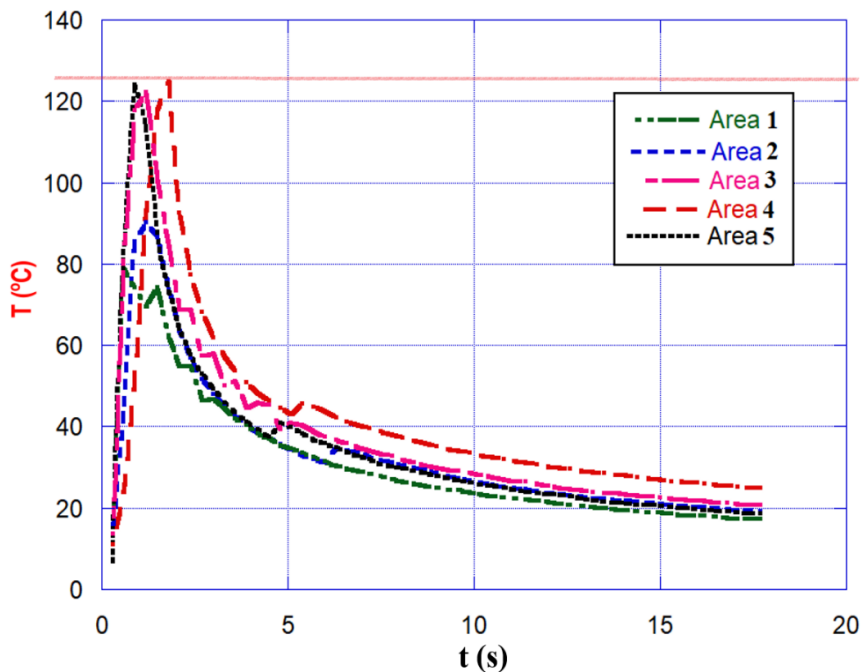


Fig. 5.3: The record of the temperature changes at the sub-ns n-IR laser by utilizing Thermo Cam P25 IR camera, associated with the Fig. 5.2 and Table 5.2.

When the laser irradiation is increased, the bone surface temperature rises as a result. Figure 5.3 shows the temperature variations that occurred while using sub-ns n-IR laser treatment to remove contaminants and hard blackish encrustations. Using the processing parameters listed in Table 5.2, it takes roughly 1.5 seconds to treat an area of 2 mm^2 bone surface each

time. Figure 5.3 depicts the heat generations when bone surface cleaned by utilizing 800ps n-IR laser. IR thermal camera's measuring range of -40°C to 125°C is exceeded by the maximum temperature for 0.45 GW cm^{-2} irradiance values. At a temperature of more than 125°C , melt and cracks on the bone surface started to appear. It has been observed that, on the other hand, the optimal cleaning threshold generates heat around 123°C at maximum, while the ablation threshold can reach to 75°C .

When it comes to laser fluence F_{pulse} , the term refers to the amount of energy emitted from a single laser pulse per unit area of a given spot size, while irradiance I_{pulse} refers to the amount of laser fluence emitted per pulse duration, and pulse repetition rate f_p refers to the number of pulses per second. Distance between two lines was fixed at $25\ \mu\text{m}$, and execution number was fixed at 1 in all experiments at this study. However, after conducting several irradiation trials, it was determined that the cleaning effectiveness was insufficient for eliminating this sort of hard blackish encrustations. On the other hand, when the number of treatment sessions increased, little melting began to occur and fractures became visible. For all of these trials, the incubation level was kept constant, as was the ratio of scanning speed to repetition rate, as indicated in Table 5.2. Irradiation was concentrated on the sample's dark blackish regions as seen in Fig. 5.1. (a).

Bone damage can be prevented with irradiation levels as low as $\approx 1.15\text{ GW cm}^{-2}$, according to study on sub-ns UV laser cleaning. These findings also showed that irradiation of 1.29 GW cm^{-2} caused damage to the substrate's surface. To be on the safe side, radiation values less than or equal to $\sim 1.15\text{ GW cm}^{-2}$ have been chosen for bone laser cleaning studies since they appear to cause no harm on the bone surface. It was discovered, however, following several irradiation experiments, that the cleaning efficacy was insufficient for eradicating the hard black encrustations. Willfully, increasing the execution number with the same settings, cracks became evident and colors began to shift. The scanning speed to repetition rate ratios were consistent for having similar incubation during all of these experiments, as shown in Table 5.2.

With the objective of removing the blackish colored overlayers from the bright white colored substrate, a "cleaning" threshold I_{pulse} range for n-IR beam scan irradiation at 1064 nm was identified, though it has been observed that cleaning efficiency was not good enough for being good cleaning threshold. By changing the laser system's power output from 4.39 W to 7.24 W , the irradiance levels used for the aforementioned tests ranged from 0.25 to 0.39 GW cm^{-2} (Table 5.2: sub-ns n-IR 800ps laser). Contrarily, in order to clean the

dark blackish colored overlayers, a "cleaning" threshold irradiance I_{pulse} range for UV beam scan revealed by operating different power output of the laser system (from 0.23 W to 1.39 W). The good cleaning irradiance found at around 0.90 to 1.15 GW cm⁻², while inefficient cleaning started from 0.71GW cm⁻². In both laser systems, multiple laser irradiation treatments were done on the bone surface in various locations with the identical irradiance conditions, leaving a specific area to be used as a reference for finding out the appropriate cleaning parameters. Apparently, no contamination removal below this I_L cleaning threshold settings have been observed.

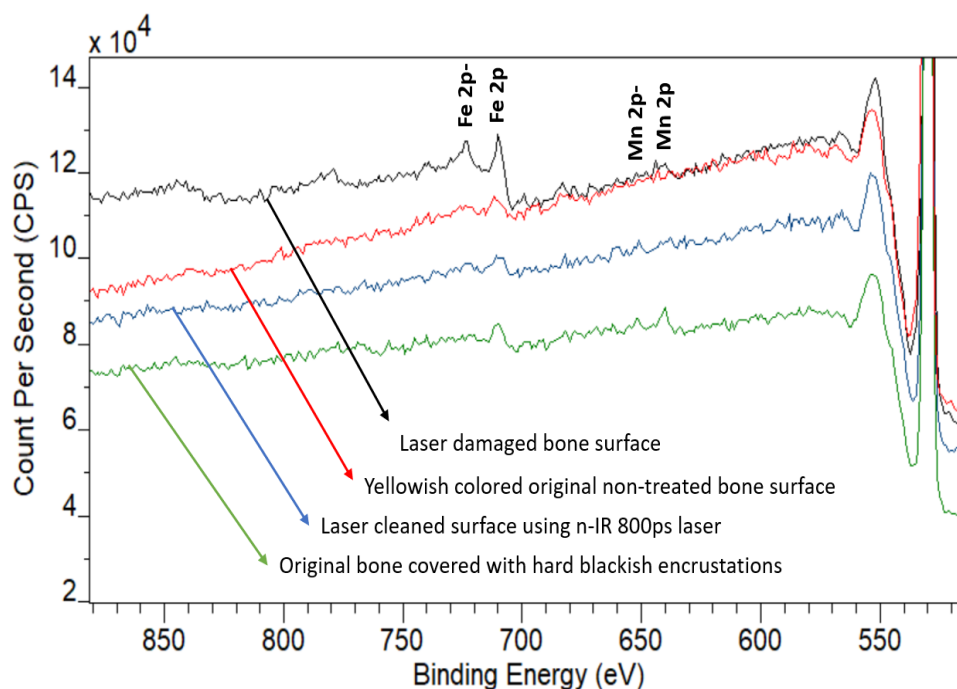


Fig. 5.4: Representative raw XPS survey spectrum of the bear rib bone. Bottom to top: green colored band obtained from the 'as received non treated' bone; blue colored band corresponding to the 'n-IR (1064nm) 800ps laser-treated bone surface; red colored band from the 'as received non treated' bone surface and black colored band obtained from the laser induced molten surface area of the bone.

To assess the chemical composition of the bone surface, specifically the hard blackish overlayers in both its "as received and laser treated" surface, we have studied the SEM-EDS and XPS data (Fig. 5.2 and Fig. 5.4) to look for the presence of Mn, Fe, and other typical elements. As a result, the existence and distribution of Ca and P, both of which are essential for bone have been observed, found that Ca/P ratio followed almost similar to the standard bone compositions [106]. Even after laser cleaning, Mn was found in substantial quantities,

according to EDS and XPS analysis. Considering prior research indicating Mn may be an element of bone, this is not surprising [48]. XPS revealed the sample's surface and vicinity contained Mn; it may have originated not just during mineralization but also from within the initial bone [106]. EDS study indicates that Mn has a similar distribution pattern to Fe (Fig. 5.4), indicating that it was incorporated during the diagenesis process. Fe and Mn, which are known to display dark stains are also responsible for the black hue seen in the latter [53].

Both characterization methods indicate that Mn and Fe are still present in appreciable amounts within the 0.45 GW cm^{-2} sub-ns IR laser irradiated area (Table 5.2: Area 5). The fact that Al and Si are detected indicates that the bone has come into touch with clay (Fig. 5.5). If bone has in addition been submerged for an extended length of time and mechanical breakdown or chemical degradation has occurred, Mn and Fe compounds might precipitate to a depth observable in the bone cross-section near the surface, resulting in blackish yellowish stains and later encrustations on the bone's topmost layer (Fig. 5.2 and Fig. 5.4).

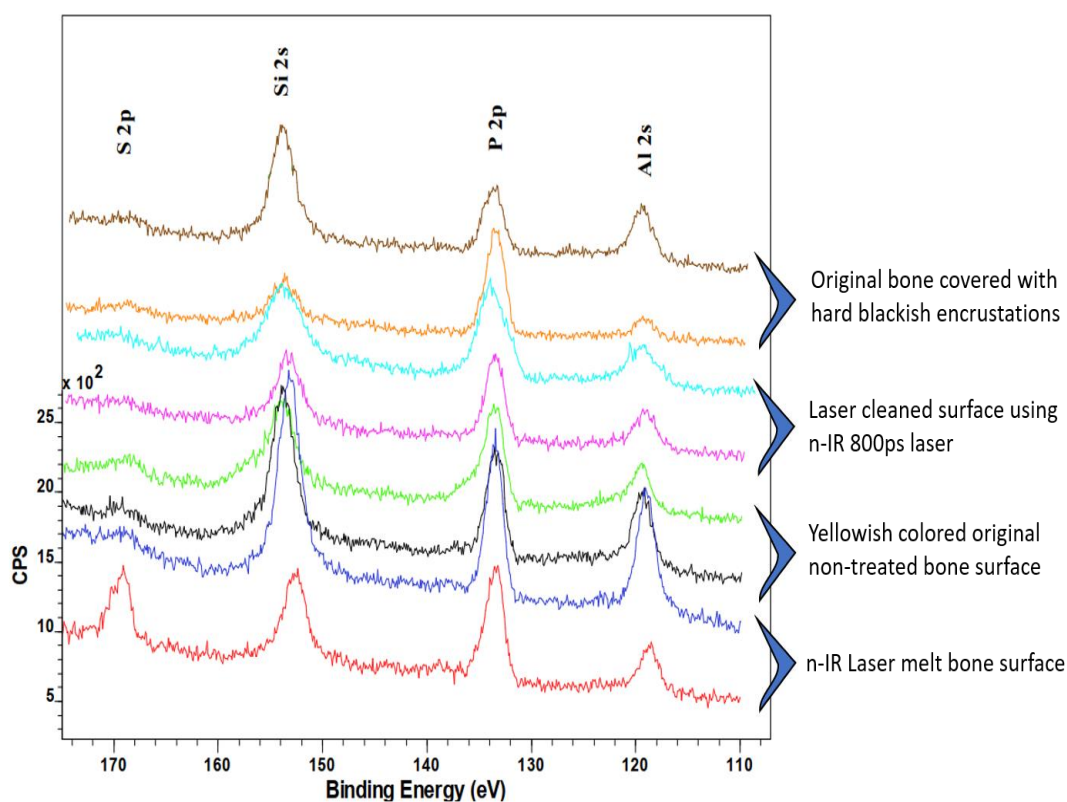


Fig. 5.5: Representative XPS survey spectrum of the bear rib bone presenting different minerals correspond to the registered HR regions. C 1s (C-C) 284.9 has been used to calibrate the spectra.

When treated with both sub-ns lasers, the dark black and yellowish contaminated crusts typically discolored into a brownish hue. EDS and XPS characterization suggest, however, that laser cleaning did not produce significant compositional changes when satisfactory cleaning threshold values were applied. It has been hypothesized that the coupled heat dissociation of the Mn and Fe compounds may be the cause of the small brownish color change observed on the samples. Analogous findings for different areas of sub-ns UV laser treatment revealed that, at I_{pulse} values slightly above the ablation threshold, hard blackish encrustation and/or mineralization are not properly removed, whereas only a very thin layer of matrix material can be removed from the over-layers of the bone surface. These are consistent with previous n-IR laser treatment observations within different areas of the artifact (Fig. 5.2).

Table 5.3: The fs UV laser interaction with Pleistocene bone was studied and reported on using different experimental parameters for the assessments.

Area	P (W)	Effective f (kHz)	E_P (J)	F_L (J/cm ²)	I_L (TW/cm ²)	Observations
1	0.42	10	2.1×10^{-6}	0.29	1.24	Good cleaning, hard blackish-yellowish encrustations steadily cleaned (Fig. 5.6 & 5.7: Laser treated Area 1, Table 5.3: Area 1)
2	0.42	10	2.1×10^{-6}	0.29	1.24	Good cleaning, hard blackish encrustations steadily cleaned (Fig. 5.6 & 5.7: Laser treated Area 2, Table 5.3: Area 2)
3	0.54	10	2.7×10^{-6}	0.38	1.60	Good cleaning, hard blackish encrustations mostly cleaned (Fig 5.6 & 5.7: Laser treated Area 3, Table 5.3: Area 3)
4	0.66	10	3.3×10^{-6}	0.46	1.96	Good cleaning, hard blackish encrustations mostly cleaned (Fig. 5.6 & 5.7: Laser treated Area 4, Table 5.3: Area 4)
5	0.80	10	4.0×10^{-6}	0.56	2.37	Good cleaning, hard blackish encrustations mostly cleaned (Fig. 5.6 & 5.7: Laser treated Area 5, Table 5.3: Area 5)
6	0.94	10	4.7×10^{-4}	0.66	2.79	Little structural damage (cracks) observed, hard blackish encrustations mostly cleaned (Fig.5.6 & 5.7: Laser treated Area 6, Table 5.3: Area 6)

In the case of fs UV laser interaction with Pleistocene bone study, pulse repetition rate f refers to the effective final frequency outcomes after using the PPD. Distance between two lines was fixed at 15 μm , and execution number was fixed at 10 in cross hatch mode (i.e., 0° and 90°) in all experiments. Controlled cleaning of bone with no indication of melting, carbonization, or cracking is possible utilizing an ultrafast laser with 238 fs pulse duration and emission at 343 nm wavelength with irradiances greater than the ablation threshold. The ablated surfaces have a slightly rounded form and are covered with irregular and non-homogeneously blackish encrustations, giving them an uneven and non-uniform appearance. The cleaning operation occurs as a result of a being above the ablation regime and whether the ablation mechanism involved is photothermal, photophysical/photomechanical or photochemical [54], for the pulse irradiances employed ranges from 1.24 TW cm^{-2} to 2.37 TW cm^{-2} . According to the study, damage on the bone surface can be avoided at irradiation intensities as low as 2.37 TW cm^{-2} . Additionally, these data indicated that irradiation at 2.79 TW cm^{-2} produced damage to the substrate's surface, where cracks and melting are evident above the damage threshold. To be safe, irradiation less than or equivalent to 2.37 TW cm^{-2} were chosen for bone laser cleaning experiments, since they appear to have no detrimental effect on the bone surface. Following multiple irradiation tests, it was determined that the cleaning efficiency was good for removing the hard black encrustations. By deliberately raising the number of laser beam scan repetitions in cross mode, while maintaining the same laser and beam scan parameters, the original appearance of the bone surface gradually revealed. The laser irradiance values applied in this study ranged from ~ 1.24 to ~ 2.79 TWcm^{-2} . A satisfactory cleaning threshold was established within the 1.24 \sim 2.37 TWcm^{-2} range for beam scanning this specific Pleistocene bear rib bone using a UV ultrafast pulsed laser emitting 238 fs pulses. The outcomes of beam scan laser cleaning are showcased in Table 5.3, while Figures 5.6 & 5.7 show the outcome of effective good cleaning threshold values and corresponding SEM images.

The optical micrographs of Fig. 5.6 show the actual region of the 'as received' bone (left side), where the blackish mineralized encrustations zone is evident; Fig. 5.7 represents the corresponding SEM images, marked as 'Original bone surface'. Due to the Gaussian spatial beam profile of the pulses, the maximum non-damaging laser irradiance I_{pulse} on the sample surface measured for contaminant removal in dark mineralized areas is 2.37 TW cm^{-2} (Table 5.3, Area 5). The dense blackish - yellowish contaminated crusts didn't show any discoloration; similarly, SEM-EDS data (Table 5.4) indicate that laser cleaning did not alter the composition of the surface under the revealed good cleaning conditions for this aforementioned fs laser system.

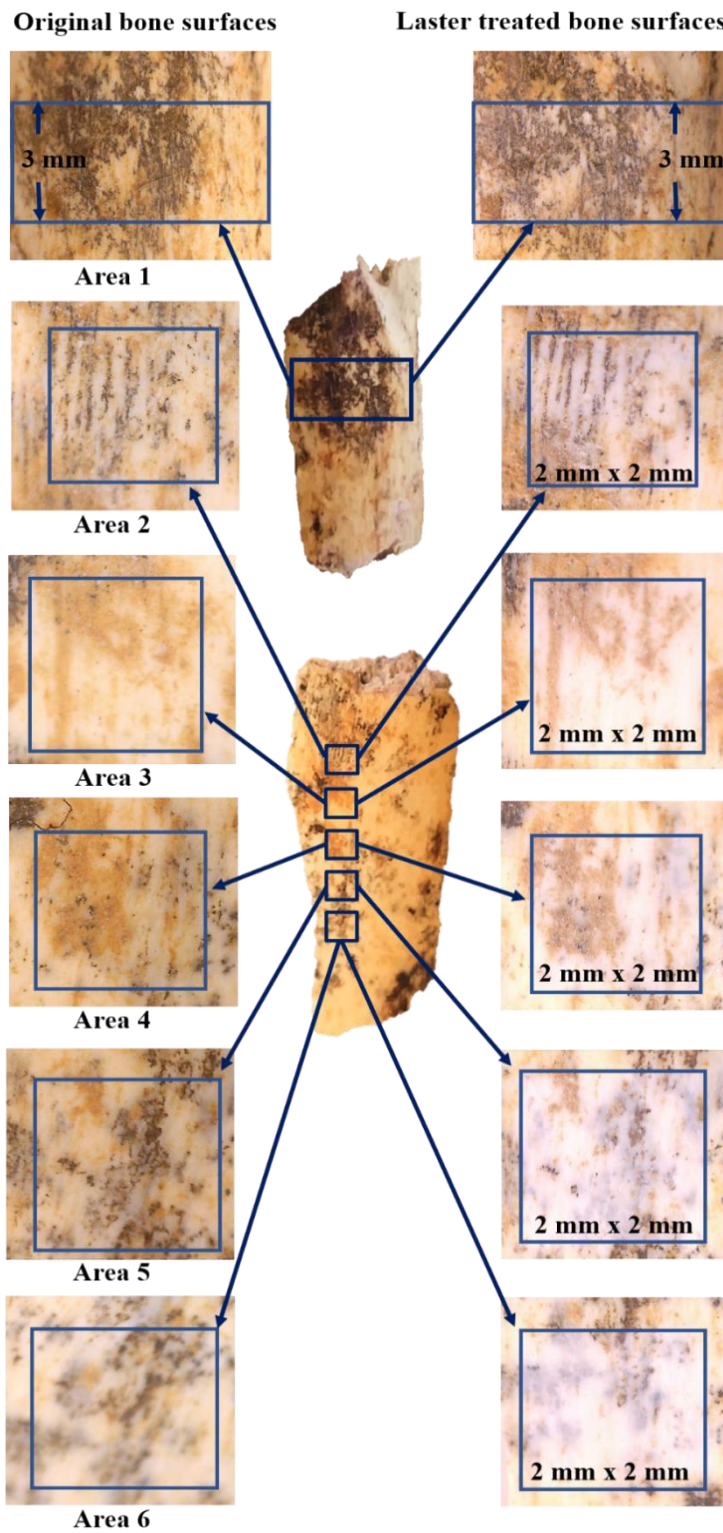


Fig. 5.6: Optical microscopy and SEM images obtained on the Pleistocene bone sample subjected to this study: Left hand side: original bone surfaces represented the different original 'as received' area (Area 1 to 6) where the right hand side laser cleaned bone surfaces correspond to the same area treated by the ultrafast fs lasers, under different irradiance values.

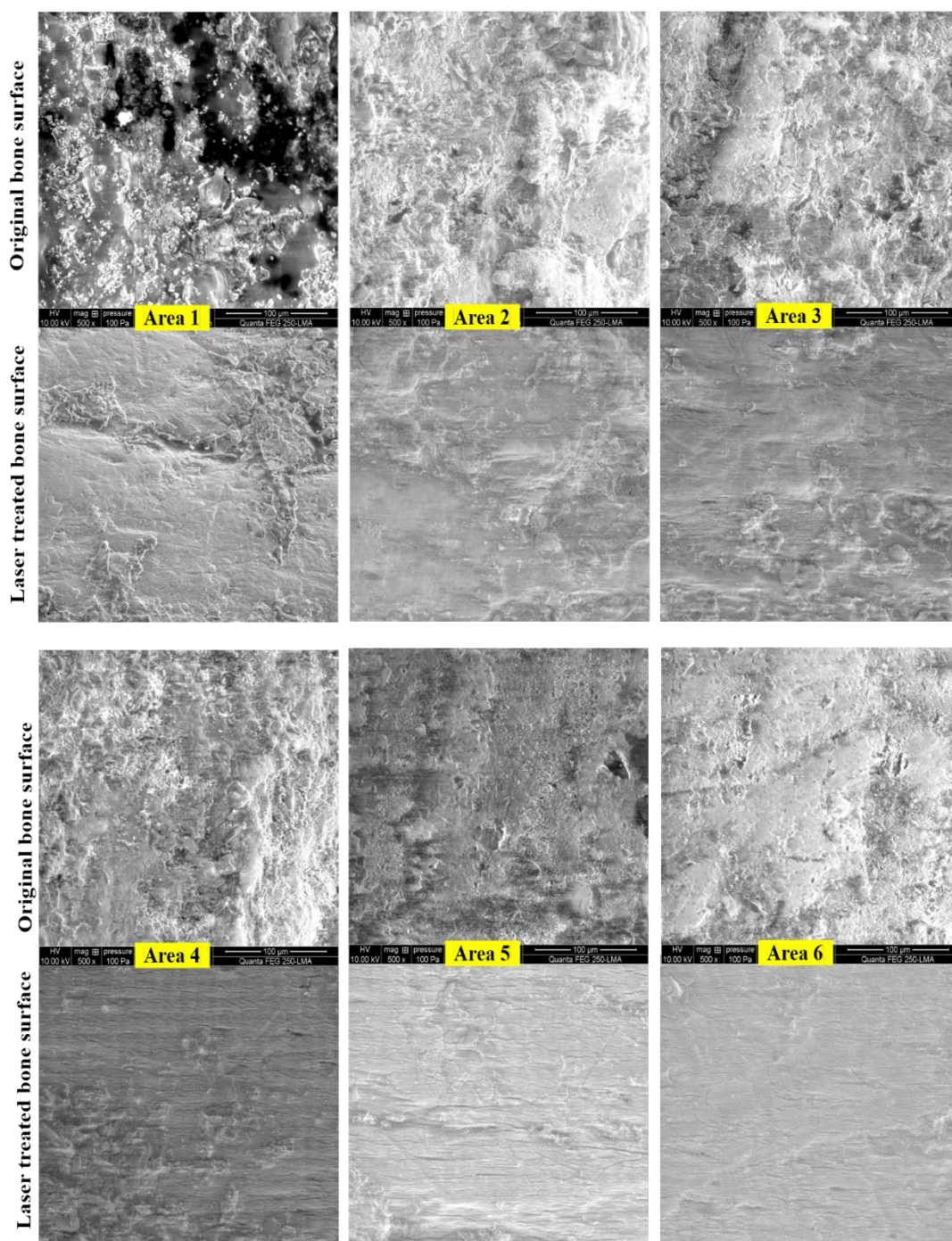


Fig. 5.7: SEM images obtained on the Pleistocene ‘as received’ and ‘laser treated’ bone surfaces subjected to this study. Columns 1 and 3 correspond to areas 1-6, (left side in Fig. 5.6). Equivalent micrographs are shown in columns 2 and 4, corresponding to laser treated areas 1-6 (right side in Fig. 5.6).

Archaeological fossilized bones have substantial compositional changes, which are reflected in the Ca/P atomic ratio, which demonstrates a constant composition connected to the fundamental Ca hydroxyapatite structure of bone. After fs laser irradiation, the amount of Si, Al, and Fe decreases while the content of Ca and P increases, which is in line with the removal of aluminosilicates and iron-containing compounds measured in the soil found at the burial area (Table 5.4) [242]. It is also possible that the increased Ca and P content following laser irradiation indicates that those elements are being stabilized by melting, which leads to surface damage. As for Fluorine (F), it has been identified in fossil bones and has been particularly linked to water intake in animal's diet [238]; F levels in fossil bones therefore vary depending on the location of the fossils. Silicates (i.e., feldspars), nitrates, sulfates, and others may be linked to the burial environment, as these elements are commonly discovered as soil components at archaeological sites, and specifically at the *Sierra de Atapuerca* site [242].

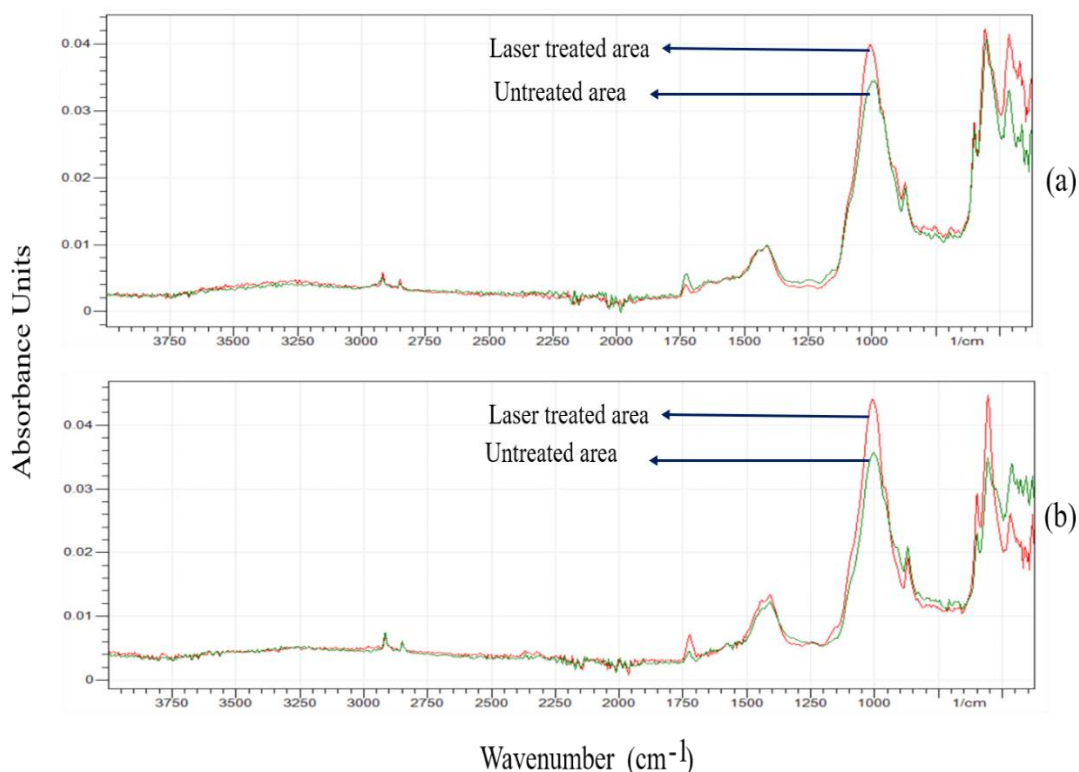


Fig. 5.8: FTIR spectra of fs laser treated and untreated samples; represents the hard blackish contaminated surface irradiated by 1.24 TWcm^{-2} (Fig. a) and 2.37 TWcm^{-2} (Fig. b) along with the untreated original surface area.

Table 5.4: Elemental composition of Pleistocene bone surface ‘as received and after fs laser treatment’ obtained from EDS (SEM) analysis. The presence and distribution of Ca and P, essential components of bone, is confirmed and observed to increase significantly after laser treatment. Mn is observed to increase with laser treatments in all of the analyzed areas. Fe content is found, however, to increase in some areas and decrease in others, as a result of laser treatment. In addition, C containing contaminants are observed to decrease considerably upon laser irradiation, suggesting that they were abundantly present in the outermost layers of the artifact, and that the laser treatment efficiently removes them from the bone substrate.

Elements (wt%)	Area 1	Laser treated Area 1	Area 2	Laser treated Area 2	Area 3	Laser treated Area 3	Area 4	Laser treated Area 4	Area 5	Laser treated Area 5	Area 6	Laser treated Area 6
C	49.12	22.03	15.66	6.66	14.83	7.44	14.86	5.95	12.38	7.15	9.54	6.93
O	26.57	37.32	38.63	34.78	38.89	34.65	38.77	38.02	36.42	35.31	40.62	35.33
Fe	1.44	1.7	5	2.11	5.45	1.98	4.3	5.6	2.8	3.5	4.95	3.48
Na	0.45	0.52	0.47	0.43	0.38	0.51	0.42	0.2	0.49	0.5	0.41	0.42
Mg	0.27	0.31	0.56	0.19	0.61	0.36	0.52	0.97	0.31	0.8	0.5	0.31
Al	2.68	3.25	6.07	2.01	6.3	2.62	4.76	8.6	2.57	5.72	5.8	2.96
Si	3.77	2.78	10.24	3.13	11.5	4.25	7.83	16.9	4.18	10.64	9	4.75
P	3.76	8.9	6.26	14.59	6.04	13.39	8.19	5.65	12.4	9.73	8.76	12.57
K	1.04	0.54	1.94	0.56	2.06	0.95	1.44	2.88	0.83	1.92	1.45	1.02
Ca	10.34	20.45	14.53	33.04	13.25	31.16	18.42	12.64	27.13	21.86	18.49	28.8
Mn	0.54	0.83	0.66	0.89	0.69	0.72	0.5	1.23	0.49	1.16	0.47	1.79

Figure 5.8 illustrates the ATR-FTIR spectra of Pleistocene bear bone in its natural state and after fs laser treatment with average irradiances of 1.24 TWcm^{-2} (Fig. 5.8a) and 2.37 TWcm^{-2} (Fig. 5.8b), respectively. The spectrum of the untreated sample exhibits a lower signal-to-noise ratio than the spectrum of the laser-treated sample, owing to the bone surface's increased reflectivity after cleaning. The phosphate and carbonate absorption bands in these spectra correspond to the mineral phase of bone, namely a calcium deficient hydroxyapatite. The most intense bands, related with PO_4^{3-} , emerge at about 1000 and 950 cm^{-1} , respectively, and correspond to the ν_3 antisymmetric PO stretching mode and the ν_1 symmetric stretching mode. The absorption bands at 1415 and 1450 cm^{-1} are due to CO_3^{2-} in the B-type PO_4^{3-} and A-type OH^- anionic sites, respectively.

The band at 873 cm^{-1} corresponds to the $\text{CO}_3 \nu_2$ mode [294][295][296]. Between 1450 and 1750 cm^{-1} , the bands of collagen, the primary organic component of bone, show the material's organic components. The bands at 1690 to 1720 cm^{-1} , 1550 to 1590 cm^{-1} , and 1250 cm^{-1} correspond to the collagen molecule's amide I (C = O bond stretching), amide II (C-N bond stretching and N-H deformation modes), and amide III groups. The wide absorption band at 2920 cm^{-1} is assigned to an amide B group. A collagen group (N-H asymmetric stretching mode), and the band between 2850 to 2950 cm^{-1} arise from CH_2 chain bond stretching [296][297]. Laser cleaning reduces the relative amplitude of the collagen-associated amide bands. The fs laser cleaning appears to have no discernible effect on the relative amplitude of the other IR absorption peaks, particularly those related with the mineral component of bone.

In this work, the usage of sub-ns vs. fs pulses is demonstrated to have significantly different benefits in terms of protecting the bone from heating-induced issues. We conducted a detailed subsurface investigation of laser intervention using sub-ns and fs pulses in UV and n-IR emission regimes to determine cleaning effectiveness and the appearance of the subsurface after cleaning. Ultrafast lasers are intriguing instruments that might be the best alternative to conventional cleaning, as fs laser bone intervention reveals that there are currently no chemical and structural changes in bone caused by laser treatment. We demonstrate that utilizing fs laser pulses to clean blackish encrustations and archeological bone stains is apparently more successful than using sub-ns pulses.

The laser ablation threshold is defined as the lowest irradiance value at which surface desorption of contaminants starts on the outermost surface of the bone exposed to laser irradiation. In this regard, E_p (Energy per pulse), defined by the output power P (W) level,

establishes laser ablation efficiency and is expected to exert a significant impact on cleaning quality. Sub-ns laser irradiation at the pulse repetition rates applied in this work induces limited thermal input to the irradiated surface. The pulsed fs laser employed, on the other hand, provides an advantage in the cleaning process because it imparts significantly very little or no heat to the majority of the material during the pulse. It has been observed that increasing the pulse repetition rate results in an increased depth feature, although in this case avoiding an excessive heat input to the material surface is a challenge.

The effect of wavelength on the efficiency of archaeological bone cleaning can be attributed to two factors. To begin with, the absorption coefficient of laser energy on the substrate varies with wavelength. Secondly, how laser irradiation interacts with contaminants is greatly dependent on the wavelength and thickness of the contamination layer. The varied wavelengths of the laser have a major influence on the cleaning process for bone samples, which is due to the strong absorptivity of the encrusted hard blackish contamination layer at different wavelengths. UV radiation at 343 nm with a pulse duration of 238 fs delivered from a Carbide model laser was shown to be highly effective at removing contaminated and degraded products from the outermost surface of Pleistocene bone.

5.4 Conclusions

The laser's fluence/irradiance is adjusted, and the post-cleaning condition of samples is determined. Color alterations, mechanical and physicochemical compositional changes are also analyzed. All wavelengths appear to be capable of removing encrusted blackish contaminants and degradation products within a specific range of irradiances without causing damage to the underlying original bone surface. Each wavelength observed with a characteristic range of operational irradiances; with the n-IR having the small range and UV having the high when applied with sub-ns pulse durations. The precise damage threshold, on the other hand, appears to be independent of the existence of Mn mineralization and Fe staining. Although both sub-ns laser radiations were capable of cleaning contaminants from the outermost layer of the bone surface, the cleaning process was found to be unsuitable and impractical in the case of the sub-ns n-IR laser when beam scan mode was used, whereas sub-ns UV beam scan irradiation appears to be significantly better when laser-induced damage, cracks, physicochemical changes, and so on are taken into account. The bone surface cleaned with a 1064nm sub-ns laser generates a significant amount of heat and develops a yellowish hue as a result of the strong heat incubation effects, potentially leading to carbonization, thermomechanical cracking, and, in extreme

situations, necrosis. This wavelength also seems to penetrate the surface without removing all the hard blackish contaminants. In contrast, 355nm sub-ns laser radiation interacts with the bone surface in a very localized, superficial way, making the process impractical from the point of view of its low material removal rate. n-IR sub-ns laser is not recommended due to the high heat accumulation; it is suggested to go for shorter pulse duration. To avoid damaging fragile materials such as archaeologically valuable bone while using laser cleaning, heat deposition to the bulk should be kept to a minimum.

Femtosecond UV laser (343nm, 238fs respectively) has been determined as the most effective laser technique in cleaning of fragile and sensitive bone surfaces. The findings from several number of experiments demonstrates that fs UV laser is quite effective in cleaning bone samples, resulting in zero or minimal discoloration, and no damage to distinguishable bone surface under microscopic examination. When compared to the application of sub-ns laser technology, this work revealed that laser pulses with a fs duration can exhibit non-thermal ablation of contaminants on bone samples. As an outcome from the different characterization techniques, the fs laser cleaning process had essentially no impact on physicochemical characteristics. Furthermore, this fs laser lends itself to further exploration of the influence of laser-bone interaction on varied laser pulse durations and emission wavelengths.

CHAPTER: 6

FEMTOSECOND UV LASER IN BONE CLEANING

CHAPTER SIX

FEMTOSECOND UV LASER IN BONE CLEANING

***Summary:** Archaeological bones are severely damaged with time as a result of inorganic mineralization weathering, encrustations, contaminations, degradations etc. in the burial environment. Due to their fragile and sensitive surfaces with varying degrees of contamination and deterioration, archaeologically significant bone cleaning is a challenge for multidisciplinary scientific development. When traditional chemical and mechanical cleaning are no longer practical, and short pulsed laser cleaning is not entirely effective, this chapter explores the femtosecond (fs) ultrafast pulsed laser technology that has recently emerged as an alternative tool for cleaning cultural heritage artifacts, providing control over ablation depth and avoiding unwanted photothermal and photochemical damage. An important Pleistocene bone excavated from Palacios de la Sierra (Sierra de Atapuerca, Spain) with surface pollutants, deterioration products, and hardened soil crusts was cleaned using an Yb:KGW fs laser with an ultraviolet emission wavelength (343 nm). Efficient cleaning parameters, ablation threshold, damage threshold, and operative cleaning threshold values in laser beam scanning mode were identified. Scanning Electron Microscopy with Energy Dispersive X-ray Spectrometry (SEM-EDS), Fourier Transform Infrared Spectroscopy (FTIR), Optical Microscopy (OM), and X-ray diffractometry (XRD) were used to characterize the physicochemical properties of the deteriorated bone before and after the laser treatment, while evaluating the degree of damage produced to the original bone surface. The study reveals the capability of this recently developed, commercially available fs UV laser in the successful conservation of archaeological bones. Results indicate their ability to remove unwanted material with nanoscale precision, while avoiding excessive heat accumulation, undesired physicochemical transformations, and catastrophic mechanical damage to the underlayers during laser bone cleaning.*

6.1 Introduction

6.1.1 Bone diagenesis

Understanding bone diagenesis is vital for effective laser interventions, because bone may reveal historical lifeways, habitats, and evolutionary histories [279]. Bones are calcified tissues that mostly consist of the mineral hydroxyapatite (HAP) [298]. Although some elements may be connected with the organic phase, trace elements are typically found in

the mineral phase of these calcified tissues. The concentration of the various elements in bone changes depending on the diet. The remodeling process [299], bone diagenesis routes [300], and direct exposure to contaminated objects [214], all have an impact on bone trace element alterations. Apparently, the bone diagenesis period is important when compared with the leaching percentage of bone minerals. Organic and mineral components in bone basically make it a composite substance. Approx. 22-23% of fresh, dry bone's weight is made up of organic matter, i.e., mostly collagen. Collagen fibers that are long and intertwined offer the tensile strength and toughness of live bones. The mineral component of bone provides the compressive strength, which is a carbonate-containing HAP with a composition similar to $\text{Ca}_{10}(\text{PO}_4)_6(\text{OH})_2$. This accounts for around 70% of the total weight. The remaining 7-8% is water that is firmly bonded and remains stable even when the bone is heated to 105°C [298] [301].

Bone deterioration is influenced dominantly by the soil environment in which the remains are buried [217]. A number of elements that are required for bone development in small and trace amounts (such as iron, magnesium, zinc, chromium, copper, manganese etc.) are known to be progressively leached from the HAP structure of the bone once they have been incorporated [291][302]. Numerous variables may affect the quantity of trace elements in bone due to the exposure to a variety of environmental circumstances; pH, soil hydrology (i.e., wetting and drying regimes), microbial activity and temperature have been recognized among the most influential. These variables, however, must not be treated as independent of one another. In a thermodynamically open soil environment, for example, simple access of ground water to a significant structural bone component might be fatal. The mineral component of ancient bone is first shielded from decomposition by its close connection with the collagen matrix. The insoluble collagen protects the mineral phase from dissolving, and hence microbes from rapidly degrading it, because microbial enzymes are too large to penetrate the extremely tiny spaces between HAP crystallites. Additionally, the inorganic phase protects the collagen from chemical hydrolysis, since it is efficiently stabilized by its close association between the organic and inorganic parts of bone. Once this close relationship between the collagen and mineral phase is damaged, the structure becomes susceptible to unraveling via a range of biological and chemical processes [285]. It's amazing that bone has survived in the archaeological record given how rich it is in protein and phosphorus [217]. Analysis of mineral and protein phases, particularly collagen, yields valuable information regarding both Paleobiology and Paleoenvironment [303]. Analysis of bone's main, minor, and trace elements has helped researchers to understand several different queries in order to reconnect the past with present [304].

6.1.2 Laser cleaning potentials

Lasers emit a highly directed beam of light which poses significant advantages towards cleaning of archaeological materials and museum artifacts. Lasers have thus been under investigation for the past decades for archaeological artifact surface contaminant desorption, because of the advantages they can provide over traditional cleaning methods [18]. A laser system may offer efficacy, selectivity, and layer-by-layer ablation, while still being quick and cost-effective due to its high interaction efficiency. On the other hand, it is still not commonly employed due to several undesirable consequences that result from the interaction of the laser with the artifact. These are mostly caused by photothermal effects and produce a direct temperature increase around the irradiated surface of the artifacts, an issue known as heat accumulation [107][227][305]. Once this heat buildup problem is overcome, laser cleaning has the potential to become more widely used than traditional procedures, which still have certain drawbacks. Mechanical cleaning, for example, may leave scratches on the artifact's surface, whilst chemical and electrochemical cleaning may result in secondary contamination. Both are yet difficult to control in cleaning processes [306]. Taking into account the diversity of environmental pollutants and contaminants on the bone surface, as well as the variety of emission parameters that a laser has to offer, it would not be surprising that previous investigations may not agree on the optimal criteria for laser cleaning of ancient bone [106]. It is widely accepted that shorter pulse duration values minimize cumulative thermal effects and the likelihood of micro-melting [105][263]. Laser parameter optimization hypotheses postulate crucial roles for laser irradiance, material absorptivity, and thermal conductivity in the safe and effective removal of foreign and undesired materials [244][276] from the bone surface.

6.1.3 Ultrafast fs pulsed laser

Most recently developed ultrashort (fs) pulse lasers appear as emerging and promising tools for cleaning archaeological materials in a variety of applications. Lasers capable of generating coherent photon pulses of fs duration have paved the way for new horizons in artifact cleaning with exceptionally high temporal resolution and photon intensity. The ultrafast nature of femtosecond lasers has been utilized to perform sophisticated characterization experiments in real time, and have appeared ideal for artifact cleaning as compared to conventional chemical and mechanical methods. Due to their ultrashort pulse irradiation duration and high intensity, fs laser pulses profoundly change the laser-material interaction processes [105]. The high intensity achieved at their focus can generate an intense plasma capable of ablating the target materials from a precisely defined area of a

substrate. This may have implications in restoring tough-to-clean artifacts, particularly delicate and sensitive bone surfaces [307][308]. A fs laser pulse has a duration substantially shorter than the time required for electron-lattice energy relaxation [309]. As a result, laser energy is absorbed before the lattice changes. Due to the extreme intensity, fs laser-material interactions are nonlinear state between electrons and lattices. Hydrodynamic motion and heat conduction through lattices during this period is negligible; thus, thermal damage (microcracks and heat-affected-zone) is greatly reduced [310][311]. Moreover, as fs laser ablation processes are deterministic and repeatable[312], practically any archaeological artifact could be cleaned with the help of this ultrafast laser. The best potential cleaning method may also be modified by varying the laser intensity and its temporal and spatial distribution in order to manage laser-artifact interactions, in addition to the above [313].

6.1.4 Objectives of this chapter

The evaluation of the efficiency of a specific laser cleaning approach and specific laser system in every given situation is critical. Moreover, when irradiated by a laser system, each artifact reacts uniquely, according to their unique optical, physicochemical, and thermal characteristics [104]. This is particularly true for archaeological bones due to their delicate and sensitive surface. In essence, a "cleaning threshold and damage threshold" is required that utilizes the optimal laser settings in each situation, and the state of each archaeological bone needs to be assessed both, before and after laser cleaning using a range of characterization techniques for identifying the cleaning efficiency.

In this work, the feasibility of ultrafast fs UV laser intervention in archaeological bone has been investigated for potential bone cleaning applications. One late middle Pleistocene bone was chosen since it contained diverse contamination and deterioration problems and was largely covered by hardened clay crusts. Moreover, the influence of wavelength on contaminants and clay matrix concretion removal, and underlying bone substrate preservation is investigated with special attention paid to the influence of laser emission wavelength, irradiance levels and pulse-to-pulse overlap, with the aim to avoid destructive thermal accumulation on the bone substrate. The novelty of this work mainly lies in the use of a fs laser which enables independent selection of Energy per pulse (E_p), pulse repetition frequency and beam scanning rate at the emission wavelength of 343 nm. The proper identification of the former parameter effects to distinguish topmost foreign materials and the underlying original bone surface enabled, in turn, satisfactory control of contaminant laser ablation and substrate damage. Analytical methods for determining optimal conditions for cleaning archaeological bone studied here include Optical Microscopy

(OM), Scanning Electron Microscope coupled with Energy-Dispersive Spectrometry (SEM–EDS), Fourier Transform Infrared Spectroscopy (FTIR), and X-ray diffraction (XRD). These techniques were employed to semi-quantitatively analyze the bone elements based on detected physicochemical properties before and after the laser intervention, in order to provide experimental data to evaluate the cleaning process.

6.2 Material and method

6.2.1 Significant archaeological bone

The study was performed on one archaeologically significant Mammal rib fragment bone covered with various thickness of hardened clay crusts, contaminants and environmental pollutants. It was excavated from *Palacios de la Sierra* (Burgos, Spain) [314], described physically as a 3.9 cm long x 2.6 cm wide x 1.1 cm thick rib fragment sample, dating back to late middle Pleistocene (120000 years). The majority of the bone was covered as inhomogeneous cemented clays, whereas one side was exposed to the environment and non-crusted.



Fig. 6.1: Front (left side photograph) and top surface (right side photograph) views of the mammal rib bone fragment, excavated at the *Palacios de la Sierra* (Burgos, Spain).

However, a significant area of this exposed side of bone exhibits varied shades of hard greyish and yellowish discoloration, which contrasts with the natural whitish-yellowish color characteristic of fossilized bones, possibly due to Fe staining. It was covered unevenly by atmospheric soil dusts and weathering patterns as shown in Fig.6.1.

Dust on the bone surface was previously removed by a standard mechanical procedure, previously been cleaned with a soft brush mechanically to remove any loose debris as a first phase of conservation. The goal of this study was to clean the hard greyish-yellowish stains and remove the clay matrix concretion from the outermost layer of the bone without altering its natural look, while the efficiency of a fs UV laser in cleaning bone and its interaction with the substrate were explored. The ablation threshold, damage threshold and cleaning threshold values were determined with the aim to identify parameters which would help avoid excessive heat buildup on the underlying substrate bone surface. Figure 6.1 illustrates the front and top side views of the bone sample.

6.2.2 Laser cleaning system and parameters

During the laser treatments, 238 fs pulses were emitted at 343 nm at a maximum average output power of 9.33 W. This corresponds with a maximum pulse energy of 46.6 μJ , and a Gaussian beam diameter of 30 μm at full width half-maximum (FWHM) [202]. As the laser system offers a PPD option, the amount of energy delivered by each pulse was determined by the resonating frequency, which was fixed at 200 kHz. The PPD index always vary the output frequency, but it never changes the E_p , and as a result, the peak power never changes. PPD suppresses a proportion of pulses to lower the effective pulse repetition rate or frequency, which resulted in the laser continuing to emit at a repetition rate of 200 kHz.

The continuous beam scanning laser pulse mode approach was explored applying a series of experiments varying the laser output level. Selective irradiation was carried out on specifically defined areas of the sample surface [205]. The sample was irradiated in the open air and the laser beam was scanned across the sample's defined surface in beam scan mode. The scan speed and line-to-line distance were selected by the CAD-like program installed on the laser system control computer. The treatments were primarily performed in 2 mm \times 2 mm regions each in 'cross-line' mode, i.e., scanned the area in 0° direction followed by scanning at 90°. Laser treatments were later applied on 5mm x 5mm regions to identify unusual phenomena related to process scale-up. Due to the use of a single distinct laser system, irradiance and fluence (the amount of energy contained in each laser pulse) are proportional in this study.

6.3 Results and Discussion

Using ultrafast UV fs pulsed laser to remove pollutants and cemented clay crusts from archaeologically important bone surface in an effort to preserve their archaeological

significance and aesthetic value are the main aim of this study. In order to understand the bone sample and diagenesis before cleaning, the bone fragment cross-section was analyzed by FESEM for concurrently exploring micro-structure within the bone artifact. EDX analysis was used to identify diagenetic minerals. FESEM analysis were carried out on embedded and polished cross-section of the bone.

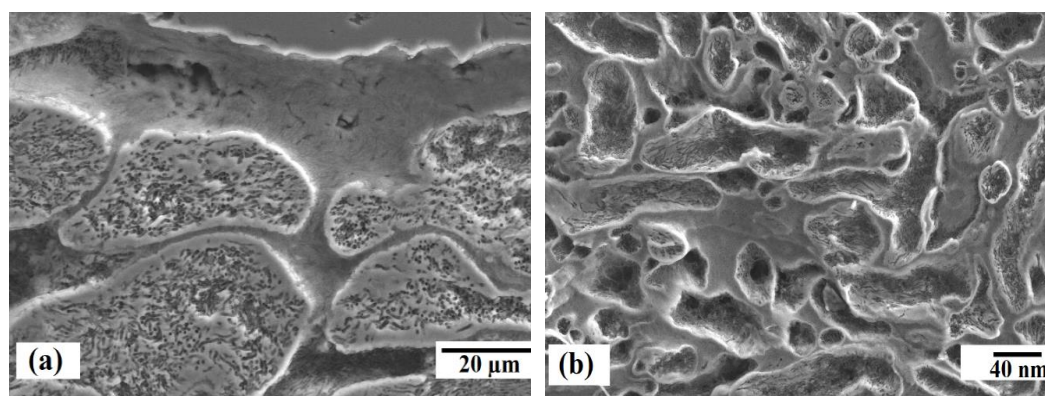


Fig. 6.2: (a) Microbe tunnels visible in the FESEM images of cross-section of late middle Pleistocene mammal rib fragment bone. (b) FESEM image of the same bone cross-section at high resolution: on the left side of the image, cross-sections of microbe tunnels with typical diameters ranging from 40 to 200 nm are observed; the stripes on the right side indicates HAP that has been re-deposited.

Circuitous microbe tunnels were seen in the FESEM micrograph of the mammal rib fragment bone, showed in Fig. 6.2(a). Microbe colonies are constrained to defined zones, many of which are encircled by a bright, electron-dense cuff of redeposited HAP. In Fig 6.2(b), the left-hand side of the figure depicts cross-sections of microbe tunnels with typical sizes of 40-200 nm. A thin network of pores with a maximum diameter of around 20 nm was observed unevenly close to or inside the tunnels. The bright stripe on the right reflects re-deposited HAP at a greater density than the demineralized, microbially tunneled area and the un-tunneled area on the right. These are the spaces created when collagen fibrils are chemically hydrolyzed. Thus, Fig. 6.2(b) demonstrates that both microbial destruction and slow chemical hydrolysis occur concurrently and in parallel in a single specimen, probably until the residual protein concentration reaches a level that renders the bone unsuitable as a food source. At this time, microorganisms may quit or delay their attack to the point that they are no longer the primary contributor in bone diagenesis.

The archaeological bone used in this study has been found as fragile material, typically reasonably inert, dimensionally stable upon drying, and does not require specific storage conditions. It is rarely regarded as "organic" archaeological materials and are hardly cleaned and maintained similarly to other excavated artifacts. Although this type of late middle Pleistocene bone often survives because it was found in anoxic conditions and hence did not face significant microbial attack (Fig.6.2), it has undergone partial demineralization and contains partly destroyed or damaged collagen. It has been revealed that when excavated from natural sediments, bone may appear in good condition but dry out to bending, shattering, or delamination. There were no noticeable Manganese mineralization phenomena [106] observed; perhaps approx. 120,000 years is not enough to start Manganese mineralization in anoxic burial conditions.

Using a steady laser beam, a high-power density irradiation to remove environmental pollutants, contaminants and clay crusts of bone artifact is achieved by laser cleaning. The scanning speed, repetition rate, scanning area, and scanning path of the laser system were optimized in order to determine their effect on the cleaning efficiency and thermal damage. Scanning at 150 mms^{-1} yielded the maximum material removal rate during the bone laser treatments herein carried out. Scan speeds over 150 mms^{-1} resulted in a greater number of scans and longer processing times, since the removal depth in bone substrate is expected to be inversely related to the beam scanning speed. Scanning at less than 150 mms^{-1} led to excessive heat accumulation and damage to the bone substrate. Thus, the scanning speed of 150 mms^{-1} has been established and set as fixed for this study, while the laser beam moves across the surface at a predetermined distance between scan lines (i.e., $15 \mu\text{m}$) to cover the entire area, streamlining the same irradiation effect and cleaning quality. In situations where the distance between successive scan lines is less than that of the laser spot diameter, increased overlap leads to a better removal rate; in situations, discontinuous material removal tracks occurred.

The other three scanning paths (i.e., unidirectional parallel lines, concentric circles from the inside to the outside, and outside to the inside) did not demonstrate the same cleaning effectiveness as the bidirectional parallel lines, thus it was chosen to optimize removal rate and reduce heat damage. While the other approaches have approximately the same removal rates, it has been shown that the laser beam takes a longer time to complete the scanning route when using a unidirectional approach. In addition, a concentric circle scanning method with apparent thermal damage was discovered. During laser processing, heat

accumulates at the center of the cleaned area due to the circular scanning routes' inability to dissipate heat so effectively.

The cleaning approach was dictated by the range of applied irradiance values, for which the bone surface is protected from altering the original surface, and which were estimated by the theoretical irradiance calculation [107][106]. During the preliminary tests, laser cleaning for smallest area treatment with proper cleaning parameters created imprints on the bone surfaces, mostly due to the non-uniform energy allocation of the Gaussian beam. Spallation, phase explosion, fragmentation, and vaporization has been observed at material removal when the ablation irradiance value is below the threshold for damage formation. Spallation has been observed only at low irradiance values, while phase explosion seems to appear at moderate irradiance levels. During high irradiance values, a plume is produced by the fragmentation and thermal vaporization of the surface layers [201]. Cleaning of this archaeological bone in the subsurface was affected by all these concurrent events. The materials removed were released from the irradiated bone surface in the form of solid debris, vapors, or as a plasma plume.

Ultrafast laser processing caused zero collateral damage because of the reduced heat conduction [236] when treated with threshold cleaning; damages observed when treated by damage threshold and more irradiances than that. The bone damage threshold was identified by the irradiance at which observable physicochemical changes of original bone surface, such as melting, color changes, cracking, spallation, phase explosion, fragmentation, and vaporization occurs. Special consideration was given to the possibility of causing damage to the bone composition, notably the Ca/P ratio, which might occur with the maximum susceptibility to the laser beam, due to the optical properties of bone and its comparatively low melting point [293]. While establishing damage thresholds for operating irradiance ranges was rather straightforward, establishing the start of contaminant removal (cleaning threshold) was certainly more complicated. Certain areas of the final surface may have been irradiated numerous times in order to fine-tune the contaminant's removal from the surface and thereby achieve satisfactory cleaning conditions for the various types of foreign undesired elements present on the bone's surface. Satisfactory cleaning may be reached as long as damage threshold values, observed using different microscopy and spectroscopy methods, are not surpassed.

Table 6.1: Parameters used in fs UV laser irradiation of Pleistocene bone. F_{pulse} denotes the Laser fluence, I_{pulse} for irradiance, and P for maximum nominal power. The pulse energy E_P was calculated by dividing the established output power level over 200 kHz, the fundamental pulse resonating frequency. The effective pulse repetition rate f_p was set at 10 kHz by dividing this resonating frequency by an arbitrary PPD integer (in this case by 20) for all experiments herein reported. The consecutive line-to-line distance was set at 15 μm , and the beam scanning speed to 150 mm s^{-1} in cross hatch mode (i.e., 0° and 90°) in all experiments.

Treated Region	P (W)	E_P (μJ)	F_{pulse} (J/cm^2)	I_{pulse} (TW/cm^2)	N_L	Cleaning Performance
Fig. 6.3a	0.23	1.15	0.16	0.68	10 x 10	Yellowish contaminants removed; cleaning achieved.
Fig. 6.3b	0.66	3.30	0.46	1.96	5 + 5	Greyish / blackish contaminants removed; good cleaning achieved.
Fig. 6.3c	0.42	2.10	0.29	1.24	10 + 10	Good cleaning achieved.
Fig. 6.3d	6.07	30.40	4.29	18.04	10 x 4	Hardened clay matrix removed; best cleaning performed.
Fig. 6.3e	0.94	4.70	0.66	2.79	1 + 9	Heat accumulation observed; melting and cracks were evident.
Fig. 6.3f	1.34	6.70	0.95	3.98	1 + 9	Cracks were evident; fragmentation and thermal vaporization observed.
Fig. 6.3g	3.33	3.30	0.47	1.96	1 + 9	No progress observed in removing clay concretions.
Fig. 6.3h	5.29	26.50	3.74	15.72	1 + 9	Hardened clay removed inefficiently.

In accordance with the final cleaning threshold values, the mammal rib fragment surface with a thin layer of pollutants and contaminants was cleaned at various specific irradiances (Table 6.1 and Fig. 6.3). Laser based damage on the mammal rib may be avoided with irradiation values as low as 0.68 TW cm^{-2} , however irradiation greater than 1.96 TW cm^{-2} resulted in surface damage to the bone substrate. To be safe, radiation values less than or equivalent to 0.68 TW cm^{-2} were chosen for bone contaminant and pollutant removal, since they appear to have no detrimental effect on the bone surface. Using irradiance levels of 0.68 TW cm^{-2} for the yellowish colored contaminants (Table 6.1 and Fig. 6.3a), and 1.96 TW cm^{-2} for the dark blackish greyish pollutants (Table 6.1 and Fig. 6.3b), apparently

excellent laser cleaning was achieved for this bone artifact. The discoloration on the bone surface can be removed to acceptable levels by using medium cleaning thresholds i.e., 1.24 TW cm^{-2} (Table 6.1 and Fig. 6.3c). These conditions, on the other hand, did not allow for the ablation of the clay accretion layers.

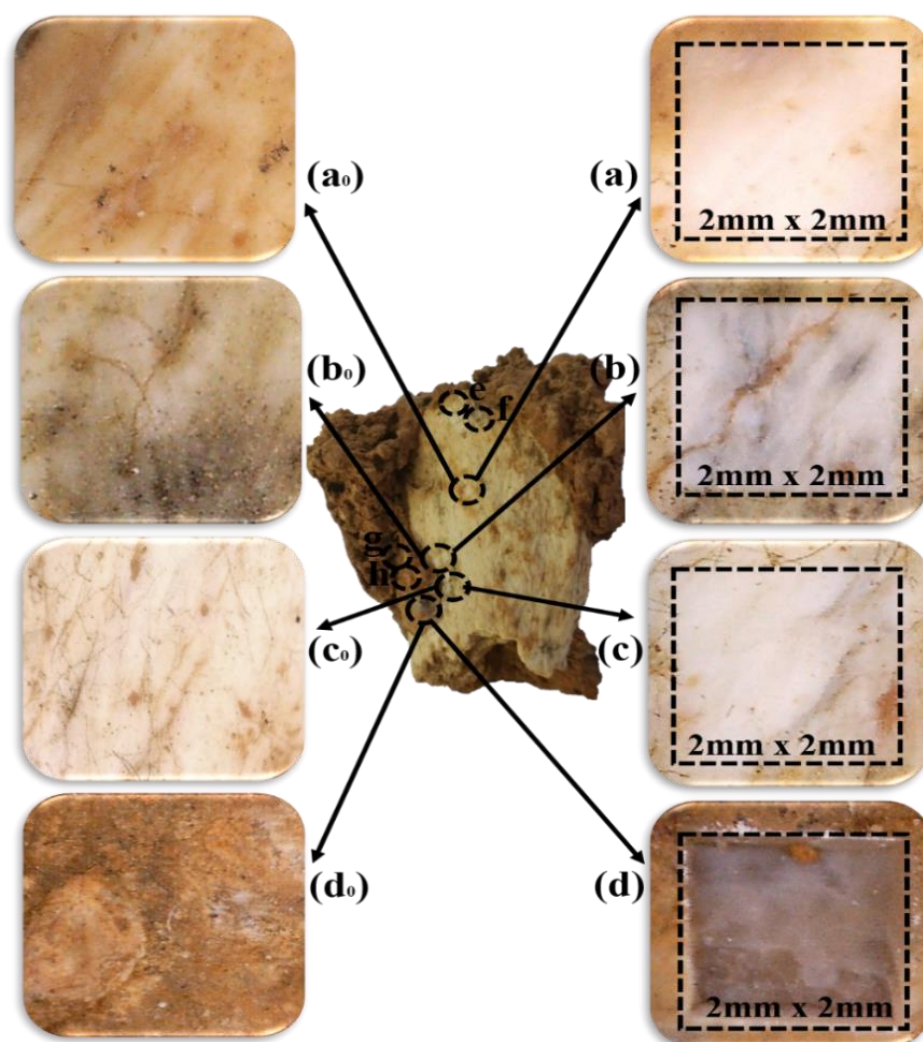


Fig. 6.3: Optical microscopy images from the original mammal rib fragment surfaces before and after UV fs laser treatment in continuous beam scan mode: fig. 'a₀ and a' correspond to the non-treated dark yellowish contaminated original surface and the laser cleaned surface; fig. 'b₀ and b' to the non-treated blackish-greyish contaminated and laser cleaned surface; fig. 'c₀ and c' to the bone surface staining area and laser treated cleaned area, and fig. 'd₀ and d' to the hardened clay covered bone surface and laser cleaned area with atmospheric dust, and loose debris. Treated areas measure 2 mm^2 each.

The thick hardened clay crust accretions have required an increase in the applied irradiances, as well as in the number of repetitive scans, until the accretion's layers were removed. This was achieved with an irradiance of 18.04 TW cm^{-2} , boosting the previously established contaminant removal value over the safe range of irradiances (Table 6.1 and Fig. 6.3d). Observed clay particles removed during laser processing might act as a shield, slowing the laser's removal rate [315]. The calculated safe irradiance value has been applied with a higher number of repetitive scans when steamed necessary to remove increased thickness of hardened clay matrix concretions. Consecutive scans were halted when the bone outermost surface was observed. A less aggressive cleaning condition was subsequently applied in order to clean the leftovers. The procedure described here is an ideal illustration of a realistic case study, involving a sample with varying thickness and composition of clay matrix concretion layers, where irradiance levels, pulse overlap, and irradiated areas are constantly assessed and evaluated using optical microscopy. This configuration might serve as the foundation for a commercial instrumentation capable of doing semi-automated cleaning in the future, provided additional acoustic and spectroscopic monitoring are implemented.

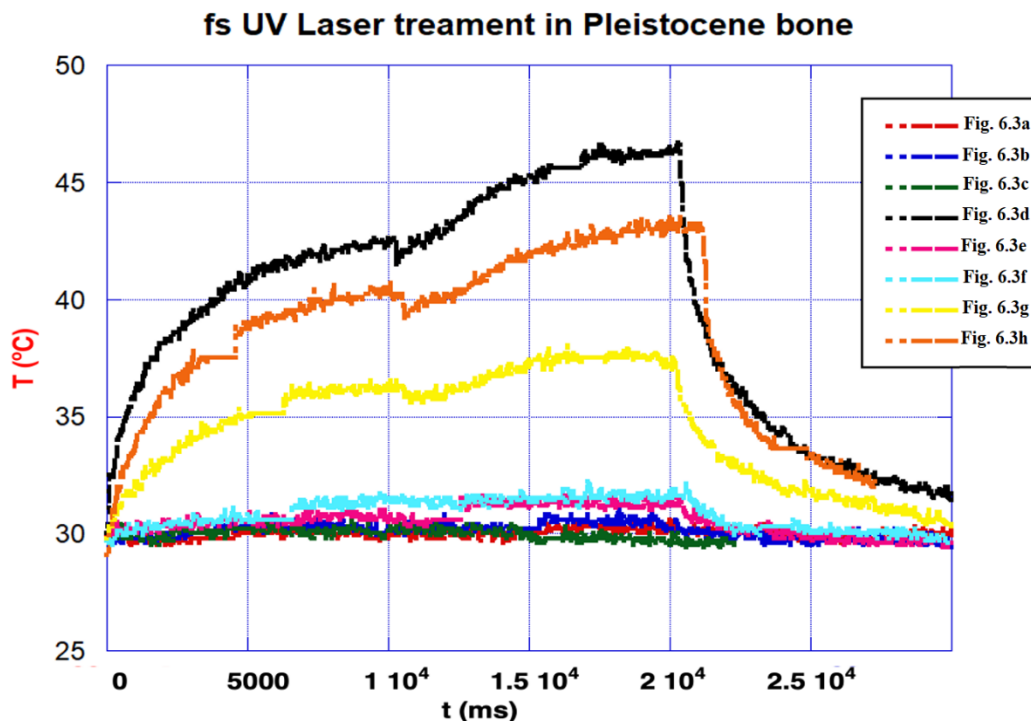


Fig. 6.4: Temperature generations during the fs UV laser treatments recorded with the Optris Xi 400 thermal camera on the bone surface, associated with the Fig. 6.3 and Table 6.1.

With the objective of cleaning the yellowish, blackish, and greyish colored overlayers/stains from the bright white colored substrate that is the natural color of fossilized bone surface, a common "cleaning" threshold should be conveniently identified. Hence, four different 5mm x 5mm areas were chosen following the diversified staining and mineralization problems observed. A series of laser tests were conducted with the same number of laser beam scan passes (herein this case, N_L was 10 for all experiments), using the three different threshold cleaning irradiances and one damage threshold as mentioned in Table 6.1 for Fig. 6.3 - a, b, c & e; the irradiance levels used ranged from 0.68 to 2.79 TW cm^{-2} by changing the laser system's power output from 0.23 W to 0.94 W (Fig. 6.3 and 4, Table 6.1). Satisfactory cleaning was observed at irradiance values ranging between 0.68 and 1.24 TW cm^{-2} (Fig. 6.5 a and b), while inefficient cleaning was observed below 0.68 TW cm^{-2} . Observation of cracks and evidence for melting started at values above 1.96 TW cm^{-2} after 10 laser scans. In the cases where higher irradiances were applied, heat accumulation was observed clearly, hence melting and cracks were evident. Bone damage appeared at 2.79 TW cm^{-2} even when there was only one laser pass (Fig. 6.5d). On the bone surface, the same irradiance values were employed for several laser irradiation treatments in order to confirm these threshold values.

Increasing the irradiance value during laser treatment will lead to an increase in the temperature of the bone surface. Figure 6.4 depicts the record of the heat generations when removing contaminants and clay accretions by fs UV laser treatment. For a total of 10 treatments, it will take approximately 13.5 seconds to treat this 2 mm^2 bone surface region each with contaminants using these laser processing parameters mentioned at Table 6.1. Figure 6.4 also shows the maximum temperature increase measured during these experiments when cleaned the hard clay accretions; measured values increase by $\Delta T = 18.5 \pm 0.5$ °C, when the room temperature was 28.8 °C. In contrast, when the temperature values increased 2.5 ± 0.3 °C, damage on the bone surface started to appear. The best cleaning threshold has been observed to increase by an amount of 0.5 ± 0.3 °C at maximum.

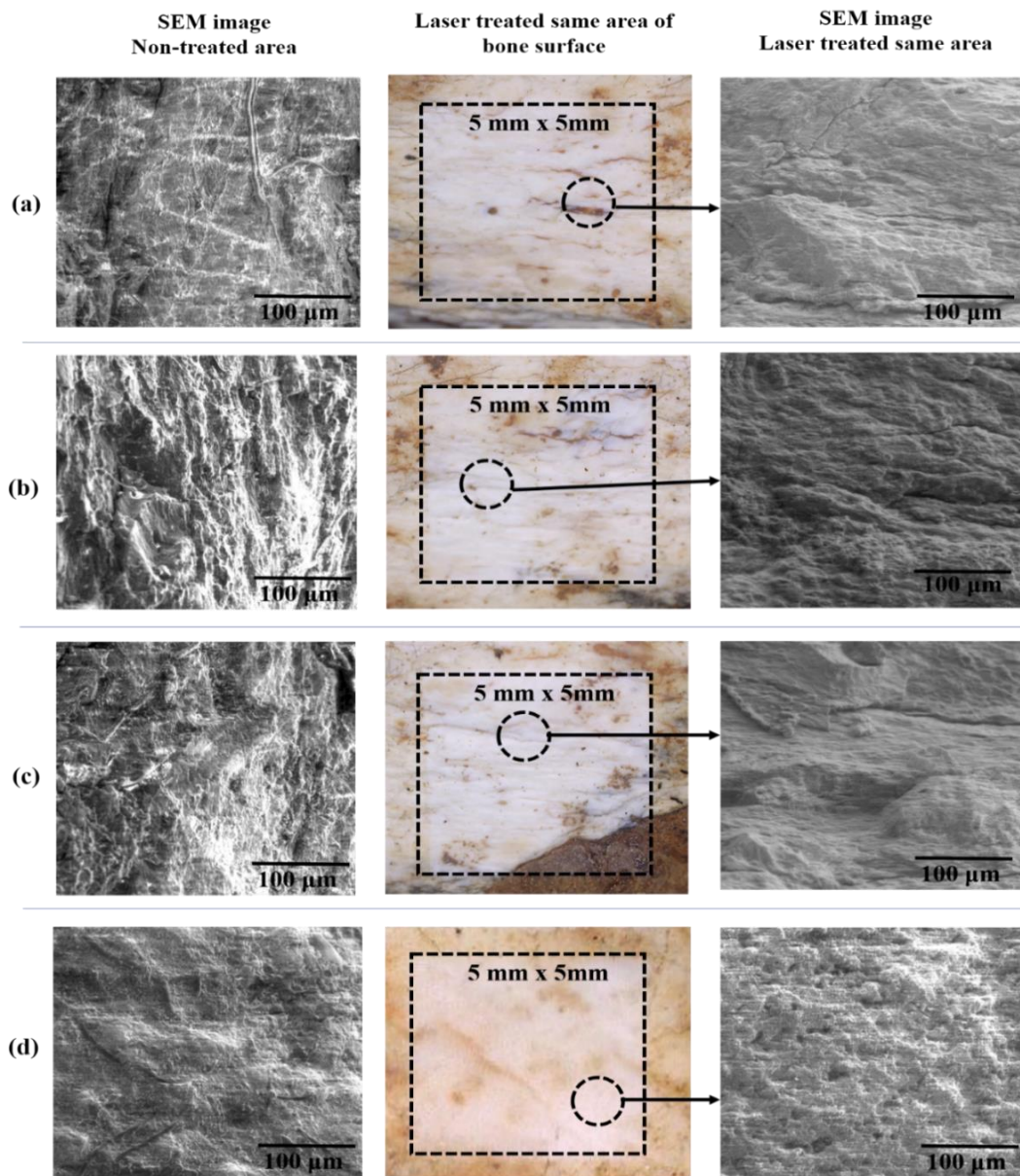


Fig. 6.5: Optical microscopy and SEM images both ‘before and after’ the laser treatment obtained on the 4 specific 5 mm² areas of a mammal rib fragment subjected to this study. Three different cleaning threshold irradiance values (Fig. a, b, & c) and the damage threshold value (Fig. d) have been applied to identify any damage as a result of the irradiation of a large area without considering the nature of the contaminants and pollutants present within the topmost layer.

The first three optical micrographs in Fig. 6.5 show the actual region of the irradiated bone containing different types of contaminants, staining and inorganic mineralization

weathering. Subsequently, the left- and right-hand side SEM images correspond to the same area before and after laser irradiation. After laser treatment, the bone surface did not show any discoloration or damage by visual inspection, nor as observed through optical microscopy. The result suggested that laser cleaning could be achieved without apparent damage to the bone surface, as long as the herein recommended parameters were employed (Table 6.2). The laser-induced alteration of the key bone components was semi quantitatively determined using EDX measurements on all treated samples.

Table 6.2: Semiquantitative elemental composition determined by EDS on SEM for a late middle Pleistocene bone surface before and after laser irradiation.

Elements (At%)	Non-treated area 'a'	Laser treated area 'a'	Non-treated area 'b'	Laser treated area 'b'	Non-treated area 'c'	Laser treated area 'c'
C	21.90	09.60	20.18	12.20	23.13	13.26
O	51.27	55.30	53.92	54.66	51.84	54.15
F	01.14	01.66	00.00	01.52	00.00	01.03
Fe	00.09	00.37	01.60	00.60	01.39	00.55
Na	00.31	00.31	00.37	00.35	00.40	00.34
Mg	00.25	00.13	00.45	00.41	00.32	00.53
Al	00.40	00.13	01.08	00.51	01.01	01.11
Si	00.48	00.14	01.45	00.93	00.71	0.07
P	07.29	09.95	06.38	07.74	06.38	06.81
S	00.03	00.05	00.00	00.03	00.08	00.00
K	00.04	00.00	00.13	00.15	00.11	00.17
Ca	16.70	19.90	14.20	18.29	14.35	17.90
Mn	00.06	00.32	00.25	00.26	00.09	00.12

Archaeological fossilized bones exhibit significant compositional variations, as seen by the Ca/P atomic ratio, which reveals a stable composition related to the bone's essential Ca hydroxyapatite structure [316]. After fs laser irradiation, the quantity of Si, Al, and Fe appears to be reduced, while the Ca and P content rises, consistent with the projected removal of aluminosilicates and iron-containing compounds from the burial soil (Table 6.2) and the penetration into the bone's original Ca hydroxyapatite composition. Fluorine (F) increases upon laser irradiation, as expected from the composition of the original fluorapatite structure of bone. F has been connected also to water intake; hence, the amount of F in fossil bones varies according to their location. In addition, F is not found within the surface contaminants of the bone, since it would be expected to lixiviate with weathering

easily. Silicates (i.e., feldspars), nitrates, and sulfates, among other elements, may be associated with the burial environment, as these elements are frequently detected as soil components in the *Sierra de Atapuerca* region [242] close to the *Palacios de la Sierra* archaeological site.

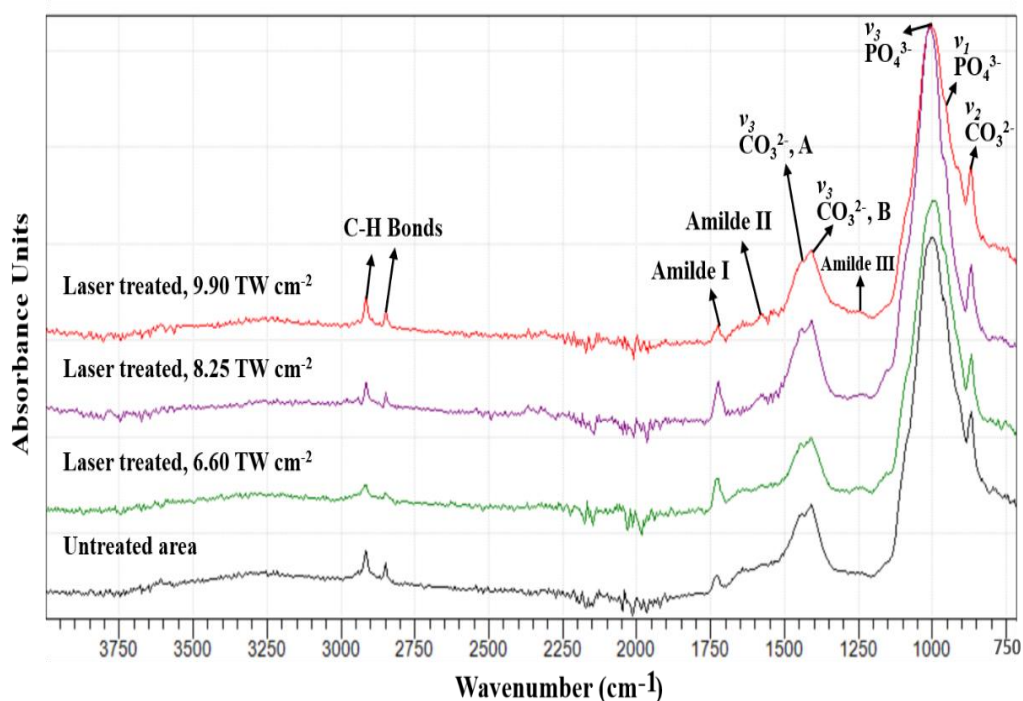


Fig. 6.6: Infrared spectra of (a) untreated bone area and laser treated area with irradiance levels of 0.68 TW cm^{-2} , 1.24 TW cm^{-2} , 1.96 TW cm^{-2} .

Both the ATR-FTIR spectra of the original and laser treated bone surface (Fig. 6.6) are identical and characteristic here in this study. We took into account three distinct cleaning thresholds when describing the "before and after" laser intervention interactions with the bone surface. An increase in reflectivity and cleanliness from the laser treatment resulted in a higher S/N ratio than the untreated sample area. According to these spectra, phosphate and carbonate absorption bands in the mineral phase of bone surface, which is low in calcium, are linked to the mineral phase of the bone surface [297].

In Fig. 6.6, the band around 870 cm^{-1} corresponds to the $\text{CO}_3^{2-} \nu_2$ mode, that around 958 cm^{-1} to the ν_3 antisymmetric PO stretching mode, and that near 1010 cm^{-1} to the ν_1 symmetric stretching mode of the PO_4^{3-} group [294]. Collagen is the primary organic

component of bone, and the amide bands observed in the spectra between 1750 and 1200 cm^{-1} are characteristic of this substance [317]. The bands at 1250, 1570 and 1725 cm^{-1} are responsible for amide III bands of collagen, amide II (C–N stretching and N–H deformation modes) and, amide I (C–O bond), respectively. In the presence of B-type anionic PO_4^{3-} sites and A-type anionic OH^- sites, the absorption bands at 1410 and 1450 are ascribed to the $\text{CO}_3^{2-} - \nu_3$ mode [318]. C–H bonds in organic molecules often correlate to the 2950 cm^{-1} and 2850 cm^{-1} bands [296]. Laser intervention had no effect on the FTIR-ATR absorption band location or relative amplitude, consistent with the fact that the laser treatment didn't produce any damage on the bone surface.

It has been observed that the optimal set of laser processing parameters is attained at the lowest effective repetition rate and highest scanning speed, which enables higher ablation rates while leaving the bone surface intact. This study can be connected to the different responses when applied with different threshold fluences on the bone surface. However, the physicochemical composition of bone artifact and the distribution of its absorbing chromophores are highly reliant on the specific archaeological bone characteristics, making it challenging to establish a comprehensive optical response for UV wavelength regimes in terms of energy penetration depths.

When cleaning cemented clay matrix concretions from the bone surface, the role of heat buildup and clay particle shielding is noticeable by observing a reduction in cleaning efficiency. As the scanning speed is decreased, the closer the laser pulses are to each other (i.e., higher overlap among pulses) and the greater the heat load deposited per unit surface area into the bone volume for a certain effective repetition rate.

Laser-induced heat effects are adverse to cleaning efficiency improvement as well as to bone surface discolorations. The combination of a low repetition rate and a fast-scanning speed results in the best cleaning parameters, where the dominating absorption at this UV wavelength may be attributable to the mineral phase of the ancient bone. Because the HAP as an inorganic matrix, it is more thermo-resistant and allows the archaeological bone surface to withstand heat loads, that are just too high to prevent the bone surface from being discoloring (specifically, calcination). When this happens, the cleaned surfaces will have a gray-white color and a significant drop in C content (Table 6.2). Laser-induced discoloration of the bone surface might be seen in a variety of hues when the damage threshold is exceeded. SEM examinations reveal significant micrometric fissures in the

laser-irradiated bone (Fig. 6.5d); spherical micro- and nano-particles emerge at the top of these micrometric structures, as is characteristic of laser-induced thermal processes.

6.4 Conclusion

Archaeological bone from anoxic environments has been reported to decay by a combination of slow chemical hydrolysis and mineral solubilization, resulting in a more open and weaker structure. The use of an ultrafast laser with a pulse duration of 238 fs and a wavelength of 343 nm, as well as cleaning threshold irradiances (~ 0.68 to $\sim 1.96 \text{ TWcm}^{-2}$) greater than the ablation threshold, allows for controlled cleaning of archaeological bone with no indications of melting, cracking, or discoloration. The lowest possible irradiance that interacts with the contaminated bone surface and clay matrix should be employed to protect the bone surface from apparent damage. The cleaning treatments are also affected by the thickness of the foreign material accretions and environmental pollutants, which are independent of the archaeological bone composition. Higher irradiance values were employed on the cemented clay matrix to remove thick clay accretion layers, while also protecting the bone by selecting and controllably irradiating these regions and lowering the irradiance when approaching the bone surface. It appears that the effectiveness of this UV laser cleaning procedure is compatible with the optical parameters of laser energy interaction with the contaminated bone artifacts; thus, cleaning parameters were optimized and experimentally validated, allowing the development of more effective and safer laser cleaning procedures for the removal of surface pollutants, deterioration products, and hardened clay crusts from the significant archaeological bone surface. This study clearly demonstrates that laser cleaning of archaeological bones is achievable using a YB: KGW fs UV laser; it has been found to have a significant advantage and state-of-the-art solution in bone cleaning, and can successfully guide future conservation strategies.

CHAPTER: 7

LASER FOR FLINTS CLEANING

CHAPTER SEVEN

LASER FOR FLINTS CLEANING

***Summary:** The laser's ability to remove surface deposits and crusts without affecting the original substrate surface makes it an ideal cleaning method for archaeological stones. However, archaeologically significant flints got limited care to date when it comes to cleaning the flint patina containing the contaminated ferruginous brown colored encrustations, despite the considerable attention given to laser stone cleaning. When dealing with issues that demand an enhanced level of conservation and the competency of the cleaning procedures, it is common for restoration attempts to fail if typical traditional cleaning methods are applied. Controlled laser cleaning is one of the most important elements to consider. The ultrafast UV femtosecond lasers with effective low repetition rates might boost the effectiveness of ancient flints cleaning by maintaining pulse energy below the damage threshold. This chapter comprises two Neogene and Cretaceous flint artifacts from the Fuente Mudarra and La Paredaja, open-air archaeological sites in the Sierra de Atapuerca (Spain). The cleaning process was carried out in beam scan mode with the utilization of recently developed Yb:KGW laser that emitted 238 fs of ultraviolet light with an emission wavelength of 343 nm, Nd:YAG lasers that emitted 800 ps of near-infrared light emission at 1064 nm, and 300 ps of ultraviolet light at 355 nm. Although irradiance values for laser cleaning intervention regulates some factors, the cleaning threshold of the flints might be inferred following irradiation with a number of treatments. Consequently, flints' thermal properties introduce structural and chemical defects due to the high treatment numbers even if the absorbed laser energy is below the damage threshold.*

Encrustation and surface deposit removal efficiency and substrate damage due to laser irradiation were studied using Optical Microscopy, Scanning Electron Microscopy - with Energy Dispersive X-ray Spectrometry (SEM-EDS), and X-ray diffractometry (XRD). UV laser irradiation with fs pulses produced excellent results in photomechanical, photochemical and thermal incubation processes in this investigation. Laser-flint interactions can be better managed by altering the laser intensity, pulse duration, and spatial distribution of the laser irradiation. Due to the controllability of laser irradiation conditions, the ultrafast UV fs laser has been proven to be substantially safer and more efficient in flint surface deposit cleaning.

7.1 Flints

Flint, often known as flintstone, is a hard sedimentary rock and a form of microcrystalline quartz. After being cut, the surfaces of the flintstone are highly reactive, as are the surfaces of the vast majority of other inorganic materials. This is due to the fact that rupture surfaces leave the atomic boundary structure unbalanced in electrical terms, and this condition compels the material to react rapidly in the direction of a new electrical equilibrium. It is possible that this is the initial step in the process of creating a flint patina [319][320].

Flint's sensitivity to attack and the rate of penetration by water and other weathering agents are significantly impacted by the type of contaminants present, the size of those contaminants, as well as the way in which they are distributed throughout the stone. Flint is mostly made up of silica crystallites that are quite tiny. The individual crystallites may be so microscopic that even when viewed with high magnification, their borders cannot be detected, or they may be sufficiently massive to be observed even with the naked eye. Many varieties of flint preserve the outlines of fossils or fossil pieces because many flints were siliceous replacements for fossiliferous carbonate rocks in the early stages of their formation. Carbonates, iron oxides, clay minerals, carbonaceous matter, and iron sulphide are some examples of the mineral contaminants that may be found in flint [321].

7.1.1 Flint patination

Patination is a process that may occur on all flints during the long burial period. The rate at which patination occurs is dependent on a wide variety of factors, including (i) contaminants: such as type, proportion, and distribution of contaminants; (ii) flints features: such as texture, microstructure, permeability, and (iii) environmental factors: such as temperature, humidity, moisture and the chemistry of the soil. In turn, the variables of the environment interact with the surface, either through more or less violent chemical reactions or by means of a more or less intensive deposition of non-reactive aerosols and other substances [322]. These interactions might take place either directly or indirectly. At the same time, the surfaces of flints start to become places in which various forms of living organisms can develop. This can happen either because the flints provide simple physical support to the microorganisms or function as a substratum supplier of essential micronutrients. The investigation of man-made flint surfaces or natural outcrops reveals complete evidence of all the potential stages of change, beginning with the initial fresh flint surfaces and progressing all the way up to the extreme situations of their profound alteration or entire obliteration [321][323]. The depth of the patina changes during the course of its

development. The reflectivity and preferred absorption of light are altered by chemical modifications to pigments, their dispersion over intergranular surfaces, or their elimination by leaching. There are a number of elements that can affect the patina's thickness, and hence its ability to be used as a flint patina chronometer: permeability, contaminants distribution, and composition of contaminants may all be responsible [324].

7.1.2 Color of the flint patina

There are two main types of color changes that may be observed forming on flints: a ferruginous brown patina or a chalky white patina. Refraction and reflection at various intergranular surfaces, which results in internal absorption of light as well as a reflection back to the viewer in most flints, are responsible for much of the flint's hue. The brightness or value of a color is determined by the difference between the amount of light reflected and the amount of light absorbed. A natural pigment's ability to absorb light at specific wavelengths (such as iron oxide and hydrous iron oxide) is what determines the color's hue. The color variations are related to changes in the texture and contaminant compositions of the flint. The modification of the flint's reflectivity may be attributed to a number of different processes, including the formation of voids as a result of the dissolution and leaching of carbonates, the loosening of quartz crystallites, and the reflectivity of clays [325].

7.1.3 Laser intervention of flints

The constraints of traditional mechanical and chemical cleaning methods, which cannot always thoroughly clean the targeted stone surface without inflicting either microdamage or color changes, have made laser stone cleaning increasingly important in this field. Even though a particular amount of damage can only be seen with a microscope, it still increases the likelihood that the surface may gradually evolve towards damaged in the future. The parameters for the laser are chosen so that it can attain the level of precision and selectivity required to successfully separate the surface deposits and crusts or soling from the lighter-colored substrate without causing any unwanted damage.

Since the early days of laser technology and its increasing number of applications in the field of cultural heritage (CH), people have had the idea of using pulsed laser irradiation as a light eraser on stone artwork in order to remove encrustations and damaged layers of the stone's surface [110]. This early laser system technology was mainly employed within the confines of the laboratory [112][113][114], mostly due to the expensive cost of the

equipment as well as its inability to relocate for in situ cleaning treatments. Some decades ago, a great number of stone conservators were concerned about the possible negative effects of laser irradiation on stones. However, this anxiety has been alleviated as a direct result of an increased investigation into the ways in which lasers interact with stones. As a result of extensive studies since the 1970s, the laser cleaning technique has become more efficient and effective while addressing and resolving the drawbacks associated with cleaning stone artifacts [153][150] [49].

7.1.4 Objectives of this chapter

Although conservators conduct a range of experiments in the laboratory or in the field, comparing lasers to other traditional methods for stone cleaning to evaluate the cleaning effectiveness of the laser, flints cleaning conservation has received minimal attention. It is possibly due to the rising number of challenges associated with cleaning outdoor sculptures, most of which are related to environmental pollution, as well as their aesthetic value and relevance to the society. In contrast, laser cleaning techniques may be included as an outstanding example of how relatively recent technological advances may be applied to improve conservation methods for CH materials; although they have been given limited attention for indoor in-cave flint artifacts by the conservation and restoration community, most probably because of a lack of conservation understanding. This is also probably because the indoor in-cave flint artifacts typically have naturally produced patination crusts and different type of surface deposition problems. On the other hand, the idea of stone or flint patina is still a controversial concept despite the fact that it is of significant relevance to conservation [320]!

The existence of a patina on a flint surface indicates that some foreign materials have been included into the intervention. This laser flint interaction is crucial; it is likely that the ‘original’ surface, or what is left after the alterations due to the crusts and surface deposits as well as contaminants, is still present. When it comes to cleaning operations, the presence of natural patina serves as the greatest sign that the procedure has to be completed in a timely manner and without causing any damage to the flint surface. It is also very important from the conservation viewpoint to develop necessary skills to select, safely operate, and apply lasers in the surface of the flint to clean the patinated layer, as much as possible, without touching the original surface. The objective of the present chapter is to study different pulsed laser technology [59] to ascertain its potential use in cleaning contaminated crusts and surface deposits from significant flint surfaces unearthed in two different open-air sites of *Sierra de Atapuerca* (Burgos, Spain).

7.2 Materials and methods

7.2.1 Neogene and Cretaceous Flints

Two different flint artifacts, identified as (i) Neogene flint (ATA16 / FM / N5), excavated as completely covered with soil in 2016 from the *Fuente Mudarra* site, dating back to $87,077 \pm 5.23$ Ka (OSL), and as (ii) Cretaceous flint (ATA19/PDJ/N1), unearthed from the *La Paredaja* site as mineralized in 2019, dating back to the upper Pleistocene chronology. Other related essential details for both of the flints, from an archaeological standpoint, are as follows: - (i) square: K34, number: 8, z(depth): 195, category: BN, length: 80 mm, width: 52 mm, thickness: 45, and (ii) number: 212, z(depth): 985.2780, category: FRAG, length: 72 mm, width: 29 mm, thickness: 19.



Fig. 7.1: Top surface view photographs corresponding to both of the Neogene flint (left) and Cretaceous flint (right) artifacts, excavated from the *Fuente Mudarra* and *La Paredaja* site, subjected to this study.

The ferruginous brown patina and less brownish-yellowish encrustations, surface deposits, and contaminants were unevenly covering the surface of these flint samples; the Cretaceous flint was covered with a thick of the crusts, whereas the Neogene flint was covered irregularly with a thin layer. Upon excavation, the primary atmospheric soil dust was removed by applying a mechanical cleaning procedure earlier by using soft brushes. Photographs of the artifacts from topside views are shown in Fig. 7.1. The specific objective for these flints entails laser intervention on selected areas to eliminate the dark brownish-yellowish encrustations without reaching the original surface that developed due to the contamination and mineralization.

7.2.2 Laser irradiation parameters applied to flint artifacts

A series of studies have been conducted to assess the controlled laser cleaning parameters using two sub-ns pulsed laser systems with emission wavelengths in the near IR (1064 nm) and UV (355 nm) range, and one ultrafast fs UV laser emission at 343 nm wavelength. Their essential emission characteristics are summarized in Table 7.1. In all experiments, beam scanning protocols were used in attempts to clean the surface of the flint and to explore contaminant removal efficiency, while at the same time assessing the degree of damage produced to the underlying original substrate surface. In the target area of the surface where cleaning is being applied, the laser beam is scanned over the surface of a fixed sample; so that the beam scan speed and line-to-line distance must be specified in the computer CAD-like software that controls the laser and galvo scanners.

Table 7.1: Characteristic emission of the two sub-ns and one fs laser employed for the present study. Values are given for the maximum nominal power (P_{\max}), emission wavelength (λ), pulse width (τ_p), pulse repetition rate (f_p) and beam waist (D_b) by applying the $1/e^2$ criterion with a Gaussian beam distribution.

Laser type	P_{\max} (W)	λ (nm)	τ_p	f_p (kHz)	D_b (μm)
sub-ns UV	3	355	300 ps	200-800	31.4
sub-ns n-IR	8	1064	800 ps	200-800	79
fs UV	9.33	343	238 fs	200 -1000	30

7.3 Results and Discussion

When considering undesired contaminant removal from surfaces, laser emission parameters are most relevant, while substrate and surface properties must also be considered for developing cleaning and conservation methodologies. The different laser irradiation conditions contribute to various degrees of elimination of flint surface deposits, depending heavily on the level of contaminants and crusts of the flint surface substrate. It is most common that undesired contaminant layers are not uniformly distributed; even the same has been observed throughout the flints subjected to cleaning. Pollution accumulations and contaminants of flints change the initial flints color to the ferruginous

brown patina color by all sorts of sub-surface contaminants gathered within an uneven matrix of thickness varying from few micrometers to 1mm.

At the flints cleaning by laser irradiation, notable color changes and blackening phenomena have been taking place: i) dark brownish alternation on Neogene flint due to the n-IR irradiation (Fig. 7.2: d) and ii) discoloration into grey on Cretaceous flint due to UV irradiation (Fig. 7.2: h) when treating the contamination crusts and surface deposits. The fluence and irradiance values for good sub-ns n-IR cleaning has been calculated ~ 0.24 J/cm² and ~ 0.30 GW/cm² (Fig. 7.2) respectively; on the other hand, ~ 0.69 J/cm² and ~ 2.30 GW/cm² (Fig. 7.2 f, g and h) accordingly has been obtained for sub-ns UV laser in order to clean the surface smoothly without making any alteration to the original surface (Table 7.2a). It has been observed that under sub-ns UV laser irradiation, thin and homogeneous crust cleaning is possible following an increasing number of scans with the same irradiance values, although the surface slowly turns grey after a critical number of scans. On the other hand, the whitish border area of the Neogene flint surface reveals an outstanding laser cleaning performance. Irradiation of the inner dense yellowish surface reveals, however, the blackening phenomena even at the lowest ablation threshold values. It seems the surface usually turns brownish and eventually melts under n-IR irradiation, probably due to exaggerated thermal incubation as a consequence of the high pulse repetition rates characteristic to the emission of this sub-ns laser.

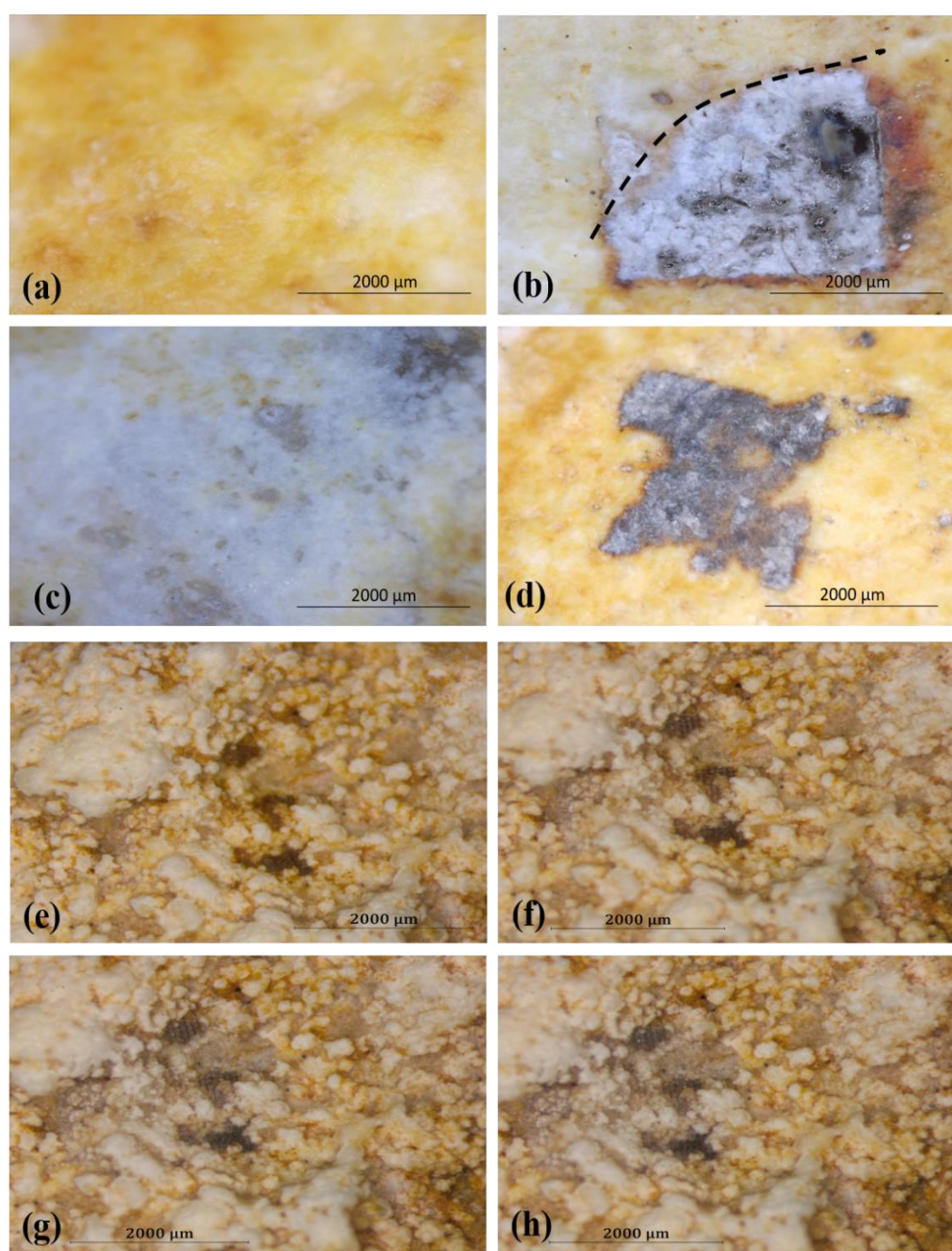


Fig. 7.2: Optical microscopy images of the Neogene Flint: ‘a and e’ represent the original surface of the sample with crusts and surface deposits, ‘b and d’ illustrate the laser damage with clearly visible melting and discoloration as evident due to the application of 800 ps n-IR laser, ‘c’ corresponds to a satisfactory cleaning result area at the outer whitish border of the sample, and ‘f, g and h’ correspond to the laser treatment outcomes upon irradiation with a 300 ps UV laser applied 3, 50 and 150 scans.

Table 7.2 (a): Experimental parameter data used for investigating laser cleaning on flints. The beam diameter was determined as 79 μm for the 800 ps n-IR laser and 31.4 μm for the 300 ps UV laser; N_L presents the number of laser treatments.

Laser type	P_{\max} (W)	Effective f_p (kHz)	Pulse Energy $E_p(\mu\text{J})$	F_L (J/cm^2)	I_L (GW/cm^2)	Speed (mm/s)	N_L	Observations
800ps n-IR emission at 1024nm wavelength	5.82	500	11.6	0.24	0.30	150	25	The inner side of the flint melted, but the whitish outer side is cleaned (Fig. 7.2: b)
	4.87	700	6.95	0.14	0.18	150	25	No damage, good cleaning result (Fig. 7.2: c)
	6.77	500	13.5	0.27	0.34	150	25	Discoloration (Fig. 7.2: d).
	7.24	600	12.1	0.24	0.30	150	25	No damage, good cleaning result
	6.29	600	10.5	0.21	0.26	150	25	No damage; cleaning efficiency is not good
300ps UV emission at 355nm wavelength	1.53	200	7.65	0.98	3.30	150	50	Damage observed; color changed.
	2.04	300	6.80	0.88	2.93	150	50	Damage observed; color changed.
	1.09	200	5.45	0.70	2.34	150	3	No damage, good cleaning result, little grey discoloration (Fig. 7.2: f).
	1.60	300	5.33	0.69	2.30	150	50	No damage, good cleaning result, little grey discoloration (Fig. 7.2: g).
	1.60	300	5.33	0.69	2.30	150	150	No damage, good cleaning result, little grey discoloration (Fig. 7.2: h).

Table 7.2 (b): Experimental parameter data used for investigating fs UV laser cleaning on flints. The beam diameter was 30 μm for this laser system. N_L presents the laser treatments number.

Laser type	P_{\max} (W)	Effective f_p (kHz)	Pulse Energy E_p (μJ)	F_L (J/cm^2)	I_L (TW/cm^2)	Speed (mm/ s)	N_L	Observations
238fs UV emission at 343nm wavelength	1.34	10	6.70	0.95	3.98	150	5	Good cleaning threshold of ferruginous brown crusts of Neogene flint, no damage (Fig. 7.3: a)
	0.94	10	4.7	0.66	2.79	150	5	Ablation threshold of ferruginous brown crusts of Neogene flint (Fig. 7.3: b)
	1.34	10	6.70	0.95	3.98	300	1	Perfect cleaning of ferruginous brown encrustations, no damage (Fig. 7.3: c)
	1.34	10	6.70	0.95	3.98	300	5	Expected cleaning of ferruginous brown encrustations of Neogene flint, no damage (Fig. 7.3: d)
	1.34	10	6.70	0.95	3.98	230	5	Discoloration observed (Fig. 7.3: e)
	1.34	10	6.70	0.95	3.98	100	5	Discoloration observed (Fig. 7.3: f)
	0.23	10	1.15	0.16	0.68	150	1	Ablation threshold of ferruginous brown crusts of Cretaceous flint (Fig. 7.4: b, c)
	0.42	10	2.10	0.29	1.24	150	1	Good cleaning threshold of ferruginous brown crusts of Cretaceous flint, no damage (Fig. 7.4: d, e)
	0.66	10	3.30	0.47	1.96	150	1	Maximum cleaning threshold of ferruginous brown crusts of Cretaceous flint, no damage (Fig. 7.4: f, g)

In terms of n-IR and UV laser cleaning, the irradiance values for the pollution crust and the natural surface deposits of the flint are all close to the respective ablation thresholds. As a result, the irradiated material is not completely removed at low irradiance levels. Thermally-induced dissolving processes are favored, potentially contributing to micro-sized melting properties. It is also crucial to establish the ranges of parameters where the irradiance values may be utilized to define the right laser treatment, as total irradiance values alone cannot be used to describe the optimal treatment. It is important to note that the value in the center of the spot for the Gaussian beam profile is twice as high as the norm; yet, the values for fluence and irradiance will remain similar if the pulse duration and wavelength values are not changed [326].

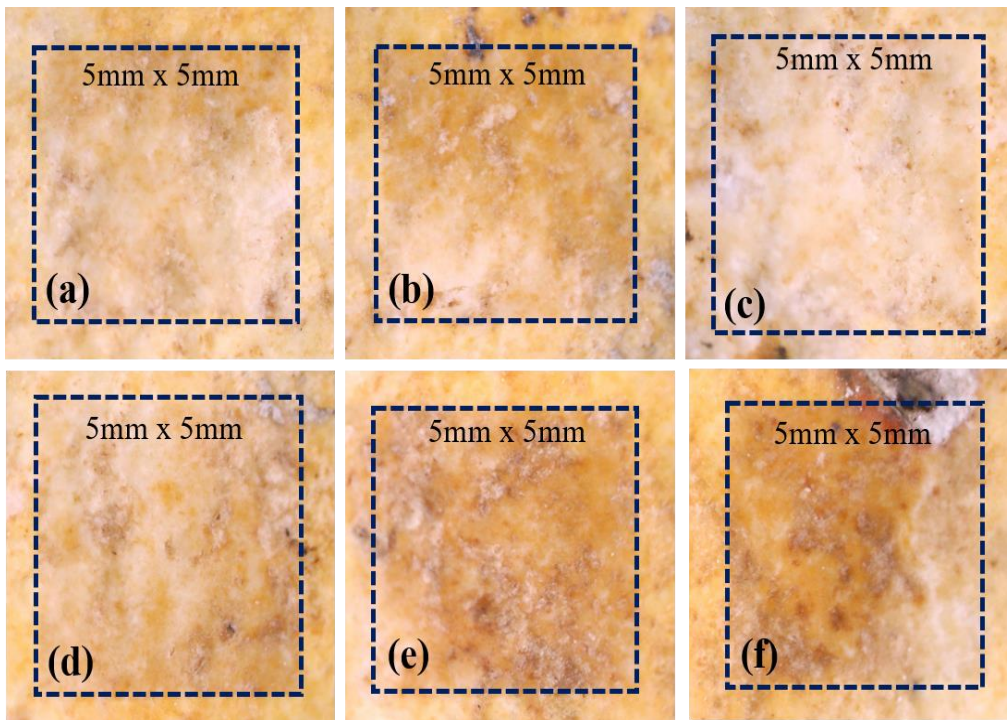


Fig. 7.3: Optical microscopy images of the Neogene Flint cleaned by 238fs UV laser, associated with Table 7.2(b): ‘a’ represents the outcomes of the laser cleaning threshold, ‘b’ shows the ablation threshold, where ‘c and d’ revealed the best laser cleaning results when cleaning the dark ferruginous brown crusts and surface deposits in micro/nanometer range taking into account the number of scans. On the other hand, ‘e and f’ present the discoloration effect at the same cleaning threshold values but differently arranged scanning speed.

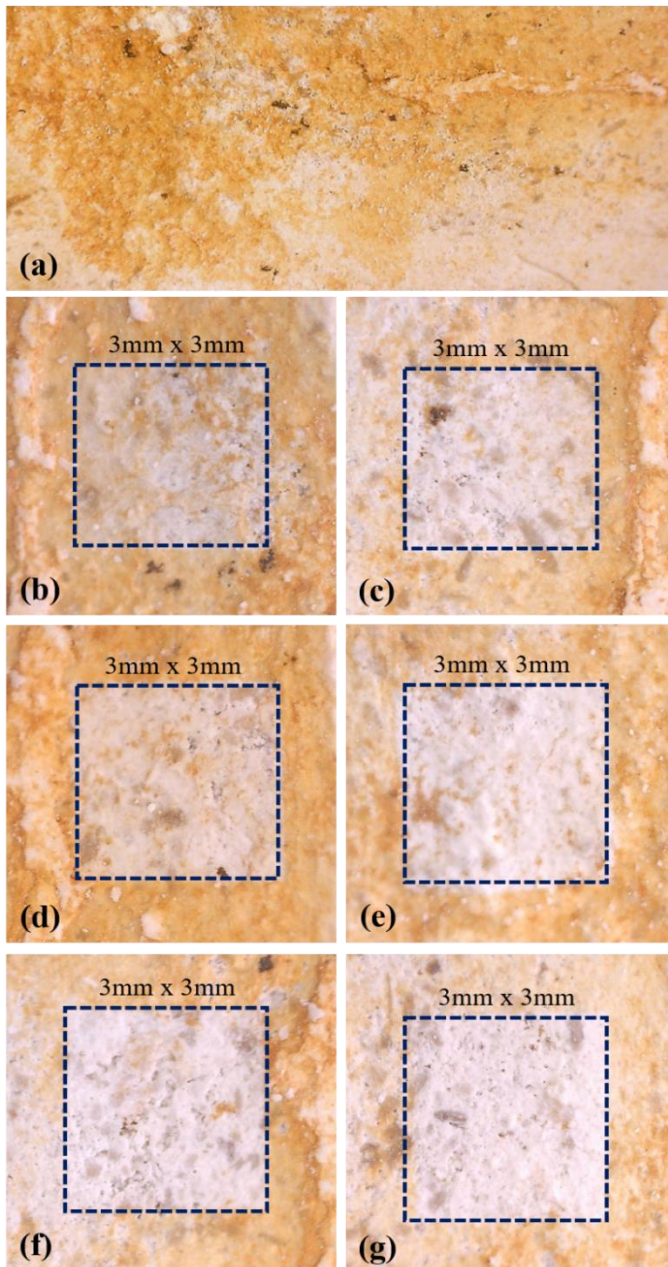


Fig. 7.4: Optical microscopy images of the Cretaceous Flint cleaned by 238fs UV laser, associated with Table 7.2 (b): ‘a’ presents the original outlook of the flint sample, ‘b and c’ represents the outcomes of the application of the ablation threshold, ‘d and e’ presents the best cleaning threshold, and ‘f and g’ presents the maximum cleaning threshold, where beyond this threshold value melting is the evidence. In all cases, only 1 treatment has been executed to rectify the best possible cleaning outcomes.

Evidently, laser wavelength and pulse duration play a crucial role in this discoloration problem [161][162]. The yellowing is often more apparent at 1064 nm and hence less apparent at the third harmonic 355 nm [168]. In contrast, no discoloration or blackening effects were seen upon application of ultrafast fs UV irradiation emission at 343 nm to contaminated crusts. The entire contamination crust and surface deposits have been

gradually eliminated at this wavelength regime based on the 'layer-by-layer' ablation mechanism for both flint samples, with the observed efficiency attributed to its self-limiting nature. Removal of the ferruginous brown patina of Cretaceous flint revealed the best cleaning results (Fig. 7.4) in comparison to the Neogene flint (Fig. 7.3). The prolonged age period of the stones and their burial may be the cause.

It has been shown that lasers of UV wavelengths and pulse durations of fs may effectively remove dark-colored overlayers from flint artifacts with light-colored substrates. Since the short pulse length prevents heat from reaching the flint surface, it would have a limited effect on the surface until the crusts and other surface deposits had been eradicated since minimal intensity normally does not create any damage on the surface cleaning. It has come to light that the crust on the region with the deepest ferruginous brown patina needs a larger number of scans (Fig. 7.3d with 5 number of treatments), whereas the crust on the area with less dark ferruginous brown patina needs less scans (Fig. 7.3c with 1 treatment number). It has also been noticed that the speed of the scanning process has a significant influence on cleaning. When the latter is performed using a larger scanning speed, a lower quantity of heat is accumulated. However, slower scan rates result in higher heat accumulation, which leads to melting (Fig. 7.3e and f).

The SEM-EDX analysis indicates that the inspected flint material mainly consists of silica (SiO_2), however, other major and minor trace elements, which can be interpreted as typical signatures caused by geographical site location factor, can be found (Fig. 7.5 and 7.6). The SEM-EDX study was carried out on both, the untreated and the fs UV laser-irradiated flint surface and found the presence of Si, O, Al, K and Fe. Trace amounts of Mg, Ca, Na, and Ti were also found in some specific regions. The irradiated surface was accomplished by performing sequential laser beam scanning in each and every experiment, ensuring that there was an area overlap of at least 70 percent. Figure 7.5a and c show the SEM-EDX spectra of the original encrusted dark colored region, and Fig. 7.5b and d show the treated surface with different cleaning thresholds (associated with Table 7.2b, and Fig: 7.3c and 7.4e, respectively) for the Neogene and Cretaceous flint. According to the treatment outcomes (shown in Fig. 7.5: b and d), practically all of the iron is removed with each subsequent cleaning.

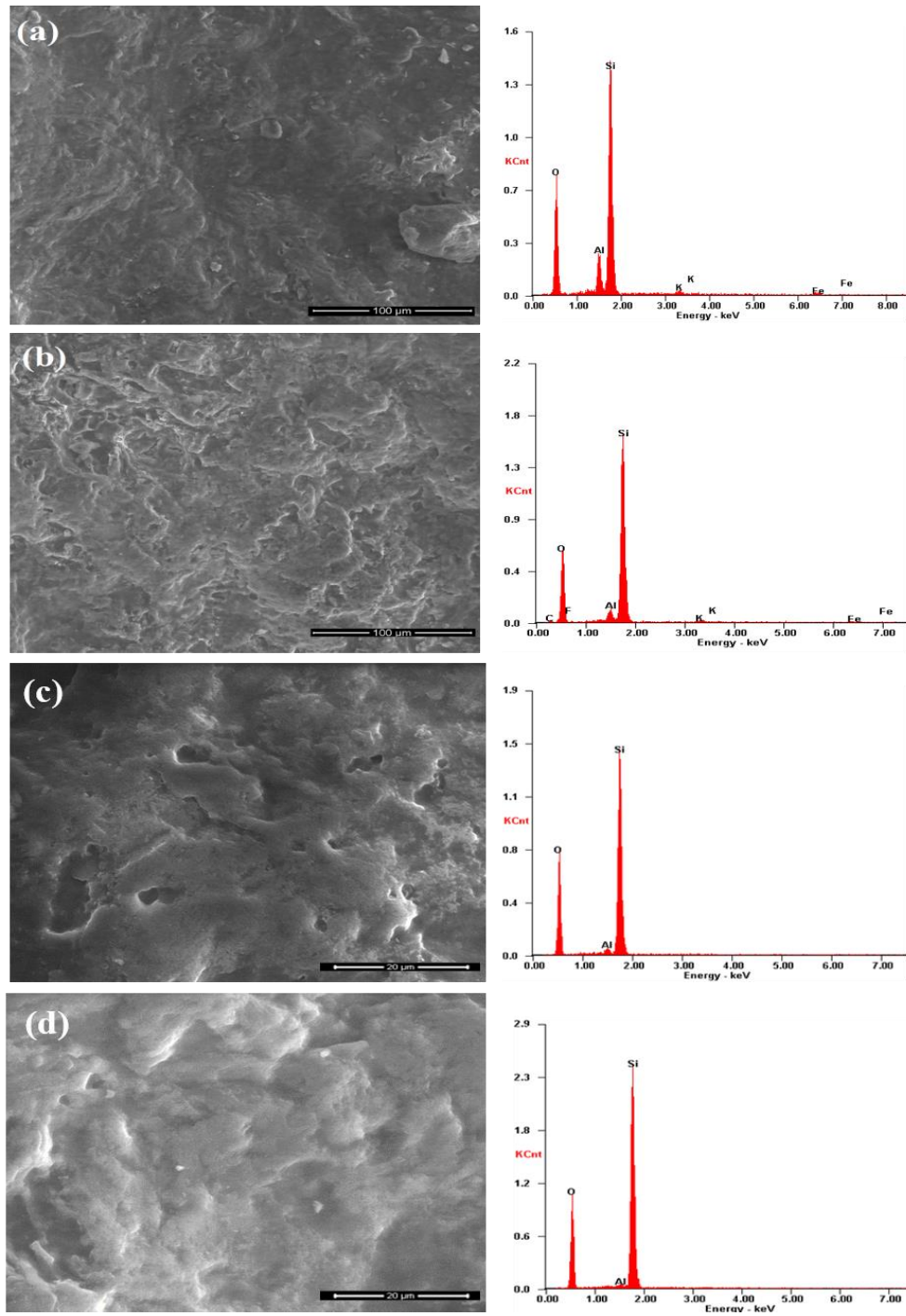


Fig. 7.5: SEM-EDS analysis of the UV laser cleaning for the non-treated Neogene and Cretaceous flint area (a and c), and the respective laser-treated flint area (b and d).

Other elements, such as Al, which owed their presence primarily to the effects of contaminants, have been significantly eliminated. According to SEM-EDX analyses, the concentration of Fe, Al and K is significantly higher near the surface than it is deeper inside the flint (Fig. 7.6). The concentrations of these elements have been lowered to the point where they are scarcely recognizable as contaminated crusts and surface deposits on the flint surface, as a consequence of the applied laser irradiation procedure.

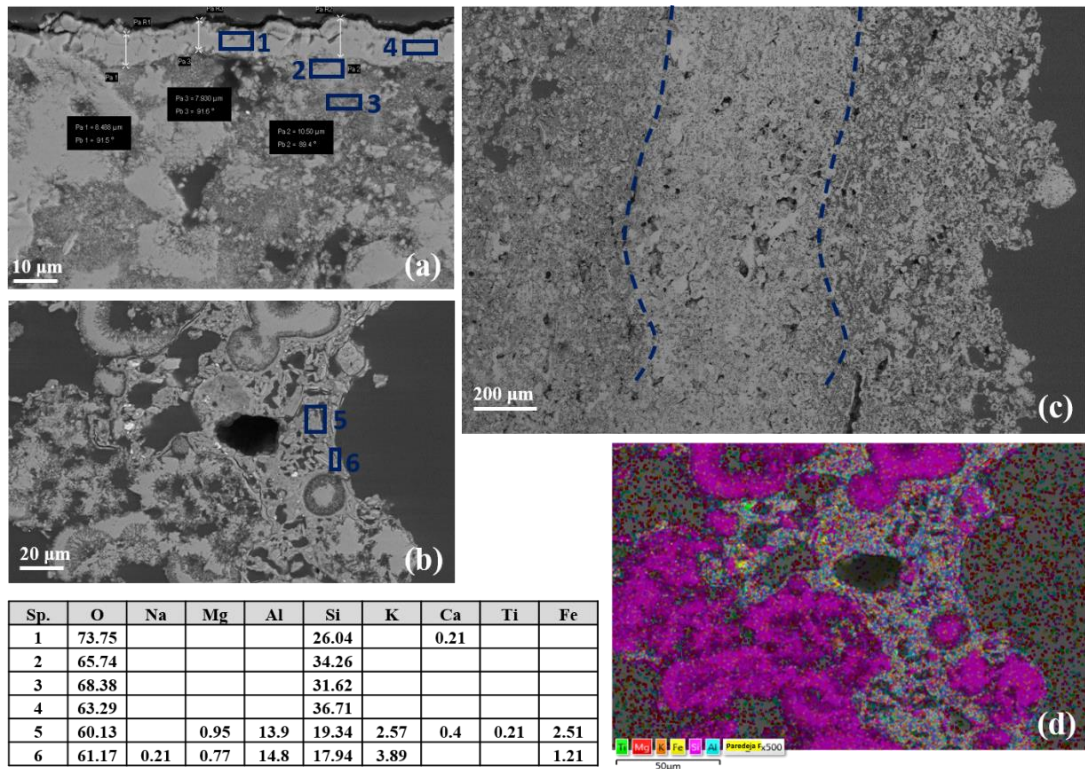


Fig. 7.6: Non-irradiated Cretaceous flint cross-section observed on micrographs obtained by FE-SEM under different magnification (1000 X, 500 X and 38 X accordingly for Fig. a, b and c).

Three different layers are observed in the micrographs of Fig. c (from right to left): outer ferruginous brown patina layer, middle denser layer and inner porous layer. Fig. d represents the elemental mapping of the cross-section of the flint sample. EDS analyses performed on the indicated representative areas are summarized in the lower left Table in Atomic Percentage (%At).

The presence and distribution of Si and O, essential components of flint, is confirmed and observed to be similar in almost every region of the flint. Contaminants, specifically crusts and surface deposits, are thus restricted to the outermost layers of several μm . K is detected within the dark ferruginous brown patina area (ca. 5-15 μm) and follows a similar trend as Al. Both, Al and Fe are consistent with the fact that the flint has been in contact with clay, as their presence is significantly reduced below a depth of ca. 5-15 μm .

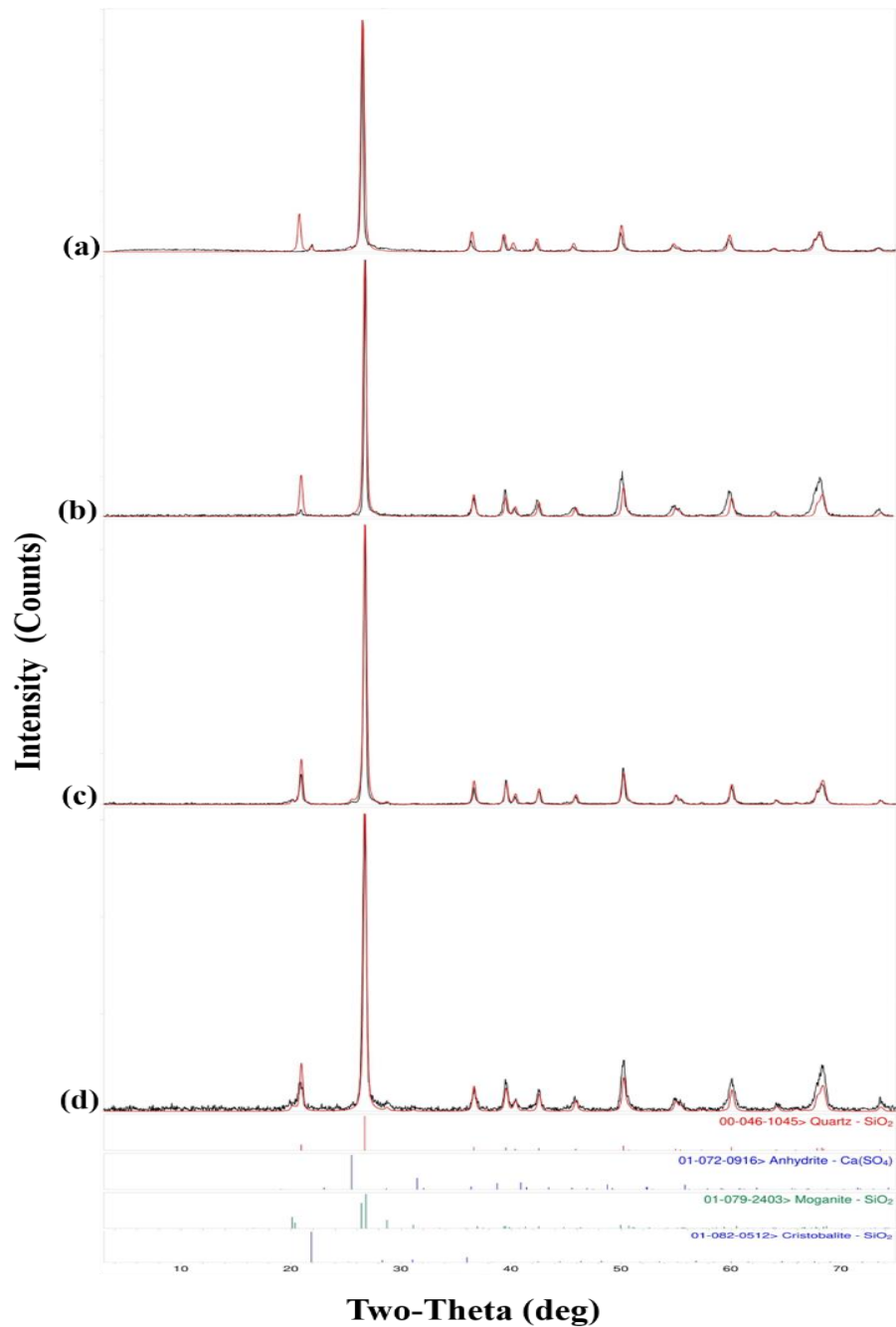


Fig. 7.7: Representative XRD peak identification of the Neogene flint sample with and without treatment of UV fs laser; experimental diffractogram peak in black compared with the theoretical one in red colored: 'a' and 'c' presents the original flint surface and 'b' and 'd' presents the fs UV laser cleaned surface. The JCPDS-International Center for Diffraction Data-2000 database has been used to determine phases.

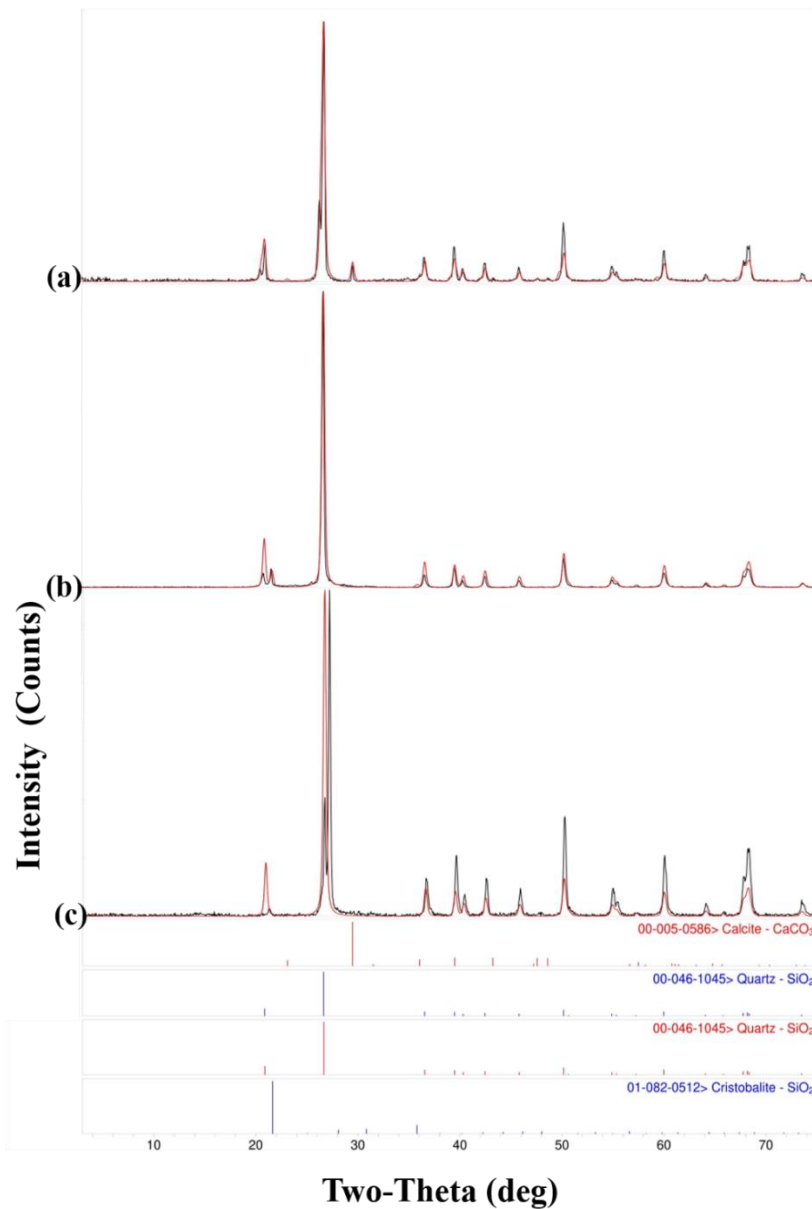


Fig. 7.8: Representative XRD peak identification of the Cretaceous flint sample with and without treatment of fs UV laser: 'a' presents the original flint surface and 'b' and 'c' presents the satisfactorily cleaned laser treated surface. The JCPDS-International Center for Diffraction Data-2000 database has been utilized to determine the phases.

EDS was used to identify the chemical composition of the flint sample in a semi-quantitative manner by analyzing the flint's cross-section (Fig. 7.6). A similar pattern is

seen in all the regions, except for a large drop in the outmost darkest ferruginous brown patina area at depths of ca. 5-15 μm , where we detected high concentrations of Si and O, the major constituents of flint, known as quartz. K is shown to have a similar trend as Al, which supports the idea that it was incorporated into the rock through mineralization. Furthermore, the content of Al and Fe in the flint is dramatically reduced below a depth of around 5-15 μm . It is clear that the presence of contaminants and crusts is limited to the topmost layers (a few micrometers) of the flint artifact. However, because the flint was buried for an extended length of time, mechanical breakdown or chemical deterioration of the surface permitted the precipitation of Fe compounds, which resulted in dark encrustations and ferruginous brown stains on the artifact's most exterior layer (Fig. 7.4a).

Figure 7.7 and 7.8 represents the experimental diffractogram (black) compared with the theoretical one (red) resulting from the sum of phases specified. In the XRD analysis for the Neogene flint sample at the original ferruginous brown patina crusts area, it has been observed that all the diffraction peaks correspond to quartz, except the first one at 2θ 20.68° (Fig. 7.7: a). A small diffraction peak is also observed, perhaps corresponding to SiO_2 -cristobalite at the nearby 2θ value of 22° (Fig. 7.7: a). Upon UV fs laser cleaning, the quartz diffraction peaks were also identified, but slightly displaced (Fig. 7.7: b). On the other hand, the original whitish colored region (Fig. 7.7: c) and the satisfactorily cleaned laser region (Fig. 7.7: d) showed very similar diffraction peak, both of the which correspond to quartz. A small diffraction peak was identified at 2θ 25.5° which might be possibly assigned to CaSO_4 , but is not confirmed as the more intense diffraction patterns has only been observed (Fig. 7.7: d). Two more low intensity lines appear at 2θ 20° and 28.7°, identified as corresponding to SiO_2 -moganite (Fig. 7.7: d).

XRD analysis of Cretaceous flint 'before and after' laser treatment (Fig. 7.8) showed double diffraction patterns at low angles. Fig. 7.8a stands for original ferruginous brown patina crusts before laser treatment. Two peaks at 2θ 20.45° and 26.25° could be SiO_2 similar to quartz but a little different. The diffraction peak at 2θ 29.15° may be assigned to calcite. In contrast, Fig. 7.8b exhibits quartz diffraction peaks. The line at 2θ 21.57° corresponds to the most intense cristobalite line, although no other diffraction patterns are observed corresponding to this compound. Only quartz lines are observed in Fig. 7.8c with the more intense double peak; perhaps the double peak is due to surface irregularities.

7.4 Conclusions

Our primary finding is that surface deposits and crusts may be effectively removed from flint surfaces using fs laser pulses operating in the UV wavelength range. The results suggest that the encrustation removal effectiveness was high and comparable to that of other laser approaches, including sub-ns lasers, despite the fact that just a small number of processing parameters were utilized in the experiment. The evidence provided by the SEM-EDX data and the XRD spectra for both, before and after laser irradiation, demonstrates that the fs UV laser is an effective tool for cleaning flint surfaces.

When compared to sub-ns lasers, fs lasers appear to better preserve the original morphology of the flint surface when viewed from such a perspective. As a result of the thermal nature of the cleaning process for the sub-ns laser, the surface of the flint becomes flattered due to the melting of rock-forming elements, and it also becomes noticeably discolored in the process. In spite of this, the morphology of the mineral grains is not changed by fs pulses; rather, the relief associated with mineral cleavage planes is preserved. This is a significant benefit of using fs, instead of sub-ns laser cleaning.

In spite of the fact that the irradiance value of the laser cleaning intervention governs some elements, the cleaning threshold of the flints may be deduced after the flints have been subjected to irradiation via successive scans. Even though the absorbed laser energy is below the damage threshold, the thermal characteristics of flint can still cause structural and chemical flaws as a consequence of heat accumulation with prolonged, repeated irradiation sequences. This is the case regardless of whether or not the damage threshold has been surpassed. During this experiment, UV laser irradiation with fs pulses generated great outcomes in photomechanical, photochemical, and thermal incubation procedures. Altering the laser power, pulse duration, and spatial distribution of the laser irradiation are some of the ways in which laser-flint interactions may be regulated more effectively. As a result of the fact that the settings of the laser irradiation may be controlled, the ultrafast UV fs laser has been demonstrated as significantly safer and more effective in cleaning flint surface deposits.

CHAPTER: 8

fs LASER INTERVENTION ON
CERAMIC ARTIFACTS

CHAPTER EIGHT

fs LASER INTERVENTION ON CERAMIC ARTIFACTS

***Summary:** Restoration using traditional cleaning methods often fails for numerous archaeological materials covered with hard concretions. This chapter investigates the impact of wavelength and pulse duration in ultrafast femtosecond (fs) laser cleaning of concretion crust from archaeologically significant ceramic artifacts. Cleaning was performed utilizing three newly developed Yb:KGW lasers: 228 fs near-Infrared laser with emission wavelength at 1030 nm, 238 fs Ultraviolet laser emission at 343 nm, and 249 fs visible Green laser at 515 nm. Beam scanning mode, pulse repetition rate, and material thermal properties are among the parameters considered to evaluate the potential that these fs lasers offer towards an increased cleaning efficiency of safeguarding original ceramic surfaces. Optical Microscopy, Scanning Electron Microscopy - with Energy Dispersive X-ray Spectrometry (SEM-EDS), and X-ray diffractometry (XRD) were used to investigate and compare the impact of these laser systems on hard concretion removal while analyzing the damage to the substrate surface. In this study, the application of fs visible Green laser irradiation leads to a very satisfactory result in photochemical, photomechanical, and thermal incubation effects. It appears to be superior in cleaning when varying the laser intensity and its temporal and spatial distribution to manage laser-artifact interactions. It has been found significantly safer and more efficient at ceramic surface cleaning, owing to the controllability of laser irradiation parameters, which allows for a systematic and accurate description of an actual laser cleaning intervention.*

8.1 Motivation of the Research

Ancient human knowledge and expertise in technical applications and innovations make archaeological ceramics a significant blend of materials, techniques, and processes. It is a complicated piece of art that mainly reveals much about human culture and history. Potters use clay and other ceramic materials to create a wide range of ceramic objects, which are then fired at high temperatures to solidify and keep their shape. Ceramic artifacts have been

used for food preparation, storage, preservation, and aesthetic purposes [327]. A number of factors, even if they're made from the same clay, can influence the quality of ceramic artifacts. Variables including the manufacturing process, duration of firing, and amount of oxygen present during combustion are all factors to consider [328]. Concerning the value of researching ceramic materials, for example - ancient pottery, each piece unearthed provides essential information about its lifespan and, more importantly, the civilization that made it [329]. Pottery sherds unearthed from archaeological sites can be studied with modern techniques to learn about their chemical composition, microstructure, the layout of minerals [330] [331][332][333][334][335], the temperature and type of firing they have gone through when manufactured [336][337][338], their use, archaeological setting and context, and their conservation status [329][339][340].

Modern archaeometry methods for studying ancient ceramics are generally various non-destructive / para-destructive and non-invasive methods that enable researchers to perform direct operations on the object. These methods include visual inspection using microscopy, reflectography, profilometry, colorimetry, etc. These processes often need the acquisition of information on the artifact's physicochemical, mineralogical, morphological, and crystallographic characteristics, which may be acquired by studies of the internal structure of the sample while taking into consideration the stratigraphic layers of the sample [341][342] [343]. Different diversified interdisciplinary techniques in collaborative or conjunction systems are used in the most recent archaeological ceramic objects investigations[344][345][346][347][348][349][350][351][352][353][348][348][353][354] [355][356].

This study focuses on the three Bronze Age ceramic pottery sherd from *Portalón de Cueva Mayor*, which is an incomparable archaeological Holocene site located in the *Sierra de Atapuerca* (Burgos, Spain) [357][98][101][99]. The *Sierra de Atapuerca* is a mountain range in northern Spain, roughly 15 kilometers east of Burgos on the Northern Plateau. Communication routes run north-south from the Duero to the Ebro basins through this region on their way through the Iberian Peninsula. Numerous Pleistocene hominid sites [72] made the mountain range archaeologically significant, which is also notable for its significant karst system, which consists of the *Cueva Mayor-Cueva del Silo* cave complexes. The "*Portalón de Cueva Mayor*" is a massive chamber near *Cueva mayor's* entrance that reveals traces of many human occupants in the recent prehistory. Many surveys and studies on *Portalón de Cueva Mayor* have shown three distinct cultural epochs that occurred throughout the course of time: the final, middle and early Bronze Age

sequence [98][101]. During the Holocene period, archaeological stratigraphic units have been found with a very rich archaeological content, including pottery, lithic industry, individual ornamental components, metallic artifacts, and human and animal remains [98].

In archaeometry research, it is important to understand the archaeological site's history from both an archaeological and anthropological standpoint when large quantities of ceramic pottery artifacts are uncovered during excavations of a particular location. Hence, it is essential to examine ceramic pottery materials while analyzing historical events [180]. An array of causes may be traced back to the degradation of the archaeological pottery legacy. Weathering and pollution, as well as mechanical pressures, are all examples of environmental degradation. The end outcome has been a decrease in artistic quality [133]. A wide range of hard deposits, soil contaminants, stains, and encrustations are commonly found on pottery artifacts excavated from archaeological sites [181][182][39]. Hard soil deposits and diverse stains have built up over time on the surface, which has resulted in concretion crusts on the sherd materials. Chemical compounds, such as calcium carbonate or iron oxide, found in soil, in the form of grains or nodules of various sizes, shapes, hardness, and colors, are known as concretions [358]. Generally, they are hard, compact masses of materials that are created by the precipitation of minerals within the gaps between particles in sedimentary soil. They are typically ovoid or spherical in shape; however other shapes can exist. Existing layers of sedimentary strata are the source of concretions, and they form within deposits of sedimentary strata that have already been deposited. Artifacts are buried in sediment and these concretions form before the sediment becomes rock-like in density. The chemical makeup of some concretions differs from that of the surrounding material. Due to the longer burial time and the ground conditions, the concretion becomes more durable and weather-resistant than the host stratum in which it is implanted. Concretion layers can be classified as weak or hard depending on storage conditions, such as soil humidity and pressure and the composition of the artifacts. Weak layers can be cleaned with brushes, whereas tougher layers need the use of scalpels, acids, or complexing agents. The concretion crusts layer provides a problem for laser cleaning restoration when combined with the sensitivity of the original pottery surface. In the vast majority of instances, cleaning the concretion matrix, which is often far more durable and resistant to the effects of chemicals than the surface of the original sherd, can be extremely challenging or even be impossible.

Keeping archaeological potsherds free of unwanted foreign materials is an important part of preventing deterioration, which is why cleaning ceramic artifacts is so essential and

common [359]. Ancient ceramic surface cleaning has traditionally been accomplished by the mechanical procedure or through the use of chemical solvents that are applied directly to the surface [360]. Ceramic artifacts, particularly the delicate pottery sherd body, are susceptible to rapid deterioration by chemical and abrasive processes, which can result in scratching and pitting on their finished surfaces. Few studies have inspected laser cleaning for ceramic materials conservation reasons, despite the widespread use of mechanical and chemical cleaning methods for ceramic artifacts for many years [133][131][132]. The utilization of laser irradiation has been used to achieve a great deal of beneficial conservation work in the cultural heritage sector, and laser cleaning as a method for cleaning ceramic objects is investigated in this research in an effort to establish its efficiency. The Yb:KGW femtosecond lasers irradiation with emission wavelengths of 1030 nm (near-Infrared), 515 nm (visible Green), and 343 nm (Ultraviolet) were utilized to clean the surfaces of three pieces of archaeological pottery sherds that had been covered with concretion crusts and contaminants.

This study aims to explore these three ultrafast fs laser wavelengths, how well they clean and interact with pottery sherds to remove matrix concretion from their outermost layer, as well as ash spots and hard environmental stains. There have been efforts to determine the optimal wavelength and pulse duration, as well as the ablation, damage, and cleaning threshold values for laser cleaning in order to prevent damaging the underlying substrate sherds surface. The cleaning experiments were evaluated in terms of the pace at which the hard matrix concretion crusts were removed and the damage impinged onto the potshers surface. The removal rate and efficiency of the employed laser systems were assessed using optical microscopy, scanning electron microscopy with energy dispersive X-ray spectroscopy (SEM-EDS), and X-ray diffractometry (XRD). Additional imaging techniques, such as optical and SEM images, were also employed to evaluate the damage to the outermost ceramic surface.

8.2 Materials and methods

8.2.1 Ceramic Artifacts

Three pieces of archaeological pottery sherds (APS) were subjected to the experimental process applied for this study. In order to identify each individual artifact throughout the study, the letter "APS" was preceded by the serial number (Fig. 8.1): APS-1 for the excavated sherd name ATP LIMP CATA (level: Sondeo 1983 Apellániz), APS-2 for the ATP LIMP EXC 2042 (level: Limpieza Excavación) and APS-3 for the ATP LIMP EXC

1979 (level: Limpieza Excavación). All the three sherds analyzed were excavated in the year 2000 from the *Portalón de Cueva Mayor* site, in the greyish brown mud layer, at various depths. Fabric composition, form, and surface treatment indicate that the sherds belong to a Chalcolithic-Bronze Age setting that dates back to the 4000 to 3000 BP period [98][99]. Because of the circumstances in which they were discovered and the morphological traits they exhibit, these sherds appear to be older than other comparable traces from the same trench. All sherds are covered with various thicknesses of hardened concretion crusts, slight contaminants and burial pollutants. The three sherds may be physically described as follows: (i) APS-1: 2.3 cm long x 1.8 cm wide x 1.0 cm thick fragment, (ii) APS-2: 3.4 cm long x 2.2 cm wide x 0.9 cm thick fragment, and (iii) APS-3: 3.6 cm long x 2.7 cm wide x 1.1 cm thick fragment.

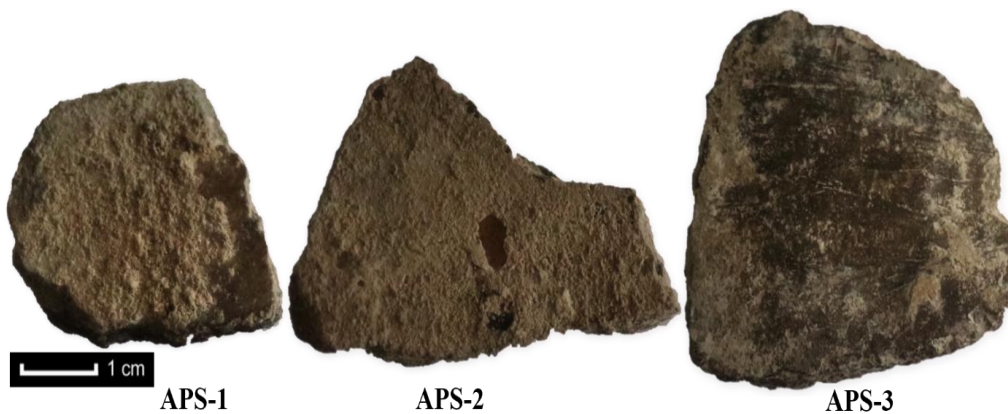


Fig. 8.1: Front surface photograph views of the three archaeological pottery sherds, excavated at the *Portalón de Cueva Mayor* (Burgos, Spain).

There was a thick layer of inhomogeneous concretion crust covering both APS-1 and APS-2, while only a small portion of the sherd surface was exposed to the burial environment and uncrusted, exhibiting shades of hard reddish contaminants, which is common with buried ceramic artifacts, possibly due to Fe mineralization. Concretion crusts, ash patches, and atmospheric soil dust marginally coated APS-3 unevenly. As a first stage in the conservation process, the soft clays and burial dust obtained on these three APS surfaces were mechanically cleaned with a soft brush to remove as much debris as possible before further laser treatments. Figure 8.1 shows the front side views of the three sherds, where these sides are subject to cleaning by the fs-laser in this study.

8.2.2 Laser cleaning systems and parameters

The schematic of the laser cleaning experimental setup subjected to this study is shown in Fig. 8.2. The Fig. 8.2(a) depicts the principal arrangement of the experimental setup for the applied fs laser system; a section of the electromagnetic spectrum is depicted in Fig. 8.2(b), which begins at the top with the ultraviolet (UV) region and moves down through the visible range and into the near-infrared (n-IR) region at the bottom. Three unique lasers are displayed on the spectrum used for this investigation, each operating at its characteristic wavelength.

Figure 8.2(c) illustrates the relationship between pulse duration and usable energy, revealing how thermal accumulation occurs throughout the pulse irradiation process. At the user's end, heat incubation, or the steady accumulation of energy input into one or more particular regions of a sample over time, was controlled by adjusting laser emission and beam scanning parameters.

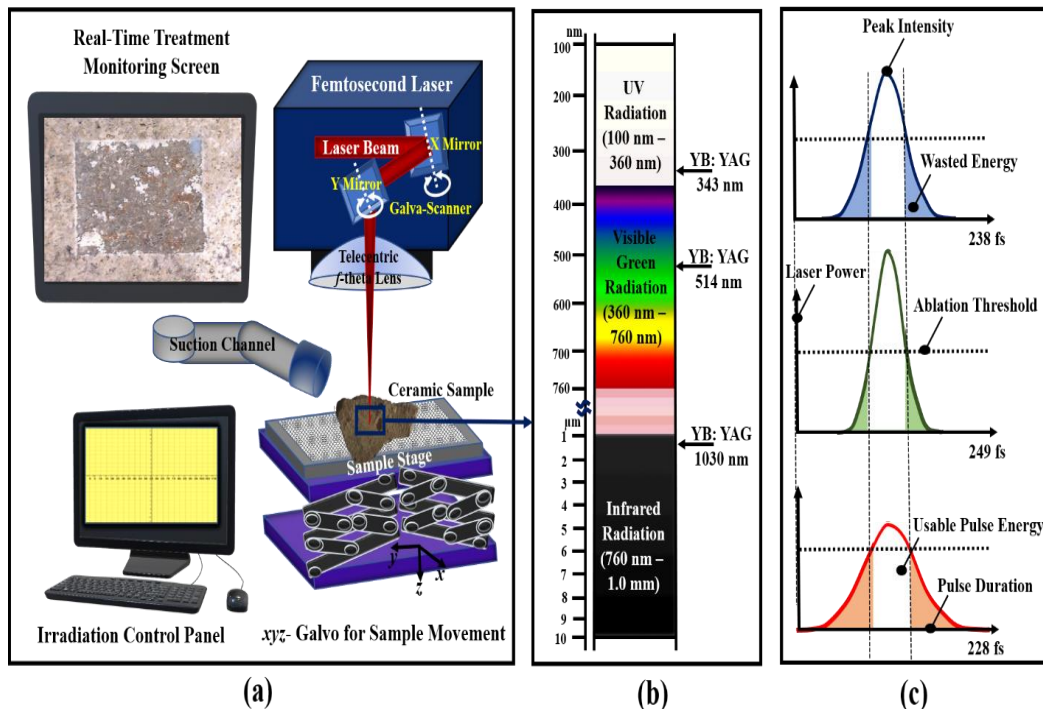


Fig. 8.2: (a) Experimental setup of the Yb:KGW fs laser cleaning system, (b) electromagnetic spectrum with three fs laser harmonics displayed at their characteristic wavelengths employed in this study and (c) the relationship between pulse duration and usable energy (adapted from [361]).

Table 8.1: Characteristic emission of three different fs laser harmonics employed in the present study. Values are specified for the pulse emission wavelength λ , pulse duration (τ), average power (P), pulse repetition rate (f), maximum pulse energy E_p , scan speed V , the distance between adjacent laser passes d and beam diameter (D_b) at full-width half-maximum (FWHM) [202] applying the $1/e^2$ criterion for a Gaussian beam distribution.

	Femtosecond n-IR	Femtosecond Green	Femtosecond UV
Wavelength λ	1030 nm \pm 10 nm	515 nm \pm 3 nm	343 nm \pm 3 nm
Pulse duration τ	228 fs	249 fs	238 fs
Average power P	40 W	20 W	9.33 W
Pulse repetition rate f	200 kHz – 1 MHz	200 kHz – 1 MHz	200 kHz – 1 MHz
Maximum pulse energy E_p	200 μ J	100 μ J	46.6 μ J
Beam diameter D_b	100 μ m	50 μ m	30 μ m
Scan speed V	150 mm/s	150 mm/s	150 mm/s
Distance between adjacent laser passes d	15 μ m	10 μ m	10 μ m

The laser power was controlled and regulated following the cleaning outcomes, and the experimental setup was maintained for selective irradiation of the desired surface region of the sherd. The laser beam was scanned in beam scan mode [205], while the scan speed and line-to-line distance were defined by selecting the values in the CAD type software provided by the laser integrator. Most of the treatments were done in three-by-three millimeter areas each that were crossed over, meaning that they were done in the zero-degree direction and then 90-degree direction simultaneously for every experiment. Hatching was used bi-directionally with no outlining mode for all experiments.

A series of laser treatments was then carried out in every fs laser system with different parameters to see whether any new phenomenon emerged. Scanning length and beam movement across the sample are controlled using XY-Galvanometer scanners, while scanning velocity is employed to fine-tune pulse spacing in the transverse direction. Optical microscopy and visual inspection were the primary methods used to analyse the cleaning outcomes. In this work, fluence (emitted energy of a given pulse per unit area of spot size) and irradiance (laser fluence divided by the pulse duration) are directly proportional to each other. It is important to note that irradiance values were used as a fundamental reference in this study, and thus as a universal reference for the best possible laser cleaning treatments.

8.3 Results and discussion

8.3.1 FESEM-EDS Analysis of the cross-section of pottery sherd-2 before laser

Whatever the sedimentary level or cultural phase, the *Portalón de Cueva Mayor* bronze age pottery sherds collection exhibits a stunning uniformity. In terms of manufacturing type, their variations, the surface treatments, the profusion and style of ornamentation, and the form and kind of manufacture, the continuity between the early and middle bronze ages has been revealed. The sedimentary bronze age at this region, which dates back 700 years, shows that manufacturing patterns have remained constant over that time [357]. A thorough understanding of the sample and the problems that need to be cleaned as a consequence of analytical studies necessitates revealing as much information as possible about the sherd's composition. As a means to maintain and enhance the aesthetic value of sherds, this investigation's main goal was to use an ultrafast fs pulsed laser to remove any concretions, ash spots, or other naturally polluted surfaces. FESEM analyzed the cross-section of the APS-2 pottery sherd to characterize the microstructural changes in ceramic compositions, while EDX analysis was used to identify the elemental compositions of the original surface and the concretions in order to better understand the ceramic sample state and the potential complexity of the cleaning problem. The formation of the concretions and the pottery's original surface are revealed by FESEM analysis of embedded and polished parts of the sherd.

The technical research literature provides information on how the pottery was produced, decorated, and fired in order to understand how they were manufactured, their color, inclusions, and pores peculiarities as well as on their practical use. Thus, the APS-2 (Fig. 8.1b) sample with a thickness of 13 mm shows mostly a tiny, spherical, well-threaded paste (i.e., lithoclast inclusions under 0.5 mm) and both sides are decorated with striations [362] (Fig. 8.3). The striations on the interior of this sherd suggest that it belongs to coarse or semi-coarse pottery that has been roughly smoothed. Angular/subangular whitish quartz grains with diameters ranging from 100 to 300 μm are the primary inclusions identified.

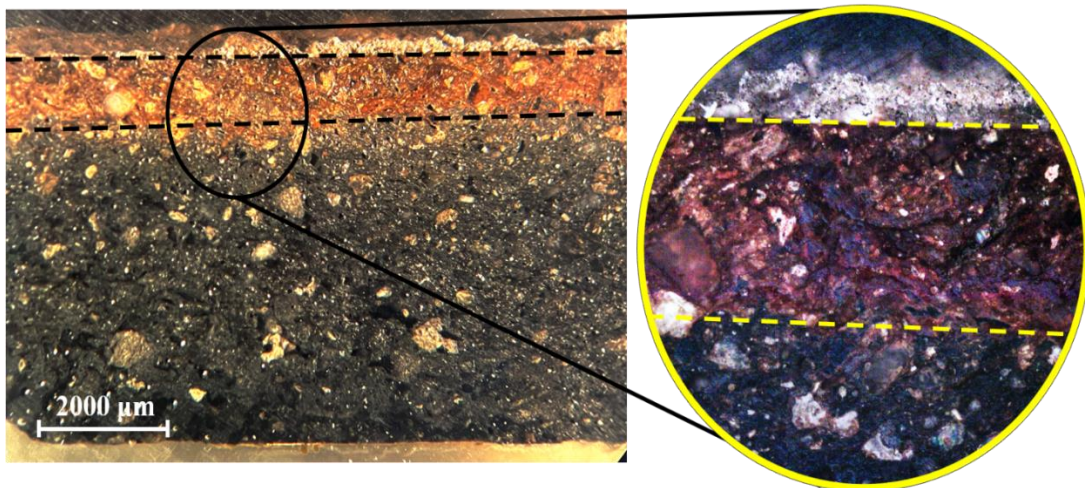


Fig. 8.3: Optical micrograph of the APS-2 sample cross-section (left), and higher resolution image (right) clearly exhibits the small details of the sample.

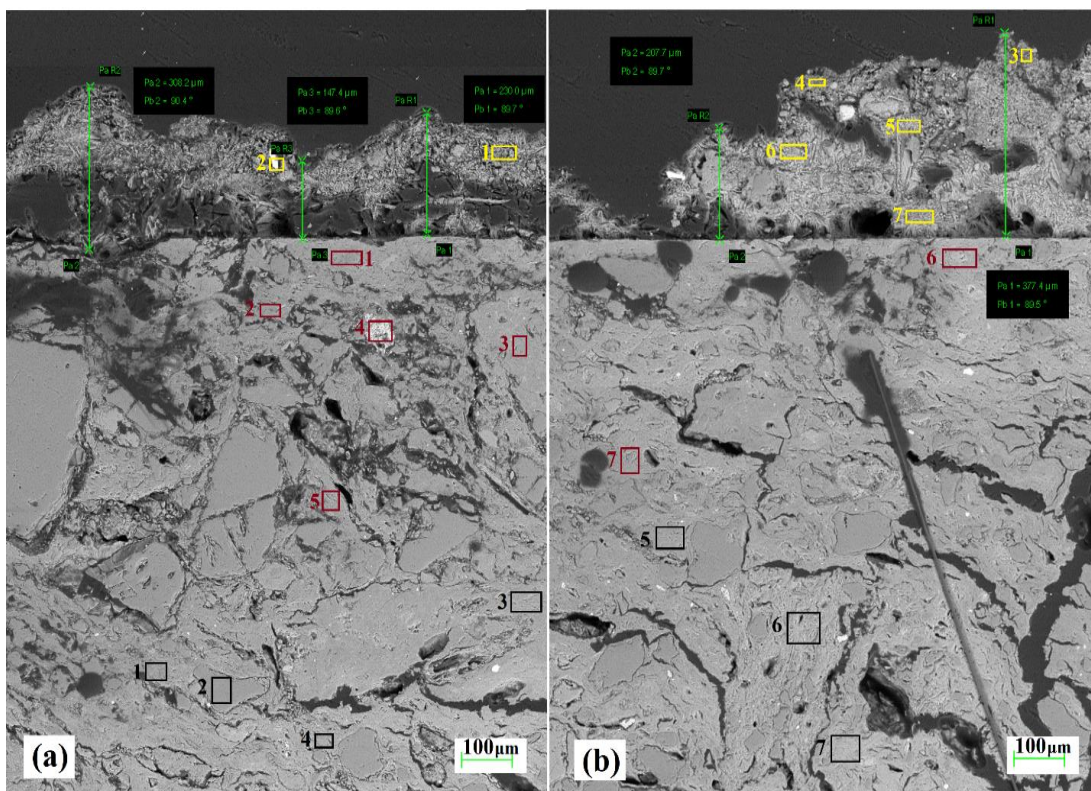


Fig. 8.4: SEM images of the cross-section of APS -2 represent the concretions' thickness, and different areas denote the interested regions characterized by the EDS analysis.

While most of the sherd color has been observed as very dark grey or black (5YR3/1) in the core of the sample, the outermost surface color (layers of 1.5–2.5 mm) varies within the array of light reddish yellow (5YR6/6) and yellowish red (5YR5/6) color, following the Munsell Soil Color Charts [363]. The thickness of the matrix concretions has been observed to be around ~150 to 380 μm (Fig. 8.3).

As shown in Table 8.2, the EDS measurements were acquired on cross-sections of the sample and concretions with varying shades of color. Thus, with the exception of the reddish color area and concretions that contain very little V with a much lower amount (under 0.5% Wt), the following chemical elements were identified in all areas of the reddish and blackish colored area of the sherd and the concretions: O, Ca, Si, Fe, Al, S, Mg, K, Na, and Ti, whose components are found in the lithic material utilized and the soil pollutants that were present throughout the subterranean laying process.

Na, Cl, P and Cu have also been identified but only in trace amounts: Na is under 0.4% Wt, Cl is less than 0.2% Wt in the sherd body and around 0.8% Wt in the concretions, P is less than 0.2% Wt in the sherd body and under 1.2% Wt in the concretions, and Cu is around 0.2% Wt. Concretions, on the other hand, contain a significant quantity of Mn, around 3 %Wt at maximum, indicating that the sample was polluted due to the grounded burial environment. The quantity of S in concretions is highly evident, reaching up to a maximum of 20% of the weight of the material in some regions, but it is insignificant in the sample. Almost all of the sherd's areas contain a significant quantity of Al, with maximum concentrations of roughly 15 %Wt, but with concentrations as low as 5 %Wt at the concretions. Fe concentration (about 6-8% by weight) in the sample indicates that ferruginous clay was utilized in the production of the pottery artifact. The absence of carbon from the sample's composition indicates that the artifact was fired at more than 800 °C, confirming that Calcite can withstand these temperatures.

Table 8.2: EDS analysis of the elemental composition on the cross-section of the sherd sample APS-2, associated with the Fig. 8.4.

Elemental composition of ceramic samples in weight percentage (%Wt)																	
Layer	Area	Label	O	Na	Mg	Al	Si	P	S	Cl	K	Ca	Ti	V	Mn	Fe	Cu
Concretion crust	a	1	54.54	0.19	0.44	2.21	10.85	0.48	7.21	0.22	1.03	21.83	0.03			0.97	0
		2	27.74	0.03	0.12	0.52	2.57	0.14	0.12	0.07	0.22	2.21	38.42	0.48	2.79	24.57	0
	b	3	45.39	0.33	0.96	5.21	9.69	9.43	0.34	0.78	1.96	22.1	0.18		1.19	2.37	0.07
		4	48.83	0.19	1.09	4.96	20.24	1.62	0.45	0.43	2.08	17.67	0.33			2	0.1
		5	54.51	0.12	0.24	1.88	12.37	0.69	11.22	0.05	0.67	17.32	0.09			0.75	0.09
		6	56.79	0.05	0.48	1.41	3.93	0.29	13.81	0.05	0.5	21.83	0			0.85	0
		7	50.51	0	0.11	0.62	1.75	0.34	18.86	0.06	0.28	26.99	0.05			0.44	0
Reddish colored	a	1	46.12	0.16	1.27	12.81	28.45	0.08	0.11	0.01	3.65	1.47	0.38			5.46	0.03
		2	44.92	0.15	1.51	13.59	26.65	0.21	0.14	0.13	3.93	1.65	0.66			6.37	0.09
		3	44.8	0.29	0.71	16.33	25.22	0.18	0	0.11	3.15	1.32	0.34			7.46	0.08
		4	43.42	0.11	0.7	3.96	4.95	0.02	0	0	1.13	0.04	42.24	0.47		2.94	0.04
		5	45.11	0.26	1.5	13.71	27.64	0.07	0	0.08	4.06	1.19	0.38			6.01	0
	b	6	45.59	0.27	1.14	13.15	27.02	0.14	0.11	0.04	5.54	1.35	0.37			5.28	0
		7	47.53	0.13	0.74	7.68	37.21	0.02	0.05	0.06	2.53	0.59	0.13			3.27	0.06
Blackish colored	a	1	43.5	0.15	1.46	12.72	31.17	0.06	0	0.13	3.12	1.12	0.39			6.17	0
		2	50.23	0.01	0.01	0.04	49.52	0	0	0	0	0	0.07			0.12	0
		3	44.63	0.34	0.6	14.85	27.34	0.17	0	0.09	3.36	1.41	0.43			6.8	0
		4	44.98	0.18	1.51	14.78	27.29	0.08	0.01	0.08	3.45	1.25	0.25			6.13	0
	b	5	45.72	0.19	1.25	12.2	30.42	0	0.02	0.08	3.33	1.07	0.36			5.17	0.17
		6	45.23	0.1	1.94	12.5	27.94	0.07	0.03	0.06	3.71	1.7	0.27			6.33	0.12
		7	45.69	0.24	1.5	14.61	26.97	0.04	0	0	3.53	1.1	0.39			5.87	0.05

8.3.2 Femtosecond laser cleaning on pottery sherds

Laser cleaning uses a steady laser beam to irradiate ceramic pottery sherds to remove concretions and contaminants. The laser system's scanning speed, repetition rate, scanning area, and scanning direction were adjusted for cleaning efficiency and thermal damage. Irradiance thresholds I_L were obtained by dividing the pulse energy delivered on the target by the pulse duration of a specified unit area, while the pulse energy E_P was found by dividing the energy (P) released by the laser by the number of pulses delivered in one second, respectively (f). It is important to note that while the pulse duration is kept constant, the fluence and irradiance values are always proportional. To clean pottery sherds using lasers, the irradiance value of all three fs laser wavelengths is used to define 'ablation threshold', 'cleaning threshold', and 'damage threshold'. As the beam scan irradiation mode employed in this study, it is feasible to produce a homogeneous energy distribution along the scanning direction by varying the spacing between lines and dots, and vice versa.

The best cleaning rate in this study was obtained when scanning at 150 mms^{-1} . Cleaning depth in pottery sherd substrates is inversely linked to the scanning speed. Scanning at less than 150 mms^{-1} caused severe heat buildup and substrate degradation. The laser beam sweeps over the surface at a predefined distance between scan lines (i.e., 10 to $15 \mu\text{m}$) to cover the whole area, streamlining the same irradiation impact and cleaning quality. The larger overlapping leads to improved cleaning rate when the distance between successive scan lines is less than the laser spot diameter; when it is larger, discontinuous material cleaning tracks occur. When PPD 20 is set at the 200kHz resonating pulse frequency, the effective pulse repetition rate output is 10kHz, but the energy per pulse and peak power are fixed by the former and seem adequate to remove foreign materials without increasing pulse-to-pulse overlap and thus heat accumulation on the irradiated surface. As a result, contaminant removal rates increased with increasing number of laser surface scans. The pottery sherds were not wetted at any point throughout the laser irradiation process.

An appropriate cleaning strategy was determined by the irradiances that were present. Imprints on the sherd surfaces were caused mostly by the non-uniform energy distribution of the Gaussian beam during the earliest experiments of laser cleaning for small area treatments. Satisfactory cleaning was observed at material removal when the ablation irradiance value correctly identified. Ablation usually takes place when a plasma plume forms, with the associated shock waves. It is a complex mixture of phenomena with direct sublimation, some melting (not so much in the fs regime, unless there is a significant incubation component) and ejection of particles (sub nm size in the case of fs lasers, μm

size in the case of ns lasers) and liquid droplets (ns lasers). For these pottery sherd materials, the damage threshold is determined by the level of radiation at which physical and chemical changes may be observed under the optical microscope and SEM. The probable harm to the ceramic sherds' composition was given particular attention. Even while it was rather simple to figure out the damage thresholds for the various operating irradiance ranges, the good starting point for concretions removal (i.e., the cleaning threshold) was a lot more difficult. This may have resulted in some sections of the final surface being irradiated numerous times with the same parameters instead of just once to fine-tune and determine the satisfactory cleaning threshold values for each laser system. Thus, the numbers for cleaning and damage thresholds that have been established in this work are the result of several tests and observations. When the irradiated sherd surfaces were scraped clean, materials were liberated in various forms, including solid debris, vapors, and a growing cloud of plasma.

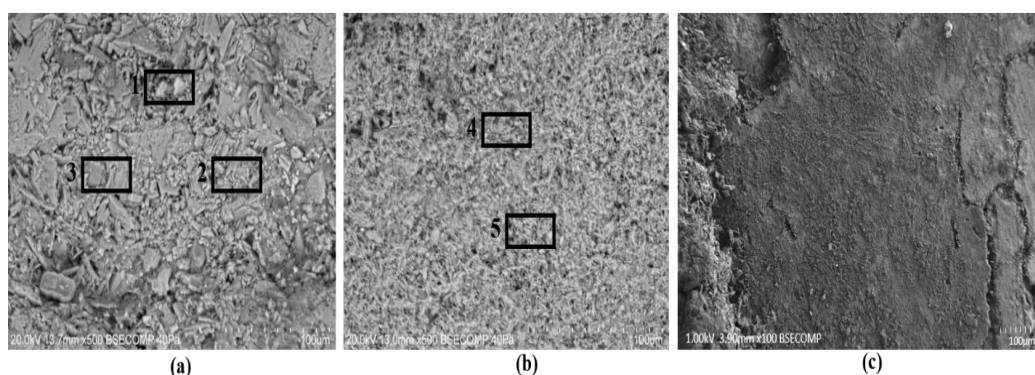


Fig. 8.5: Non-irradiated matrix concretions observed on representative micrographs obtained by SEM under different magnification: (a) corresponds to hard matrix concretions of APS-2, (b) corresponds to ash spots, and less concretions of APS-3, and (c) corresponds to the reddish surface of APS-2 without having any concretions. The summary of EDS analyses conducted in the designated locations has been shown below in Table 8.4.

In addition to providing information on the degree of refinement or cracks after laser treatment, as well as the morphology and chemistry of the final product, Scanning Electron Microscopy has been used to determine whether any modification occurs to the sample surface as a result of the laser treatment. Figure 8.5 shows representative micrographs obtained on the non-irradiated matrix concretions and contaminated layer before laser application, while Figures 8.6, 8.7 and 8.8 show micrographs taken with a SEM for each of the three ceramic sherd samples and subsequent laser cleaning.

Table 8.3: Parameters employed for the irradiation of pottery sherds using three different fs laser wavelengths. F_{pulse} denotes the laser fluence, I_{pulse} the irradiance, and P the set power level. Pulse energy E_P is calculated by dividing the power (J/s) over the resonant pulse frequency (200 kHz). For all experiments, the effective pulse repetition rate f_p was set at 10 kHz, employing a PPD integer value of 20 ($200/20 = 10$ kHz). The distance between two lines was set to 10 μm for both, Green and UV emission, and 15 μm for the n-IR emission. The beam scan speed was set to 150 mms^{-1} in cross line hatch mode (i.e., 0° and 90°) in all experiments. N_L presents the experiments numer.

Laser	Treated Region	P (W)	E_P (μJ)	F_{pulse} (J/cm^2)	I_{pulse} (TW/cm^2)	N_L	Cleaning Performance
fs n-IR (1030nm) 228 fs Laser	Fig. 8.6 (a _{n-IR})	6.0	30.0	0.38	1.67	25+275	Very little cleaning; not appreciable.
	Fig. 8.6 (b _{n-IR})	7.2	36.0	0.46	2.01	25+500	Cleaning efficiency is good, but cracks and drains are generated.
	Fig. 8.6 (c _{n-IR})	7.2	30.0	0.46	2.01	750	Increased cracks and drains size appeared.
fs Green (515nm) 249 fs Laser	Fig. 8.7 (a _G)	2.71	13.6	0.69	2.77	10	Cleaning efficiency is not much appreciable; ablation threshold.
	Fig. 8.7 (b _G)	3.78	18.9	0.96	3.86	10+10	Perfect cleaning; cleaning threshold for concretions.
	Fig. 8.7 (c _G)	4.31	21.6	1.10	4.40	10	Overcleaning; melting and fractures observed; damage threshold.
	Fig. 8.7 (d _{G1})	4.31	21.6	1.10	4.40	10	Overcleaning in the reddish area; melting is observed.
	Fig. 8.7 (d _{G2})	2.71	13.6	0.69	2.77	10	Good cleaning was observed in the reddish area.
fs UV (343nm) 238 fs Laser	Fig. 8.8 (a _{UV})	0.23	1.15	0.16	0.68	10	No cleaning, but melting was observed.
	Fig. 8.8 (b _{UV})	0.66	3.30	0.47	1.97	10	No cleaning; melting boosted due to the heat accumulation.
	Fig. 8.8 (c _{UV})	1.34	6.70	0.95	3.98	10	Entirely melted and damaged the surface.

Apparently, optimum laser cleaning appears to have been achieved on these ceramic materials by observing these pottery sherds at the same magnification; two different magnifications for each cleaned region on all the samples treated with all the three fs laser harmonics have been shown in Figures 8.6, 8.7 and 8.8.

8.3.2.1 Femtosecond n-IR laser cleaning on pottery sherds

A laser cleaning system with a fs n-IR laser may prevent damaging pottery sherds surface when irradiation intensities are as low as 1.67 TW/cm^2 (Table 8.3, Fig. 8.6a_{n-IR}); nevertheless, cleaning is not practicable at this threshold, only a limited amount of ablation is observed. The findings showed that irradiation at 2.01 TW/cm^2 damaged the substrate surface, causing fractures and drains to develop beyond the damage threshold (Table 8.3, Fig. 8.6b_{n-IR}). With n-IR radiation, the matrix concretions in the treated region were progressively cleaned away by what appeared to be a significant thermal accumulation, since the surrounding original layer was slightly yellowed as a result of heat buildup (Figure 8.6 c_{n-IR}). The laser beam interaction with the pottery sherds surface and the concretions causes this heat effect. Some of the laser light is reflected back and absorbed by the concretion layer during n-IR irradiation laser treatment, while the rest is transferred through it. There will be some reflection, absorption, and transmission of the incident radiation when it finally reaches the original surface. To develop a noticeable thermal effect, n-IR irradiation is significantly absorbed by the sherd surfaces, which usually have high absorption coefficients for this irradiation wavelength [131] [132].

Pottery sherd laser cleaning investigations used an irradiation threshold less than or comparable to 1.67 TW/cm^2 since it appears to have no negative impact on the material's surface. For best potential cleaning, the irradiation results were found to be insufficient after a series of experiments. By systematically increasing the cross-mode execution count while keeping the same parameters, the original surface appearance of the sherds was gradually exposed, but generations of cracks and drains were also evident. However, surface damage occurred beyond a threshold irradiance (Table 8.3 and Fig. 8.6 bn-IR) as the irradiance values increased. The cracks and drains were developed on the damaged surface in regions where the laser intensity was higher.

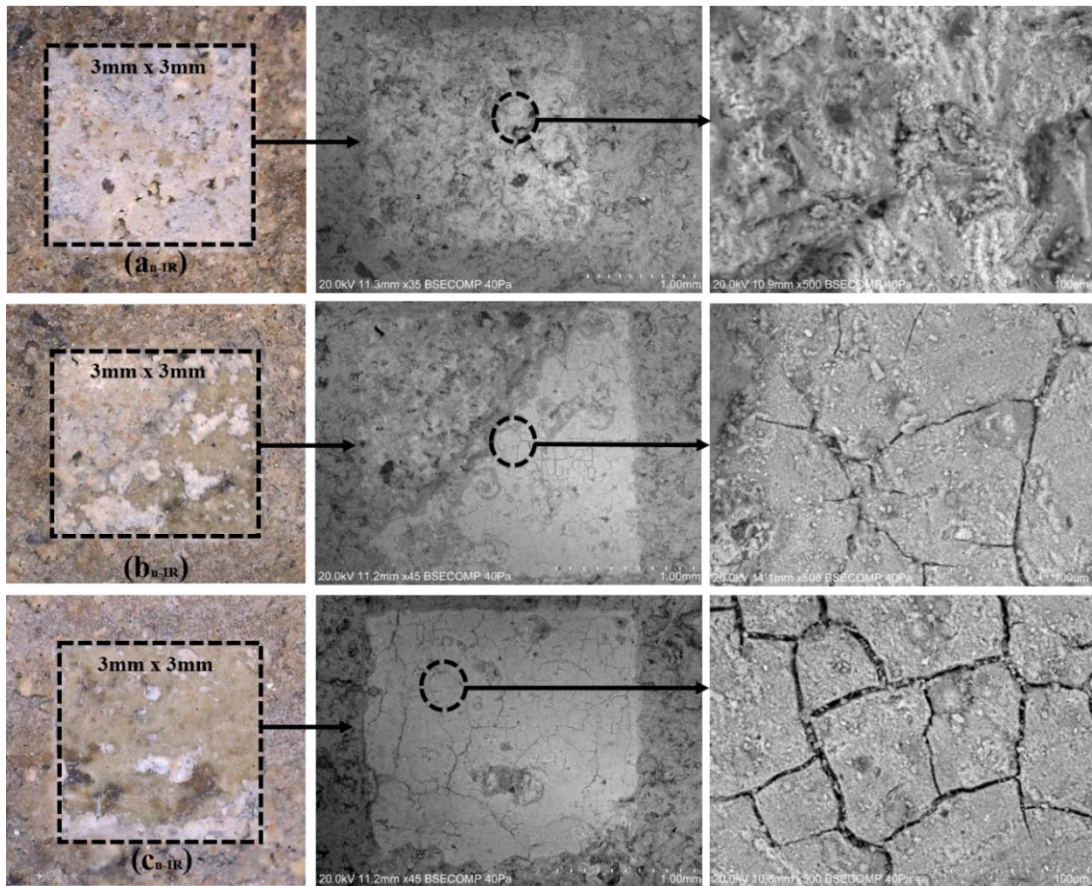


Fig. 8.6: Optical microscopy images obtained on the fs n-IR ‘laser treated’ sherd APS-1 surface in column 1 presents the concretion crusts on the sides as uncleaned, and SEM images of the same areas showed in column 2 and 3 with two different magnifications following the interested region subjected to this study.

Damaged areas were left with a thick concretion layer even at high irradiation values. If the irradiances were higher, 1030 nm irradiation was able to penetrate and damage the surface via the concretion matrix, as predicted, as seen in this experiment. Based on the results of this work, a cleaning threshold for this specific concretion problem was at or about 1.67 TW/cm^2 for beam scanning utilizing a 228fs n-IR ultrafast pulsed laser, but ended with the development of cracks. The non-self-limiting character of this process at this n-IR wavelength is another finding that may be drawn from optical microscopic investigation. As can be seen in Table 8.3, the results of laser cleaning are presented with the cleaning and damage threshold values, and accompanying SEM micrographs in Fig. 8.6 (a, b, and c).

8.3.2.2 Femtosecond Green laser cleaning on pottery sherds

Results from the fs visible Green laser cleaning showed that irradiation levels lower than $\sim 4.10 \text{ TW/cm}^2$ prevented damage to pottery sherds, while $\sim 3.86 \text{ TW/cm}^2$ provided the optimum cleaning (Table 8.3 and Fig. 8.7a_G). This study also found that the substrate surface was damaged at an irradiance level of 4.40 TW/cm^2 (Table 8.3 and Fig. 8.7c_G). A safety buffer was taken into consideration, and irradiation values lower than 4.10 TW/cm^2 were selected for future cleaning studies. A number of irradiation experiments have shown, however, that while cleaning with the same threshold (i.e., $\sim 3.86 \text{ TW/cm}^2$), performance was boosted for removing reddish-colored contaminated sherds' surfaces; thus, the optimum cleaning has been fixed at $\sim 2.77 \text{ TW/cm}^2$ (Table 8.3, Fig. 8.7d_{G2}). Evidence for melting and cracks became apparent, however, with an increase in concretion cleaning scans. As specified in Table 8.3, both the incubation level and scanning speed/repetition rate ratio were kept constant throughout all of these experiments.

The cleaning rate was increased when green irradiation was used instead of n-IR irradiation; in spite of the fact that surface damage occurred at lower irradiances under n-IR irradiation (Table 8.3). In this specific case, it was possible to completely remove the matrix concretions layer in the visible Green irradiated area, without causing any harm to the surface of the original sherds during the cleaning procedure. Quite a significant achievement. It has been observed that the pottery surface has a lower absorption coefficient for visible Green radiation than for n-IR; therefore, the irradiation transferred to the original surface over the concretion layer is absorbed less strongly by the surface and transmitted through it instead of being absorbed. The removal of concretions is not as localized as it was in the prior study of n-IR irradiation, which implies that the majority of the radiation that passes through the concretions is reflected back when it reaches the interaction between the concretions and the surface of the pottery surface substrate. As a result, the visible Green laser light is more effectively utilized, and the concretion removal rate increases. SEM-EDX was also used to investigate the interaction between visible (515 nm) radiation and the original surface (Fig. 8.7, Table 8.4). It is very much practicable that adjusting the number of scans or switching to burst pulse mode, considering the varied laser characteristics, will prevent any laser-induced damage to the original pottery surface.

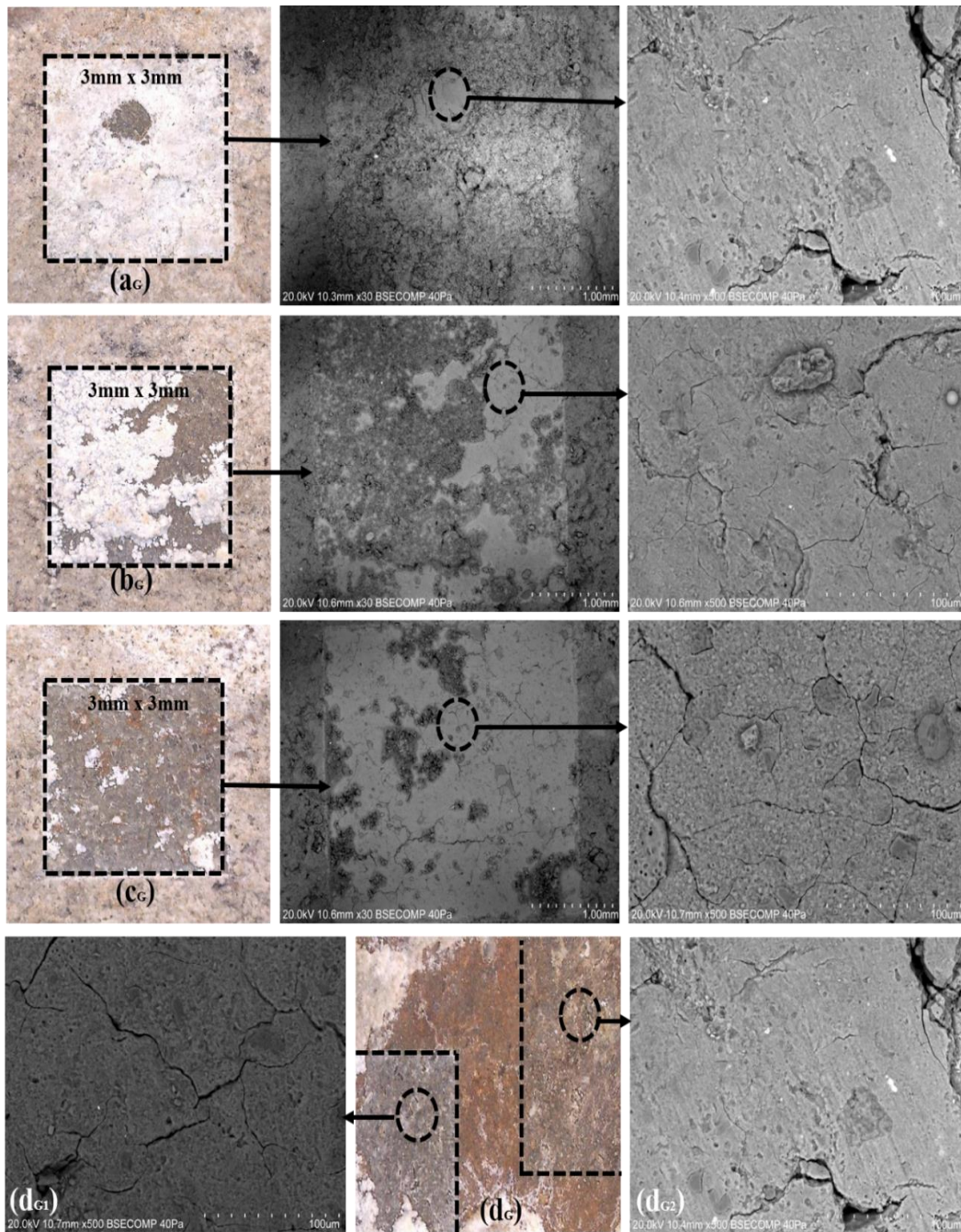


Fig. 8.7: Optical micrographs obtained on the fs Green ‘laser treated’ sherd APS-2 surface present the concretion crusts (Fig. a_G, b_G and c_G) and reddish contaminated surface (d_G) on the sides of the square area as uncleaned, and corresponding SEM images of the same areas shown adjacent with different magnifications.

8.3.2.3 Femtosecond UV laser cleaning on pottery sherds

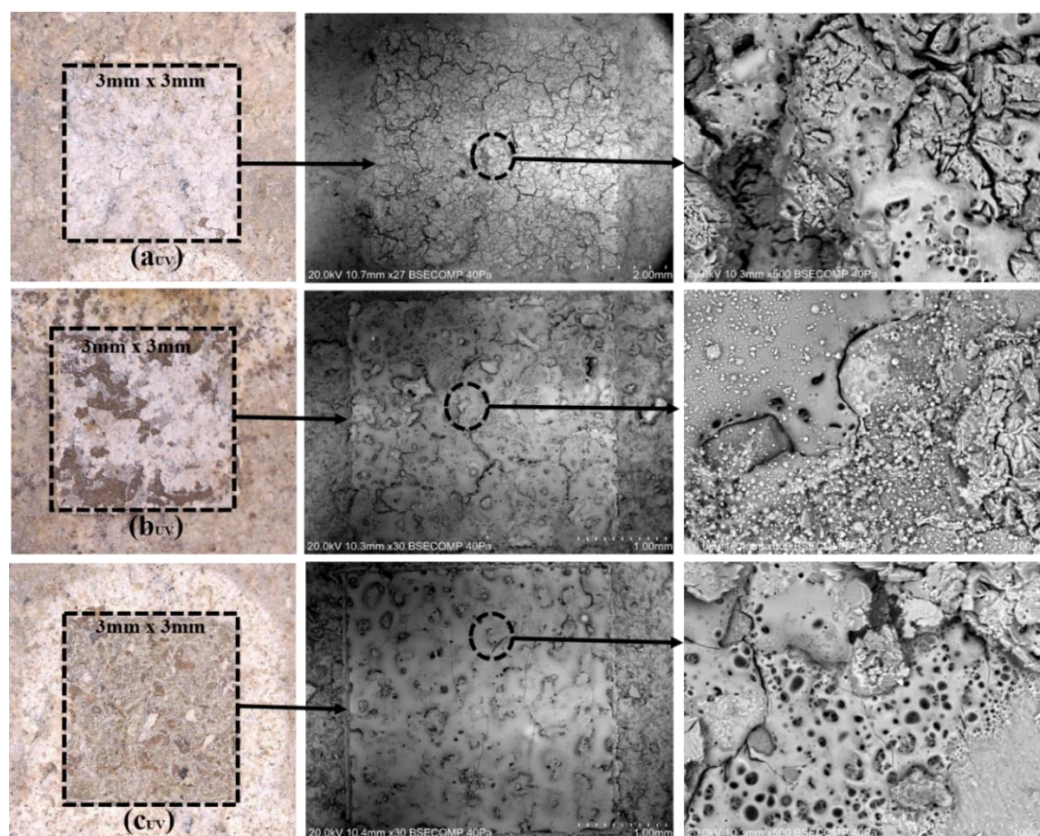


Fig. 8.8: Optical micrographs obtained on the fs UV ‘laser treated’ pottery sherd APS-2 surface. The 1st column (left) presents the concretion crusts on the sides of the square area as uncleaned, and SEM images of the same areas shown in the 2nd and 3rd columns (center and right, respectively) with different magnifications.

Damage on the pottery sherds surface was entirely uncontrollable when cleaning with the lowest possible ablation threshold, with irradiation levels as low as $\sim 0.68 \text{ TW/cm}^2$, according to cleaning attempts using the 238 fs UV laser emission (Table 8.3, Fig. 8.8a_G). This finding also demonstrated that exposing the substrate to irradiation of 0.68 TW/cm^2 damaged it severely and apparently induced melting to the substrate's surface. Matrix concretions cleaning was carried out at irradiance levels below 0.68 TW/cm^2 to be safe, but no ablation was observed. The cleaning efficiency was shown to be completely insufficient for removing the concretion crusts; however, following a number of irradiation studies with a higher number of scans (i.e., with 500) while maintaining the same parameters resulted in melting and cracking, as well as in color shifts (Table 8.3, Fig. 8.8).

UV irradiation causes localized and extremely distinctive damage to emerge on the material's surface. This damage appears to be connected with localized, thin layer surface melting, as opposed to the damage related to irradiation of the surface at 515 and 1030 nm, which appears to be associated with the formation of a deeper molten layers.

8.3.3 SEM-EDX and XRD analysis of the laser cleaning outcomes

The mineral phases in the ceramic sherd samples were found to be constituted predominantly of Si, O, Ca, Fe, Al, K, and rarely Mg and Ti. In this study, these SEM-EDX observations were supported by the XRD results (Fig. 8.9), which demonstrated the presence of quartz, gypsum, $\text{CaSO}_4 \cdot 0.5\text{H}_2\text{O}$ in all cleaned areas (Fig. 8.7 a, b, c and d) of sample APS-2 and other minerals, such as mullite (Fig. 8.7 a, b, and c), illite (Fig. 8.7 d_{G2}) and calcium feldspar (Fig. 8.7 c, d_{G1} and d_{G2}). Aside from that, the EDS analysis indicated a significant concentration of Ca and Al in all of the samples tested. Carbonates, oxides, and silicates, among other compounds, can be found in the presence of these elements. Additionally, S and P were found in trace amounts, indicating that those elements were already in the raw material at the time of pottery manufacture. In this experimental situation, it is possible that S is connected with gypsum, which would support the identification of gypsum by XRD. Finally, the surface of the pottery sherds was found to have a laminar structure due to the presence of long and flat mineral phases, most likely originating from the mica group. It was also observed that the elements Ca and Mg appeared before and after laser cleaning to be associated to these samples.

A detailed EDS study of the elemental composition of the actual region of the well-cleaned pottery sherd surface, which contained hard concretions and reddish colored contaminants, is shown in Table 8.4. Following that, it shows the difference between the untreated original and the laser treated surfaces, as evidenced by the concretions and contaminations present, as well as if there is any damage took place after laser cleaning is evident. Through optical microscopy and visible inspection, it was observed that the ceramic surface had not been discolored or damaged as a result of the fs visible Green laser treatment. When the proper cleaning conditions were followed and the fs Green laser was used (Table 8.3), the results demonstrated that laser cleaning had no detrimental effect on the elemental composition of the pottery sherd. Using EDS measurements on all of the treated samples, it was possible to determine the amount of laser-induced alteration in the weight percentage of the ceramic minerals.

Table 8.4: SEM-EDS elemental analysis of the APS-2 sherd, before and after laser irradiation, with elemental composition provided in weight percentage (%Wt)

EDS analysis of elemental composition of ceramic samples 'before and after laser cleaning' in weight percentage														
Region	Area	Label	O	Na	Mg	Al	Si	P	S	Cl	K	Ca	Ti	Fe
Original surface with concretions	Matrix concretions (uncleaned); Fig. 8.5 (a)	1	44.5	0	0.6	3.9	14.6	1	8.1	0.2	3.4	19.5	1.9	2.3
		2	44.8	0.1	0.7	3.8	14.8	1	8.1	0	1.6	22.7	0	2.5
		3	45.7	0.2	0.9	4.7	15.9	1	5.2	0	2.4	20.5	0	3.7
Cleaning threshold	Laser cleaned area; Fig. 8.7 (a _G)	1	43.9	0.5	1.1	8.5	24.5	0.2	0.4	0.1	4.9	11	0	5
		2	42.7	0.4	1	5.7	25.2	0.1	2.8	0.1	3.4	14.6	0	4.1
	Laser cleaned area; Fig. 8.7 (b _G)	1	46.08	0.2	0.8	5.4	30.7	0	1.6	0	2.2	8.7	0	3.8
Required selective cleaning on some areas	Semi-cleaned area; Fig. 8.7 (a _G)	2	36.5	0.1	0.4	1.2	7.6	0.7	16.3	0.1	1.1	36.5	0	0.8
	Semi-cleaned area; Fig. 8.7 (b _G)	1	35.3	0	0.3	1.2	11.6	0.5	12	0	2	35.9	0	1.1
Damage threshold	Laser over cleaned area; Fig. 8.7 (c _G)	1	40.3	0.5	1	9.1	23.5	0.4	0.8	0.1	6.8	11.1	0	6.4
		2	42.4	0.3	1.4	9.2	26.1	0.4	1.1	0	5.7	6.3	0	7.1
Reddish colored surface	Reddish colored (uncleaned);	1	46.5	0	0.8	3.3	17.4	0.6	1.5	0.3	1.7	24	2	2
		2	44	0.1	0.6	2.4	17.3	0.3	2.8	0	2	28.9	0	1.5
Cleaning threshold	Reddish area; laser cleaned; Fig. 8.7 (d _{G2})	3	41.1	0.4	0.8	6.5	26	0.3	2.5	0.2	5.2	12.1	0	5
Damage threshold	Reddish area; laser over cleaned; Fig. 8.7 (d _{G1})	2	42.3	0.1	0.9	7	24.1	0.1	5	0	3.9	12.4	0.1	4.2

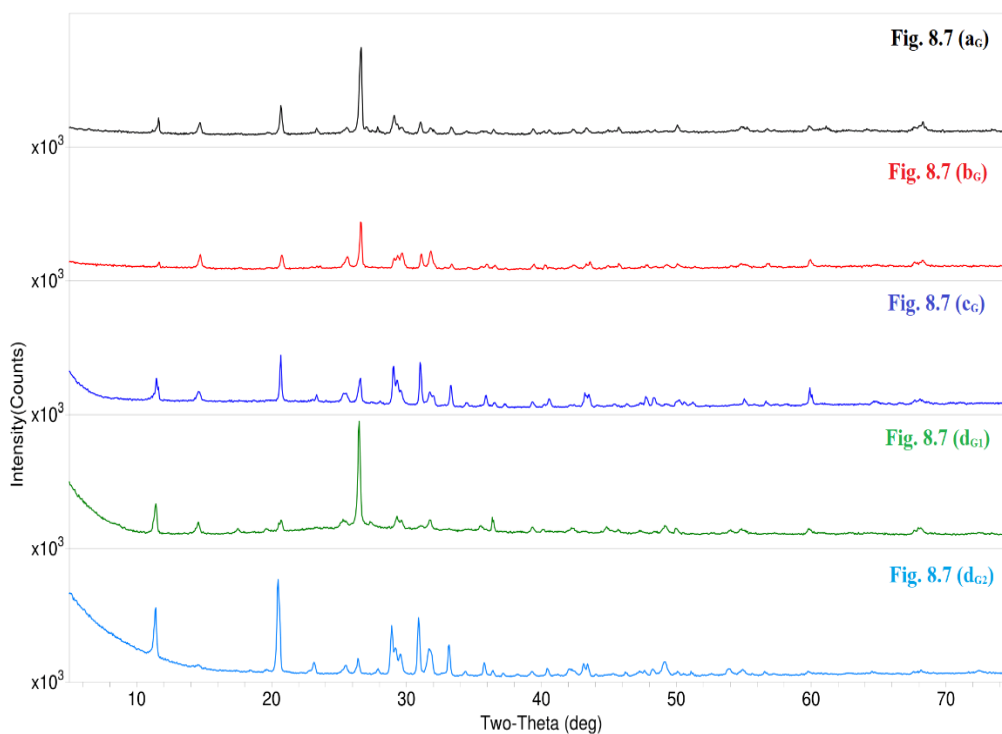


Fig. 8.9: The XRD patterns of the fs visible green laser treated APS-2 ceramic surface, associated with Fig. 8.7. For the determination of phases, the JCPDS-International Center for Diffraction Data-2000 database was used.

A substantial amount of fluctuation in the composition of archaeologically significant pottery sherds may be detected in the weight percentage ratios of different minerals, which indicates a rather stable ceramic composition. Characteristic concretions deposited on the surface include feldspar, iron silicates, and carbonate minerals. The pottery sherds' temper is dominated by feldspars and quartz, which are resistant to chemical alteration and mechanical attrition. FESEM analysis confirmed the presence of Al, Ti-rich mineral inclusions, and ilmenite (FeTiO_3) crystals. Specific minerals, like Ti, which resist weathering and is unique to particular types of magmatic or metamorphic rocks, can be used to pinpoint the origin of ceramics [352][364][365]. Following the fs visible Green laser irradiation, the amounts of Ca, S, and P decrease, while the amounts of Si, Al, Mg, K and Fe increase (Table 8.4). This is compatible with the anticipated cleaning of aluminosilicates and iron-rich compounds from the burial soil. Silicates, feldspars, and sulphates, among other distinctive minerals, may be related to the burial environment, since these elements are often found as soil components in the *Sierra de Atapuerca* region [242].

8.4 Conclusions

Three emission wavelengths from a fs laser, corresponding to its first, second and third harmonics at 1030, 515 and 343 nm were used to irradiate hard matrix concretions and contaminated pottery sherds surface. Physicochemical compositional alterations, mechanical changes, color variations, etc., and other effects were assessed, both as-received and laser irradiated samples, enabled to conclude that laser irradiation of the n-IR and the visible green wavelengths are capable of cleaning concretions. But the visible wavelength laser has been shown to be successful and efficient, as shown by the fact that n-IR laser irradiation may produce cracking and melting even at the lowest ablation threshold values, which is not ideal. When using beam scan mode, the cleaning results of an n-IR fs laser were determined to be inappropriate and impracticable; the heat accumulation effects led to thermomechanical cracking, and substantial color changes occurred. Drains and fissures began to appear on the original outermost surface as the laser penetrated much into the surface without removing all of the matrix concretions on the potsherds surface. The fs UV laser irradiation, on the other hand, was demonstrated to be entirely damaging at whatever threshold value investigated. In comparison to the n-IR laser, it heated up far more quickly, resulting in a much worse quality of outcomes.

In order to prevent excessive heat accumulation, fs visible Green beam scan irradiation appeared to be significantly better when laser-induced damage, cracks, drainage, physicochemical changes etc. were taken into account. The irradiation has been found as much more localized and superficial interaction with the sherd surface, making it a very efficient cleaning method. This investigation has yielded an outstanding performance of fs visible Green laser cleaning concretion crusts from potsherds, which may be utilized as a foundation for future research to expand our understanding of the laser's interaction with a different sort of ceramic artifacts.

CHAPTER: 9

fs VISIBLE LASER FOR
IRON OBJECT CLEANING

CHAPTER NINE

fs VISIBLE LASER FOR IRON OBJECT CLEANING

***Summary:** Corroded iron artifacts are frequently fragile and flaky. Surprisingly, even among the same type of corroded iron objects, the chemical and physical properties can vary dramatically. Depending on the physicochemical properties of an object, laser cleaning efficacy may vary significantly [135]. Using low-energy pulses and irradiating iron artifacts with varied wavelengths and pulse durations allowed for the effective removal of corrosion rusts; nevertheless, darkening phenomena occurred at nearly all wavelengths and pulse durations [63][139]. The change of yellowish-brown goethite, the primary component of iron corrosion, into black magnetite, led to darkening [198]. On the other hand, corrosion removal has been observed as extremely slow and impractical, according to the journal published on iron object cleaning [199]. Despite the fact that a layer of magnetite on the surface of iron objects may be beneficial for their long-term preservation [366][367][200], this study aimed to determine if an ultrafast fs visible green laser could clean the corroded surface of iron artifacts without causing discoloration on the original outer surface. As there was no record of applying fs green laser emission at 515nm, the outcomes apparently contributed to the state of the art of the laser intervention of iron artifacts. This study demonstrates the efficacy of this fs green laser technology in the effective conservation of artifacts by establishing its capacity to remove corrosion crusts with nanoscale accuracy, while maintaining control over ablation depth and protecting the underlayers.*

9.1 Background of the study

One of the most essential things that our civilization does is to make sure that its cultural artifacts are preserved for future generations. The knowledge that may be gleaned from such artifacts is an invaluable key to comprehend important events from our past. The process of conservation involves applying a wide variety of strategies. The stabilization of

the CH artifacts and the revelation of previously concealed characteristics on the surface of the artifact in question is accomplished via the cleaning process, which is one of the most important steps in conservation. It is of the utmost importance to select appropriate cleaning strategies and procedures in order to prevent damaging and discoloring of artifacts, as they are frequently fragile and cannot be replaced. Currently, ongoing research is being carried out to develop new or improved cleaning methodologies. In the realm of conservation work, one of these innovative methods involves laser cleaning, which has demonstrated promising success as a tool across a wide variety of artifact categories.

To eliminate contaminants that cannot be removed by typical cleaning methods (mechanically or chemically) such as deep-seated corrosion particles, laser cleaning is a chemical free, contactless technology that may be conveniently applied [368]. Some cleaning objectives, such as removing corrosion crusts from iron objects or cleaning up contaminants that are regularly necessary for the conservation of artwork, can only be completed with laser-based cleaning intervention [135][139][200]. Ancient iron objects often deteriorate due to chemical modification rather than physical depreciation [367]. Weathering and deterioration are apparent signs of corrosion, which happens when various ambient chemicals mix with iron objects to form more stable compounds [19]. The artifact's original iron components are destroyed and replaced by corrosion products during redox processes. There is a strong correlation between corrosion products and iron's source material [140].

For archaeological purposes, preservation of iron artifacts is extremely critical. One of the most critical steps in the restoration of iron artifacts is thorough cleaning as a necessary component of the stabilizing procedure [306]. Cleaning an object entirely removes all traces of contaminants, preventing any further damage to the object. In order to ensure the long-term preservation of an artifact, cleaning techniques are the most difficult to regulate. An iron artifact's stability may be maintained by eliminating as many corrosion sources as possible.

9 1.1 Iron objects conservation

An inhomogeneously formed thick crust layer containing burial deposits from the ground and iron corrosion products, such as the most common goethite and magnetite, typically protects ancient iron objects when they are buried. They have likely evolved during the course of the artifacts' burial history [19]. In order to reveal the original artifact's surface, conservators are attempting to remove the bulk of these contaminants. The majority of the

laser irradiation pulse energy is absorbed by the plasma formed during laser cleaning interventions (when the repetition rate is high), reducing the cleaning efficiency. As a result, vigilance is required in order to avoid concerns with the rust's surface dryness and color. Additionally, any iron oxide that accumulates might melt and cause permanent damage. A detailed investigation of the implemented irradiance values and the parameter settings used to clean specific iron objects might help avoid such problems. After mastering the application of different laser parameters, it is feasible to handle archaeological iron objects with a higher inherent value.

Some case studies have shown that using longer wavelength lasers to clean iron objects to remove corrosion products only partially removes the corrosion layers [199]. On the other hand, almost all studies investigating the ns laser-based treatments on ancient iron artifacts found that the iron surface darkened after treatment. Goethite (FeOOH), a yellow-brownish iron corrosion product, was the predominant source of darkening at all wavelengths and pulse durations reported in the literature [63][139][136]. Some laser experiments have found removal of rust or corrosion to be a time-consuming and impractical task. Magnetite (i.e., darkening) has been usually added to the surface of iron objects in order to help maintain them for a long term without suffering from corrosion, even if darkening has a substantial influence on the aesthetic appearance of the laser-cleaned iron objects [135][19][200]. Magnetite protects the underlying iron from further environmental erosion as a fairly stable oxide [137].

9.1.2 Objectives of the study

The cleaning technique is affected by the surface's structure, color, and porosity. The absorptivity of a surface can be affected, for example, by its roughness. Rough surfaces are more efficient in absorbing energy than smooth ones. Additionally, the operating parameters settings must be adjusted if the thickness of a deposited layer that has to be cleaned varies. A variety of factors may influence the results of laser cleaning, and even the same laser may provide different results depending on the artifact it is employed on. The physicochemical evaluation of the iron materials to be treated is critical when selecting a laser for surface cleaning, avoiding any future darkening on the surface prior to the conservation treatment.

The objective of this investigation is to examine if an ultrafast fs laser emitting in the green, visible part of the spectrum, can clean the corroded surface of iron artifacts without altering the original color of the surface. In addition, an attempt to find the effectiveness of this type

of laser for cleaning this sort of artifacts, while preserving control over ablation depth and conserving the underlayers of the substrate surface.

9.2 Material and method

9.2.1 Iron object

Archaeological excavations at the *Portalón Cueva Mayor* site in *Sierra de Atapuerca* (Spain), have unearthed one piece of iron object of an indeterminate handle of a contemporary tool, referred to as ATP-19 no. 221. It is seemingly 40-50 years old, most probably grounded up as the leftover of former excavators who worked there at this archaeological site. The reference level for excavation of this iron object is: R. Perf. Norte, Sector III (collected from northern profile, Sector III). As this artifact does not have archaeological significance but has been preserved for many years, in order to investigate the different cleaning methodologies, we were allowed to cut it into two pieces to study the different laser irradiations to find the best possible cleaning without any darkening upon controlled parameter settings.



Fig. 9.1: Top surface view photographs corresponding to two pieces of the unearthed iron object found at the *Portalón Cueva Mayor* site in *Sierra de Atapuerca* (Spain).

The surface of the iron object was covered irregularly with brownish thick corrosion crusts. During excavation, the major atmospheric soil dust was cleaned by employing soft brushes and a mechanical cleaning method. Figure 9.1 shows photographs of the topside perspectives of two pieces of the iron object. The particular goal of this study comprises laser intervention in chosen places to clean the dark rich corrosion crust in order to expose the original surface, while avoiding the development of darkening phenomena on the surface caused mostly by heat accumulation or chemical alterations.

9.2.2 Laser irradiation parameters applied to iron object

Controlled cleaning parameters utilizing a 515 nm wavelength ultrafast visible Green laser have been evaluated in a number of investigations. Table 9.1 summarizes the most important emission parameters. Wavelength (λ), pulse duration (fs), pulse repetition rate (f_p), and selected power (P) are the most critical. The laser beam's energy distribution follows a circular Gaussian mode as described in a previous chapter of this thesis. Beam scanning techniques were utilized in all experiments to clean the corroded surface and to investigate cleaning effectiveness while also analyzing the extent of damage to the original substrate surface.

Table 9.1: Characteristic emission of the fs green laser employed for the present study. Values are given for the nominal power (P_{\max}), emission wavelength (λ), pulse width (τ_p), pulse repetition rate (f_p) and beam waist (D_b) by applying the $1/e^2$ criterion with a Gaussian beam distribution.

Laser type	P_{\max} (W)	λ (nm)	τ_p	f_p (kHz)	D_b (μm)
fs visible	20	515 ± 3 nm	249 fs	200 -1000	50

9.3 Results and Discussion

9.3.1 Corrosion crusts characterization by SEM-EDX

A sub-micron-thick layer of corrosion crusts has appeared on the surface of the sample following the burial period. According to EDX examination (Table 9.3: left side) of an inhomogeneous section of the substrate, the presence of Fe found in the less corroded areas (Fig. 9.2b), as well as the presence of other elements including carbon and oxygen (Fig. 9.2a), is typical for exposed iron surfaces. A mineralization process would explain why Fe is found in varying concentrations in regions with thick and thin corroded crusts. Furthermore, the presence of Al and Si in every region indicates that the object has been in touch with clay. This is consistent with the fact that corrosion appears to be limited to the uppermost layers (several μm) of the iron object, as measured by this analysis. When an object is buried for a lengthy time, mechanical or chemical deterioration of its surface allows soil compounds to interact with it to observable depths, resulting, for the case of Fe, in brownish and greyish stains on its outermost layer (Fig. 9.1). The original iron components of the artifact are destroyed when corrosive activities are carried out, and the

resulting corrosion crusts take their place (Table 9.3 - left side). There is a strong connection between corrosion products and the substance from which iron is derived.

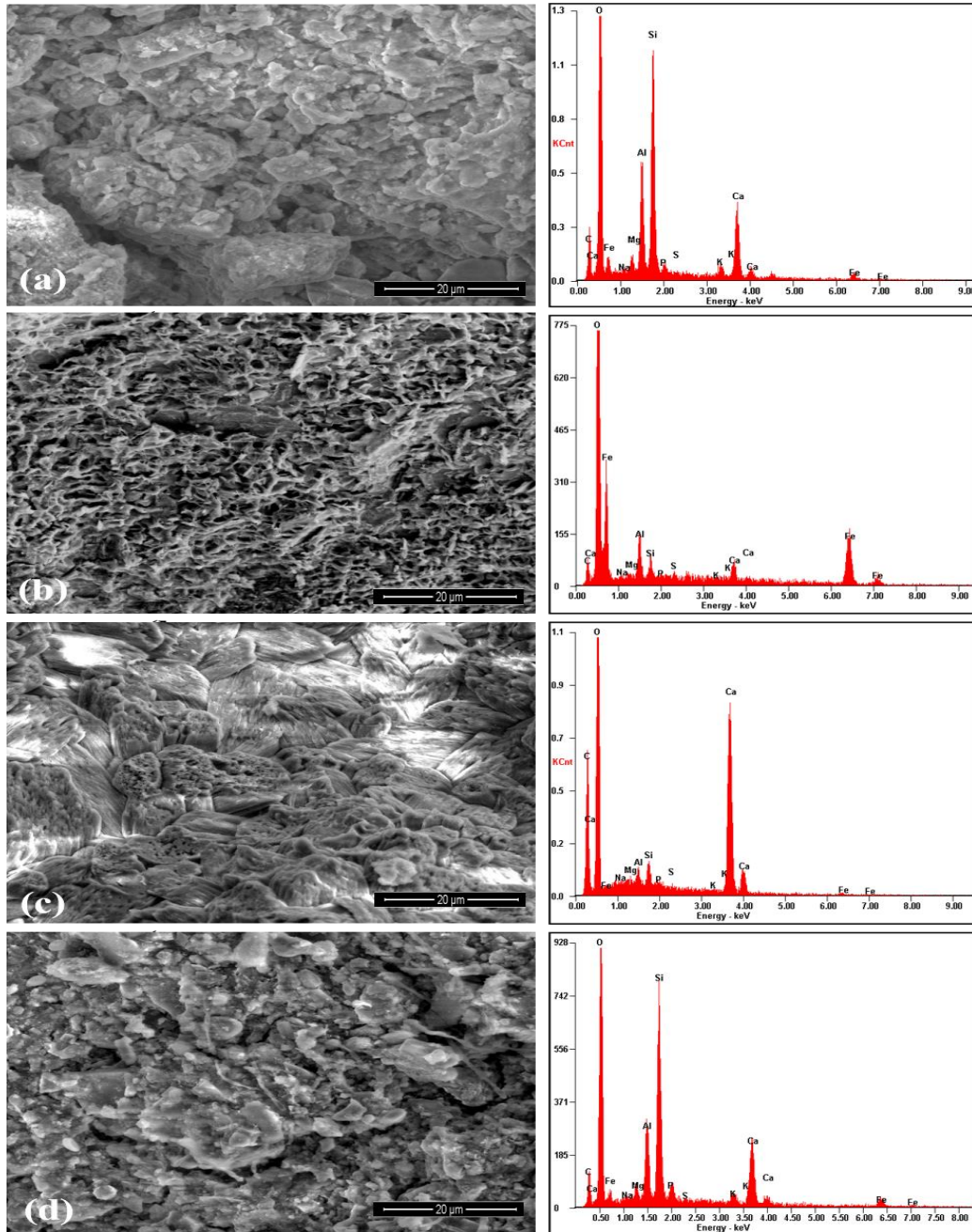


Fig. 9.2: SEM micrographs of corroded iron object (left) and corresponding EDX analysis spectra (right).

9.3.2 Laser cleaning for iron object

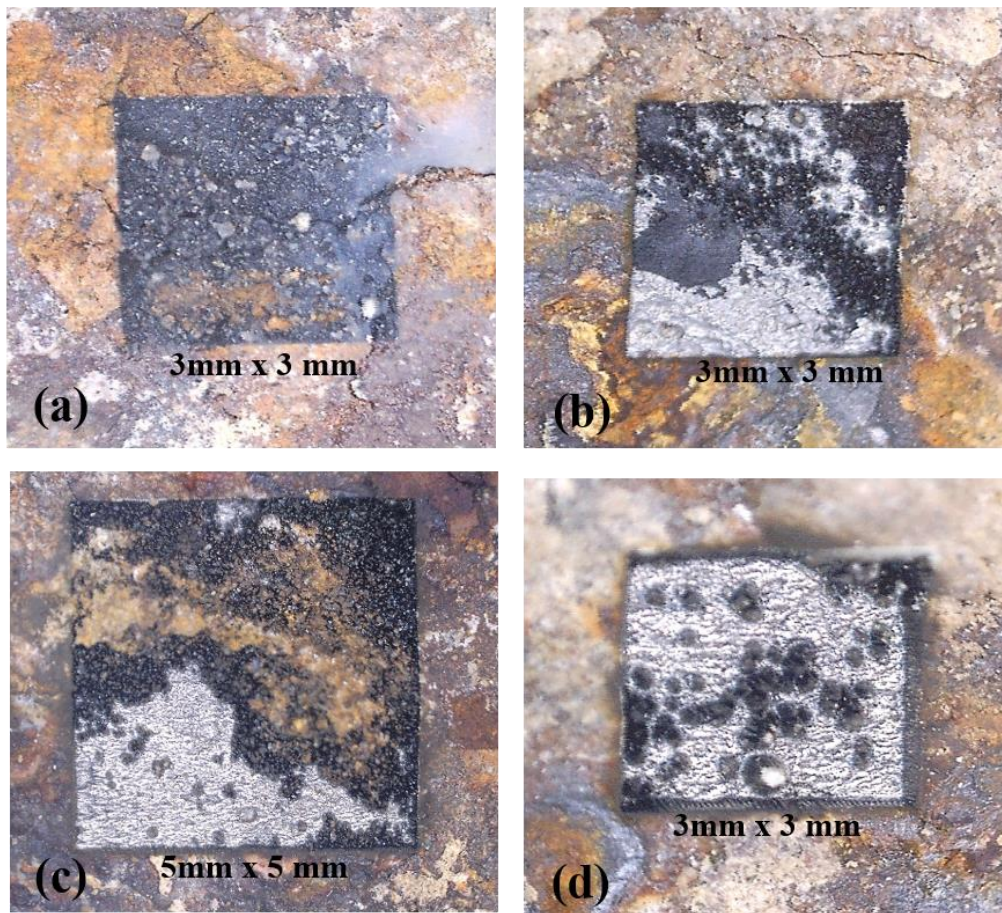


Fig. 9.3: Optical photograph of corroded iron object cleaned by fs visible laser: ‘a’ presents the darkening phenomena when the threshold cleaning values are applied for 50 scans, ‘b and c’ correspond to the exposed original surface after 100 and 250 scans, respectively, following the thickness of the corrosion crusts, and ‘d’ corresponds to the damage threshold associated to an increased number of scans (i.e., 500), where evidence for melting appears.

The mid-levels of radiation intensity (i.e., 50% of the maximum power of the employed laser technology) were utilized during fs visible laser cleaning, and corrosion rust removal was accomplished through the process of evaporation. In this scenario, the heat effect on the substrate is relatively minimal. There are many different ways to tweak the laser output parameters with this laser apparatus, thus a convenient set of parameters has been selected to effectively remove the projected depth of crusts following a series of laser tests.

Increasing the number of treatments after starting with the cleaning threshold values promotes the darkening phenomena. (Fig. 9.3a and Table 9.2). Darkening has been found to be caused most probably by the transformation of the main component in iron corrosion, yellowish-brownish goethite (FeOOH) to hard black magnetite (Fe₃O₄) [199][63][139].

Table 9.2: Experimental parameter data used for investigating laser cleaning on iron objects reported in this work. The beam diameter for the 249 fs visible green laser was 50 μm, and the distance between two consecutive lines was fixed at 20 μm. N_L presents the treatments number.

P _{max} (W)	Effecti -ve f _p (kHz)	Pulse Energy E _p (μJ)	F _L (J/cm ²)	I _L (TW/cm ²)	Speed (mm/s)	N _L	Observations
3.78	20	18.90	0.96	3.86	400	50	Good cleaning threshold for cleaning corrosion crusts, no damage, darkening phenomena observed (Fig. 9.3: a)
3.78	20	18.90	0.96	3.86	400	100	With a good cleaning, the original surface started to expose (Fig. 9.3: b)
3.78	20	18.90	0.96	3.86	400	250	With a good cleaning, the original surface started to expose (Fig. 9.3: c)
3.78	20	18.90	0.96	3.86	400	500	Melting appeared due to the application of a higher number of treatments number (Fig. 9.3: d)

It has been demonstrated that irradiation with the cleaning threshold values and increasing the number of laser scans both contribute to the darkening process. This phenomenon carried on and displayed a surface that was entirely black until it reached the original surface. In this particular instance, we have also seen that the pace at which corrosion was being removed was rather sluggish. After a significant number of treatments, the original surface began to become visible; further applications at a lower intensity coupled with an increase in the total number of scans assisted in gradually revealing the original surface (Fig. 9.3b and c; Table 9.2) following the thickness of the corrosion crusts. It has been discovered that it is a good idea to lower the intensity as soon as the original surface starts to appear. This helps prevent the accumulation of more heat and seemingly no chemical changes of the surface occur; on the other hand, more heat accumulations might lead to melting and surface alterations (Fig. 9.3d; Table 9.2).

9.3.3 Laser cleaned surface characterization by SEM-EDX

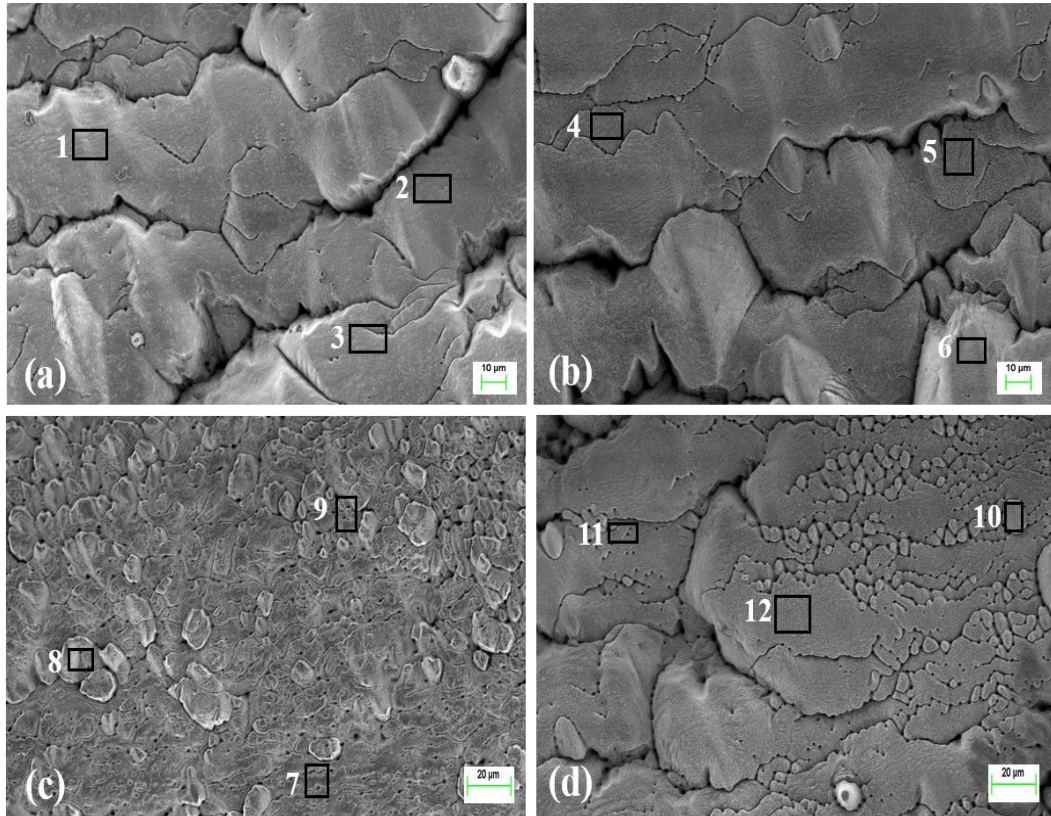


Fig. 9.4: SEM micrographs of cleaned iron object; “a and b” correspond to the samples irradiated with 250 scans at irradiance values of 3.86 TW/cm^2 , and “c and d” correspond to a partially cleaned surface with the same irradiance value, but only 50 and 100 scans, respectively.

During laser cleaning, except for the removal of the corroded layer, the substrate could also be affected by the irradiation of the laser under a certain condition. Thus, the exposed original surface of the cleaned iron object was investigated after laser cleaning by utilizing SEM-EDX (Fig. 9.4). When the laser treated with the irradiance threshold cleaning values of 3.86 TW/cm^2 and the number of scans reached 250, an original surface layer was exposed and the effect of the laser irradiation could be observed in Fig. 9.4 a and b (Table 9.3 - right side: spectrum level 1-3 for Fig. 9.4a, and 4-6 for 9.4b); apparently, no damage has been observed.

Table 9.3: The EDS analysis of the elemental composition on the iron object; the original surface before laser cleaning associated with the Fig. 9.2 (left side table) and the surface after laser cleaning associated with Fig. 9.4 (right side table).

Element	Fig. 9.2a	Fig. 9.2b	Fig. 9.2c	Fig. 9.2d	Spectrum Label	Element	
						O	Fe
CK	14.47	9.1	19.39	12.04	1	3.5	96.5
OK	50.89	58.53	56.7	51.4	2	2.77	97.23
FeL	3.25	21.87	0.41	2.43	3	3.34	96.66
NaK	0.08	0.35	0.12	0.06	4	2.23	97.77
MgK	0.78	0.33	0.12	0.72	5	3.02	96.98
AlK	5.75	3.77	0.58	5.05	6	4.57	95.43
SiK	13.54	1.81	1.21	15.06	7	27.22	72.78
PK	0.59	0.11	0.23	1.41	8	27.38	72.62
SK	0	0.31	0	0.09	9	27.49	72.51
KK	1.4	0.3	0.15	1.34	10	20.42	79.58
CaK	9.24	3.51	21.08	10.4	11	21.58	78.42
					12	18.06	81.94

On the other hand, when the number of scans applied reached 50 and 100 (Fig 9.4 c, Table 9.3 - right side: spectrum level 7-9; Fig 9.4 c, Table 9.3 - right side: spectrum level 10-12, respectively) with the same irradiance value, the effect of the laser irradiation found was not enough to expose the original surface. Hence the Fe and O content is also consistent with a larger difference (Table 9.3 – right side: spectrum level 7-14) when comparing with Fig 9.4 a and b (Table 9.3 - right side: spectrum level 1-6). Moreover, comparison of the left and right-side elemental analyses of Table 9.3 also establishes a clear difference between the original and the laser irradiated areas. Elemental analysis of the exposed, laser cleaned layer suggests that the fs visible laser is adequate for effective iron object cleaning.

9.4 Conclusions

This work explored the interaction of a 249 fs ultrashort pulsed visible Green laser, with emission at 515 nm, with the corrosion crust layers present in an iron object sample which has undergone severe weathering throughout last 40-50 years. The laser was operated in beam scan mode, and laser parameters which avoid damaging the surface of the iron object sample were identified. A laser irradiance of 3.86 TW/cm² was determined as the threshold cleaning value, though the number of scans plays a relevant role in this particular case; below this value, the laser irradiation appears safe and may lead the way to an efficient and

satisfactory cleaning of surface rust and contaminants. SEM-EDS characterization studies comparing both, as-received and laser irradiated samples, enabled to conclude that corrosion crusts had been removed entirely from the surface of the sample, and the original outermost surface exposed. Furthermore, there are no significant compositional changes on the bulk of the sample during irradiation. The darkened surface became disappeared when the original surface was reached by increased treatment numbers; however, increasing laser irradiation scans assisted in finding satisfactory cleaning results.

There is still more work to be done to determine whether or not the fs visible laser system can be used to clean other sorts of metal artifacts, despite the fact that this case study showed effective cleaning of an iron object. Although no apparent damage was observed when reaching the original metal substrate surface, further studies are necessary to advance our understanding of the fs visible laser interaction with Fe and other metal and alloy artifacts.

CHAPTER: 10

GENERAL CONCLUSIONS

CHAPTER TEN

GENERAL CONCLUSIONS

10.1 Conclusions

Archaeological materials and museum artifacts are severely damaged with time as a result of mineralization, weathering, encrustations, contaminations, degradations etc. in the burial environment. Due to their fragile and sensitive surfaces with varying degrees of contamination and deterioration, the development of efficient, respectful cleaning methods is a challenge that requires a multidisciplinary scientific approach. The present research effort entailed the study of the phenomena caused by laser irradiation of actual archaeological samples exposed to contaminants on their outmost surface. It has thus focused on the development of laser-based cleaning methodology to safely remove surface contaminants from archaeological and museum heritage artifacts. The laser cleaning experiments and the physicochemical analyses performed on the archaeological bones, stones, ceramics and iron objects have served to obtain a better insight into the characteristics of these artifacts, their subsequent cleaning problems, and the laser-material interaction phenomena. According to the findings of this research, the results of laser cleaning attempts were in general satisfactory, contributing to better performance and to the development of more respectful cleaning and conservation solutions.

As the objective of this thesis, this study reviews the wide range of applications of laser cleaning and the accompanying laser-material interaction regimes in the conservation of CH materials, and focuses on the methods used to address typical cleaning challenges. The different criteria for selecting a suitable laser technique for the conservation of significant artifacts have been investigated by considering laser emission characteristics and the nature of the material to be intervened, particularly regarding its physico-chemical properties. Based on the comparison of different laser cleaning methods and subsequent cleaning results versus alternative methods (mechanical and chemical), ideal laser conservation strategies have been explored. In this study, we evaluated the potential of new short and ultrashort pulse lasers in CH materials conservation and developed specific laser processing protocols for archaeologically relevant samples excavated in the *Sierra de Atapuerca* site.

Ultrashort pulsed lasers have been explored in the sub-ns and fs regimes and with emission in the n-IR (1064 and 1030 nm), visible (515 nm), and UV (355 and 343 nm) wavelengths. To our knowledge, recently developed ultrafast fs lasers have been applied for the first time on different archaeological samples (such as bones and ceramics) since there were no similar reports found in the scientific literature. These lasers have allowed the observation of phenomena not reported until now and enabled, therefore, advances in the state of the art. In contrast to the long-pulsed laser systems that induce heat accumulation, ultrashort pulse lasers frequently yielded better results when it comes to archaeological artifact surface cleaning.

When determining the best feasible laser parameters for optimal laser cleaning, careful consideration has been given to the physicochemical properties of the artifacts as well as their subsequent interactions with the laser. This has enabled identification of the optimal laser cleaning settings. The investigations conducted to characterize the samples have utilized the appropriate approaches in order to explore the surface modifications generated by the laser on the samples under analysis. The topological and morphological modifications, together with changes in elemental composition were studied by characterizing the deteriorated artifacts before and after laser irradiation. These required the use of Scanning Electron Microscopy with Energy Dispersive X-ray Spectrometry (SEM-EDS), X-ray Diffractometry (XRD), Fourier Transform Infrared Spectroscopy (FTIR), X-ray Photoelectron Spectroscopy (XPS), IR Thermal Camera and Optical Microscopy (OM).

Although irradiance values for laser cleaning intervention may be taken as universal reference parameters, the cleaning threshold of the artifacts might be inferred following irradiation with a consecutive number of laser surface scans and taking into account other laser emission parameters, such as wavelength, together with some of the fundamental physical properties of the material subject to irradiation. Consequently, the artifact's optical and thermal properties may be determinant in the appearance of structural and chemical defects when an increasing number of laser scans are applied on the same area of the surface, even when the absorbed laser energy is below the material's damage threshold. During this investigation, laser irradiation with fs pulses has been observed as an outstanding success towards avoiding excessive thermal incubation/accumulation. While the sub-ns laser demonstrates capability in removing contaminants from significant artifacts, fs-laser irradiation paved the way to respectful, efficient and previously unachievable satisfactory cleaning results. One particular laser approach has been

demonstrated to be capable of better regulating the interactions between the laser and the material. This has been accomplished by adjusting the laser intensity, pulse duration, emission wavelength, and spatial distribution of the laser irradiation. It has been demonstrated that the ultrafast fs laser is significantly safer and more effective in the process of cleaning contaminants, surface deposits, crusts, concretions, environmental pollutants, etc. than other types of lasers due to the fact that its emission characteristics enable thermal management to an unprecedented level of control.

In this thesis, several research lines have been explored and developed based on ultrashort fs and sub-ns pulse burst and beam scan modes. A summary of the most relevant specific conclusions reached in the present thesis project, based on results obtained on the laser-based intervention on significant archaeological bones, stones, ceramics and iron objects follows.

10.1.1 Archaeological bones cleaned by laser

The interaction of an 800 ps pulsed n-IR laser with contaminants and degraded layers in a Pleistocene bear bone sample was investigated. Laser parameters that don't damage bone surface were determined; below this, laser irradiation of Pleistocene bone was observed safe and effective on surface cleaning. Surface analysis by different characterization techniques, comparing as-received and laser-irradiated sample, showed that contaminants including predominantly clay components, have been eliminated from the bone artifact. Alumino-silicates were mostly discovered at its surface, reduced significantly as the presence of Ca and P increased towards the sample's interior and upon laser irradiation. During irradiation, the bone artifact showed no substantial compositional changes; irradiation over the damage threshold darkens its surface, possibly due to the presence of Fe and Mn. Different explanations may account for their presence; Fe and Mn compounds may come from the soil in contact with the artifact, whereas Mn might also be a bone component, as it is discovered in adequate amounts in the sample cross-section and distant from its surface.

Although both sub-ns lasers were capable of cleaning contaminants from the outermost layer of the bone surface, the cleaning process was found to be unsuitable and impractical in the case of the sub-ns n-IR laser when beam scan mode was used, whereas sub-ns UV beam scan irradiation appears to be significantly better, particularly when laser-induced damage, cracks and physicochemical changes are taken into account. The bone surface cleaned with a sub-ns n-IR laser generates a significant amount of heat and develops a

yellowish hue as a result of the strong heat incubation affects, potentially leading to carbonization, thermomechanical cracking, and, in extreme situations, necrosis. This wavelength also seems to penetrate the surface without removing all the hard blackish contaminants. In contrast, sub-ns UV laser radiation interacts with the bone surface in a very localized, superficial way, making the process impractical due to its low material removal rate. The n-IR sub-ns laser in beam scan mode is not recommended due to the high heat accumulation observed. To avoid damaging fragile materials, such as archaeologically valuable bone, while using laser cleaning, heat deposition to the bulk should be kept to a minimum.

Ultrafast 238 fs UV laser (343 nm) has been found as the most effective laser method to clean delicate and subtle Pleistocene bone surfaces. The findings from several number of experiments demonstrate that this laser is quite effective, resulting in zero or minimal discoloration, and no indications of melting and cracking to the distinguishable bone surface under microscopic and spectroscopic examination. Compared to the application of sub-ns laser technology, this thesis revealed that laser pulses with a fs duration could induce non-thermal ablation of contaminants on bone samples. The cleaning treatments were affected by the thickness of the foreign material accretions and environmental contaminants, which are independent of the archaeological bone composition. Higher irradiance values were employed on the cemented clay matrix to remove thick clay accretion layers, while also protecting the bone by selecting and controllably irradiating these regions and lowering the irradiance when approaching the bone surface. As an outcome of the different characterization techniques, the fs laser cleaning process had essentially no negative impact on the material's physicochemical properties. This study clearly demonstrates that laser cleaning of archaeological bones is achievable using a Yb:KGW (ytterbium-doped potassium gadolinium tungstate) fs UV laser; it has been found to have a significant advantage and to pose a state-of-the-art solution in bone cleaning, and can successfully guide future conservation strategies.

10.1.2 Archaeological stones cleaned by laser

The cleaning process was carried out in beam scan mode with the utilization of recently developed Yb:KGW laser that emitted 238 fs of ultraviolet light with an emission wavelength of 343 nm, and two Nd:YAG lasers that emitted 800 ps of near-infrared light emission at 1064 nm, and 300 ps of ultraviolet light at 355 nm. Despite the fact that laser cleaning irradiance values govern several parameters, it has been discovered that the cleaning threshold of flints may be inferred after a number of treatments. Even though the

laser energy is below the threshold for damaging the flint surface, it has been found that utilizing a high number of treatments can still produce damage.

The most important finding that we revealed was the fact that surface deposits and crusts may be efficiently removed off flint surfaces by applying fs UV laser pulses. Though only a limited number of processing parameters have been investigated, the results suggest that the encrustation removal effectiveness was high and better capable of maintaining the flint's natural morphology compared to that of other sub-ns lasers approaches. This is ascribed to the very short pulse duration of fs lasers. As the cleaning process for the sub-ns laser is thermal in nature, the surface of the flint gets flattered as a consequence of the melting of rock-forming components, also becoming significantly discolored. In addition, fs pulses do not alter the morphology of the mineral grains; rather, the notable advantage and relief that is associated with mineral cleavage planes is maintained.

10.1.3 Archaeological ceramic materials cleaned by laser

All three fs n-IR, visible and UV irradiation wavelengths had different interactions with the hard matrix concretions and contaminated pottery sherds surface. Laser irradiation of the n-IR and the visible wavelengths are capable of cleaning concretions, but the visible wavelength seems more successful, as evidenced by the fact that even at the lowest ablation threshold values, n-IR laser irradiation causes cracking and melting, which is detrimental. The cleaning results of n-IR fs laser were thus found unsuitable and impractical under beam scan mode. Visible fs beam scan irradiation appears, in contrast, to be significantly better with respect to avoiding cracks, drainage and induced physicochemical changes. The fs n-IR laser caused significant heat and color changes as a result of strong heat accumulation effects, leading to thermomechanical cracking in extreme situations. It has been observed that the laser penetrated deeper into the surface; drains and fissures began to form on the original outermost surface without eliminating all the matrix concretions.

The fs UV laser irradiation, on the other hand, was proven to be fully damaging at any of the threshold values examined. It induced significantly faster heat accumulation than the n-IR laser, and the results were substantially poorer. In order to avoid excessive heat buildup, the fs UV and n-IR lasers should not be used; instead, fs visible lasers are recommended because the irradiation has a much more localized and superficial interaction with the sherd surface, making it a most practical technique in terms of its high cleaning rate.

As an outcome of multiple characterization techniques, the fs visible laser cleaning procedure had practically no negative impact on the physicochemical parameters of the ceramic artifacts; thus, the fluence and irradiance of the fs laser have been determined. The best laser cleaning conditions were found by balancing all of the parameters in a given scenario. This investigation has yielded an outstanding performance of fs visible green laser cleaning ceramic material, that may be used as the basis for further studies to advance the understanding of the laser interaction with different types of ceramic artifacts. The fs visible laser lends itself to further exploration of the influence of laser-ceramic interactions on varied fs visible laser pulse durations; consequently, it leads to the question that needs to be explored in great detail: is the visible green laser the new panacea for cleaning ceramic artifacts?

10.1.4 Archaeological iron object cleaned by laser

Using a 249 fs ultrashort pulsed visible laser with 515 nm emission, this thesis investigated how the corrosion crust layers in an iron object sample, which has weathered over the last 40-50 years, were affected by the laser's intervention. The laser was operated in beam scan mode, and laser parameters that didn't damage the iron item sample's surface were determined. Although the number of scans plays a significant role in this specific situation, the laser irradiance threshold cleaning value has been identified; below this, the laser irradiation appears entirely safe to an effective and satisfying surface cleaning. Corrosion crusts had been completely removed from the iron object and exposed to the original outermost surface.

On the other hand, irradiation does not seem to have any discernible effect on the majority of the sample's composition in any way. The surface darkened even with the cleaning threshold and a small number of scans. The darkness vanished when the original surface was reached; nevertheless, increasing the number of laser irradiation scans helped discover adequate cleaning results.

10.2 Recommendations for further work

Throughout this PhD thesis, all of the results and conclusions that have been presented thus far are part of the goals that were met, and each of them opens new avenues for future investigation.

The laser-based intervention of archaeologically significant materials and museum-stored artifacts could be improved by using a unique "sample by sample", "surface by surface" and "problem by problem" approach between the laser source and the artifact. A database following satisfactory laser cleaning results would be handy in the near future for the conservation specialists and museums to decide whether and how to clean the artifacts under their care, considering their aesthetic and historical values.

Further research on ultrashort pulsed laser-surface interaction using a variety of pulse durations and emission wavelengths, based on the advancements achieved within this thesis project will pave the way towards future respectful and environmentally advantageous conservation practices.

When considering how well different sub-ns laser irradiation emissions at n-IR and UV wavelengths and ultrafast fs-laser irradiation emissions at n-IR, visible green and UV wavelengths have cleaned contaminations, degradations, deterioration products, crusts, corrosion layers, concretions, etc. on different archaeological and CH material surfaces, intelligent laser system development will certainly be an essential part of the future. This will be essential to achieve more dynamic, respectful and effective cleaning protocols via automated laser conservation in the fields of Archaeology and Cultural Heritage.

CAPÍTULO DIEZ

CONCLUSIONES GENERALES

10.1 Conclusiones

Los materiales arqueológicos y las piezas de museos se dañan gravemente con el tiempo como resultado de la mineralización, la intemperie, las incrustaciones, las contaminaciones, las degradaciones, etc. en el entorno del subsuelo. Debido a sus superficies frágiles y sensibles con diversos grados de contaminación y deterioro, el Desarrollo de métodos de limpieza eficientes y respetuosos es un desafío que requiere un enfoque científico multidisciplinar. El presente esfuerzo de investigación ha implicado el estudio de los fenómenos causados por la irradiación láser de muestras arqueológicas actuales expuestas a contaminantes en su superficie exterior. Por lo tanto, se ha centrado en el Desarrollo de una metodología de limpieza basada en láser para eliminar de forma Segura los contaminantes superficiales de las piezas arqueológicas y de patrimonio museístico. Los experimentos de limpieza láser y los análisis físicoquímicos realizados en los huesos, piedras, cerámicas y objetos de hierro arqueológicos han servido para obtener una mayor comprensión de las características de estas piezas, sus problemas de limpieza posterior y los fenómenos de interacción láser-material. Según los resultados de esta investigación, los resultados de los intentos de limpieza con láser fueron en general satisfactorios, contribuyendo a un mayor rendimiento y al desarrollo de soluciones de limpieza y conservación más respetuosas.

Como objetivo de esta tesis, este estudio revisa la amplia gama de aplicaciones de la limpieza con láser y los regimens de interacción láser-material que la acompañan en la conservación de materiales del Patrimonio Cultural, y se centra en los métodos utilizados para abordar los desafíos típicos de la limpieza. Se han investigado los diferentes criterios para seleccionar una técnica láser adecuada para la conservación de piezas significativas considerando las características de emisión del láser y la naturaleza del material a intervenir, particularmente en lo que respecta a sus propiedades físico-químicas. Sobre la base de comparación de diferentes métodos de limpieza con láser y los resultados de limpieza posteriores frente a métodos alternativos (mecánicos y químicos), se han explorado estrategias ideales de conservación con láser. En este estudio, evaluamos el potencial de los nuevos láseres de pulso corto y ultracorto en la conservación de materiales del patrimonio cultural y desarrollamos protocolos de procesamiento láser específicos para piezas arqueológicas relevantes excavadas en el yacimiento de la Sierra de Atapuerca.

Los láseres de pulso ultracorto se han explorado en los regimenes de sub-ns y fs y con emission en las longitudes de onda n-IR (1064 y 1030nm), visible (515 nm) y UV (355 y 343 nm). Hasta donde sabemos, los láseres fs ultrarrápidos desarrollados recientemente se han aplicado por primera vez en diferentes muestras arqueológicas (como huesos y cerámica) ya que no se encontraron informes similares en la literatura científica. Estos láseres han permitido la observación de fenómenos no reportados hasta el momento y posibilitaron, por tanto, avances en el estado del arte. En contraste con los sistemas láser de pulsos largos que inducen la acumulación de calor, los láseres de pulsos ultracortos con frecuencia arrojaron mejores resultados cuando se trata de la limpieza de superficies de piezas arqueológicas.

A la hora de determinar los mejores parámetros láser factibles para una limpieza láser óptima, se han tenido muy en cuenta las propiedades físicoquímicas de las piezas, así como sus interacciones posteriores con el láser. Esto ha permitido la identificación de los ajustes óptimos de limpieza láser. Las investigaciones realizadas para caracterizar las muestras han utilizado los enfoques apropiados para explorar las modificaciones superficiales generadas por el láser en las muestras bajo análisis. Se estudiaron las modificaciones tipológicas y morfológicas, junto con los cambios en la composición elemental, caracterizando las piezas deterioradas antes y después de la irradiación con láser. Estos requerían el uso de microscopía electronica de barrodi con espectrometría de rayos X de dispersion de energía (SEM-EDS), difracción de rayos X (XRD), espectroscopía infrarroja transformada de Fourier (FTIR), espectroscopía de fotoelectrones de rayos X (XPS), cámara térmica IR y microscopía óptica (MO).

Aunque los valores de irradiancia para la intervención de limpieza con láser pueden tomarse como parámetros de referencia universales, el umbral de limpieza de las piezas puede deducirse después de la irradiación con un número consecutivo de escaneos de superficie con láser y teniendo en cuenta otros parámetros de emission del láser, como la longitud de onda, junto con algunas de las propiedades físicas fundamentales del material sujeto a irradiación. En consecuencia, las propiedades ópticas y térmicas de la pieza pueden ser determinantes en la aparición de defectos estructurales y químicos cuando se aplica un número creciente de escaneos láser en el mismo área de la superficie, incluso cuando la energía láser absorbida está por debajo del umbral de daño del material. Durante esta investigación, la irradiación láser con pulsos fs se ha observado como un éxito destacado para evitar una incubación / acumulación térmica excesiva. Si bien el láser sub-ns

demuestra su capacidad para eliminar contaminantes de piezas significativas, la irradiación con láser fs allanó el camino hacia resultados de limpieza respetuosos, eficientes y anteriormente inalcanzables. Se ha demostrado que un enfoque láser particular es capaz de regular mejor las interacciones entre el láser y el material. Esto se ha logrado ajustando la intensidad del láser, la duración del pulso, la longitud del pulso, la longitud de onda de emisión y la distribución espacial de la irradiación del láser. Se ha demostrado que el láser ultrarrápido fs es significativamente más seguro y efectivo en el proceso de limpieza de contaminantes, depósitos superficiales, costras, concreciones, contaminantes ambientales, etc. que otros tipos de láseres debido a que sus características de emisión permiten la gestión térmica a un nivel de control sin precedentes.

En esta tesis se han explorado y desarrollado varias líneas de investigación basadas en modos de barrido de haces y ráfagas de pulsos ultracortos fs y sub-ns. A continuación se presenta un resumen de las conclusiones específicas más relevantes a las que se ha llegado en el presente Proyecto de tesis, en base a los resultados obtenidos en la intervención con láser sobre huesos, piedras, cerámicas y objetos de hierro arqueológicos significativos.

10.1.1 Huesos arqueológicos limpiados con láser

Se ha investigado la interacción de un láser n-IR pulsado de 800 ps con contaminantes y capas degradadas en una muestra de hueso del Pleistoceno. Se determinaron parámetros láser que no dañan la superficie ósea; por debajo de esto, se observa que la irradiación con láser del hueso del Pleistoceno era segura y eficaz en la limpieza de la superficie. El análisis de la superficie mediante diferentes técnicas de caracterización, comparando la muestra tal como se recibió la irradiada con láser, mostró que los contaminantes, incluidos predominantemente componentes de arcilla, se eliminaron de la pieza ósea. Los aluminosilicatos se descubrieron principalmente en su superficie, y se redujeron significativamente a medida que aumentaba la presencia de Ca y P hacia el interior de la muestra y tras la irradiación con láser. Durante la irradiación, la pieza ósea no mostró cambios sustanciales en su composición; la irradiación por encima del umbral de daño oscurece su superficie, posiblemente debido a la presencia de Fe y Mn. Diferentes explicaciones pueden dar cuenta de su presencia; los compuestos de Fe y Mn pueden provenir del suelo en contacto con la pieza, mientras que el Mn también puede ser un componente óseo, ya que se descubre en cantidades adecuadas en la sección transversal de la muestra y distante de su superficie.

Aunque ambos láseres sub-ns eran capaces de limpiar los contaminantes de la capa más externa de la superficie del hueso, se encontró que el proceso de limpieza era unadecuado y poco práctico en el caso del láser sub-ns n-IR cuando se usaba el modo de escaneo de haz, mientras que la irradiación de barrido con haz UV sub-ns parece ser significativamente mejor, particularmente cuando se tienen en cuenta los daños inducidos por láser, las grietas y los cambios físicoquímicos. La superficie del hueso limpiada con un láser sub-ns n-IR genera una cantidad significativa de calor y desarrolla un tono amarillento como resultado de los fuertes efectos de la incubación del calor, lo que puede provocar carbonización, agrietamiento termomecánico y, en situaciones extremas, necrosis. Esta longitud de onda también parece penetrar en la superficie sin eliminar todos los contaminantes negruzcos duros. Por el contrario, la radiación láser UV sub-ns interactúa con la superficie del hueso de una manera muy localizada y superficial, lo que hace que el proceso sea poco práctico debido a su baja tasa de eliminación de material. No se recomienda el láser n-IR sub-ns en modo de exploración de haz debido a la gran acumulación de calor observada. Para evitar dañar materiales frágiles, como huesos valiosos para la arqueología, mientras se utiliza la limpieza láser, la deposición de calor en la masa debe reducirse al mínimo.

Se ha descubierto que el láser UV ultrarrápido de 238 fs (343 nm) es el método láser más efectivo para limpiar superficies óseas delicadas y sutiles del Pleistoceno. Los hallazgos de varios experimentos demuestran que este láser es bastante efectivo, lo que da como resultado una decoloración mínima o nula, y no hay indicios de fusión o agrietamiento en la superficie distinguible del hueso bajo el examen microscópico. En comparación con la aplicación de la tecnología láser sub-ns, esta tesis reveló que los pulsos de láser con una duración de fs podrían inducir la ablación no térmica de contaminantes en muestras de hueso. Los tratamientos de limpieza se vieron afectados por el espesor de las acumulaciones de material extraño y los contaminantes ambientales, que son independientes de la composición del hueso arqueológico. Se emplearon valores de irradiancia más altos en la matriz de arcilla cementada para eliminar las capas grasas de acumulación de arcilla, al mismo tiempo que se protegía el hueso seleccionando e irradiando de forma controlada estas regiones y reduciendo la irradiancia al acercarse a la superficie del hueso. Como resultado de las diferentes técnicas de caracterización, el proceso de limpieza con láser fs prácticamente no tuvo un impacto negativo en las propiedades físicoquímicas del material. Este estudio demuestra claramente que la limpieza con láser de los huesos arqueológicos se puede lograr utilizando un láser UV Yb: KGW (tungstato de potasio y gadolinio dopado con iterbio) fs; se ha encontrado que tiene una ventaja significativa y que plantea una

solución de vanguardia en la limpieza de huesos, y puede guiar con éxito futuras estrategias de conservación.

10.1.2 Piedras arqueológicas limpiadas con láser

El proceso de limpieza se llevó a cabo en modo de exploración de haz con la utilización de un láser Yb:KGW recientemente desarrollado que emitía 238 fs de luz ultravioleta con una longitud de onda de emisión de 343 nm, y dos láseres Nd: YAG que emitían 800 ps de luz infrarroja cercana, emisión a 1064 nm, y 300 ps de luz ultravioleta a 355 nm. A pesar del hecho de que los valores de irradiancia de la limpieza con láser gobiernan varios parámetros, se ha descubierto que el umbral de limpieza de los Pedernales se puede infringir después de una serie de tratamientos. Aunque la energía del láser está por debajo del umbral para dañar la superficie del pedernal, se ha descubierto que la utilización de una gran cantidad de tratamientos aún puede producir daños.

El hallazgo más importante que revelamos fue el hecho de que los depósitos superficiales y las costras se pueden eliminar de manera eficiente de las superficies de sílex mediante la aplicación de pulsos de láser UV fs. Aunque solo se ha investigado un número limitado de parámetros de procesamiento, los resultados sugieren que la eficacia de eliminación de incrustaciones fue alta y más capaz de mantener la morfología natural del pedernal en comparación con otros enfoques de láseres sub-ns. Esto se atribuye a la muy corta duración del pulso de los láseres fs. Como el proceso de limpieza del láser sub-ns es de naturaleza térmica, la superficie del pedernal se aplana como consecuencia de la fusión de los componentes que forman las rocas, y también se decolora significativamente. Además, los pulsos fs no alteran la morfología de los granos minerales; más bien, se mantiene la notable ventaja que se asocia con los planos de clivaje mineral.

10.1.3 Materiales cerámicos arqueológicos limpiados con láser

Las tres longitudes de onda de radiación fs n-IR, visible y UV tuvieron diferentes interacciones con las concreciones de la matriz dura y la superficie de las cerámicas contaminadas. La irradiación láser de n-IR y las longitudes de onda visibles son capaces de limpiar concreciones, pero la longitud de onda visible parece tener más éxito, como lo demuestra el hecho de que incluso en los valores de umbral de ablación más bajos, la irradiación láser n-IR provoca agrietamiento y fusión, lo que es perjudicial, por lo tanto, los resultados de limpieza del láser n-IR fs se consideraron inadecuados y poco prácticos en el modo de exploración del haz. La irradiación de barrido con haz fs visible parece, por el contrario, ser significativamente mejor con respecto a evitar grietas, drenaje y cambios

físicoquímicos inducidos. El láser fs n-IR provocó cambios significativos de calor y color como resultado de los fuertes efectos de acumulación de calor, lo que provocó el agrietamiento termomecánico en situaciones extremas. Se ha observado que el láser penetraba más profundamente en la superficie; comenzaron a formarse drenajes y fisuras en la superficie más externa original sin eliminar todas las concreciones de la matriz.

La irradiación láser UV fs, por otro lado, demostró ser completamente dañona en cualquiera de los valores de umbra examinados. Indujo una acumulación de calor significativamente más rápida que el láser n-IR y los resultados fueron sustancialmente peores. Para evitar una acumulación excesiva de calor, no se deben utilizar los láseres fs UV y n-IR; en cambio, se recomiendan los láseres visibles fs porque la irradiación tiene una interacción mucho más localizada y superficial con la superficie de la cerámica, lo que la convierte en una técnica muy práctica en términos de su alta tasa de limpieza.

Como resultado de múltiples técnicas de caracterización, el procedimiento de limpieza con láser visible fs prácticamente no tuvo un impacto negativo en los parámetros físicoquímicos de las piezas cerámicas; por lo tanto, se han determinado la fluencia y la irradiancia del láser fs. Las mejores condiciones de limpieza con láser se encontraron equilibrando todos los parámetros en un escenario dado. Esta investigación ha arrojado un rendimiento sobresaliente del material cerámico de limpieza con láser verde visible fs, que puede usarse como base para estudios posteriores para avanzar en la comprensión de la interacción del láser con diferentes tipos de piezas cerámicas. El láser visible de fs se presta a una mayor exploración de la influencia de las interacciones láser-cerámica en diversas duraciones de pulso de láser visible de fs; en consecuencia, lleva a la pregunta que necesita ser explorada en gran detalle: ¿es el láser verde visible la nueva panacea para la limpieza de piezas cerámicas?

10.1.4 Limpieza de objetos arqueológicos de hierro con láser

Usando un láser visible pulsado ultracorto de 249 fs con emisión de 515 nm, esta tesis ha investigado cómo las capas de la costra de corrosión en una muestra de hierro, que se había desgastado durante los últimos 40-50 años, se vieron afectadas por la intervención del láser. El láser se manejó en modo de escaneo de haz y se determinaron los parámetros del láser que no dañaron la superficie de la muestra de hierro. Aunque el número de escaneos juega un papel importante en esta situación específica, se ha identificado el valor de limpieza del umbral de irradiación láser; por debajo de esto, la irradiación láser parece completamente segura para una limpieza superficial efectiva y satisfactoria. Las costras de corrosión

se habían eliminado por completo de la pieza de hierro y se habían expuesto a la superficie exterior original.

Por otro lado, la irradiación no parece tener ningún efecto perceptible en la mayor parte de la composición de la muestra. La superficie se oscureció incluso con el umbral de limpieza y una pequeña cantidad de escaneos. La suciedad desapareció cuando se alcanzó la superficie original; sin embargo, aumentar el número de escaneos de irradiación láser ayudó a descubrir resultados de limpieza adecuados.

10.2 Recomendaciones para trabajos futuros

A lo largo de esta tesis doctoral, todos los resultados y conclusiones que se han presentado hasta el momento forman parte de los objetivos cumplidos, y cada uno de ellos abre nuevas vías para futuras investigaciones.

La intervención basada en láser de materiales arqueológicamente significativos y piezas almacenadas en museos podría mejorarse mediante el uso de un enfoque único de “muestra por muestra”, “superficie por superficie” y “problema por problema” entre el láser y la pieza. Una base de datos que siga los resultados satisfactorios de la limpieza láser sería útil en un futuro cercano para que los especialistas en conservación y los museos decidan si limpiar las piezas bajo su cuidado y cómo hacerlo, considerando sus valores estéticos e históricos.

La futura investigación sobre la interacción de la superficie del láser de pulso ultracorto utilizando una variedad de duraciones de pulso y longitudes de onda de emisión, basada en los avances logrados dentro de este proyecto de tesis, allanará el camino a futuras prácticas de conservación respetuosas y ambientalmente ventajosas.

Al considerar cómo son de buenas las diferentes emisiones de irradiación láser sub-ns en longitudes de onda n-IR y UV y las emisiones ultrarrápidas de irradiación láser fs en n-IR, longitudes de onda UV y verde visible han limpiado contaminaciones, degradaciones, costras, capas de corrosión, concreciones, etc. en diferentes superficies de material arqueológico y del patrimonio cultural, el desarrollo de sistemas láser inteligentes será sin duda una parte esencial del futuro. Esto será fundamental para conseguir protocolos de limpieza más dinámicos, respetuosos y eficaces mediante la conservación láser automatizada en los campos de la Arqueología y el Patrimonio Cultural.

REFERENCES & APPENDIX

REFERENCES

- [1] M. Cooper, *Laser cleaning in conservation: an introduction*. Butterworth-Heinemann, 1998.
- [2] B. Szmygin, Protection of historic monuments and sites – achievements, problems, perspectives. In *Heritage for Future 1(3)*. *Heritage in Transformation: cultural heritage protection in XXI century - problems, challenges, predictions.*, vol. 1, no. 3. Lublin, Poland: ICOMOS International Scientific Committee for Theory and Philosophy of Conservation and Restoration, 2016.
- [3] *Lasers in the Conservation of Artworks VIII*. 2010.
- [4] S. Siano, “Principles of Laser Cleaning in Conservation,” in *Handbook on the Use of Lasers in Conservation and Conservation Science, COST G7 (2007)*, 2007, vol. 7, pp. 1–26.
- [5] J. L. Bromberg, “The birth of the laser,” *Phys. Today*, vol. 41, no. 10, pp. 26–33, 1973, doi: 10.1063/1.881155.
- [6] T. Maiman, “Stimulated Optical Radiation in Ruby,” *Nature*, vol. 187, pp. 493–494, 1960.
- [7] M. S. Ettore Carpena, Maria Dinescu, Henry Helvajian, Jörg Hermann, Daniel Höche, Daniel Höche, Thomas Lippert, Frank E. Livingston, Ion N. Mihailescu, Paolo M. Ossi, Jürgen Reif, Peter Schaaf, Christof W. Schneider, *Laser Processing of Materials: Fundamentals, Applications and Developments*, no. 139. Springer Heidelberg Dordrecht London New York.
- [8] E. Kannatey, *Materials Processing Principles of Laser*. 2009.
- [9] J. H. Breck Hitz, J.J. Ewing, *Introduction to Laser Technology*, Third Edit. IEEE Press, 2001.
- [10] B. Muralikrishnan, S. Phillips, and D. Sawyer, “Laser trackers for large-scale dimensional metrology: A review,” *Precis. Eng.*, vol. 44, no. Cmm, pp. 13–28, 2016, doi: 10.1016/j.precisioneng.2015.12.001.
- [11] W. Kapłonek and C. Łukianowicz, “Non-contact optical metrology for automated in-process inspection of machined surfaces,” *11th IMEKO TC14 Int. Symp. Meas. Qual. Control. ISMQC 2013*, pp. 36–39, 2013.
- [12] P. D. F. Träger, Ed., *Springer Handbook of Lasers and Optics*. New York, 2007.
- [13] M. Sugo, H. Suzuki, and Y. Kondo, “Applications of Telecom Light Sources to Non-telecom Fields,” pp. 12–14.
- [14] L. Summerer and O. Purcell, “Concepts for Wireless Energy Transmission via Laser,” *ESA-Advanced Concepts Team*, pp. 1–10, 2008.
- [15] S. T. Khanna and K. Sharma, “Laser Technology Improving Wireless Communication: A Comprehensive Study on Laser Communicator,” *IOSR J.*

-
- Comput. Eng., vol. 19, no. 04, pp. 26–33, 2017, doi: 10.9790/0661-1904022633.
- [16] D. C. M. P. Dr Raimund Hibst, Ed., *Medical laser application.*, Volume 26., Urban & Fischer, 2011.
- [17] Q. Peng et al., “Lasers in medicine,” *Prog. Phys.*, vol. 71, 2008, doi: 10.1088/0034-4885/71/5/056701.
- [18] C. Fotakis, W. Kautek, and M. Castillejo, “Lasers in the Preservation of Cultural Heritage,” *Laser Chem.*, vol. 2006, no. February, pp. 1–1, 2006, doi: 10.1155/2006/74791.
- [19] S. Siano et al., “Laser cleaning in conservation of stone, metal, and painted artifacts: State of the art and new insights on the use of the Nd:YAG lasers,” *Appl. Phys. A Mater. Sci. Process.*, vol. 106, no. 2, pp. 419–446, 2012, doi: 10.1007/s00339-011-6690-8.
- [20] J. Reif, “Basic Physics of Femtosecond Laser Ablation,” Springer, Berlin, Heidelberg, 2010, pp. 19–41.
- [21] G. M. Bilmes, C. Freisztav, D. Schinca, and A. Orsetti, “Cleaning and characterization of objects of cultural value by laser ablation,” *Opt. Methods Arts Archaeol.*, vol. 5857, no. 1900, p. 585704, 2005, doi: 10.1117/12.612671.
- [22] B. Wagner, O. Syta, and M. Sawicki, “A moderate microsampling in Laser Ablation Inductively Coupled Plasma Mass Spectrometry analysis of cultural heritage objects: a review,” pp. 155–178, 2017, doi: 10.12775/3875-4.11.
- [23] P. Leiderer, “Laser-induced particle removal from silicon wafers,” no. 2000, pp. 249–259, 2004, doi: 10.1117/12.407353.
- [24] R. Fischer, “Laser cleaning of Tire Molds,” *4 SURfaces - Laser Technol. Mag. by 4JET*, vol. 43, no. 2, pp. 46–47, 2018.
- [25] “Lasers for cleaning – LASCAM systems.” <https://www.lascam.cz/en/laser-cleaning/> (accessed Sep. 06, 2019).
- [26] “Paint removal and decoating - residue-free cleaning with cleanLASER.” <https://www.cleanlaser.de/en/applications/application-fields/paint-removal-and-decoating/> (accessed Sep. 06, 2019).
- [27] R. Salimbeni, “Laser Techniques for Conservation of Artworks,” *Archeometriai Mühelly*, vol. 1, no. January 2006, pp. 34–40, 2006.
- [28] M. Schreiner, M. Strlič, and R. Salimbeni, *Handbook of the use of lasers in conservation and conservation science*. COST Office, 2008.
- [29] W. H. Asmus, J. F., Murphy, C.G., Munk, “Studies on the interaction of laser radiation with art artifacts,” *Dev. laser Technol. II*, no. Proc. SPIE 41, pp. 19-30.
- [30] M. L. Lazzarini, L., Asmus, J.F., “Lasers for the cleaning of statuary: initial results and potentialities,” *Jour. Vac. Sci. Tech.*, pp. 89–94, 1973.
- [31] S. Siano, M. Giamello, L. Bartoli, A. Mencaglia, V. Parfenov, and R. Salimbeni, “Laser cleaning of stone by different laser pulse duration and wavelength,” *Laser Phys.*, vol. 18, no. 1, pp. 27–36, Jan. 2008, doi: 10.1134/S1054660X08010064.
-

-
- [32] J. F. Asmus, V. A. Parfenov, and J. P. Elford, "Final Endeavors of 'Monument Man,'" pp. 15–24, 2017, doi: 10.12775/3875-4.01.
- [33] J. F. Asmus, "More light for art conservation," *IEEE Circuits Devices Mag.*, vol. March Issu, pp. 6–14, 1986.
- [34] P. Bromblet, M. Labouré, and G. Oriol, "Diversity of the cleaning procedures including laser for the restoration of carved portals in France over the last 10 years," *J. Cult. Herit.*, vol. 4, no. SUPPL. 1, pp. 17–26, 2003.
- [35] N. Schiavon et al., *Applying the Techniques on Materials II: The Application of Back-Scattered Scanning Electron Microscopy to Unravel Building Stone Decay Mechanisms in Urban Environments From a petrographical point of view.* 2013.
- [36] R. Abd-Allah, "Chemical cleaning of soiled deposits and encrustations on archaeological glass: A diagnostic and practical study," *J. Cult. Herit.*, vol. 14, no. 2, pp. 97–108, 2013, doi: 10.1016/j.culher.2012.03.010.
- [37] K. Singley and D. L. Hamilton, "Basic Methods of Conserving Underwater Archaeological Material Culture," *J. Am. Inst. Conserv.*, vol. 37, no. 3, p. 379, 1998, doi: 10.2307/3179822.
- [38] "Iron Conservation: Part I - Introduction and Equipment - Conservation Manual - Conservation Research Laboratory - Center for Maritime Archaeology and Conservation - Texas A&M University." <https://nautarch.tamu.edu/CRL/conservationmanual/File10a.htm> (accessed Jun. 05, 2022).
- [39] M. P. Casaletto et al., "Chemical cleaning of encrustations on archaeological ceramic artefacts found in different Italian sites," *Appl. Phys. A Mater. Sci. Process.*, vol. 92, no. 1, pp. 35–42, 2008, doi: 10.1007/s00339-008-4519-x.
- [40] N. P. Ema and M. Á. de Buergo, "Adverse effects arising from conservation treatments on archaeological sites: theory, practice and review," *COALITION*, no. 24, pp. 14–23, 2013.
- [41] G. Turner-Walker, "The Nature of Cleaning: Physical and Chemical Aspects of Removing Dirt, Stains and Corrosion.," *Proc. Int. Symp. Cult. Herit. Conserv. Tainan, Taiwan 6th-8th Novemb. 2012.*, no. November, p. 19, 2012.
- [42] Martin Cooper, "Recent Developments in Laser Cleaning - Martin Cooper." <https://www.buildingconservation.com/articles/laser/laser.htm> (accessed Sep. 06, 2019).
- [43] R. Salimbeni, "Laser Cleaning of Artworks," *COST Action G7 "Artworks Conserv. by Laser,"* 2016.
- [44] A. F. Elhagrassy, A. Hakeem, and A. F. Alhagrassy, "Comparative Study of Biological Cleaning and Laser Techniques for Conservation of Weathered Stone in Failaka Island, Kuwait," *A.F. ELHAGRASSY al Sci. Cult.*, vol. 4, no. 2, pp. 43–50, 2018, doi: 10.5281/zenodo.1214561.
- [45] R. A. Kaczkowski, B. A. Dajnowski, and E. P. Vicenzi, "From Earth to Outer Space: Laser cleaning semiprecious quartz and a novel application for meteoritic metal," pp. 47–62, 2017, doi: 10.12775/3875-4.03.
-

-
- [46] E. Di Francia, R. Lahoz, E. Angelini, S. Grassini, and M. Parvis, “Pulsed laser cleaning of metallic heritage,” *IMEKO Int. Conf. Metrol. Archeol. Cult. Heritage, MetroArcheo 2016*, vol. 2016-Octob, pp. 77–82, 2016.
- [47] M. Cooper and J. Larson, “The use of laser cleaning to preserve patina on marble sculpture,” *Conserv.*, vol. 20, no. 1, pp. 28–36, 1996, doi: 10.1080/01410096.1996.9995100.
- [48] Horst-Günter Rubahn, *Laser Applications in Surface Science and Technology*. 1999.
- [49] A. Zanini, V. Trafeli, and L. Bartoli, “The laser as a tool for the cleaning of Cultural Heritage,” *IOP Conf. Ser. Mater. Sci. Eng.*, vol. 364, no. 1, 2018, doi: 10.1088/1757-899X/364/1/012078.
- [50] J. M. Lee and K. G. Watkins, “In-process monitoring techniques for laser cleaning,” *Opt. Lasers Eng.*, vol. 34, no. 4–6, pp. 429–442, 2000, doi: 10.1016/S0143-8166(00)00073-7.
- [51] C. Emmelmann, J. Pablo, and C. Urbina, “Analysis of the Influence of Burst-Mode Laser Ablation by Modern Quality Tools,” vol. 12, pp. 172–181, 2011, doi: 10.1016/j.phpro.2011.03.119.
- [52] Y. S. Koh, “Cleaning of metal artefacts using pulsed lasers,” 2002, [Online]. Available: <http://epubl.ltu.se/1402-1757/2002/38/index-en.html>.
- [53] P. Sanjeevan and A. J. Klemm, “A Review of Laser Technique Application in Cleaning Process of Porous Construction Materials,” *Pulse*, pp. 463–472.
- [54] D. Bäuerle, “Thermal, Photophysical, and Photochemical Processes,” *Laser Process. Chem. Adv. Texts Physics*. Springer, Berlin, Heidelb., pp. 1–2, 2000, doi: 10.1007/978-3-662-04074-4_2.
- [55] M. Cooper, “Laser cleaning of sculpture, monuments and architectural detail,” *J. Archit. Conserv.*, vol. 11, no. 3, pp. 105–119, 2005, doi: 10.1080/13556207.2005.10784955.
- [56] S. Klein et al., “Discoloration of marble during laser cleaning by Nd:YAG laser wavelengths,” *Appl. Surf. Sci.*, vol. 171, no. 3–4, pp. 242–251, 2001, doi: 10.1016/S0169-4332(00)00706-6.
- [57] C. Varotsos, C. Tzani, and A. Cracknell, “The enhanced deterioration of the cultural heritage monuments due to air pollution,” *Environ. Sci. Pollut. Res.*, vol. 16, no. 5, pp. 590–592, 2009, doi: 10.1007/s11356-009-0114-8.
- [58] M. Carvalhão and A. Dionísio, “Evaluation of mechanical soft-abrasive blasting and chemical cleaning methods on alkyd-paint graffiti made on calcareous stones,” *J. Cult. Herit.*, vol. 16, no. 4, pp. 579–590, 2015, doi: 10.1016/j.culher.2014.10.004.
- [59] A. H. Hamad, “Effects of Different Laser Pulse Regimes (Nanosecond, Picosecond and Femtosecond) on the Ablation of Materials for Production of Nanoparticles in Liquid Solution,” *High Energy Short Pulse Lasers*, no. September, 2016, doi: 10.5772/63892.
- [60] M. A. Iglesias-Campos and J. L. Prada-Pérez, “Actual laser removal of black soiling
-

-
- crust from siliceous sandstone by high pulse repetition rate equipment: Effects on surface morphology,” *Mater. Constr.*, vol. 66, no. 321, 2016, doi: 10.3989/mc.2016.02215.
- [61] “Reasons Behind the Growth of Laser Cleaning in the Conservation Sector.” <https://www.azom.com/article.aspx?ArticleID=18216> (accessed Sep. 19, 2019).
- [62] T. Ersoy, T. Tunay, M. Uğuryol, G. Mavili, and S. Akturk, “Femtosecond laser cleaning of historical paper with sizing,” *J. Cult. Herit.*, vol. 15, no. 3, pp. 258–265, 2014, doi: 10.1016/j.culher.2013.07.002.
- [63] D. S. Prokuratov et al., “Laser cleaning of archaeologically corroded iron objects with inlays,” *Opt. Quantum Electron.*, vol. 52, no. 2, 2020, doi: 10.1007/s11082-020-2231-z.
- [64] G. Turner-Walker, “The nature of cleaning: physical and chemical aspects of removing dirt, stains and corrosion ArchSci2020 View project Mineralised Textiles View project,” , *Proc. Int. Symp. Cult. Herit. Conserv. Tainan, Taiwan 6th-8th Novemb*, no. November 2012, p. 19, 2012, [Online]. Available: <https://www.researchgate.net/publication/235788601>.
- [65] “Preparation and Conservation – Vertebrate Paleontology Collection.” <https://www.floridamuseum.ufl.edu/vertpaleo/amateur-collector/preparation/#Mechanical> (accessed Jun. 05, 2022).
- [66] G. Turner-Walker, “The West Runton fossil elephant: A pre-conservation evaluation of its condition, chemistry and burial environment,” *Conserv.*, vol. 22, no. 1, pp. 26–35, Jan. 1998, doi: 10.1080/01410096.1998.9995124.
- [67] M. R. Graham and L. Allington-Jones, “The air-abrasive technique: A re-evaluation of its use in fossil preparation,” *Palaeontol. Electron.*, vol. 21, no. 2, 2018, doi: 10.26879/815.
- [68] S. Çelik, “Use of a Vibro-Graver tool for mechanical cleaning of copper alloy stamp seals,” *Anatol. Archaeol. Stud.*, vol. 15, pp. 277–281, 2006.
- [69] R. Oltra et al., “Modelling and diagnostic of pulsed laser-solid interactions applications to laser cleaning: a TMR programme,” *Conf. Lasers Electro-Optics Eur. - Tech. Dig.*, vol. 3385, no. 2000, p. 307, 1998, doi: 10.1109/cleoe.1998.719457.
- [70] I. Maxwell, “Cleaning Sandstone,” *Inf. Hist. Scotl.*, pp. 1–8, 2007, [Online]. Available: www.historic-scotland.gov.uk/publicationsresults.html.
- [71] M. Coladonato, B. Di Odoardo, and E. Prunas, “Removal of Calcareous Concretions from Natural and Manufactured Stone Archaeological Artefacts through the Use of CO2 Water Solutions,” *Procedia Chem.*, vol. 8, pp. 65–71, 2013, doi: 10.1016/j.proche.2013.03.009.
- [72] E. Carbonell et al., “The first hominin of Europe,” *Nature*, vol. 452, no. 7186, pp. 465–469, 2008, doi: 10.1038/nature06815.
- [73] M. Maru, *Paleodemography - Encyclopedia of Geoarchaeology*. 2017.
- [74] J. M. Bermúdez de Castro, M. Martínón-Torres, R. Blasco, J. Rosell, and E.
-

-
- Carbonell, “Continuity or discontinuity in the European Early Pleistocene human settlement: The Atapuerca evidence,” *Quat. Sci. Rev.*, vol. 76, pp. 53–65, 2013, doi: 10.1016/j.quascirev.2013.06.023.
- [75] J. M. Bermúdez De Castro et al., “The Atapuerca Sites and Their Contribution to the Knowledge of Human Evolution in Europe,” *Evol. Anthropol.*, vol. 13, no. 1, pp. 25–41, 2004, doi: 10.1002/evan.10130.
- [76] J. M. Carretero et al., “Stature estimation from complete long bones in the Middle Pleistocene humans from the Sima de los Huesos, Sierra de Atapuerca (Spain),” *J. Hum. Evol.*, vol. 62, no. 2, pp. 242–255, 2012, doi: 10.1016/j.jhevol.2011.11.004.
- [77] A. I. Ortega et al., “Evolution of multilevel caves in the Sierra de Atapuerca (Burgos, Spain) and its relation to human occupation,” *Geomorphology*, vol. 196, pp. 122–137, 2013, doi: 10.1016/j.geomorph.2012.05.031.
- [78] A. Benito-Calvo and A. Pérez-González, “Erosion surfaces and Neogene landscape evolution in the NE Duero Basin (north-central Spain),” *Geomorphology*, vol. 88, no. 3–4, pp. 226–241, 2007, doi: 10.1016/j.geomorph.2006.11.005.
- [79] E. Carbonell, M. Esteban, P. Rodri, and A. Ollé, “The Pleistocene site of Gran Dolina , Sierra de Atapuerca , Spain : a history of Maria Bermu dez de Castro Ana Isabel Ortega,” *J. Hum. Evol.*, 1999.
- [80] L. J. Arnold, M. Demuro, M. Navazo, A. Benito-Calvo, and A. Pérez-González, “OSL dating of the Middle Palaeolithic Hotel California site, Sierra de Atapuerca, north-central Spain,” *Boreas*, vol. 42, no. 2. pp. 285–305, 2013, doi: 10.1111/j.1502-3885.2012.00262.x.
- [81] M. Navazo, “Sierra de Atapuerca archaeological sites. 2014. Pleistocene and Holocene hunter-gatherers in Iberia and the Gibraltar Strait. The current archaeological record.,” no. January, 2015, [Online]. Available: http://www.researchgate.net/profile/Maria_Galindo-Pellicena2/publication/266061253_Sierra_de_Atapuerca_archaeological_sites._2014._Pleistocene_and_Holocene_hunter-gatherers_in_Iberia_and_the_Gibraltar_Strait._The_current_archaeological_record/links/54241c.
- [82] A. Benito-calvo and A. Pérez-gonzález, “Geomorphology of the Sierra de Atapuerca and the Middle Arlanzón Valley (Burgos , Spain),” *J. Maps*, vol. 0, no. 0, pp. 1–10, 2015, doi: 10.1080/17445647.2014.909339.
- [83] J. M. B. de C. and E. C. A. Pérez-González (Coord.); A. Benito Calvo, M. Bernat Rebolal, A. Martín-Serrano, E. Molina, F. Nozal , J.A. Rodríguez, M. Santonja, J.L. Arsuaga, “Landforms and Geomorphological Processes in The Duero Basin. Pleistocene Geoaerchology of Ambrona And Atapuerca Sites.,” *Sixth Int. Conf. Geomorphol. LANDFORMS*, vol. C8, 2005, [Online]. Available: https://geomorfologia.es/sites/default/files/C8_Duero_Basin.pdf.
- [84] M. Navazo and E. Carbonell, “Neanderthal settlement patterns during MIS 4-3 in sierra de atapuerca (Burgos, Spain),” *Quat. Int.*, vol. 331, pp. 267–277, 2014, doi: 10.1016/j.quaint.2014.03.032.
- [85] J. S. Smith, J. Chandler, and J. Rose, “Quantitative reconstruction of Late Cenozoic
-

-
- landscapes: a case study in the Sierra de Atapuerca (Burgos, Spain),” *Earth Surf. Process. Landforms*, vol. 34, no. August 2007, pp. 155–161, 2009, doi: 10.1002/esp.
- [86] M. Navazo, A. Benito-Calvo, R. Alonso-Alcalde, J. F. Jordá Pardo, and E. Carbonell, “Archaeological surveys today: Projects, methods and results. The case of Sierra de Atapuerca (Burgos, Spain),” *Quat. Int.*, vol. 435, pp. 5–12, 2017, doi: 10.1016/j.quaint.2015.09.070.
- [87] A.I. Ortega Martínez, “Evolución geomorfológica del Karst de la Sierra de Atapuerca (Burgos) y su relación con los yacimientos pleistocenos que contiene,” Universidad de Burgos, Burgos, Spain, 2009.
- [88] A. Ollé et al., “The Early and Middle Pleistocene technological record from Sierra de Atapuerca (Burgos, Spain),” *Quat. Int.*, vol. 295, pp. 138–167, 2013, doi: 10.1016/j.quaint.2011.11.009.
- [89] “Atapuerca | American Museum of Natural History.” <https://web.archive.org/web/20051026105931/http://amnh.org/exhibitions/atapuerca/caves/index.php> (accessed Sep. 02, 2019).
- [90] “Atapuerca | Castilla y León World Heritage UNESCO.” <http://www.patrimonio.castillayleon.com/en/atapuerca> (accessed Sep. 02, 2019).
- [91] J. L. Arsuaga et al., “Sima de los Huesos (Sierra de Atapuerca, Spain). The site,” *J. Hum. Evol.*, vol. 33, no. 2–3, pp. 109–127, 1997, doi: 10.1006/jhev.1997.0132.
- [92] N. García, J. L. Arsuaga, and T. Torres, “The carnivore remains from the Sima de los Huesos Middle Pleistocene site (Sierra de Atapuerca, Spain),” *J. Hum. Evol.*, vol. 33, no. 2–3, pp. 155–174, 1997, doi: 10.1006/jhev.1997.0154.
- [93] “Archaeological Site of Atapuerca - UNESCO World Heritage Centre.” <http://whc.unesco.org/en/list/989> (accessed Sep. 02, 2019).
- [94] M. Santamaría and M. Navazo, “Fuente Mudarra: La industria lítica de un asentamiento musteriense en la Sierra de Atapuerca (Burgos),” *Arqueol. en el Val. del Duero Del Paleolítico a la edad Media.*, vol. 5, pp. 19–34, 2016.
- [95] M. Navazo, A. Colina, S. Domínguez-Bella, and A. Benito-Calvo, “Raw stone material supply for Upper Pleistocene settlements in Sierra de Atapuerca (Burgos, Spain): flint characterization using petrographic and geochemical techniques,” *J. Archaeol. Sci.*, vol. 35, no. 7, pp. 1961–1973, 2008, doi: 10.1016/j.jas.2007.12.009.
- [96] “Fuente Mudarra «destapa» un taller neandertal de industria lítica - Diario de Burgos.” <https://www.diariodeburgos.es/noticia/Z5A277C00-91D9-D189-18A44CEBE5D159B8/20140711/fuente/mudarra/destapa/taller/neandertal/industria/litica> (accessed Aug. 19, 2019).
- [97] “Fuente Mudarra - Fundación Atapuerca.” <https://www.atapuerca.org/es/atapuerca/Fuente-Mudarra> (accessed Aug. 19, 2019).
- [98] J. M. Carretero et al., “A Late Pleistocene–Early Holocene archaeological sequence of Portalón de Cueva Mayor (Sierra de Atapuerca, Burgos, Spain),” *Munibe (Antropol.)*, vol. 59, no. 2, pp. 67–80, 2008.
- [99] A. Pérez-Romero et al., “An unusual Pre-bell beaker copper age cave burial context
-

-
- from El Portalón de Cueva Mayor site (Sierra de Atapuerca, Burgos),” *Quat. Int.*, vol. 433, pp. 142–155, 2017, doi: 10.1016/j.quaint.2015.06.063.
- [100] M. Á. Galindo-Pellicena et al., “The equids from the Bronze Age levels of the El Portalón site (Atapuerca, Burgos, Spain),” *Quat. Int.*, vol. 433, pp. 124–141, 2017, doi: 10.1016/j.quaint.2015.11.120.
- [101] A. Alday Ruiz et al., “La industria osea de El Portalón de Cueva Mayor (Sierra de Atapuerca, Burgos). Biapuntados, puntas de flecha y agujas, morfología y funcionalidad,” *Munibe (Antropologia-Arkeologia)*, vol. 62, no. 3, pp. 227–249, 2011.
- [102] M. Bass, “Lasers for use in medicine,” *Endoscopy*, vol. 18, no. 1, pp. 2–5, doi: 10.1055/s-2007-1018399.
- [103] E. Khalkhal, M. Rezaei-Tavirani, M. R. Zali, and Z. Akbari, “The evaluation of laser application in surgery: A review article,” *J. Lasers Med. Sci.*, vol. 10, no. 4, pp. S104–S111, 2019, doi: 10.15171/jlms.2019.S18.
- [104] S. Siano et al., “Laser cleaning in conservation of stone, metal, and painted artifacts: State of the art and new insights on the use of the Nd:YAG lasers,” *Appl. Phys. A Mater. Sci. Process.*, vol. 106, no. 2, pp. 419–446, 2012, doi: 10.1007/s00339-011-6690-8.
- [105] A. V. Rode et al., “Ultrafast laser ablation for restoration of heritage objects,” *Appl. Surf. Sci.*, vol. 254, no. 10, pp. 3137–3146, 2008, doi: 10.1016/j.apsusc.2007.10.106.
- [106] M. A. Rahman et al., “Sub-ns-pulsed laser cleaning of an archaeological bone from the Sierra de Atapuerca, Spain: a case study,” *SN Appl. Sci.*, vol. 3, no. 12, 2021, doi: 10.1007/s42452-021-04850-8.
- [107] E. M. Maingi et al., “Historical stained-glass window laser preservation: the heat accumulation challenge,” *Bol. Soc. Esp. Ceram. Vid.*, pp. 1–14, 2021, doi: 10.1016/j.bsecv.2021.12.003.
- [108] T. Burmester, M. Meier, H. Haferkamp, S. Barcikowski, J. Bunte, and A. Ostendorf, “Femtosecond Laser Cleaning of Metallic Cultural Heritage and Antique Artworks,” pp. 61–69, 2005, doi: 10.1007/3-540-27176-7_8.
- [109] C. G. M. J. F. Asmus and W. H. Munk, “Studies on the interaction of laser radiation with art artifacts,” *Dev. Laser Technol. II*, R. F. Wuerker, ed., *Proc. SPIE* 41, pp. 19–30, 1973.
- [110] A. L. Schawlow, “Lasers,” *Science (80-.)*, vol. 149, no. 3679, pp. 13–22, 1965.
- [111] J. F. Asmus, C. G. Murphy, and W. H. Munk, “Studies on the Interaction of Laser Radiation With Art Artifacts.,” *SPIE Semin Proc*, vol. 4, pp. 19–27, 1974, doi: 10.1117/12.953831.
- [112] J. F. Asmus, “Thirty-seven years of lasers in the conservation of art,” vol. 27, no. 1, pp. 3–8, 2010.
- [113] J. F. Asmus, G. Guattari, L. Lazzarini, G. Musumeci, and R. F. Wuerker, “Holography in the conservation of statuary,” *Stud. Conserv.*, vol. 18, no. 2, pp. 49–
-

-
- 63, 1973, doi: 10.1179/sic.1973.005.
- [114] L. Lazzarini and John F. Asmus, “The Application of Laser Radiation to the Cleaning of Statuary,” *First Annu. Meet. Am. Inst. Conserv. Hist. Artist. Work.*, vol. 13, no. 2, pp. 39–49, 1973.
- [115] L. Lazzarini, L. Marchesini, and J. F. Asmus, “Lasers for the Cleaning of Statuary: Initial Results and Potentialities,” *J. Vac. Sci. Technol.*, vol. 10, no. 6, pp. 1039–1043, 1973, doi: 10.1116/1.1318462.
- [116] K. G. Watkins, J. H. Larson, D. C. Emmony, and W. M. Steen, “Laser Cleaning in Art Restoration: A Review,” *Laser Process. Surf. Treat. Film Depos.*, pp. 907–923, 1996, doi: 10.1007/978-94-009-0197-1_50.
- [117] W. Z. A.C. Tam, W.P. Leung, W. Zapka, “Lasercleaning techniques for removal of surface particulates,” *J. Appl. Phys.*, vol. 71 (7), pp. 3515–3523, 1992.
- [118] G. M. Bilmes, C. Freisztav, D. Schinca, and A. Orsetti, “Cleaning and characterization of objects of cultural value by laser ablation,” *Opt. Methods Arts Archaeol.*, vol. 5857, no. 1900, p. 585704, 2005, doi: 10.1117/12.612671.
- [119] W. Al Sekhaneh, A. El Serogy, and M. El-Bakri, “Yag-laser cleaning of archaeological materials in Jordanian museums,” *Mediterr. Archaeol. Archaeom.*, vol. 15, no. 3, pp. 157–164, 2015, doi: 10.5281/zenodo.19297.
- [120] R. Ostrowski, J. Marczak, M. Strzelec, and A. Koss, “Laser damage thresholds of bone objects,” *O3A Opt. Arts, Archit. Archaeol.*, vol. 6618, p. 66181D, 2007, doi: 10.1117/12.726117.
- [121] R. Pini et al., “Application of a new laser cleaning procedure to the mausoleum of Theodoric,” *J. Cult. Herit.*, vol. 1, no. 2, pp. 93–97, 2000, doi: 10.1016/S1296-2074(00)00189-8.
- [122] I. Osticioli, M. Mascalchi, D. Pinna, and S. Siano, “Removal of *Verrucaria nigrescens* from Carrara marble artefacts using Nd:YAG lasers: comparison among different pulse durations and wavelengths,” *Appl. Phys. A Mater. Sci. Process.*, vol. 118, no. 4, pp. 1517–1526, 2015, doi: 10.1007/s00339-014-8933-y.
- [123] P. Barreiro, A. Andreotti, M. P. Colombini, P. González, and J. S. Pozo-Antonio, “Influence of the laser wavelength on harmful effects on granite due to biofilm removal,” *Coatings*, vol. 10, no. 3, pp. 1–18, 2020, doi: 10.3390/coatings10030196.
- [124] G. Grammatikakis, K. D. Demadis, K. Melessanaki, and P. Pouli, “Laser-assisted removal of dark cement crusts from mineral gypsum (selenite) architectural elements of peripheral monuments at Knossos,” *Stud. Conserv.*, vol. 60, no. March 2016, pp. S3–S11, 2015, doi: 10.1179/0039363015Z.000000000201.
- [125] A. Aldrovandi, C. Lalli, G. Lanterna, and M. Matteini, “Laser cleaning: A study on greyish alteration induced on non-patinated marbles,” *J. Cult. Herit.*, vol. 1, no. 2, pp. S55–S60, 2000, doi: 10.1016/S1296-2074(00)00152-7.
- [126] S. Siano, F. Fabiani, R. Pini, R. Salimbeni, M. Giamello, and G. Sabatini, “Determination of damage thresholds to prevent side effects in laser cleaning of pliocene sandstone of Siena,” *J. Cult. Herit.*, vol. 1, no. 2, pp. 47–53, 2000, doi:
-

-
- 10.1016/S1296-2074(00)00194-1.
- [127] M. Labouré, P. Bromblet, G. Oriol, G. unter Wiedemann, and C. Simon-Boisson, “Assessment of laser cleaning rate on limestones and sandstones,” *J. Cult. Herit.*, vol. 1, no. 2, pp. 21–27, 2000, doi: 10.1016/S1296-2074(00)00195-3.
- [128] F. Margheri et al., “SMART CLEAN: A new laser system with improved emission characteristics and transmission through long optical fibres,” *J. Cult. Herit.*, vol. 1, no. 2, pp. 119–123, 2000, doi: 10.1016/S1296-2074(00)00187-4.
- [129] G. Lanterna and M. Matteini, “Laser cleaning of stone artefacts: A substitute or alternative method?,” *J. Cult. Herit.*, vol. 1, no. 2, pp. 29–35, 2000, doi: 10.1016/S1296-2074(00)00136-9.
- [130] R. Chapoulie, S. Cazenave, and M. Duttine, “Laser cleaning of historical limestone buildings in Bordeaux appraisal using cathodoluminescence and electron paramagnetic resonance,” *Environ. Sci. Pollut. Res.*, vol. 15, no. 3, pp. 237–243, 2008, doi: 10.1065/espr2007.07.436.
- [131] H. IMAM, K. ELSAYED, and F. MADKOUR, “A Comparative Study of Laser Cleaning of Archaeological Inorganic Materials With Traditional Methods,” pp. 239–250, 2011, doi: 10.1142/9789814317511_0028.
- [132] T. Stratoudaki, A. Manousaki, V. Zafirooulos, N. Huet, S. Pétreumont, and A. Vinçotte, “Cleaning of Ceramics Using Lasers of Different Wavelength,” *Opt. Lasers Biomed. Cult.*, pp. 213–217, 2000, doi: 10.1007/978-3-642-56965-4_42.
- [133] P. Gaspar, A. Kearns, R. Vilar, K. G. Watkins, and M. M. M. Gomes, “A study of the effect of wavelength on Q-switched Nd:Yag laser cleaning of eighteenth-century portuguese tiles,” *Stud. Conserv.*, vol. 45, no. 3, pp. 189–200, 2000, doi: 10.1179/sic.2000.45.3.189.
- [134] J. Hildenhagen, K. Dickmann, and H. G. Hartke, “Removal of Strong Sinter Layers on Archaeological Artworks with Nd:YAG Laser,” Nimmrichter, J., Kautek, W., Schreiner, M. *Lasers Conserv. Artworks. Springer Proc. physics*, Springer, Berlin, Heidelberg., vol. 116, 2007, doi: https://doi.org/10.1007/978-3-540-72310-7_21.
- [135] Y. Koh and I. Sárady, “Cleaning of corroded iron artefacts using pulsed TEA CO₂- and Nd:YAG-lasers,” *J. Cult. Herit.*, vol. 4, no. SUPPL. 1, pp. 129–133, 2003, doi: 10.1016/s1296-2074(02)01140-8.
- [136] M. A. Yandrisevits, P. Londero, F. Carò, A. Rizzo, and C. Cappuccini, “Wavelength-dependent absorption and scattering effects on laser cleaning of a corroded iron alloy European scale armor,” *Lasers Conserv. Artworks XI, Proc. LACONA XI*, P. Targ. al. (Eds.), NCU Press. Toruń 2017, pp. 27–45, 2017, doi: 10.12775/3875-4.02.
- [137] I. Osticioli and S. Siano, “Dependence of Nd:YAG laser derusting and passivation of iron artifacts on pulse duration,” *Fundam. Laser-Assisted Micro-Nanotechnologies 2013*, vol. 9065, p. 906513, 2013, doi: 10.1117/12.2049808.
- [138] J. Chamón, J. Barrio, E. Catalán, M. Arroyo, and A. I. Pardo, “Nd:YAG laser cleaning of heavily corroded archaeological iron objects and evaluation of its effects,” *Lasers Conserv. Artworks - Proc. Int. Conf. LACONA 7*, pp. 297–302,
-

-
- 2008.
- [139] K. Dickmann, J. Hildenhagen, J. Studer, and E. Müsch, “Archaeological Ironwork: Removal of Corrosion Layers by Nd:YAG-Laser,” pp. 71–77, 2005, doi: 10.1007/3-540-27176-7_9.
- [140] C. Korenberg, A. M. Baldwin, and P. Pouli, “Investigating and optimising the laser cleaning of corroded iron,” *Lasers Conserv. Artworks LACONA VII Proc.*, pp. 291–296, 2008.
- [141] L. Pereira-Pardo and C. Korenberg, “The use of erbium lasers for the conservation of cultural heritage. A review,” *J. Cult. Herit.*, vol. 31, no. July 2019, pp. 236–247, 2018, doi: 10.1016/j.culher.2017.10.007.
- [142] A. Decruz, M. L. wolbarsht, A. Andreotti, M. P. Colombini, D. Pinna, and C. F. Culberson, “Investigation of the Er:YAG laser at 2.94 μm to remove lichens growing on stone,” *Stud. Conserv.*, vol. 54, no. 4, pp. 268–277, 2009, doi: 10.1179/sic.2009.54.4.268.
- [143] L. N. Melita, K. Węłowska, D. Tamburini, and C. Korenberg, “Investigating the Potential of the Er:YAG Laser for the Removal of Cemented Dust from Limestone and Painted Plaster,” *Coatings MDPI*, vol. 10(11);, no. 1099, 2020, doi: 10.3390/coatings 10111099.
- [144] A. D. Karoutis and E. Hellidonis, “A new method of cleaning ancient skulls by means of ArF excimer laser,” *LACONA I, Restaur. Sonderband, Wien, Austria*, pp. 99–102, 1997.
- [145] P. Maravelaki-Kalaitzaki, V. Zafirooulos, and C. Fotakis, “Excimer laser cleaning of encrustation on Pentelic marble: Procedure and evaluation of the effects,” *Appl. Surf. Sci.*, vol. 148, no. 1, pp. 92–104, 1999, doi: 10.1016/S0169-4332(99)00125-7.
- [146] S. I. Kholodova, D. A. Goryachkin, and L. V. Koval’chuk, “The cleaning of works of art made from stone with laser radiation at wavelengths of 106 and 106 μm ,” *J. Opt. Technol.*, vol. 77, no. 5, p. 309, 2010, doi: 10.1364/jot.77.000309.
- [147] G. Pereira, M. Pires, B. Costa, and F. Costa, “Laser selectivity on cleaning museologic iron artefacts,” *XVI Int. Symp. Gas Flow, Chem. Lasers, High-Power Lasers*, vol. 6346, no. 1, p. 63461G, 2006, doi: 10.1117/12.738153.
- [148] T. Rivas et al., “Comparative study of ornamental granite cleaning using femtosecond and nanosecond pulsed lasers,” *Appl. Surf. Sci.*, vol. 278, pp. 226–233, 2013, doi: 10.1016/j.apsusc.2012.12.038.
- [149] M. Matteini, C. Lalli, I. Tosini, A. Giusti, and S. Siano, “Laser and chemical cleaning tests for the conservation of the Porta del Paradiso by Lorenzo Ghiberti,” *J. Cult. Herit.*, vol. 4, no. SUPPL. 1, pp. 147–151, 2003, doi: 10.1016/s1296-2074(02)01190-1.
- [150] S. Samolik, M. Walczak, M. Plotek, A. Sarzynski, I. Pluska, and J. Marczak, “Investigation into the removal of graffiti on mineral supports: Comparison of nanosecond Nd:YAG laser cleaning with traditional mechanical and chemical methods,” *Stud. Conserv.*, vol. 60, pp. S58–S64, 2015, doi: 10.1179/0039363015Z.
-

00000000208.

- [151] M. Strzelec, J. Marczak, R. Ostrowski, A. Koss, and R. Szambelan, “Results of Nd:YAG laser renovation of decorative ivory jug,” *Springer Proc. Physics, Proc. Int. Conf. LACONA V, Lasers Conserv. Artworks, Osnabrück, Ger.*, vol. 100, pp. 163–168.
- [152] P. Maravelaki-Kalaitzaki et al., “Short free running Nd:YAG laser to clean different encrustations on Pentelic marble: Procedure and evaluation of the effects,” *J. Cult. Herit.*, vol. 4, no. SUPPL. 1, pp. 77–82, 2003, doi: 10.1016/s1296-2074(02)01151-2.
- [153] L. Bartoli, P. Pouli, C. Fotakis, S. Siano, and R. Salimbeni, “Characterization of Stone Cleaning by Nd:YAG Lasers with Different Pulse Duration,” *Laser Chem.*, vol. 2006, pp. 1–6, 2006, doi: 10.1155/2006/81750.
- [154] R. Salimbeni, R. Pini, S. Siano, and G. Calcagno, “Assessment of the state of conservation of stone artworks after laser cleaning: Comparison with conventional cleaning results on a two-decade follow up,” *J. Cult. Herit.*, vol. 1, no. 4, pp. 385–391, 2000, doi: 10.1016/S1296-2074(00)01094-3.
- [155] S. S. Potgieter-Vermaak, R. H. M. Godoi, R. Van Grieken, J. H. Potgieter, M. Oujja, and M. Castillejo, “Micro-structural characterization of black crust and laser cleaning of building stones by micro-Raman and SEM techniques,” *Spectrochim. Acta - Part A Mol. Biomol. Spectrosc.*, vol. 61, no. 11–12, pp. 2460–2467, 2005, doi: 10.1016/j.saa.2004.09.010.
- [156] P. Pouli et al., “The two-wavelength laser cleaning methodology; Theoretical background and examples from its application on CH objects and monuments with emphasis to the Athens Acropolis sculptures,” *Herit. Sci.*, vol. 4, no. 1, pp. 1–11, 2016, doi: 10.1186/s40494-016-0077-2.
- [157] P. Pouli, M. Oujja, and M. Castillejo, “Practical issues in laser cleaning of stone and painted artefacts: Optimisation procedures and side effects,” *Appl. Phys. A Mater. Sci. Process.*, vol. 106, no. 2, pp. 447–464, 2012, doi: 10.1007/s00339-011-6696-2.
- [158] J. Delivré, “Laser cleaning: Is there specific laser esthetics?,” *J. Cult. Herit.*, vol. 4, no. SUPPL. 1, pp. 245–248, 2003, doi: 10.1016/s1296-2074(02)01204-9.
- [159] V. Verges-Belmin and C. Dignard, “Laser yellowing: Myth or reality?,” *J. Cult. Herit.*, vol. 4, no. SUPPL. 1, pp. 238–244, 2003, doi: 10.1016/s1296-2074(02)01203-7.
- [160] P. Pouli et al., “The laser-induced discoloration of stonework; a comparative study on its origins and remedies,” *Spectrochim. Acta - Part A Mol. Biomol. Spectrosc.*, vol. 71, no. 3, pp. 932–945, 2008, doi: 10.1016/j.saa.2008.02.031.
- [161] S. S. Amaral, M. Pires, M. D. Carvalho, and F. M. Costa, “Laser cleaning of calcareous stones: influence of laser irradiation in colour changes of different layers,” *XVII Int. Symp. Gas Flow, Chem. Lasers, High-Power Lasers*, vol. 7131, p. 713127, 2008, doi: 10.1117/12.818140.
- [162] V. Zafirooulos et al., “Yellowing effect and discoloration of pigments: Experimental and theoretical studies,” *J. Cult. Herit.*, vol. 4, no. SUPPL. 1, pp. 249–
-

-
- 256, 2003, doi: 10.1016/s1296-2074(02)01205-0.
- [163] C. De Oliveira, P. Bromblet, A. Colombini, and V. Vergès-Belmin, “Medium-wave ultraviolet radiation to eliminate laser-induced yellowing generated by the laser removal of lamp black on gypsum,” *Stud. Conserv.*, vol. 60, pp. S34–S40, 2015, doi: 10.1179/0039363015Z.000000000205.
- [164] J. Berthonneau et al., “Yellowing of laser-cleaned artworks: Formation of residual hydrocarbon compounds after Nd:YAG laser cleaning of gypsum plates covered by lamp black,” *J. Cult. Herit.*, vol. 39, pp. 57–65, 2019, doi: 10.1016/j.culher.2019.02.014.
- [165] J. Chloros, H. Salmon, and V. Talland, “Laser cleaning at the Isabella Stewart Gardner Museum, Boston, USA: Sixteen Roman sculptures, fourteen months, and three conservators,” *Stud. Conserv.*, vol. 60, pp. S41–S48, 2015, doi: 10.1179/0039363015Z.000000000206.
- [166] S. Siano, F. Margheri, R. Pini, P. Mazzinghi, and R. Salimbeni, “Cleaning processes of encrusted marbles by Nd:YAG lasers operating in free-running and Q-switching regimes,” *Appl. Opt.*, vol. 36, no. 27, p. 7073, 1997, doi: 10.1364/ao.36.007073.
- [167] P. Ortiz et al., “Comparative study of pulsed laser cleaning applied to weathered marble surfaces,” *Appl. Surf. Sci.*, vol. 283, pp. 193–201, 2013, doi: 10.1016/j.apsusc.2013.06.081.
- [168] P. Pouli et al., “A comprehensive study of the coloration effect associated with laser cleaning of pollution encrustations from stonework,” *Conf. Lasers Electro-Optics Eur. - Tech. Dig.*, p. 687, 2005, doi: 10.1109/CLEOE.2005.1568463.
- [169] J. Zhang, A. J. Birnbaum, Y. Lawrence Yao, F. Xu, and J. R. Lombardi, “Effect of fluence on the discoloration of marble cleaned with UV lasers,” *Appl. Surf. Sci.*, vol. 253, no. 6, pp. 3083–3092, 2007, doi: 10.1016/j.apsusc.2006.06.056.
- [170] S. Klein, T. Stratoudaki, Y. Marakis, V. Zafirooulos, and K. Dickmann, “Comparative study of different wavelengths from IR to UV applied to clean sandstone,” *Appl. Surf. Sci.*, vol. 157, no. 1, pp. 1–6, 2000, doi: 10.1016/S0169-4332(99)00561-9.
- [171] G. Marakis, P. Pouli, V. Zafirooulos, and P. Maravelaki-Kalaitzaki, “Comparative study on the application of the 1st and the 3rd harmonic of a Q-switched Nd:YAG laser system to clean black encrustation on marble,” *J. Cult. Herit.*, vol. 4, no. SUPPL. 1, pp. 83–91, 2003, doi: 10.1016/s1296-2074(02)01208-6.
- [172] B. T. Gameda, R. Lahoz, A. T. Caldeira, and N. Schiavon, “Efficacy of laser cleaning in the removal of biological patina on the volcanic scoria of the rock-hewn churches of Lalibela, Ethiopia,” *Environ. Earth Sci.*, vol. 77, no. 2, pp. 1–12, 2018, doi: 10.1007/s12665-017-7223-3.
- [173] M. Sanz et al., “Infrared and ultraviolet laser removal of crustose lichens on dolomite heritage stone,” *Appl. Surf. Sci.*, vol. 346, pp. 248–255, 2015, doi: 10.1016/j.apsusc.2015.04.013.
- [174] M. Speranza et al., “Nd-YAG laser irradiation damages to *Verrucaria nigrescens*,” *Int. Biodeterior. Biodegrad.*, vol. 84, pp. 281–290, 2013, doi:
-

-
- 10.1016/j.ibiod.2012.02.010.
- [175] T. Rivas, J. S. Pozo-Antonio, M. E. López de Silanes, A. Ramil, and A. J. López, “Laser versus scalpel cleaning of crustose lichens on granite,” *Appl. Surf. Sci.*, vol. 440, pp. 467–476, 2018, doi: 10.1016/j.apsusc.2018.01.167.
- [176] S. Pozo, P. Barreiro, T. Rivas, P. González, and M. P. Fiorucci, “Effectiveness and harmful effects of removal sulphated black crust from granite using Nd:YAG nanosecond pulsed laser,” *Appl. Surf. Sci.*, vol. 302, pp. 309–313, 2014, doi: 10.1016/j.apsusc.2013.10.129.
- [177] A. Zanini, F. Margheri, S. Modi, and M. Scortecci, “Line of laser systems for applications in the restoration yard and in the restorer’s studio,” *Laser Tech. Syst. Art Conserv.*, vol. 4402, no. I, p. 108, 2001, doi: 10.1117/12.445651.
- [178] R. M. Esbert et al., “Application limits of Q-switched Nd:YAG laser irradiation for stone cleaning based on colour measurements,” *J. Cult. Herit.*, vol. 4, no. SUPPL. 1, pp. 50–55, 2003, doi: 10.1016/s1296-2074(02)01227-x.
- [179] J. S. Pozo-Antonio, M. P. Fiorucci, T. Rivas, A. J. López, A. Ramil, and D. Barral, “Suitability of hyperspectral imaging technique to evaluate the effectiveness of the cleaning of a crustose lichen developed on granite,” *Appl. Phys. A Mater. Sci. Process.*, vol. 122, no. 2, pp. 1–9, 2016, doi: 10.1007/s00339-016-9634-5.
- [180] 2015 Archaeology, A Standard for Pottery Analysis in, “A Standard for Pottery Analysis in Archaeology,” *Archaeol. Data Serv.*, no. October, 2015, [Online]. Available: http://www.archaeologists.net/sites/default/files/Standard_for_Pottery_Analysis_Full_Draft_v4.pdf.
- [181] M. S. Tite, “Ceramic production, provenance and use - A review,” *Archaeometry*, vol. 50, no. 2, pp. 216–231, 2008, doi: 10.1111/j.1475-4754.2008.00391.x.
- [182] V. Oakley and K. K. Jain., “Essentials in the Care and Conservation of Historical Ceramic Objects,” Archetype Publ. Ltd, Gt. Britain, 2002.
- [183] M. Dondi, G. G., M. Raimondo, and S. F., “Influence of mineralogy and particle size on the technological properties of ball clays for porcelain stoneware tiles,” *Tile Brick Int.*, vol. 20, no. January, pp. 2–11, 2003.
- [184] I. P. Nikolov, T. Popmintchev, T. Todorova, I. C. Buchvarov, M. Surtchev, and S. Tzaneva, “Laser restoration of ceramic artifacts with archeological value,” *11th Int. Sch. Quantum Electron. Laser Phys. Appl.*, vol. 4397, no. June 2014, p. 343, 2001, doi: 10.1117/12.425162.
- [185] L. S. Selwyn and P. R. Roberge, *Rouging of Stainless Steel in High-Purity Water*. 2006.
- [186] B. Jegdić, S. Polić-Radovanović, S. Ristić, A. Alil, and V. Rajaković-Ognjanović, “Corrosion of an archaeological find from the Roman period in Serbia,” *Zaštita Mater.*, vol. 53, no. 3, pp. 247–252, 2012.
- [187] L. S. Selwyn and V. Argyropoulos, “Removal of chloride and iron ions from archaeological wrought iron with sodium hydroxide and ethylenediamine
-

-
- solutions,” *Stud. Conserv.*, vol. 50, no. 2, pp. 81–100, 2005, doi: 10.1179/sic.2005.50.2.81.
- [188] D. Watkinson, “Preservation of metallic cultural heritage,” *Shreir’s Corros.*, pp. 3307–3340, 2010, doi: 10.1016/B978-044452787-5.00172-4.
- [189] T. Kamimura, S. Hara, H. Miyuki, M. Yamashita, and H. Uchida, “Composition and protective ability of rust layer formed on weathering steel exposed to various environments,” *Corros. Sci.*, vol. 48, no. 9, pp. 2799–2812, 2006, doi: 10.1016/j.corsci.2005.10.004.
- [190] F. Kergourlay et al., “Mechanisms of the dechlorination of iron archaeological artefacts extracted from seawater,” *Corros. Sci.*, vol. 53, no. 8, pp. 2474–2483, 2011, doi: 10.1016/j.corsci.2011.04.003.
- [191] R. Balasubramaniam, A. V. Ramesh Kumar, and P. Dillmann, “Characterization of rust on ancient Indian iron,” *Curr. Sci.*, vol. 85, no. 11, pp. 1546–1555, 2003.
- [192] D. Dwivedi and J. P. Mata, “Archaeometallurgical investigation of ancient artefacts’ degradation phenomenon,” *npj Mater. Degrad.*, vol. 3, no. 1, 2019, doi: 10.1038/s41529-019-0097-y.
- [193] L. S. Selwyn, P. J. Sirois, and V. Argyropoulos, “The corrosion of excavated archaeological iron with details on weeping and akaganeite,” *Stud. Conserv.*, vol. 44, no. 4, pp. 217–232, 1999, doi: 10.1179/sic.1999.44.4.217.
- [194] L. Selwyn, “Overview of archaeological iron: the corrosion problem, key factors affecting treatment, and gaps in current knowledge,” *Proc. Met. 2004 Natl. Museum Aust. Canberra ACT ABN 70 592 297 967*, no. October, p. 303, 2004.
- [195] D. Watkinson and M. T. Lewis, “Desiccated storage of chloride-contaminated archaeological iron objects,” *Stud. Conserv.*, vol. 50, no. 4, pp. 241–252, 2005, doi: 10.1179/sic.2005.50.4.241.
- [196] S. Réguer, P. Dillmann, and F. Mirambet, “Buried iron archaeological artefacts: Corrosion mechanisms related to the presence of Cl-containing phases,” *Corros. Sci.*, vol. 49, no. 6, pp. 2726–2744, 2007, doi: 10.1016/j.corsci.2006.11.009.
- [197] A. A. Bore Jegdic, Suzana Polic-Radovanovic, Slavica Ristic, “Corrosion of archaeological artefact made of forged iron,” *Assoc. Met. Eng. Serbia*, vol. 18, no. 3, pp. 233–240, 2012.
- [198] Y. S. Koh, “Laser Cleaning as a Conservation Technique for Corroded Metal Artifacts,” p. 144, 2006, [Online]. Available: <http://epubl.ltu.se/1402-1544/2006/02/LTU-DT-0602-SE.pdf>.
- [199] M. Bertasa and C. Korenberg, “Successes and challenges in laser cleaning metal artefacts: A review,” *J. Cult. Herit.*, vol. 53, pp. 100–117, 2022, doi: 10.1016/j.culher.2021.10.010.
- [200] P. Dillmann, F. Mazaudier, and S. Hoerlé, “Advances in understanding atmospheric corrosion of iron. I. Rust characterisation of ancient ferrous artefacts exposed to indoor atmospheric corrosion,” *Corros. Sci.*, vol. 46, no. 6, pp. 1401–1429, 2004, doi: 10.1016/j.corsci.2003.09.027.
-

-
- [201] R. Lahoz, G. F. De La Fuente, J. M. Pedra, and J. B. Carda, "Laser engraving of ceramic tiles," *Int. J. Appl. Ceram. Technol.*, vol. 8, no. 5, pp. 1208–1217, 2011, doi: 10.1111/j.1744-7402.2010.02566.x.
- [202] J. M. Liu, "Simple technique for measurements of pulsed Gaussian-beam spot sizes," *Opt. Lett.*, vol. 7, no. 5, p. 196, 1982, doi: 10.1364/ol.7.000196.
- [203] P. Schaaf, "Laser Processing of Materials: Fundamentals, Applications and Developments," in *Springer Series in Materials Science*, Springer Science & Business Media, ISBN 32812, 9783642132810, Volume 139, Chapter 3, 2010.
- [204] E. Kannatey-Asibu and Jr., "Principles of Laser Materials Processing," in Wiley, ISBN 978-0-470-17798-3, Chapter 14, 2009.
- [205] A. V. Rode, D. Freeman, K. G. H. Baldwin, A. Wain, O. Uteza, and P. Delaporte, "Scanning the laser beam for ultrafast pulse laser cleaning of paint," *Appl. Phys. A Mater. Sci. Process.*, vol. 93, no. 1, pp. 135–139, 2008, doi: 10.1007/s00339-008-4656-2.
- [206] A. Stratan, A. Zorila, L. Rusen, and G. Nemes, "Measuring effective area of spots from pulsed laser beams," *Opt. Eng.*, vol. 53, no. 12, p. 122513, 2014, doi: 10.1117/1.oe.53.12.122513.
- [207] A. Cubero et al., "Effects of laser-induced periodic surface structures on the superconducting properties of Niobium," *Appl. Surf. Sci.*, vol. 508, no. September 2019, p. 145140, 2020, doi: 10.1016/j.apsusc.2019.145140.
- [208] G. F. Marshall and G. E. Stutz, Eds., *Handbook of Optical and Laser Scanning*, 2nd Editio. 2018.
- [209] Alvaro Cubero Ruiz, "Technological solutions and laser processes for the development of superconductor-based applications," PhD Thesis, INMA (CSIC-University of Zaragoza), pp. 88–91, 2021.
- [210] J. L. Arsuaga et al., "Neandertal roots: Cranial and chronological evidence from Sima de los Huesos," *Science (80-.)*, vol. 344, no. 6190, pp. 1358–1363, 2014, doi: 10.1126/science.1253958.
- [211] R. E. M. Hedges, "Bone diagenesis: An overview of processes," *Archaeometry*, vol. 44, no. 3, pp. 319–328, 2002, doi: 10.1111/1475-4754.00064.
- [212] H. Pfrezschner, "Fossilization of Haversian bone in aquatic environments," vol. 3, pp. 605–616, 2004, doi: 10.1016/j.crpv.2004.07.006.
- [213] R. Florencio-Silva, G. R. D. S. Sasso, E. Sasso-Cerri, M. J. Simões, and P. S. Cerri, "Biology of Bone Tissue: Structure, Function, and Factors That Influence Bone Cells," *Biomed Res. Int.*, vol. 2015, 2015, doi: 10.1155/2015/421746.
- [214] R. A. Nicholson, "Bone degradation in a compost heap," *J. Archaeol. Sci.*, vol. 25, no. 5, pp. 393–403, 1998, doi: 10.1006/jasc.1997.0208.
- [215] I.J. Higgins and R. G. Burns, "The chemistry and microbiology of pollution," Acad. Press London; New York, 1975.
- [216] W. D. Middleton et al., "The Study of Archaeological Floors : Methodological Proposal for the Analysis of Anthropogenic Residues by Spot Tests , ICP-OES , and
-

-
- GC-MS Ortiz , Laura Salvini and Roberto Rodriguez Suárez Published by : Springer
Stable URL : <http://www.jstor.org/stable>,” *J. Archaeol. Method*, vol. 17, no. 3, pp. 183–208, 2010.
- [217] E. M. White and L. A. Hannus, “Chemical Weathering of Bone in Archaeological Soils,” *Am. Antiq.*, vol. 48, no. 2, pp. 316–322, 1983, doi: 10.1017/S0002731600100423.
- [218] P.H. Bethell and M.O.H. Carver, “Detection and enhancement of decayed inhumations at Sutton Hoo. In: Boddington A, Garland AN, Janaway RC (eds),” *Death, decay Reconstr. approaches to Archaeol. forensic Sci.* Manchester Univ. Press. Manchester, pp. 10–21, 1987.
- [219] H. Piepenbrink, “Two examples of biogenous dead bone decomposition and their consequences for taphonomic interpretation,” *J. Archaeol. Sci.*, vol. 13, no. 5, pp. 417–430, 1986, doi: 10.1016/0305-4403(86)90012-9.
- [220] R. A. Queiroz et al., “First forensic records of termite activity on non-fossilized human bones in Brazil,” *Brazilian J. Biol.*, vol. 77, no. 1, pp. 127–131, 2016, doi: 10.1590/1519-6984.11415.
- [221] M. M. E. Jans et al., “In situ preservation of archaeological bone: A histological study within a multidisciplinary approach,” *Archaeometry*, vol. 44, no. 3, pp. 343–352, 2002, doi: 10.1111/1475-4754.t01-1-00067.
- [222] M. Cooper, “Laser cleaning in conservation: an introduction,” *Butterworth-Heinemann*, Oxford, vol. 79, no. 6, 1998.
- [223] R. Lahoz, L. A. Angurel, U. Brauch, L. C. Estepa, and G. F. de la Fuente Leis, “Laser Applications in the Preservation of Cultural Heritage: An Overview of Fundamentals and Applications of Lasers in the Preservation of Cultural Heritage,” *Conserv. Sci. Cult. Heritage. Appl. Instrum. Anal.*, pp. 294–332, 2013.
- [224] J. Marczak et al., “Characterization of laser cleaning of artworks,” *Sensors (Switzerland)*, vol. 8, no. 10, pp. 6507–6548, 2008, doi: 10.3390/s8106507.
- [225] W. Al Sekhaneh, A. El Serogy, and M. El-Bakri, “Yag-laser cleaning of archaeological materials in Jordanian museums,” *Mediterr. Archaeol. Archaeom.*, vol. 15, no. 3, pp. 157–164, 2015, doi: 10.5281/zenodo.19297.
- [226] A. Andreotti, M. P. Colombini, A. Nevin, K. Melessanaki, P. Pouli, and C. Fotakis, “Multianalytical Study of Laser Pulse Duration Effects in the IR Laser Cleaning of Wall Paintings from the Monumental Cemetery of Pisa,” *Laser Chem.*, vol. 2006, pp. 1–11, 2006, doi: 10.1155/2006/39046.
- [227] F. Di Niso, C. Gaudiuso, T. Sibillano, F. P. Mezzapesa, A. Ancona, and P. M. Lugarà, “Role of heat accumulation on the incubation effect in multi-shot laser ablation of stainless steel at high repetition rates,” *Opt. Express*, vol. 22, no. 10, p. 12200, 2014, doi: 10.1364/oe.22.012200.
- [228] C. Gaudiuso, G. Giannuzzi, A. Volpe, P. M. Lugarà, I. Choquet, and A. Ancona, “Incubation during laser ablation with bursts of femtosecond pulses with picosecond delays,” *Opt. Express*, vol. 26, no. 4, p. 3801, 2018, doi: 10.1364/oe.26.003801.
-

-
- [229] J. Arenberg, “A Set of Standard Definitions for Laser Damage Parameters and Procedures,” *Laser Induc. Damage Opt. Mater.* ed. H. Bennett, L. Chase, A. Guenther, B. Newnam, M. Soileau, West Conshohocken, p. PA: ASTM International, 9-9, 1990, 1989, doi: 10.1117/12.2294411.
- [230] E. Besozzi et al., “Nanosecond laser pulses for mimicking thermal effects on nanostructured tungsten-based materials,” *Nucl. Fusion*, vol. 58, no. 3, p. 036019, Mar. 2018, doi: 10.1088/1741-4326/aaa5d5.
- [231] A. Aranburu, J. L. Arsuaga, and N. Sala, “The stratigraphy of the Sima de los Huesos (Atapuerca, Spain) and implications for the origin of the fossil hominin accumulation,” *Quat. Int.*, vol. 433, pp. 5–21, 2017, doi: 10.1016/j.quaint.2015.02.044.
- [232] J. L. Bischoff et al., “Geology and preliminary dating of the hominid-bearing sedimentary fill of the Sima de los Huesos Chamber, Cueva Mayor of the Sierra de Atapuerca, Burgos, Spain,” *J. Hum. Evol.*, vol. 33, no. 2–3, pp. 129–154, 1997, doi: 10.1006/jhev.1997.0130.
- [233] C. A. Suarez, E. M. Morschhauser, M. B. Suarez, H. You, D. Li, and P. Dodson, “Rare earth element geochemistry of bone beds from the Lower Cretaceous Zhonggou Formation of Gansu Province, China,” *J. Vertebr. Paleontol.*, vol. 38, no. sup1, pp. 22–35, 2018, doi: 10.1080/02724634.2017.1400441.
- [234] E. Yakovlev, G. Shandybina, and A. Shamova, “Modelling of the heat accumulation process during short and ultrashort pulsed laser irradiation of bone tissue,” *Biomed. Opt. Express*, vol. 10, no. 6, p. 3030, 2019, doi: 10.1364/boe.10.003030.
- [235] E. Di Francia, L. A. Angurel, E. Angelini, S. Grassini, R. Lahoz, and M. Parvis, “Laser cleaning of archaeological bronze artefacts,” *Eur. Corros. Congr. EUROCORR 2016*, vol. 2, pp. 1031–1039, 2016.
- [236] F. Rey-García, F. Gutiérrez-Mora, C. J. Borrel, L. C. Estepa, L. A. Angurel, and G. F. De La Fuente, “Microstructural characterization and tribological behavior of Laser Furnace processed ceramic tiles,” *Ceram. Int.*, vol. 44, no. 6, pp. 6997–7005, 2018, doi: 10.1016/j.ceramint.2018.01.133.
- [237] G. J. Cheng, M. C. D. Pirzada, P. Mohanty, and A. Bandyopadhyay, *Materials Science and Engineering*. 2005.
- [238] G. Della Pepa and M. L. Brandi, “Microelements for bone boost: The last but not the least,” *Clin. Cases Miner. Bone Metab.*, vol. 13, no. 3, pp. 181–185, 2016, doi: 10.11138/ccmbm/2016.13.3.181.
- [239] B. Wopenka and J. D. Pasteris, “A mineralogical perspective on the apatite in bone,” *Mater. Sci. Eng. C*, vol. 25, no. 2, pp. 131–143, 2005, doi: 10.1016/j.msec.2005.01.008.
- [240] M. J. Kohn and T. E. Cerling, “Stable isotope compositions of biological apatite,” *Phosphates Geochemical, Geobiol. Mater. Importance*, vol. 48, no. McCrea 1950, pp. 455–488, 2019, doi: 10.2138/rmg.2002.48.12.
- [241] C. N. Trueman and N. Tuross, “Trace elements in recent and fossil bone apatite,” *Phosphates Geochemical, Geobiol. Mater. Importance*, vol. 48, no. Nriagu 1983,
-

-
- pp. 489–522, 2019, doi: 10.2138/rmg.2002.48.13.
- [242] F. J. B. A. Matilla Gutiérrez, M. Navazo Ruiz, “Estudio experimental acerca de la pátina que adquieren los materiales de sílex neógeno procedente de la sierra de Atapuerca,” *Arqueol. en el Val. del Duero Del Paleolítico a la Edad Media*, vol. 5, pp. 35–52.
- [243] Y. Deng et al., “Preparation and Coloration of Colored Ceramics Derived from the Vanadium-Titanium Slags,” *Adv. Mater. Sci. Eng.*, vol. 2018, 2018, doi: 10.1155/2018/5085031.
- [244] A. Nevin, P. Pouli, S. Georgiou, and C. Fotakis, “Laser conservation of art,” *Nat. Mater.*, vol. 6, no. 5, pp. 320–322, 2007, doi: 10.1038/nmat1895.
- [245] T. Palomar et al., “Evaluation of laser cleaning for the restoration of tarnished silver artifacts,” *Appl. Surf. Sci.*, vol. 387, pp. 118–127, 2016, doi: 10.1016/j.apsusc.2016.06.017.
- [246] G. Buccolieri, V. Nassisi, A. Buccolieri, F. Vona, and A. Castellano, “Laser cleaning of a bronze bell,” *Appl. Surf. Sci.*, vol. 272, pp. 55–58, 2013, doi: 10.1016/j.apsusc.2012.03.132.
- [247] S. Siano and R. Salimbeni, “Advances in laser cleaning of artwork and objects of historical interest: The optimized pulse duration approach,” *Acc. Chem. Res.*, vol. 43, no. 6, pp. 739–750, 2010, doi: 10.1021/ar900190f.
- [248] A. Kearns et al., “Laser removal of oxides from a copper substrate using Q-switched Nd:YAG radiation at 1064 nm, 532 nm and 266 nm,” *Appl. Surf. Sci.*, vol. 127–129, pp. 773–780, 1998, doi: 10.1016/S0169-4332(97)00741-1.
- [249] G. X. Chen, T. J. Kwee, K. P. Tan, Y. S. Choo, and M. H. Hong, “Laser cleaning of steel for paint removal,” *Appl. Phys. A Mater. Sci. Process.*, vol. 101, no. 2, pp. 249–253, 2010, doi: 10.1007/s00339-010-5811-0.
- [250] M. Sanz et al., “Influence of wavelength on the laser removal of lichens colonizing heritage stone,” *Appl. Surf. Sci.*, vol. 399, pp. 758–768, 2017, doi: 10.1016/j.apsusc.2016.12.032.
- [251] W. Svendsen, J. Schou, B. Thestrup, and O. Ellegaard, “Ablation from metals induced by visible and UV laser irradiation,” *Appl. Surf. Sci.*, vol. 96–98, pp. 518–521, 1996, doi: 10.1016/0169-4332(95)00506-4.
- [252] U. Keller, “Recent developments in compact ultrafast lasers,” *Nature*, vol. 424, no. August, pp. 831–838, 2003.
- [253] R. Salimbeni, R. Pini, and S. Siano, “A variable pulse width Nd:YAG laser for conservation,” *J. Cult. Herit.*, vol. 4, no. SUPPL. 1, pp. 72–76, 2003, doi: 10.1016/s1296-2074(02)01149-4.
- [254] M. Oujja et al., “Wavelength and pulse duration effects on laser induced changes on raw pigments used in paintings,” *Spectrochim. Acta - Part A Mol. Biomol. Spectrosc.*, vol. 102, pp. 7–14, 2013, doi: 10.1016/j.saa.2012.10.001.
- [255] M. Oujja, A. García, C. Romero, J. R. Vázquez De Aldana, P. Moreno, and M. Castillejo, “UV laser removal of varnish on tempera paints with nanosecond and
-

-
- femtosecond pulses,” *Phys. Chem. Chem. Phys.*, vol. 13, no. 10, pp. 4625–4631, 2011, doi: 10.1039/c0cp02147d.
- [256] M. Walczak et al., “Evaluation of femtosecond laser pulse irradiation of ancient parchment,” *Appl. Surf. Sci.*, vol. 255, no. 5 PART 2, pp. 3179–3183, 2008, doi: 10.1016/j.apsusc.2008.09.011.
- [257] N. A. Vasantgadkar, U. V. Bhandarkar, and S. S. Joshi, “A finite element model to predict the ablation depth in pulsed laser ablation,” *Thin Solid Films*, vol. 519, no. 4, pp. 1421–1430, 2010, doi: 10.1016/j.tsf.2010.09.016.
- [258] R. Le Harzic et al., “Pulse width and energy influence on laser micromachining of metals in a range of 100 fs to 5 ps,” *Appl. Surf. Sci.*, vol. 249, no. 1–4, pp. 322–331, 2005, doi: 10.1016/j.apsusc.2004.12.027.
- [259] E. G. Gamaly, “The physics of ultra-short laser interaction with solids at non-relativistic intensities,” *Phys. Rep.*, vol. 508, no. 4–5, pp. 91–243, 2011, doi: 10.1016/j.physrep.2011.07.002.
- [260] P. Pouli, I. A. Paun, G. Bounos, S. Georgiou, and C. Fotakis, “The potential of UV femtosecond laser ablation for varnish removal in the restoration of painted works of art,” *Appl. Surf. Sci.*, vol. 254, no. 21, pp. 6875–6879, 2008, doi: 10.1016/j.apsusc.2008.04.106.
- [261] T. Lippert and J. T. Dickinson, “Chemical and spectroscopic aspects of polymer ablation: Special features and novel directions,” *Chem. Rev.*, vol. 103, no. 2, pp. 453–485, 2003, doi: 10.1021/cr010460q.
- [262] P. Paraskevi, S. Alexandros, G. Savas, and F. Costas, “Recent Studies of Laser Science in Paintings Conservation and Research,” *Acc. Chem. Res.*, vol. 43, no. 6, pp. 771–781, 2010.
- [263] P. Hillips, G. Andhi, M. Azur, and S. Undaram, “Ultrafast laser processing of materials : a review,” vol. 7, no. 4, pp. 684–712, 2015.
- [264] J. K. Chen, D. Y. Tzou, and J. E. Beraun, “A semiclassical two-temperature model for ultrafast laser heating,” *Int. J. Heat Mass Transf.*, vol. 49, no. 1–2, pp. 307–316, 2006, doi: 10.1016/j.ijheatmasstransfer.2005.06.022.
- [265] M. Kono, K. G. H. Baldwin, A. Wain, and A. V. Rode, “Treating the untreatable in art and heritage materials: Ultrafast laser cleaning of ‘cloth-of-Gold,’” *Langmuir*, vol. 31, no. 4, pp. 1596–1604, 2015, doi: 10.1021/la504400h.
- [266] L. Jiang, A. D. Wang, B. Li, T. H. Cui, and Y. F. Lu, “Electrons dynamics control by shaping femtosecond laser pulses in micro/nanofabrication: Modeling, method, measurement and application,” *Light Sci. Appl.*, vol. 7, no. 2, pp. 1–27, 2018, doi: 10.1038/lsa.2017.134.
- [267] S. S. Mao et al., “Dynamics of femtosecond laser interactions with dielectrics,” *Appl. Phys. A Mater. Sci. Process.*, vol. 79, no. 7, pp. 1695–1709, 2004, doi: 10.1007/s00339-004-2684-0.
- [268] K. Mensink, E. H. Penilla, P. Martínez-Torres, N. Cuando-Espitia, S. Mathaudhu, and G. Aguilar, “High repetition rate femtosecond laser heat accumulation and
-

-
- ablation thresholds in cobalt-binder and binderless tungsten carbides,” *J. Mater. Process. Technol.*, vol. 266, pp. 388–396, 2019, doi: 10.1016/j.jmatprotec.2018.09.030.
- [269] C. M. Kruse, “Two-phase pool boiling and flow boiling heat transfer enhancement with femtosecond laser processed metallic surfaces,” 2018.
- [270] A. Žemaitis, M. Gaidys, M. Brikas, P. Gečys, G. Račiukaitis, and M. Gedvilas, “Advanced laser scanning for highly-efficient ablation and ultrafast surface structuring: experiment and model,” *Sci. Rep.*, vol. 8, no. 1, pp. 1–14, 2018, doi: 10.1038/s41598-018-35604-z.
- [271] K. Liu and E. Garmire, “Paint removal using lasers,” *Appl. Opt.*, vol. 34, no. 21, p. 4409, 1995, doi: 10.1364/ao.34.004409.
- [272] X. Liu, D. Du, and G. Mourou, “Laser ablation and micromachining with ultrashort laser pulses,” *IEEE J. Quantum Electron.*, vol. 33, no. 10, pp. 1706–1716, 1997, doi: 10.1109/3.631270.
- [273] A. Y. Vorobyev and C. Guo, “Direct femtosecond laser surface nano/microstructuring and its applications,” *Laser Photonics Rev.*, vol. 7, no. 3, pp. 385–407, 2013, doi: 10.1002/lpor.201200017.
- [274] B. Gunness, “Laser cleaning,” *Corros. Mater.*, vol. 43, no. 3, pp. 46–47, 2018, doi: 10.1201/9780203882085.ch52.
- [275] C. H. Crouch, J. E. Carey, J. M. Warrender, M. J. Aziz, E. Mazur, and F. Y. Génin, “Comparison of structure and properties of femtosecond and nanosecond laser-structured silicon,” *Appl. Phys. Lett.*, vol. 84, no. 11, pp. 1850–1852, 2004, doi: 10.1063/1.1667004.
- [276] B. N. Chichkov, C. Momma, S. Nolte, F. von Alvensleben, and A. Tünnermann, “Femtosecond, picosecond and nanosecond laser ablation of solids,” *Appl. Phys. A Mater. Sci. Process.*, vol. 63, no. 2, pp. 109–115, 1996, doi: 10.1007/s003390050359.
- [277] L. Goldman, P. Hornby, R. Meyer, and B. Goldman, “Impact of the laser on dental caries [27],” *Nature*, vol. 203, no. 4943, p. 417, 1964, doi: 10.1038/203417a0.
- [278] J. D. Featherstone and D. G. Nelson, “Laser effects on dental hard tissues.,” *Adv. Dent. Res.*, vol. 1, no. 1, pp. 21–26, 1987, doi: 10.1177/08959374870010010701.
- [279] K. Müller, C. Chadefaux, N. Thomas, and I. Reiche, “Microbial attack of archaeological bones versus high concentrations of heavy metals in the burial environment. A case study of animal bones from a mediaeval copper workshop in Paris,” *Palaeogeogr. Palaeoclimatol. Palaeoecol.*, vol. 310, no. 1–2, pp. 39–51, 2011, doi: 10.1016/j.palaeo.2011.03.023.
- [280] P. Zioupos, J. D. Currey, and A. Casinos, “Exploring the effects of hypermineralisation in bone tissue by using an extreme biological example,” *Connect. Tissue Res.*, vol. 41, no. 3, pp. 229–248, 2000, doi: 10.3109/03008200009005292.
- [281] S. Weiner and H. D. Wagner, “The material bone: Structure-mechanical function
-

-
- relations,” *Annu. Rev. Mater. Sci.*, vol. 28, no. 1, pp. 271–298, 1998, doi: 10.1146/annurev.matsci.28.1.271.
- [282] I. Reiche, C. Vignaud, and M. Menu, “The crystallinity of ancient bone and dentine: New insights by transmission electron microscopy,” *Archaeometry*, vol. 44, no. 3, pp. 447–459, 2002, doi: 10.1111/1475-4754.00077.
- [283] A. Boskey, “Bone mineral crystal size.,” *Osteoporos. Int.*, vol. 14 Suppl 5, pp. 16–21, 2003, doi: 10.1007/s00198-003-1468-2.
- [284] L. Wilson and A. M. Pollard, “Here today, gone tomorrow? Integrated experimentation and geochemical modeling in studies of archaeological diagenetic change,” *Acc. Chem. Res.*, vol. 35, no. 8, pp. 644–651, 2002, doi: 10.1021/ar000203s.
- [285] M. J. Collins et al., “the Survival of Organic Matter in Bone: a Review,” *Archaeometry*, vol. 3, no. 44, pp. 383–394, 2002.
- [286] F. Berna, A. Matthews, and S. Weiner, “Solubilities of bone mineral from archaeological sites: The recrystallization window,” *J. Archaeol. Sci.*, vol. 31, no. 7, pp. 867–882, 2004, doi: 10.1016/j.jas.2003.12.003.
- [287] S. Von Ew et al., “Bone mineral: new insights into its chemical composition,” *Sci. Rep.*, vol. 9, no. 1, pp. 1–11, 2019, doi: 10.1038/s41598-019-44620-6.
- [288] A. A. Hassan and D. J. Ortner, “Inclusions in Bone Material as a Source of Error in Radiocarbon Dating,” *Archaeometry*, vol. 19, no. 2, pp. 131–135, 1977, doi: 10.1111/j.1475-4754.1977.tb00190.x.
- [289] J. D. Hem, “Study and interpretation of the chemical characteristics of natural water.,” *US Geol. Surv. Water-Supply Pap.*, vol. 2254, 1985.
- [290] C. Reimann and P. de Caritat, *Chemical elements in the environment: Factsheets for the geochemist and environmental scientist*, vol. 1. New York: Springer, Berlin Heidelberg, 1998.
- [291] B. B. Dent, S. L. Forbes, and B. H. Stuart, “Review of human decomposition processes in soil,” *Environ. Geol.*, vol. 45, no. 4, pp. 576–585, 2004, doi: 10.1007/s00254-003-0913-z.
- [292] P. Dericquebourg, A. Person, L. Ségalen, M. Pickford, B. Senut, and N. Fagel, “Bone diagenesis and origin of calcium phosphate nodules from a hominid site in the Lukeino Formation (Tugen Hills, Kenya),” *Palaeogeogr. Palaeoclimatol. Palaeoecol.*, vol. 536, p. 109377, 2019, doi: 10.1016/j.palaeo.2019.109377.
- [293] K. Absolonová, M. Dobisíková, M. Beran, J. Zocová, and P. Velemínský, “The temperature of cremation and its effect on the microstructure of the human rib compact bone,” *Anthropol. Anzeiger*, vol. 69, no. 4, pp. 439–460, 2012, doi: 10.1127/0003-5548/2012/0213.
- [294] G. Dal Sasso, M. Lebon, I. Angelini, L. Maritan, D. Usai, and G. Artioli, “Bone diagenesis variability among multiple burial phases at Al Khiday (Sudan) investigated by ATR-FTIR spectroscopy,” *Palaeogeogr. Palaeoclimatol. Palaeoecol.*, vol. 463, pp. 168–179, 2016, doi: 10.1016/j.palaeo.2016.10.005.
-

-
- [295] M. C. Chang and J. Tanaka, "FT-IR study for hydroxyapatite/collagen nanocomposite cross-linked by glutaraldehyde," *Biomaterials*, vol. 23, no. 24, pp. 4811–4818, 2002, doi: 10.1016/S0142-9612(02)00232-6.
- [296] I. Rehman and W. Bonfield, "Characterization of hydroxyapatite and carbonated apatite by photo acoustic FTIR spectroscopy," *J. Mater. Sci. Mater. Med.*, vol. 8, no. 1, pp. 1–4, 1997, doi: 10.1023/A:1018570213546.
- [297] S. Eugénio, M. Sivakumar, R. Vilar, and A. M. Rego, "Characterisation of dentin surfaces processed with KrF excimer laser radiation," *Biomaterials*, vol. 26, no. 33, pp. 6780–6787, 2005, doi: 10.1016/j.biomaterials.2005.03.047.
- [298] G. Turner-Walker, "Degradation pathways and conservation strategies for ancient bone from wet anoxic sites," *Proc. 10th ICOM Gr. Wet Org. Archaeol. Mater. Conf. Amsterdam 2007*, no. September 2007, pp. 659–675, 2009.
- [299] A. Fabig and B. Herrmann, "Trace elements in buried human bones: Intra-population variability of Sr/Ca and Ba/Ca ratios - Diet or diagenesis?," *Naturwissenschaften*, vol. 89, no. 3, pp. 115–119, 2002, doi: 10.1007/s00114-001-0294-7.
- [300] C. T. WILLIAMS and P. J. POTTS, "Element Distribution Maps in Fossil Bones," *Archaeometry*, vol. 30, no. 2, pp. 237–247, 1988, doi: 10.1111/j.1475-4754.1988.tb00450.x.
- [301] L. T. Canguero, R. Vilar, A. M. Botelho do Rego, and V. S. F. Muralha, "Femtosecond laser ablation of bovine cortical bone," *J. Biomed. Opt.*, vol. 17, no. 12, p. 125005, 2012, doi: 10.1117/1.jbo.17.12.125005.
- [302] H. S. Vuorinen, S. Pihlman, H. Mussalo-Rauhamaa, U. Tapper, and T. Varrela, "Trace and heavy metal analyses of a skeletal population representing the town people in Turku (Åbo), Finland in the 16th-17th centuries: With special reference to gender, age and social background," *Sci. Total Environ.*, vol. 177, no. 1–3, pp. 145–160, 1996, doi: 10.1016/0048-9697(95)04892-8.
- [303] T. Tütken and T. W. Vennemann, "Fossil bones and teeth: Preservation or alteration of biogenic compositions?," *Palaeogeogr. Palaeoclimatol. Palaeoecol.*, vol. 310, no. 1–2, pp. 1–8, 2011, doi: 10.1016/j.palaeo.2011.06.020.
- [304] M. A. Kasem, R. E. Russo, and M. A. Harith, "Influence of biological degradation and environmental effects on the interpretation of archeological bone samples with laser-induced breakdown spectroscopy," *J. Anal. At. Spectrom.*, vol. 26, no. 9, pp. 1733–1739, 2011, doi: 10.1039/c1ja10057b.
- [305] H. Zhang, S. M. Eaton, J. Li, and P. R. Herman, "Heat accumulation during high repetition rate ultrafast laser interaction: Waveguide writing in borosilicate glass," *J. Phys. Conf. Ser.*, vol. 59, no. 1, pp. 682–686, 2007, doi: 10.1088/1742-6596/59/1/144.
- [306] A. Siatou, D. Charalambous, V. Argyropoulos, and P. Pouli, "A Comprehensive Study for the Laser Cleaning of Corrosion Layers due to Environmental Pollution for Metal Objects of Cultural Value: Preliminary Studies on Artificially Corroded Coupons," *Laser Chem.*, vol. 2006, pp. 1–7, 2006, doi: 10.1155/2006/85324.
-

-
- [307] T. Guo, C. Spielmann, B. C. Walker, and C. P. J. Barty, “Generation of hard x rays by ultrafast terawatt lasers,” *Rev. Sci. Instrum.*, vol. 72, no. 1 I, pp. 41–47, 2001, doi: 10.1063/1.1327309.
- [308] N. Zhavoronkov, Y. Gritsai, G. Korn, and T. Elsaesser, “Ultra-short efficient laser-driven hard X-ray source operated at a kHz repetition rate,” *Appl. Phys. B Lasers Opt.*, vol. 79, no. 6, pp. 663–667, 2004, doi: 10.1007/s00340-004-1658-4.
- [309] S. Juodkazis et al., “Laser-induced microexplosion confined in the bulk of a sapphire crystal: Evidence of multimegabar pressures,” *Phys. Rev. Lett.*, vol. 96, no. 16, pp. 1–4, 2006, doi: 10.1103/PhysRevLett.96.166101.
- [310] S. K. Sundaram and E. Mazur, “Inducing and probing non-thermal transitions in semiconductors using femtosecond laser pulses,” *Nat. Mater.*, vol. 1, no. 4, pp. 217–224, 2002, doi: 10.1038/nmat767.
- [311] M. Sakakura and M. Terazima, “Initial temporal and spatial changes of the refractive index induced by focused femtosecond pulsed laser irradiation inside a glass,” *Phys. Rev. B - Condens. Matter Mater. Phys.*, vol. 71, no. 2, pp. 1–12, 2005, doi: 10.1103/PhysRevB.71.024113.
- [312] L. Jiang and H. L. Tsai, “Repeatable nanostructures in dielectrics by femtosecond laser pulse trains,” *Appl. Phys. Lett.*, vol. 87, no. 15, pp. 1–3, 2005, doi: 10.1063/1.2093935.
- [313] H. Park, X. Wang, S. Nie, R. Clinite, and J. Cao, “Mechanism of coherent acoustic phonon generation under nonequilibrium conditions,” *Phys. Rev. B - Condens. Matter Mater. Phys.*, vol. 72, no. 10, pp. 1–4, 2005, doi: 10.1103/PhysRevB.72.100301.
- [314] E. Carmona Ballester, “Releyendo las estelas epigráficas de la necrópolis de ‘El Castillo’ (Palacios de la Sierra, Burgos),” *Arqueol. y Territ. Mediev.*, vol. 26, pp. 139–156, 2019, doi: 10.17561/aytm.v26.6.
- [315] S. Döring, T. Ullsperger, F. Heisler, S. Richter, A. Tünnermann, and S. Nolte, “Hole formation process in ultrashort pulse laser percussion drilling,” *Phys. Procedia*, vol. 41, pp. 431–440, 2013, doi: 10.1016/j.phpro.2013.03.099.
- [316] H. Liu, H. Yazici, C. Ergun, T. J. Webster, and H. Bermek, “An in vitro evaluation of the Ca/P ratio for the cytocompatibility of nano-to-micron particulate calcium phosphates for bone regeneration,” *Acta Biomater.*, vol. 4, no. 5, pp. 1472–1479, 2008, doi: 10.1016/j.actbio.2008.02.025.
- [317] A. Martínez Cortizas and O. López-Costas, “Linking structural and compositional changes in archaeological human bone collagen: an FTIR-ATR approach,” *Sci. Rep.*, vol. 10, no. 1, pp. 1–14, 2020, doi: 10.1038/s41598-020-74993-y.
- [318] A. El-Hussein, I. Yousef, and M. A. Kasem, “Exploiting FTIR microspectroscopy and chemometric analysis in the discrimination between Egyptian ancient bones: a case study,” *J. Opt. Soc. Am. B*, vol. 37, no. 11, p. A110, 2020, doi: 10.1364/josab.397419.
- [319] K. Mathewson et al., “Patina: A Profane Archaeology,” *AAG Rev. Books*, vol. 7, no. 2, pp. 113–125, 2019, doi: 10.1080/2325548x.2019.1579579.
-

-
- [320] J. Delgado Rodrigues, “Stone patina. A controversial concept of relevant importance in conservation,” *Int. Semin. Theory Pract. Conserv. a Tribut. to Cesare Brand.*, no. May 2006, pp. 127–138, 2006.
- [321] V. J. Hurst and A. R. Kelly, “Patination of cultural flints,” *Science (80-.)*, vol. 134, no. 3474, pp. 251–256, 1961, doi: 10.1126/science.134.3474.251.
- [322] G. Letavernier and J. C. Ozouf, “La gélifraction des roches et des parois calcaires,” *Bull. l’Association française pour l’étude du Quat.*, vol. 24, no. 3, pp. 139–145, 1987, doi: 10.3406/quate.1987.1841.
- [323] C. D. Howard and C. D. Howard, “The Gloss Patination of Flint Artifacts,” *JSTOR*, vol. 47, no. 182, pp. 283–287, 2016.
- [324] J. P. Lautridou and J. C. Ozouf, “Experimental frost shattering,” *Prog. Phys. Geogr. Earth Environ.*, vol. 6, no. 2, pp. 215–232, 1982, doi: 10.1177/030913338200600202.
- [325] B. Efrati, R. Barkai, S. N. Cesaro, and F. Venditti, “Function, life histories, and biographies of Lower Paleolithic patinated flint tools from Late Acheulian Revadim, Israel,” *Sci Rep.* 2022 Mar 3;12(1)2885., doi: 10.1038/s41598-022-06823-2.
- [326] M. G.F. and Stutz G.E., “Handbook of optical and laser scanning,” Taylor Fr., 2012.
- [327] P. M. Rice, “On the origins of pottery,” *J. Archaeol. Method Theory*, vol. 6, no. 1, pp. 1–54, 1999, doi: 10.1023/A:1022924709609.
- [328] V. A. Drebuschak, L. N. Mylnikova, T. N. Drebuschak, and V. V. Boldyrev, “The investigation of ancient pottery: Application of thermal analysis,” *J. Therm. Anal. Calorim.*, vol. 82, no. 3, pp. 617–626, 2005, doi: 10.1007/s10973-005-0942-9.
- [329] A. Iordanidis, J. Garcia-Guinea, and G. Karamitrou-Mentessidi, “Analytical study of ancient pottery from the archaeological site of Aiani, northern Greece,” *Mater. Charact.*, vol. 60, no. 4, pp. 292–302, 2009, doi: 10.1016/j.matchar.2008.08.001.
- [330] R. Palanivel and G. Velraj, “FTIR and FT-Raman spectroscopic studies of fired clay artifacts recently excavated in Tamilnadu, India,” *Indian J. Pure Appl. Phys.*, vol. 45, no. 6, pp. 501–508, 2007.
- [331] D. Barilaro et al., “FT-IR absorbance spectroscopy to study Sicilian ‘protomajolica’ pottery,” *Vib. Spectrosc.*, vol. 48, no. 2, pp. 269–275, 2008, doi: 10.1016/j.vibspec.2008.01.005.
- [332] C. Manoharan, R. Venkatachalapathy, S. Dhanapandian, and K. Deenadayalan, “FTIR and Mössbauer spectroscopy applied to study of archaeological artefacts from Maligaimedu, Tamil Nadu, India,” *Indian J. Pure Appl. Phys.*, vol. 45, no. 10, pp. 860–865, 2007.
- [333] S. Shoval, E. Yadin, and G. Panczer, “Analysis of thermal phases in calcareous Iron Age pottery using FT-IR and Raman spectroscopy,” *J. Therm. Anal. Calorim.*, vol. 104, no. 2, pp. 515–525, 2011, doi: 10.1007/s10973-011-1518-5.
- [334] R. P. Freitas, F. A. Coelho, V. S. Felix, M. O. Pereira, M. A. T. de Souza, and M. J. Anjos, “Analysis of 19th century ceramic fragments excavated from Pirenópolis
-

-
- (Goiás, Brazil) using FT-IR, Raman, XRF and SEM,” *Spectrochim. Acta - Part A Mol. Biomol. Spectrosc.*, vol. 193, pp. 432–439, 2018, doi: 10.1016/j.saa.2017.12.047.
- [335] R. A. Goodall, J. Hall, R. Viel, and P. M. Fredericks, “A spectroscopic investigation of pigment and ceramic samples from Copán, Honduras,” *Archaeometry*, vol. 51, no. 1, pp. 95–109, 2009, doi: 10.1111/j.1475-4754.2007.00382.x.
- [336] G. Velraj, K. Janaki, A. M. Musthafa, and R. Palanivel, “Estimation of firing temperature of some archaeological pottery shreds excavated recently in Tamilnadu, India,” *Spectrochim. Acta - Part A Mol. Biomol. Spectrosc.*, vol. 72, no. 4, pp. 730–733, 2009, doi: 10.1016/j.saa.2008.11.015.
- [337] A. Krapukaityte, S. Tautkus, A. Kareiva, and E. Zalieckiene, “Thermal analysis - A powerful tool for the characterization of pottery,” *Chemija*, vol. 19, no. 2, pp. 4–8, 2008.
- [338] R. Palanivel and U. R. Kumar, “Thermal and spectroscopic analysis of ancient potteries,” *Rom. Reports Phys.*, vol. 56, no. 1–2, pp. 195–208, 2011.
- [339] E. Manzano, A. García, E. Alarcón, S. Cantarero, F. Contreras, and J. L. Vílchez, “An integrated multianalytical approach to the reconstruction of daily activities at the Bronze Age settlement in Peñalosa (Jaén, Spain),” *Microchem. J.*, vol. 122, pp. 127–136, 2015, doi: 10.1016/j.microc.2015.04.021.
- [340] V. Cotiuga, I. Sandu, V. Vasilache and N. Ursulescu, “Atypical Local Accumulation of Calcium Carbonate Deposits in Prehistoric Ceramics during Underground Lying,” *Interdisciplinarity Research in Archaeology. Proceedings of the First Arheoinvest Congress, 10-11 June 2011.*
- [341] M. Hajjaji, S. Kacim, and M. Boulmane, “Mineralogy and firing characteristics of a clay from the valley of Ourika (Morocco),” *Appl. Clay Sci.*, vol. 21, no. 3–4, pp. 203–212, 2002, doi: 10.1016/S0169-1317(01)00101-6.
- [342] C. Ionescu, L. Ghergari, M. Horga, and G. Rădulescu, “Early Medieval ceramics from the Viile Tecii archaeological site (Romania): an optical and XRD study,” *Stud. Univ. Babeş-Bolyai, Geol.*, vol. 52, no. 2, pp. 29–35, 2007, doi: 10.5038/1937-8602.52.2.4.
- [343] G. E. De Benedetto, R. Laviano, L. Sabbatini, and P. G. Zambonin, “Infrared spectroscopy in the mineralogical characterization of ancient pottery,” *J. Cult. Herit.*, vol. 3, no. 3, pp. 177–186, 2002, doi: 10.1016/S1296-2074(02)01178-0.
- [344] G. Velraj, S. Tamilarasu, and R. Ramya, “FTIR, XRD and SEM-EDS Studies of Archaeological Pottery Samples from Recently Excavated Site in Tamil Nadu, India,” *Mater. Today Proc.*, vol. 2, no. 3, pp. 934–942, 2015, doi: 10.1016/j.matpr.2015.06.012.
- [345] J. Froh, “Archaeological ceramics studied by scanning electron microscopy,” *Hyperfine Interact.*, vol. 154, no. 1–4, pp. 159–176, 2004, doi: 10.1023/B:HYPE.0000032074.98045.cc.
- [346] a. Merkevičius et al., “XRD and SEM characterization of archaeological findings excavated in Lithuania,” *Chemija*, vol. 18, no. 1, pp. 36–39, 2007.
-

-
- [347] R. Ravisankar, S. Kiruba, C. Shamira, A. Naseerutheen, P. D. Balaji, and M. Seran, "Spectroscopic techniques applied to the characterization of recently excavated ancient potteries from Thiruverkadu Tamilnadu, India," *Microchem. J.*, vol. 99, no. 2, pp. 370–375, 2011, doi: 10.1016/j.microc.2011.06.012.
- [348] C. A. Rios-Reyes, E. D. Nunez-Alarcon, L. S. Puentes-Arguello, J. C. BarriosLopez, L. Moreno-Gonzalez, and J. A. H. Martinez, "Mineralogical characterization of an ancient pottery from the la Candelaria archaeological site, Santa Helena del Opón, Santander (Colombia)," *Mater. Sci. Eng. Int. J.*, vol. 3, no. 4, pp. 118–124, 2019, doi: 10.15406/mseij.2019.03.00101.
- [349] N. Forster, P. Grave, N. Vickery, and L. Kealhofer, "Non-destructive analysis using PXRF: Methodology and application to archaeological ceramics," *X-Ray Spectrom.*, vol. 40, no. 5, pp. 389–398, 2011, doi: 10.1002/xrs.1360.
- [350] C. Papachristodoulou, A. Oikonomou, K. Ioannides, and K. Gravani, "A study of ancient pottery by means of X-ray fluorescence spectroscopy, multivariate statistics and mineralogical analysis," *Anal. Chim. Acta*, vol. 573–574, pp. 347–353, 2006, doi: 10.1016/j.aca.2006.02.012.
- [351] A. M. W. Hunt and R. J. Speakman, "Portable XRF analysis of archaeological sediments and ceramics," *J. Archaeol. Sci.*, vol. 53, pp. 626–638, 2015, doi: 10.1016/j.jas.2014.11.031.
- [352] M. Verde et al., "Minero-petrographic investigation on Roman pottery found in a dump in the workshop area of Cumae (southern Italy)," *J. Archaeol. Sci. Reports*, vol. 42, no. October 2021, p. 103376, 2022, doi: 10.1016/j.jasrep.2022.103376.
- [353] A. Tsolakidou and V. Kilikoglou, "Comparative analysis of ancient ceramics by neutron activation analysis, inductively coupled plasma-optical-emission spectrometry, inductively coupled plasma-mass spectrometry, and X-ray fluorescence," *Anal. Bioanal. Chem.*, vol. 374, no. 3, pp. 566–572, 2002, doi: 10.1007/s00216-002-1444-2.
- [354] İ. Tarhan, Z. Derin, and M. Akif Erdem, "The study of Middle Bronze Age pottery from Yassitepe Höyük site in İzmir, Turkey, by FTIR and XRD with chemometrics," *J. Archaeol. Sci. Reports*, vol. 42, no. February, 2022, doi: 10.1016/j.jasrep.2022.103401.
- [355] M. Özçatal et al., "Characterization of lead glazed potteries from Smyrna (İzmir/Turkey) using multiple analytical techniques; Part II: Body," *Ceram. Int.*, vol. 40, no. 1 PART B, pp. 2153–2160, 2014, doi: 10.1016/j.ceramint.2013.07.132.
- [356] D. Mitchell, P. Grave, M. Maccheroni, and E. Gelman, "Geochemical characterisation of north Asian glazed stonewares: A comparative analysis of NAA, ICP-OES and non-destructive pXRF," *J. Archaeol. Sci.*, vol. 39, no. 9, pp. 2921–2933, 2012, doi: 10.1016/j.jas.2012.04.044.
- [357] A. Pérez-romero et al., "La cerámica de la Edad del Bronce en el yacimiento de El Portalón de Cueva Mayor (Sierra de Atapuerca, Burgos, España)," *Munibe Antropol.*, vol. 67, no. 3, pp. 105–126, 2016, doi: 10.21630/maa.2016.67.06.
- [358] X. L. Hao, T. Q. Zhu, J. J. Xu, Y. R. Wang, and X. W. Zhang, "Microscopic study
-

-
- on the concretion of ceramics in the ‘Nanhai I’ shipwreck of China, Southern Song Dynasty (1,127–1,279 A.D.),” *Microsc. Res. Tech.*, vol. 81, no. 5, pp. 486–493, 2018, doi: 10.1002/jemt.23002.
- [359] F. S. Madkour and M. K. Khallaf, “Degradation Processes of Egyptian Faience Tiles in the Step Pyramid at Saqqara,” *Procedia - Soc. Behav. Sci.*, vol. 68, pp. 63–76, 2012, doi: 10.1016/j.sbspro.2012.12.207.
- [360] Sáenz-Martínez, M. S. Andrés, M. Alvarez de Buergo, I. Blasco, and R. Fort, “Removing calcium carbonate deposits from archaeological ceramics. Traditional methods under review,” *Mediterr. Archaeol. Archaeom.*, vol. 19, no. 3, pp. 107–117, 2019, doi: 10.5281/zenodo.3583061.
- [361] O. Haupt and F. Gäbler, “Short-Pulse Q-Switched Lasers Enhance Precision Marking Applications,” 2022. https://www.photonics.com/Articles/Short-Pulse_Q-Switched_Lasers_Enhance_Precision/a54075 (accessed May 06, 2022).
- [362] V. Vasilache, V. Kavruk, and F. A. Tencariu, “OM, SEM–EDX, and micro-FTIR analysis of the Bronze Age pottery from the Băile Figa salt production site (Transylvania, Romania),” *Microsc. Res. Tech.*, vol. 83, no. 6, pp. 604–617, 2020, doi: 10.1002/jemt.23451.
- [363] M. soil color Charts., “Munsell Soil-Color Charts with genuine Munsell (R) color chips.” 2009.
- [364] R. Padilla, P. Van Espen, and P. P. G. Torres, “The suitability of XRF analysis for compositional classification of archaeological ceramic fabric : A comparison with a previous NAA study,” vol. 558, pp. 283–289, 2006, doi: 10.1016/j.aca.2005.10.077.
- [365] J. Riederer, “Thin section microscopy applied to the study of archaeological ceramics,” *Hyperfine Interact.*, vol. 154, no. 1–4, pp. 143–158, 2004, doi: 10.1023/B:HYPE.0000032029.24557.b1.
- [366] B. Radojković, “SURFACE MODIFICATION ON IRON INDUCED BY Nd : YAG PULSED LASER TREATMENT.”
- [367] B. Jegdić, S. Polić-Radovanović, S. Ristić, and A. Alil, “Corrosion stability of corrosion products on an archaeological iron artefact,” *Int. J. Conserv. Sci.*, vol. 3, no. 4, pp. 241–248, 2012.
- [368] V. P. Veiko, T. J. Mutin, V. N. Smirnov, E. A. Shakhno, and S. A. Batishche, “Laser Cleaning of Metal Surfaces: Physical Processes and Applications,” vol. 6985, pp. 69850D-69850D-8, 2008, doi: 10.1117/12.786975.

APPENDIX - A

ABBREVIATIONS AND ACRONYMS

Al	: Aluminum
AM	: Archaeological Materials
Approx.	: Approximately
APS	: Archaeological Pottery Sherd
ArF	: Argon fluoride
At.	: Atomic
ATP	: Atapuerca Mountain in Spain
ATR	: Attenuated Total Reflection
Ca	: Calcium
CAD	: Computer-aided design
CH	: Cultural Heritage
cm	: Centimeter
CO ₂	: Carbon dioxide
CW	: Continuous Wave
°C	: Degree Celsius
<i>d</i>	: Distance between adjacent laser passes
<i>Db</i>	: Beam diameter
EDS	: Energy Dispersive X-ray Spectrometry
Er:YAG	: Yttrium Aluminum Garnet doped with Erbium
e.g.	: Example gratia, for example
<i>Ep</i>	: Maximum pulse energy
et. al.	: et alia and others
Etc	: et cetra, and the rest
Fe	: Iron
Fig.	: Figure(s)
fs	: Femtosecond
<i>f</i>	: Pulse repetition rate, or frequency
<i>F_{pulse}</i> , or <i>F_L</i>	: Laser fluence
FTIR	: Fourier-Transform Infrared Spectroscopy
FWHM	: Full Width at Half-Maximum
i.e.	: id est, which to say in other words

GW	: Gigawatt
I_{pulse} , or I_L	: Laser irradiance
IR	: Infrared
Jcm ⁻²	: Joule per centimeter square
K	: Potassium
KrF	: Krypton fluoride
λ	: Wavelength
Mg	: Magnesium
Mn	: Manganese
M	: Meter
μ	: Micron
μm	: Micrometer
μs	: Microsecond
mm	: Millimeter
mms^{-1}	: Millimeter per second
min(s)	: Minutes
Na	: Sodium
Nd:YAG	: Yttrium Aluminum Garnet doped with Neodymium
n-IR	: near- Infrared
No.	: Number
nm	: Nanometer
ns	: Nanosecond
O	: Oxygen
OM	: Optical Microscopy
P	: Power
P	: Phosphorus (Chemical Name)
pH	: Negative logarithm of Hydrogen ion concentration (H^+)
ps	: Picosecond
%	: Percentage
S	: Sulphur
SEM	: Scanning Electron Microscopy
Si	: Silicon
sub-ns	: Sub- nanosecond
τ	: Pulse duration
Ti	: Titanium
TW	: Terawatt

UV	: ultra violet
V	: Scan speed
W	: Watt
Wt.	: Weight
XeBr	: Xenon bromide
XeCl	: Xenon monochloride
XeF	: Xenon fluoride
XRD	: X-ray Diffractometry
XRF	: X-ray Fluorescence Spectrometry
XPS	: X-ray Photoelectron Spectroscopy
YAG	: Yttrium Aluminium Garnet
Yb: YAG	: Yttrium Aluminium Garnet with Ytterbium

APPENDIX – B

LIST OF UNITS

Basic Physical Quantities

Physical Quantity	Symbol	Variable	Unit
Length	S	Meter	m
Time	T	Second	sec
Temperature	T	Degree Celsius	$^{\circ}\text{C}$
Angle	Theta	Radians	none

Electrical Physical Quantities

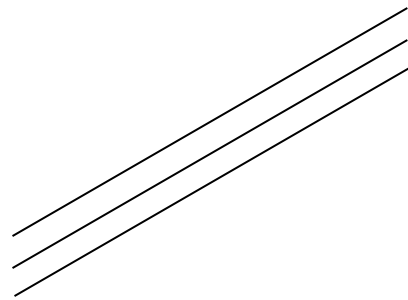
Physical Quantity	Symbol	Variable	Unit
electric current	I	ampere	A
voltage, potential	E	volt	V
frequency	f	hertz	s^{-1}
Power	P	Watt	joule/sec
wave length	λ	meters	m

Physical Constants

Physical Quantity	Symbol	MKS Value	Unit
atmospheric pressure	A	1.01325	newton/m ²
electron volt	e	1.60210E-10	joule
Pi, ratio of circumference to diameter	Pi	3.14159265	radians

Prefixes with SI Units

Prefix	Symbol	Multiple	Amount
tera	T	10 ¹²	1 million millions
giga	G	10 ⁹	1 thousand millions
mega	M	10 ⁶	1 million
kilo	k	10 ³	1 thousand
Prefix	Symbol	Sub-multiple	Fraction
milli	m	10 ⁻³	1 thousandth
micro	μ	10 ⁻⁶	1 millionth
nano	n	10 ⁻⁹	1 thousandth of a millionth
pico	p	10 ⁻¹²	1 millionth of a millionth
femto	f	10 ⁻¹⁵	1 thousandth of a millionth of a millionth



NOTHING WRITTEN,

NOTHING EXIST!!

